System Identification, State Estimation, And Control Approaches to Gestational Weight Gain Interventions

by

Penghong Guo

A Dissertation Presented in Partial Fulfillment
of the Requirements for the Degree
Doctor of Philosophy

Approved November 2018 by the
Graduate Supervisory Committee:

Daniel E. Rivera, Chair
Shuguang Deng
Erica Forzani
Theodore P. Pavlic
Matthew M. Peet

ARIZONA STATE UNIVERSITY

December 2018

ABSTRACT

Excessive weight gain during pregnancy is a significant public health concern and has been the recent focus of novel, control systems-based interventions. Healthy Mom Zone (HMZ) is an intervention study that aims to develop and validate an individually tailored and intensively adaptive intervention to manage weight gain for overweight or obese pregnant women using control engineering approaches. Motivated by the needs of the HMZ, this dissertation presents how to use system identification and state estimation techniques to assist in dynamical systems modeling and further enhance the performance of the closed-loop control system for interventions.

Underreporting of energy intake (EI) has been found to be an important consideration that interferes with accurate weight control assessment and the effective use of energy balance (EB) models in an intervention setting. To better understand underreporting, a variety of estimation approaches are developed; these include back-calculating energy intake from a closed-form of the EB model, a Kalman-filter based algorithm for recursive estimation from randomly intermittent measurements in real time, and two semi-physical identification approaches that can parameterize the extent of systematic underreporting with global/local modeling techniques. Each approach is analyzed with intervention participant data and demonstrates potential of promoting the success of weight control. In addition, substantial efforts have been devoted to develop participant-validated models and incorporate into the Hybrid Model Predictive Control (HMPC) framework for closed-loop interventions. System identification analyses from Phase I led to modifications of the measurement protocols for Phase II, from which longer and more informative data sets were collected. Participant-validated models obtained from Phase II data significantly increase predictive ability for individual behaviors and provide reliable open-loop dynamic information for HMPC implementation. The HMPC algorithm that assigns optimized dosages in response to participant real time intervention outcomes relies on a Mixed Logical Dynamical framework which can address the categorical nature of dosage components, and translates sequential decision

rules and other clinical considerations into mixed-integer linear constraints. The performance of the HMPC decision algorithm was tested with participant-validated models, with the results indicating that HMPC is superior to "IF–THEN" decision rules.

ACKNOWLEDGEMENTS

First and foremost, I would like to express my deepest gratitude to my research advisor, Dr. Daniel E. Rivera. I have been part of Dr. Rivera's Control Systems Engineering Laboratory since early 2015. These past four years that I spent in this lab are the most important time in my life. Dr. Rivera has not only been an academic father for me, but also a mentor in my life. He changed my attitude towards professionalism, profoundly influenced my career, and made me become a responsible and self-motivated person. This is far more important than the valuable knowledge and skill set that I have learned from research and courses.

I would also like to thank Drs. Erica Forzani, Theodore P. Pavlic, Matthew M. Peet and Shuguang Deng for serving on my graduate committee, offering their time, sharing their comments and knowledge to guide and expand my research.

This work cannot be completed without our collaborators at Pennsylvania State University. First, I would like to thank Drs. Danielle Symons Downs and Jennifer S. Savage who serve as PI and co-PI respectively, of an NHLBI-funded study upon which this work is based. They have provided me with valuable suggestions and professional advice on adaptive interventions during every R01 meeting, and shared with me their enthusiasm and passion toward searching solutions for important behavioral medicine related problems. I would also like to express my appreciation to Abigail M. Pauley, Krista. S. Leonard and Dr. Emily E. Hohman. Without the hard work from these lovely people at Penn State University, I could not have fulfilled the research tasks in this project.

I am grateful for having excellent colleagues: César Martín and Mohammad Freigoun, two brilliant gentlemen who always stand by the naive Penny. We attended and presented at conferences together; we took various graduate courses and helped each other with homework and course projects; we discussed and figured out very difficult technical problems in research. Those made my years at ASU the most memorable time in my life. I would also like to wish them all the best in their future endeavors.

An important thanks goes to my parents for their unconditional love and tremendous support throughout the years. Without their blessing and encouragement, I would not have accomplished my Ph.D. with so much enthusiasm. My most heartfelt thanks goes to them for standing on my side, believing in me all the time, and encouraging me to do my best in everything.

This work would not have been completed without the financial support from the National Heart, Lung, and Blood Institute (NHLBI) through grant R01 HL119245.

TABLE OF CONTENTS

CHAPTER Page

CHAPTER Page

LIST OF TABLES

Table Page

Table Page

LIST OF FIGURES

Figure Page

Figure Page

Figure Page

Figure Page

Chapter 1

INTRODUCTION

1.1 Motivation

Obesity has become a worldwide health concern due to its high prevalence and related adverse health consequences. According to the National Health and Nutrition Examination Survey (NHANES) conducted in 2011–2012, the prevalence of being overweight (OW) or obese (OB; defined as a body mass index [BMI] $\geq$ 25 kg/m^2) is 68.5% among adults in the US, including 34.9% of adults being considered as obese (fBMI $\geq$ 30 kg/m^2) [Ogden *et al.* (2014)]. High BMI is significantly associated with increased risks of cardiovascular diseases, diabetes, and other clinical comorbidities [Bastien *et al.* (2014)]. Parental obesity may also affect the offspring obesity through heredity [Wu and Suzuki (2006)]. The growing prevalence of obesity and related health problems calls for effective clinical intervention approaches to weight control.

Among the general OW/OB population, there is a specialized group which is of greater risk of obesity-related health problems and requires immediate and deliberate attention: pregnant OW/OB women. Studies have shown that maternal obesity and high gestational weight gain (GWG) are strongly related to and independently predict adverse obstetric outcomes (e.g., preterm delivery, gestational diabetes, hypertension, preeclampsia) and elevate negative risks for macrosomia and early onset of obesity in the offspring (Rasmussen and Yaktine (2009)). Infants of OW/OB mothers are more likely to be preterm, large for gestational age, and have an increased risk of developing obesity from infancy to adulthood (Gilmore *et al.* (2015); Schack-Nielsen *et al.* (2010)). GWG is a modifiable factor that can be targeted to reduce these adverse risks, and managing it can impact the etiology of obesity for offspring at a crucial time in the life cycle. In 2009, the US Institute of Medicine (IOM) revised the recommendations for total and rate of GWG for pregnant

women by different categories of pre-pregnancy BMI in order to optimize the health of the mother and the welfare of the infant (Rasmussen and Yaktine (2009)). A 2014 study shows that 71% of overweight women and 61% of obese women gained weight in excess of the IOM recommendations (Haugen *et al.* (2014)). GWG higher than the IOM recommendations substantially increases the risk of gestational diabetes mellitus (Chu *et al.* (2007); Carreno *et al.* (2012)), preeclampsia (Haugen *et al.* (2014)), emergency cesarean delivery (Haugen *et al.* (2014)), and postpartum weight retention (Nehring *et al.* (2011)) in pregnant women. Therefore, there exists a great need to develop interventions which can help pregnant women maintain weight gain within IOM guidelines and further improve maternal and infant health.

Theoretical support for the success of such interventions to manage GWG is to consider that pregnancy can be a powerful "teachable moment" for weight control, during which a woman's emotional responses due to the change of her personal and social roles to a mother may provide her extra motivation to adopt healthy eating and activity behaviors for the sake of the fetal health (Phelan (2010)). An intervention to avoid high weight gain during pregnancy will be more likely to succeed in achieving desired maternal and infant outcomes than in other times of life.

This work is motivated by such needs of an intervention study funded by the National Heart, Lung, and Blood Institute (NHLBI; R01 HL119245). The *Healthy Mom Zone* program (HMZ, Symons Downs *et al.* (2018)) being conducted at Pennsylvania State University aims to develop and validate an individually tailored, intensively adaptive intervention involving healthy eating, physical activity, goal-setting, and self-monitoring to effectively manage weight gain in pregnancy. The study relies on systems science concepts involving dynamical systems modeling and control engineering approaches to optimize the adaptive behavioral intervention, and the details of the study will be elaborated in the following section.

Table 1.1: Revised recommendations for total and rate of gestational weight gain by pre-pregnancy BMI from Institute of Medicine in 2009.

Category	Prepreg BMI (kg/m^2)	GWG Range (pounds)	Rates of GWG 2nd-3rd TRI (M range in pounds/week)
Underweight	< 18.5	28–40	1 (1–1.3)
Normal	18.5–24.9	25–35	1 (0.8–1)
Over weight	25.0–29.9	15–25	0.6 (0.5–0.7)
Obese	≥ 30.0	11–20	0.5 (0.4–0.6)

1.2 Description of the Healthy Mom Zone Intervention

Excessive gestational weight gain is a major contributor to adverse pregnancy and birth outcomes (Baeten *et al.* (2001); Galtier-Dereure *et al.* (2000)). In 2009, the IOM report on reexamining the GWG guidelines called for effective interventions to manage weight gain, especially in OW/OB women who often gain more weight in pregnancy than is recommended (see Table 1.1). However, there is currently no "gold standard" intervention to prevent high GWG in OW/OB pregnant women. Past randomized interventions have shown that GWG can be effectively managed when they "mirror" effective programs used in non-pregnant adults (e.g., frequent contact, weight or dietary intake monitoring, engaging in exercise); however, the effects have largely been limited to normal weight women (Polley *et al.* (2002); Olson *et al.* (2004); Phelan *et al.* (2011)). Overweight or obese pregnant women may require a more hands-on approach, like a program that helps an OW/OB pregnant woman to control her GWG on a weekly basis and adapts to her unique needs over pregnancy. In other words, an intervention strategy to vary the component dosages in response to an individual's needs may be more helpful for this special population (Kumar *et al.* (2013)); the intervention treatment of this kind is much like clinical practice. Such an intervention has been developed, described below as *Healthy Mom Zone*, which used control systems engineering to construct a comprehensive dynamical model to describe how changes in GWG responds to changes in energy intake, exercise, and planned/self-regulatory behaviors for a customized program for each woman. This novel intervention has the potential to shift the

focus of weight management from a "one size fits all" method to an individually tailored and intensively adaptive approach to effectively manage GWG and promote optimal maternal and infant health.

The conceptual framework of the HMZ intervention (see Fig. 1.2) is based on a dynamical model that describes how a behavioral intervention can influence GWG and relies on integrating mechanistic energy balance and dynamical models of planned/self-regulatory behaviors describing how internal psychological processes can reinforce positive program outcomes (Dong *et al.* (2012, 2013); Dong (2014)). This model includes: (a) 2-compartment energy balance model predicting changes in body mass as a result of energy intake and exercise, (b) two Theory of Planned Behavior (TPB; Ajzen (1991)) models describing how energy intake and exercise are affected by behavioral variables (including women's attitude, social influences, perceived control and motivation), (c) a program delivery module relating magnitude and duration of components to inflows of the TPB models, and (d) two self-regulation units modeling how success expectancies in the intervention influence one's goal achievement motivation. A set of decision rules were developed based on the IOM (2009) GWG guidelines, the prior research (e.g., Dong (2014); Thomas *et al.* (2012); Symons Downs *et al.* (2014); Symons Downs (2016)), and clinical insights that inform when and how to adapt the components. Decision rules define changes to the intervention and correspond with altering the dosage (Collins *et al.* (2004)). The dosage level is based on variables that are expected to impact the effect of the component (e.g., effect of exercise on GWG), called tailoring variables, and the level of intervention required to address the needs of individuals varies according to tailoring variables (e.g., GWG). In HMZ, GWG is evaluated weekly and the collective weight gain is assessed over a 3–4 week period. If a woman is within her GWG goal, she continues to receive the same level of dosage of the intervention. If she exceeds her goal, her intervention dosage is adapted or "stepped up". If she is under her goal, we use clinical guidance to decide if and how the dosage change should be made. To achieve optimal weight control, an advanced decision algorithm has been developed based

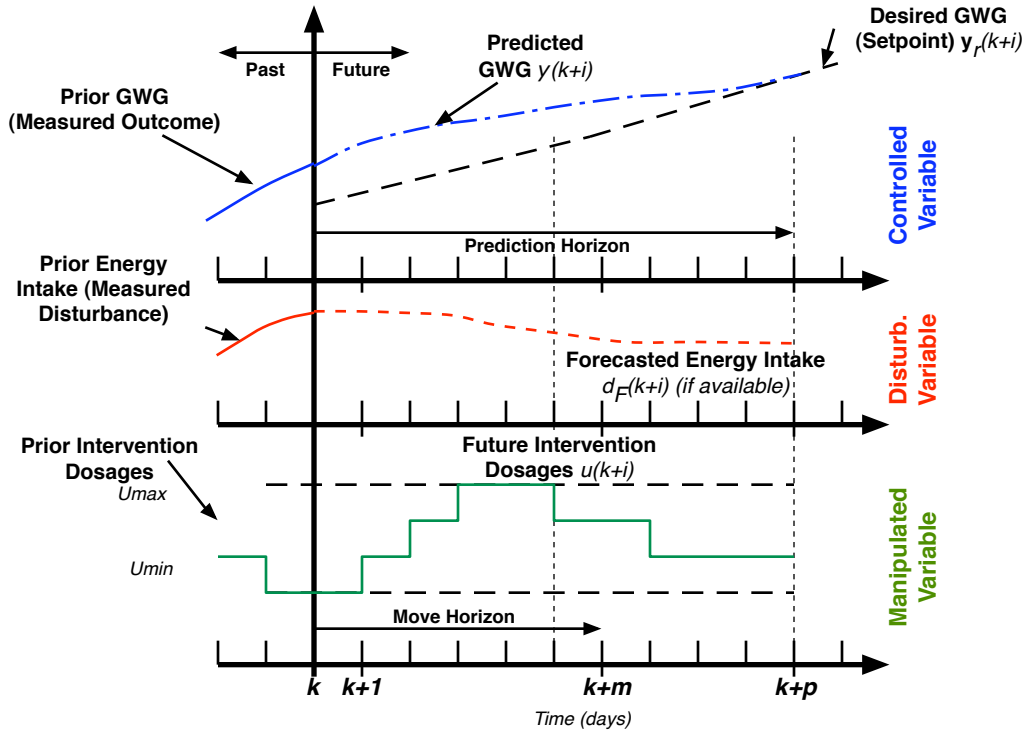

Figure 1.1: Conceptual demonstration of the receding horizon control strategy in MPC, contextualized for a GWG intervention.

on the Hybrid Model Predictive Control (HMPC) algorithm (Nandola and Rivera (2013)). Comparing to the simple decision rules, the HMPC algorithm optimizes the intervention dosage and shows better performance in terms of the intervention outcomes.

The HMPC algorithm is based on the same general principles as conventional Model Predictive Control (MPC) but is extended to a hybrid system. The MPC controller can determine optimal control actions based on model-predicted responses over a future horizon of finite length (Camacho and Bordons Alba (2013)). Such optimization is implemented online at each time point in a recursive manner by keeping shifting the prediction horizon forward as shown in Fig. 1.1. Based on the consideration of the categorical (i.e., discrete) dosages used for decisions, a hybrid system is used for describing intervention problems. Because MPC allows for user-defined constraints, the sequential decision rules and other clinical considerations can be converted into mixed integer constraints and further incorporated into the MPC for optimization. This novel framework allows the user to have greater flexi-

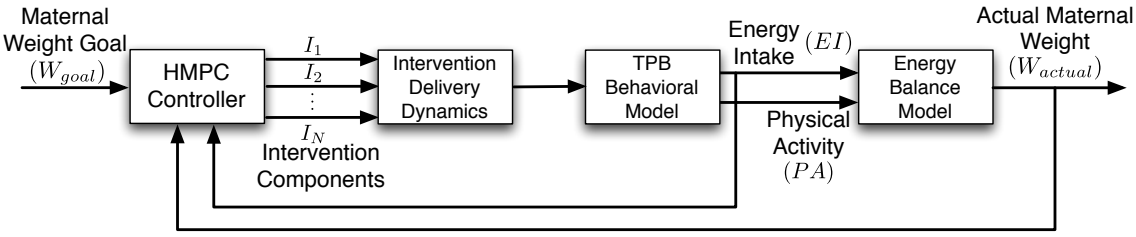

Figure 1.2: Block diagram depicting the closed-loop intervention for gestational weight gain developed in the *Healthy Mom Zone* Study. Energy intake and maternal weight changes can be used by a hybrid model predictive control (HMPC) algorithm to determine optimized intervention dosages of intervention components (such as healthy eating active learning, physical activity active learning, goal setting)

Table 1.2: HMZ intervention components and content description.

Component	Content Description
Education	Appropriate GWG, risks of high GWG, principles of energy balance, consuming a low energy dense diet, portion size, meal preparation/planning, benefits/safety of exercise, strategies to promote exercise in daily life, weekly plans for tailored meals to meet caloric and exercise goals.
Goal-Setting	Goal-setting principles (identifying where, when, how to accomplish goals); goals are reviewed; feedback/encouragement and problem-solving strategies to overcome barriers are provided on weekly basis.
Self-Monitoring	Participants use m-Health tools to self-monitor their behaviors: Aria Wi-Fi scale to record weight on daily basis, MyFitnessPal app to track dietary intake, Jawbone and Actigraph activity monitors to track exercise; output is reviewed and feedback and problem-solving strategies given on weekly basis to help overcome barriers.
Active Learning	Hands-on strategies: using a scale at home to weigh food, meal preparation demonstrations, meal replacements led by registered dietician; guided 30-min moderate-intensity exercise sessions led by exercise specialist.

bility in the specification of different requirements in real-life clinical trials and to generate the sequential decision policies with time-dependent relationships on manipulated variables, which are usually addressed by temporal logic specification in the control engineering.

The HMZ intervention components (see Table 1.2) were informed by past research and the data collected in the pilot study of the HMZ (Diabetes Prevention Program (DPP) Research Group (2002); The Look AHEAD Research Group (2006); Dong (2014); Symons

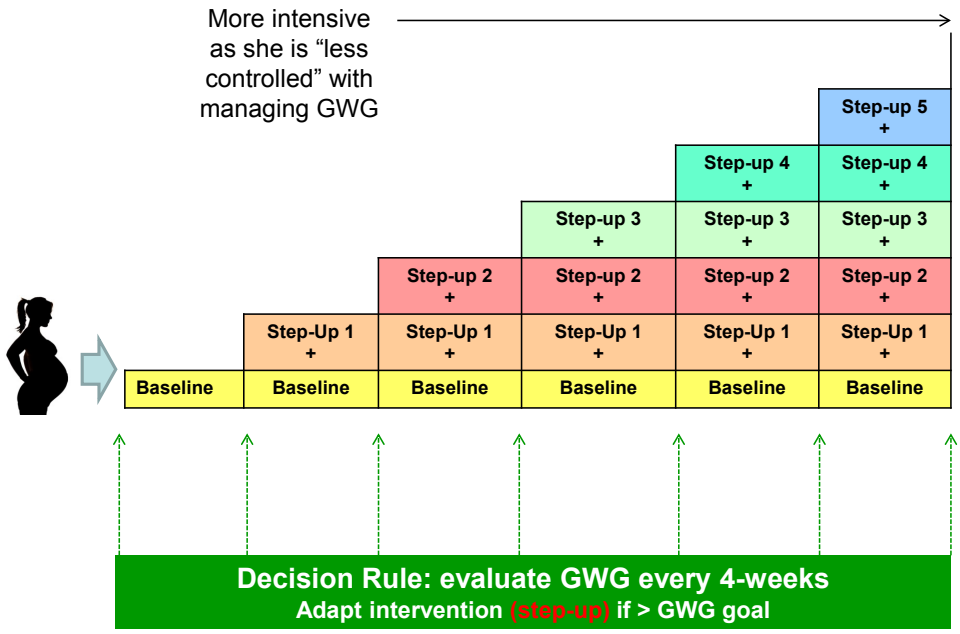

Figure 1.3: Illustration of dosage adaptations in the HMZ study.

Gestational Week	Study Week	Lesson #	Adaptation
8	1		**BASELINE ASSESSMENT** (Onsite visit + home surveys and GWG/HE/EX monitoring)
9	2	1	**BASELINE INTERVENTION**
10	3	2	Education Modules [GWG, HE/EX, Self-Monitoring, Goal-Setting; Using guideline recommendations (GWG, HE, EX)]; Focus on health of baby/weekly "fun facts"
11	4	3	Encouraged to get 150 min MVPA/week [to meet goal, promote 10,000 steps/day, increase intensity (e.g., jogging/workout) as appropriate, phone call with
12	5	4	instructor to review barriers/safety/concerns/goals]; GWG/EX/HE education, goal-setting, self-monitoring content delivered F2F by RD
GWG Assessment and Decision Rules for Adapting Intervention			
13 (2nd Tri)	6	5	**Baseline Intervention +** **STEP-UP 1: Active Learning I**
14	7	6	**HE Active Learning:** 4 Pearls Integrated into Cooking/Grocery Store Demo's: Reinforcing Messages + Recipe Booklet
15	8	7	**EX Active Learning:** 1st MVPA Session in Lab (combo treadmill, cycle, low impact aerobics, resistance exercises) in addition to 10,000 steps
16	9	8	**Self-Regulation Active Learning[a]:** If-Then Action Plans (attach mental contrasting and implementation intentions to goal-setting)
GWG Assessment and Decision Rules for Adapting Intervention			
17	10	9	**Baseline Intervention +** **Step-Up 1 +** **STEP-UP 2: Active Learning II**
18	11	10	**HE Active Learning:** Portion Sizes and Containers
19	12	11	**EX Active Learning:** 2nd MVPA: Choice of Lab workout or walking with instructor + Workout Booklet & 10,000 steps
20	13	12	**Self-Regulation Active Learning[b]:** Women chart own HE/EX behaviors; use weight data to regulate eating and exercise behaviors; tie this process into action plans
GWG Assessment and Decision Rules for Adapting Intervention			
21	14	13	**Baseline Intervention +** **Step-Up 1 +** **Step-Up 2 +** **STEP-UP 3: Active Learning III**
22	15	14	**HE Active Learning:** Grocery store receipt/pantry analysis/tour/activities; favorite recipe make-over
23	16	15	**EX Active Learning:** 3rd MVPA session: Onsite in lab or at home workout + Workout Booklet & 10,000 steps
24	17	16	**Self-Regulation Active Learning:** We monitor HE/PA daily and provide feedback "check" (EMA-I)
GWG Assessment and Decision Rules for Adapting Intervention			
25	18	17	**Baseline Intervention +** **Step-Up 1 +** **Step-Up 2 +** **Step-Up 3 +** **STEP-UP 4: Active Learning IV**
26	19	18	**HE Active Learning:** 1 MR/day for 7 days (give bulk frozen 7 meals for either lunch/dinner)
27	20	19	**EX Active Learning:** 4th MVPA session: Onsite in lab or at home workout + Workout Booklet & 10,000 steps
28 (3rd TRI)	21	20	**Self-Regulation Active Learning:** (1 x/week) Text/Call/Email Feedback & Encourage
GWG Assessment and Decision Rules for Adapting Intervention			
29	22	21	**Baseline Intervention +** **Step-Up 1 +** **Step-Up 2 +** **Step-Up 3 +** **Step-Up 4 +** **STEP-UP 5: Active Learning V**
30	23	22	**HE Active Learning:** Same as step-up 4
31	24	23	**EX Active Learning:** Same as step-up 4
32	25	24	**Self-Regulation Active Learning:** (3 x/week) Text/Call/Email FB & Encourage
33	26	25	
34	27	26	
35	28		**FOLLOW-UP ASSESSMENT** (Onsite visit + home surveys and GWG/HE/EX monitoring)

[a] = Stadler et al. (2009); [b] = Wing et al. (2006)

Figure 1.4: Demonstration of intervention planning with step-up layout in the HMZ study .

Downs and Hausenblas (2004); Symons Downs *et al.* (2010)); it has been shown that when individuals are taught how to set appropriate goals, self-monitor, and effectively manage their time, they are more likely to achieve their goals and see positive behavioral outcomes (e.g., eating healthy, engaging in exercise, managing weight). All women start in HMZ with the baseline intervention which includes standard prenatal care, education on GWG, healthy eating, and exercise, and self-monitoring. The intervention adapts or "steps-up" based on the GWG evaluation and decision rule criteria described above and includes different variations of hands-on active learning strategies that are added to the baseline intervention in a sequential order (e.g., step-up 1 = baseline intervention + active learning healthy eating demonstrations + exercise session; step-up 2 = step-up 1 + second weekly exercise session + daily meal replacement (lunch or dinner), and so forth). Such sequential decision rules are illustrated in Fig. 1.3 and 1.4. Self-monitoring of GWG, healthy eating, and exercise behaviors includes the use of m-Health tools (e.g., Wi-Fi scale, dietary intake smartphone app, activity monitors) to facilitate self-regulation, motivation, and behavior change.

Intensive longitudinal data is used in HMZ to assess the primary study outcome of GWG and several biobehavioral/psychological secondary outcomes (see Table 1.3). Pre- and post-intervention assessments are conducted at the Clinical Research Center in Pennsylvania State University, and the secure data capture (RedCAP) system is used to collect electronic survey data. Women use the Aria Wi-Fi scale (daily), Jawbone activity monitor (daily) and MyFitnessPal smartphone app (weekly) at home to measure their weight, kcal activity expenditure and intake respectively.

The HMZ involves two longitudinal studies: the pilot study in Phase I which is designed as a feasibility test, followed by a Phase II study designed for proof of concept. The Phase I study, as a trial study of the interventions, aims to establish the feasibility of the intervention dosages and the intensive measurement protocols. Hence, the intervention is designed for a shorter period of time with less participants recruited: each participant is only subject to a six-week intervention between the 2nd and the 3rd trimester of gestation, resulting

in smaller data sets. Despite the small sample being a strong limitation for the Phase I data, some insights can still be gained on the dynamical characteristics of data, as well as improvements on the model-based estimation techniques. The findings from Phase I study can be used to inform any necessary modifications on the intervention design for Phase II.

The Phase II study is to establish proof of concept of the fully adaptive intervention, including the criterion rule for making adaptive decisions. The target for the Phase II study of the HMZ is 30 overweight and obese pregnant women (BMI>25; >40 with physician approval). Eligible participants (e.g., singleton pregnancies, ages 18–38 years, able to read and understand English, no obstetric/medical complications limiting participation) are screened, enrolled, and consented. They complete pre-intervention assessments both on-site at the PSU Clinical Research Center (e.g., body composition, bloodwork) and at-home (e.g., electronic surveys) and are then randomized to either the control condition (standard of care) or treatment condition (HMZ intervention) from early (e.g., 6–12 weeks gestation) through late pregnancy (e.g., 37 weeks gestation;). Hence in the Phase II study, the intervention is delivered for a longer period of time with more data available. GWG is evaluated in 3–4 week cycles and the intervention dosage is adapted as necessary to help women stay within their GWG goals. To better understand how the interventions influences individual participant, modeling of energy balance and individual behaviors, as well as control algorithms, can be used to achieve the best intervention outcomes through system identification and control engineering principles, which is the ultimate goal of the current work.

1.3 Research Goals

A comprehensive dynamical systems model has been previously postulated for GWG adaptive interventions (Dong *et al.* (2012)), among which a first-principles maternal energy balance model can accurately predict individual weight change given the changes in energy intake and energy expenditure, while a TPB behavioral model integrated with a model for intervention delivery dynamics is well established based on the concept of fluid analogies for predictions of participant behaviors in response of dosage changes. This model has been

Table 1.3: The variables and assessments involved in *Heathy Mom Zone*.

Variable	**Assessments**
Weight and Height	High Precision Stand-On Adult Scale (stadiometer for height) Wi-Fi Smart Scale
Metabolism	Mobile metabolism device
Biomarkers	Blood, Urine
Adiposity	Body composition
Healthy Eating Behaviors	Smartphone dietary intake app (kcal intake) Back-calculation method to estimate energy intake (kcal intake) Eating inventory
Exercise Behaviors	Activity monitors and survey (expenditure) Exercise Log
Motivational Determinants	Attitude, Subjective Norm, Perceived Behavioral Control, Intention Surveys
Self-Regulation	Self-Regulation Index and Questionnaire
Socio-Demographic	Health and History Questionnaire

illustrated with the conceptual diagram in Fig. 1.2.

The development of this model uses the fluid analogy from the production-inventory systems, where the inventory is represented as a tank containing fluid, as shown in Fig. 1.5. It can be considered that the tank is depleted by exogenous disturbances and is replenished by the interventions. The goal then would be to manipulate the inflow to the production node (represented by a pipe) in order to replenish an inventory that satisfies exogenous demand. Here, the inflows to the GWG intervention system are the intervention components, while the controlled output in this problem is inventory of maternal weight gain.

To achieve this goal of GWG control, a novel intervention decision paradigm using the HMPC framework can be applied to generate sequential decision policies based on the closed-loop responses. Clinical constraints and considerations were systematically taken into account for the HMPC formulations through a user-specified dosage sequence table

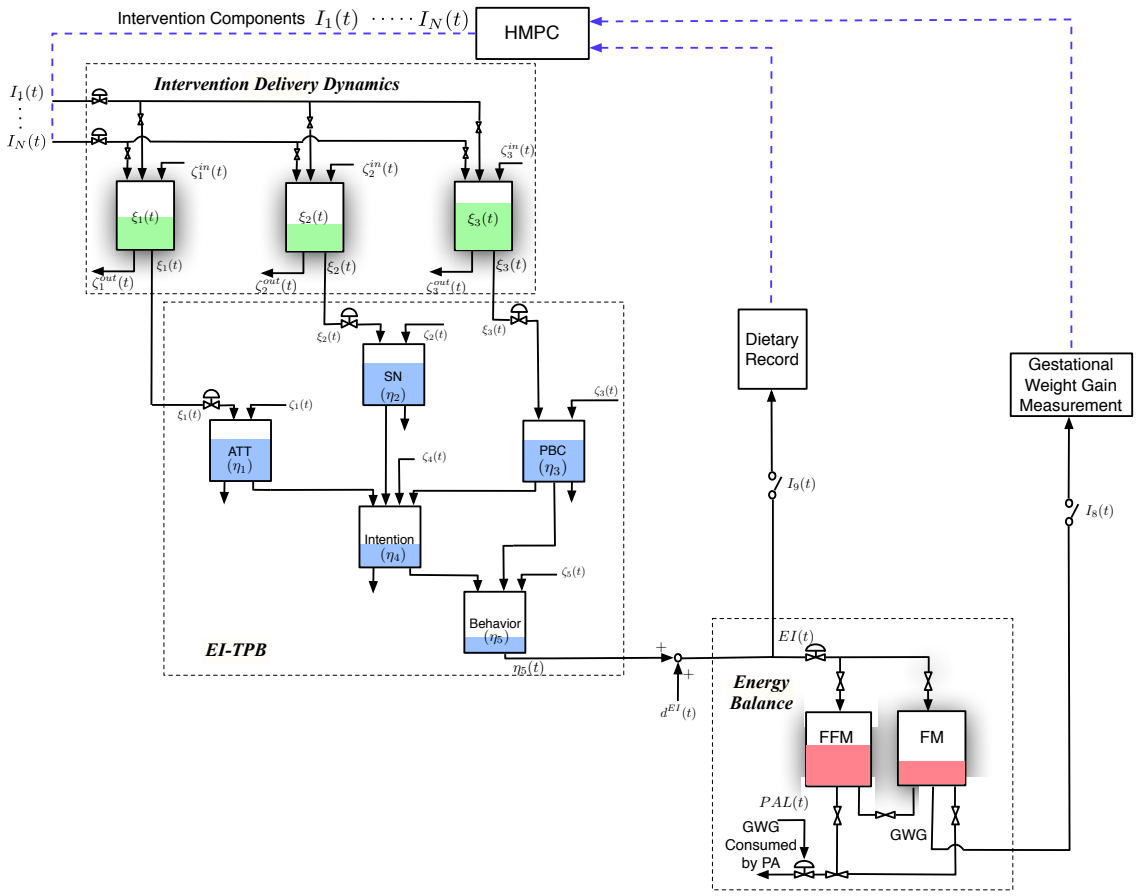

Figure 1.5: Comprehensive fluid analogy and interrelationship between systems in GWG Interventions; shown for the energy intake loop.

corresponding to the sequence rules.

The dynamical systems modeling, as well as the effectiveness of the control algorithms, has only been tested in simulations with hypothetical participants under assumption of no measurement noise or loss. Because data collection has been completed for both Phase I and Phase II studies, we are able to re-evaluate the proposed theoretical models and the control algorithms against real participant data. Specifically in the current work, the development of participant-validated behavioral models from intervention data using semi-physical identification approach is possible. Once integrated with re-formulated energy balance model, the "open-loop" dynamics for individual participants can be reliably provided, based on which the closed-loop framework that has been developed before can be implemented and validated.

In the following, the research goals for current work are briefly introduced and detailed efforts to achieve these goals will be elaborated in later chapters of this document.

1.3.1 Energy Intake Estimation

The energy balance model involved in the comprehensive model is originally developed by Thomas *et al.* (2012). In this work, we reformulated the model into a closed-form which is amenable to control purpose and favors the development of estimation methods to address the issue of energy intake underreporting. The effectiveness of the reformulated energy balance model is further evaluated against the measured data of the overweight or obese pregnant women from the HMZ study. Theoretically, the model can provide accurate prediction of maternal weight change based on reliable measurements of energy intake and energy expenditure. However, bias between the measured weight and the model predicted weight is observed in most intervention participants. This is assumed to be mostly due to the underreporting of energy intake in participants using self-reported measures.

Underreporting of energy intake has been found to be an issue of most concern in GWG interventions and is a commonly observed problem in weight interventions using self-reported measures. This can affect participant self-monitoring process and is also disturbing for clinicians to monitor the outcomes of interventions or provide informative health counseling. More importantly to this study, energy intake as an input in the HMPC algorithm determines the performance of the closed-loop control.

In addition to the self-reported measures of energy intake, most of the participant data in the HMZ study is collected through self-reported and self-monitored measures. Practically, self-reported data by participants through questionnaires or self-monitored via electronic tracking devices usually contains significant noise in the data collection along with missing data due to lack of participant adherence to interventions. This might create additional issues if quantitative models are used for sequential weight prediction or real-time calculation of caloric intake or expenditure change during an intervention.

Consequently in this work, we aim to develop estimation techniques that can address

this issue of energy-intake underreporting and the presence of missing data and measurement noise. In order to enable an continuously informative health guidance to participants throughout an intervention, an on-line estimation algorithm that can address random loss of measurements is particularly necessary. Because these issues of erroneous measurements or noise and missingness in data are commonly seen in general intervention applications, any developed methods will have the potential of being extended to the application of weight interventions targeted for the general population as well.

1.3.2 System Identification of Participant-Validated Models

The theoretical energy balance model has been well-developed with categorical model parameters (system gains) that are sufficiently accurate to predict maternal weight gain for women with different levels of BMI or weights. However, the behavioral model based on TPB and the intervention delivery dynamics are only provided with model structures, leaving the model parameters undetermined or individualized. Hence, these model parameters need to be identified for individual participants in order to be used for the design of adaptive interventions, or more specifically, for control purpose.

In the HMZ study, longitudinal measurements of the variables in the TPB models have been collected for individual participants, hence can be used to estimate these models with a semi-physical identification approach. Once obtained, the accuracy of the model prediction can be significantly improved to ensure the good performance of the control algorithms. Yet efforts needs to be made to integrate with the energy balance model, from which the measurements of the behavioral constructs can be used as input to predict individual weight gain (output). Integration of the individual-based models is amenable for the implementation of the advanced closed-loop decision rules, such as the Hybrid Model Predictive Control (HMPC) which will be addressed in next section.

1.3.3 Hybrid Model Predictive Control For Dosage Optimization

The obtained participant-validated models can reliably describe the "open-loop" dynamics for individual participants, and the decision for dosage changes can be made based on the predicted outcomes of the intervention, such as participant's weight gain or energy intake. From an engineering perspective to optimize an adaptive intervention, a controller can be designed to assign optimized dosages of each intervention component to the participant as dictated by model dynamics, problem constraints, and disturbances. In behavioral medicine problem settings, the intervention components are usually delivered in pre-determined categorical (i.e., discrete) doses, and the decision is made in a discrete manner, which requires us to consider the use of hybrid system. Hence an Model Predictive Control (MPC) algorithm for linear hybrid systems with discrete inputs is a well suited option for this application. Specifically, the Mixed Logic Dynamical (MLD) framework can be used to address categorical intervention dosages and convert sequential decision policies and other clinical considerations into mixed-integer linear constraints, In this way, various time-dependent relationships between manipulated variables can be appropriately described.

In previous work, this novel HMPC framework was developed but only illustrated with simulations based on hypothetical participant models and compared with standard "IF–THEN" rules. In this work, we aim to test the designed closed-loop schemes using participant-validated models, validate the proper generation of postulated dosage sequence, and demonstrate the benefits of HMPC framework for optimized adaptive interventions in contrast to adaptive intervention using simple decision rules. In addition, the HMZ study has modified the "IF–THEN" rules based on clinical considerations. For example, due to the length of the educating modules in the education component, intervals between decision making for dosage changes are constrained to 3 to 4 weeks in the HMZ study, instead of as frequent as two weeks proposed in previous work. In order to maintain the potency of interventions, the decision rules were changed to allow for augmentation of both healthy eating and physical activity active learning components at the same time to compensate the

longer decision intervals. Forecast of participant future weight trajectory is also included in HMZ IF–THEN decisions so that the interventions can respond ahead to any anticipated excessive weight gain. Hence, it is useful to compare the HMPC algorithms with the HMZ modified decision rules, and to examine how the different decision rules perform and respond under difference circumstances or uncertainties.

1.4 Contributions of the Dissertation

This document presents new results from the evaluation of the models and the HMPC framework against real participant data of the HMZ, from which some extensions beyond the prior use of the model has been developed and the performance of the HMPC framework has be validated. Because the Phase I Study of the HMZ and the Phase II feature different measurement frequencies and lengths, most of the estimation or identification approaches presented in this document are demonstrated with the data from both phases.

A summary of the contributions are listed below,

1. In the current work, we re-evaluate the energy balance model in the context of the HMZ study and develop some extensions. Specifically, we start from the first-principles model of Thomas *et al.* (2012) and reformulate the original energy balance model as a parsimonious dynamical system with one output (maternal weight change) and three inputs (energy intake, physical activity and resting metabolic rate). This closed-form energy balance model is amenable to control analysis and compensates for the limitations of the original model that did not explicitly include the impact of changes in physical activity and resting metabolic rate on maternal weight change. If used as tools to assist interventions, it can help with better assessing the outcomes of weight regulation and foster patient adherence to diet or exercise plans. This reformulated model also supports the development of methods for estimating underreporting of energy intake.

2. A variety of model-based estimation approaches that can address missing data and

measurement noise have been developed to estimate and correct energy intake underreporting in real-time. Such approaches include (extended) Kalman filtering, semi-physical identification approach, and non-linear estimator based on "Model-on-Demand" concept. Estimates with developed approaches significantly enhanced controller performance for closed-loop interventions and also assisted clinicians in providing appropriate counseling advice to participants, hence have demonstrated great potential to assist real-time weight interventions.

3. Participant-validated behavioral models have been obtained using semi-physical identification approach. Estimation analyses from Phase I led to modifications of the measurement protocols for Phase II, from which longer and more informative data sets were collected and used for model estimation. The individualized model is integrated with control-oriented energy balance model for implementations of closed-loop interventions, and it significantly improves the predictive ability of participant behaviors and intervention outcomes.

4. A participant-validated model is incorporated into the HMPC formulations that can assign optimized intervention dosages based on participant responses for real-time use. The three-degree-of-freedom parametrization in the HMPC formulations that enables the user to adjust the speed of setpoint tracking, measured disturbance rejection and unmeasured disturbance rejection independently in the closed-loop system has been further evaluated and shown both fundamental and practical appeal for achieving robustness. The HMPC decision policy is compared with standard IF–THEN rules and the IF–THEN rules used in the HMZ intervention study, results demonstrating consistent superior performance of the HMPC framework over other decision rules under different uncertainties.

The estimation approaches and the control engineering techniques that are developed in this dissertation can be applied to other adaptive sequential behavioral interventions.

1.5 Publications Summary

Research from this dissertation that has been published thus far as journal papers is shown below.

[1] Guo, P., Rivera, D. E., Savage, J. S., Hohman, E. E., Pauley, A. M., Leonard, K. S. and Symons Downs, D. (2018), "System identification approaches for energy intake estimation: Enhancing interventions for managing gestational weight gain", *IEEE Transactions on Control Systems Technology*, published online, October, 2018, pp. 1–16, DOI: 10.1109/TCST.2018.2871871.

[2] Freigoun, M. T., Rivera, D. E., Guo, P., Hohman, E. E., Gernand, A. D., Symons Downs, D., Savage, J. S. (2018), "A dynamical systems model of intrauterine fetal growth", *Mathematical and Computer Modeling of Dynamical Systems*, 24:6, 641–667, DOI: 10.1080/13873954.2018.1524387

[3] Pauley, A. M., Hohman, E. E., Savage, J. S., Rivera, D. E., Guo, P., Leonard, K. S. and Symons Downs, D. (2018), "Gestational weight gain intervention impacts determinants of healthy eating and exercise in overweight/obese pregnant women", *Journal of Obesity*, vol. 2018, Article ID 6469170, 12 pages, DOI: 10.1155/2018/6469170.

[4] Symons Downs, D., Savage, J. S., Rivera, D. E., Smyth, J. M., Rolls, B. J., Hohman, E. E., McNitt, K. M., Kunselman, A. R., Stetter, C., Pauley, A. M., Leonard, K. S. and Guo, P. (2018), "Individually tailored, adaptive intervention to manage gestational weight gain: protocol for a randomized controlled trial in women with overweight and obesity", *JMIR Research Protocols*, 2018, vol. 7, no. 6, pp. e150.

Publications that have been published thus far as refereed conference papers are listed below.

[5] Guo, P., Rivera, D. E., Pauley, A. M., Leonard, K. S., Savage, J. S., Symons Downs, D. (2018), "A "Model-on-Demand" methodology for energy intake estimation to improve gestational weight control interventions," in *Proceedings of* 18^{th} *IFAC Symposium on System Identification*, 2018, Stockholm, pp. 144–149.

[6] Guo, P., Rivera, D. E., Savage, J. S., Symons Downs, D. (2017), "State estimation under correlated partial measurement losses: Implications for weight control interventions," in *Proceedings of* 20^{th} *IFAC World Congress*, 2017, Toulouse, pp. 14074–14079.

[7] Guo, P., Rivera, D. E., Savage, J. S., Symons Downs, D. (2016), "Semi-physical identification and state estimation of energy intake for interventions to manage gestational weight gain," in *Proceedings of 2016 American Control Conference (ACC)*, Boston, pp. 1271–1276.

Papers that are currently in preparation or planned for future journal submission based on this dissertation are included in the list below:

[8] Hybrid Model Predictive Control for optimizing adaptive behavioral interventions for gestational weight gain using participant-validated models.

[9] Semi-physical identification of behavioral models based on Theory of Planned Behavior.

[10] Energy intake back calculation method to guide dietary recommendations in behavioral interventions (paper for a behavioral audience).

[11] Proof of concept of using mHealth tools to manage gestational weight gain in overweight or obese pregnant women (paper for a behavioral audience).

1.6 Dissertation Outline

Following this introduction, this dissertation continues Chapter 2 with modeling overview which presents how to develop the dynamical systems model for the GWG intervention problem. The current work roots from a comprehensive dynamical system model that has been established in previous study. The model comprises of three parts: a mechanistic energy balance model from the literature (Thomas *et al.* (2012)), a behavioral model based on TPB and the model for intervention delivery dynamics. The chapter focuses on the introduction and development of each module which forms the basis of the work in later chapters. Specifically, the developed structures of the TPB behavioral model and the model for intervention delivery dynamics lead to the semi-physical identification work in Chapter

5 to obtain participant-validated models for the implementation of the HMPC framework in Chapter 6. The energy balance model is reformulated into a closed-form that is amenable for control purpose and favors the development of the estimation approaches for the key energy balance determinants in Chapter 3 and 4. At the end of this chapter, the issue of energy intake underreporting that is commonly observed in participant self-reports is introduced.

In Chapter 3 and 4, a series of estimation approaches are developed to address the underreporting of energy intake. These include the Kalman filtering approach in Chapter 3 which can perform real-time estimation under intermittent measurements, and the semi-physical approaches in Chapter 4 that can parameterize the extent of underreporting and and make corrections based on future self-reports. Chapter 4 elaborates two approaches, one features global estimation and the other local method that can address non-linearities based on the concept of "Model-on-Demand".

The goal of Chapter 5 is to participant-validated models using the semi-physicals identification approach with the developed model structures. Both the results using the small data sets from Phase I study and the long data set from Phase II are presented. The results from Phase I are used to inform the protocol changes that are introduced to Phase II. The obtained participant-validated models are used to test and validate the HMPC algorithm in Chapter 6.

Chapter 6 presents an MLD-based HMPC scheme that offers a valuable framework to implement optimized adaptive sequential behavioral interventions. The unique clinical considerations and constraints in behavioral health problem settings are summarized, and are systematically addressed through mixed-integer linear constraints in MLD structure. The simulation studies are shown to verify how HMPC-based intervention assigns the optimized discrete dosages, with its change following pre-defined dosage sequence, highlight why HMPC-based intervention can adjust the dosages of the intervention components in a timely manner through the comparison with adaptive intervention using decision rules.

We conclude the dissertation in Chapter 7 with a summary of the important conclusions and advances achieved in this study. This chapter also includes the direction and comments for future work.

Chapter 2

MODELING OVERVIEW

2.1 Overview

As introduced in Chapter 1, the primary goal of the behavioral interventions developed in the *Healthy Mom Zone* Study is to manage gestational weight gain for overweight or obese pregnant women. The intervention is implemented through the delivery of a variety of intervention components to participants via an individually tailored and "intensively adaptive" manner. Specifically, a closed-loop control strategy is employed to optimize the intervention dosages (which dictate the intervention components and their magnitudes) based on an individual participant's intervention outcomes, including their physical activity/diet behaviors and weight changes. Hence, the customized intervention strategy can adapt to individuals' unique needs. The design of the closed-loop controller algorithms requires a reliable mathematical model that can accurately describe and predict the dynamics of the underlying system, which in this case, refers to individual participants. In this chapter, the details of the dynamical modeling for the developed weight control intervention will be presented. This forms the basis of the work described in later chapters, for instance, the Hybrid Model Predictive Control (HMPC) algorithms used for the closed-loop implementation as elaborated in Chapter 6.

To build a useful model, it is necessary to understand how the intervention is expected to affect participants. More specifically, we need to answer the questions: How does the delivery of intervention components eventually achieve the internally goal of preventing excessive gestational weight gain? As shown in Table 1.2, the intervention components involve healthy eating, physical activity, goal-setting, self-monitoring, and other cognitive behavioral strategies. It is believed that continuously exposing participants to intensive information regarding the benefits and risks for appropriate and high GWG respectively as

well as some useful skills to assist weight management can potentially increase their intentions or motivations to adopt healthy eating and activity behaviors, which may facilitate healthy diets among participants or observe an increase of their physical activities. The observed changes in their behaviors will be directly reflected as the changes in their caloric intake and expenditure, and this is likely to cause a deficit of energy balance that will further lead to maternal weight gain or loss.

In fact, the described intervention process involves dynamical changes in participants through three main steps: to invoke transitions in cognitions, to stimulate changes in behaviors, and eventually to expect changes in physiology (i.e., maternal weight gain or loss). These three stages relate to each other in an intuitive way, and dynamical systems modeling techniques can weigh in to explain how the changes in one step affect the other through the use of certain functional relationships. Particularly, a behavioral model based on a well-known psychological theory can be developed to explain and predict behavioral changes from assessed changes in cognition. In this work, Theory of Planned Behavior (TPB, Ajzen (1991)) is used to describe how the different behavioral constructs are internally related with each other. For example, the theory explains the determinants of one's attitude towards healthy eating and also shows how it further determines participant actual dietary intake. Based on the TPB, the behavioral model can be developed, and if the model parameters are individualized, it is able to provide an accurate prediction of a participant's dietary intake or physical activity changes based on the changes of her cognitional measures. On the other hand, how the intervention invokes the transitions in cognitions can be described by the intervention delivery dynamics, which builds the bridge between intervention components and magnitude and variables (constructs) in the TPB behavioral model. This model makes it easy to implement the intervention, track its status, and quantify its outcome in psychological view.

To enable the prediction of weight changes, models that relate dosage changes and behavioral dynamics are not enough but need to be integrated with a physiological model

which can output the behavioral outcomes of interest, *i.e.*, maternal weight changes, as a result of the fluctuations in maternal energy intake and energy expenditure. Here, a first-principles energy balance model is involved, the details of which can be found later in this chapter. To facilitate the understanding of the overall conceptual framework for this gestational weight gain intervention, a block diagram for the comprehensive control system has been shown in Fig. 1.2, where it can be found how the three modules (the behavioral model based on TPB, the model for intervention delivery dynamics, and the energy balance model) are related and how the control system is deployed. As shown in the figure, dietary and physical activity behaviors serve as important links to connect the TPB behavioral model and the energy balance model; energy intake is also used as controller input for dosage optimization.

In this chapter, the presentation of the comprehensive dynamical systems modeling is organized as follows. The development of the TPB behavioral model is described in Section 2.2, followed by the description of the energy balance model and associated energy intake underreporting issues which are elaborated in Section 2.4 and 2.5. Since the efficiency of the dynamical models is critical in the design and evaluation of the intervention study, the modeling work presented in this chapter is trying to be individualized or categorized for different scenarios/populations while maintaining the model simplicity.

2.2 TPB Behavioral Model

In behavioral interventions, scientists are expecting to manipulate the behavioral outcomes from participants by influencing their health behaviors. Thus, desirable behavioral change is the key to the success and effectiveness of behavioral interventions, especially for the current application where dietary and exercise behaviors directly reflect maternal energy intake and energy expenditure, which can be used to predict maternal weight change by the principle of energy balance.

However, it is not an easy task to change human behaviors. Many contemporary psychological theories have been well developed for scientists to interpret and predict human

behaviors, as well as to determine effective strategies for behavioral changes, so it is useful to apply the models of social cognition to intervene behaviors. Some popular psychological models include Theory of Planned Behavior (TPB, Ajzen (1991)), Social Cognitive Theory (Bandura (1986)), Goal Setting Theory (Locke and Latham (1994)), among which TPB is perhaps the most influential model and has been widely used for developing behavior related interventions, such as weight reduction (Schifter and Ajzen (1985)), low-fat diet (Armitage and Conner (1999)), smoking cessation (Norman *et al.* (1999)), and abstinence and safer sex HIV risk-reduction interventions (Jemmott III *et al.* (1998)). Therefore, the TPB is applied in the development of the behavioral model for current weight control interventions. It has to be noted that, however, unlike the physiological energy balance model, the measures of psychological constructs need to be more carefully designed. This is due to the reason that the reliability and validity of the measures are easily impaired, leading to inaccurate behaviors prediction. This will be discussed in more detail in Chapter 5.

2.2.1 Theory of Planned Behavior

The precursor of TPB, the Theory of Reasoned Action (TRA; shown in Fig. 2.1 with unshaded boxes), was first proposed in 1976. The core of the theory relies on the directly predictive relation between behavioral intention and behaviors; intention is the most important predictor of behaviors. On the other side, the formation of intentions is lead from the combination of attitude towards behaviors and subjective norms. The detailed definitions of these constructs are shown in Table 2.1. Further to the left, attitude towards behaviors is determined by behavioral beliefs weighted by the evaluation of behavioral outcomes; similarly, the subjective norm is determined by the normative beliefs of the attitudes towards the behaviors from important others weighted by the motivation to comply with these important other.

TPB is a modification of its precursor TRA and was proposed in 1985 (Ajzen (1985)) when Ajzen and Fisher realized the volitional control over the behavior can be impaired from the environment or personal abilities. Therefore, the perceived behavioral control is

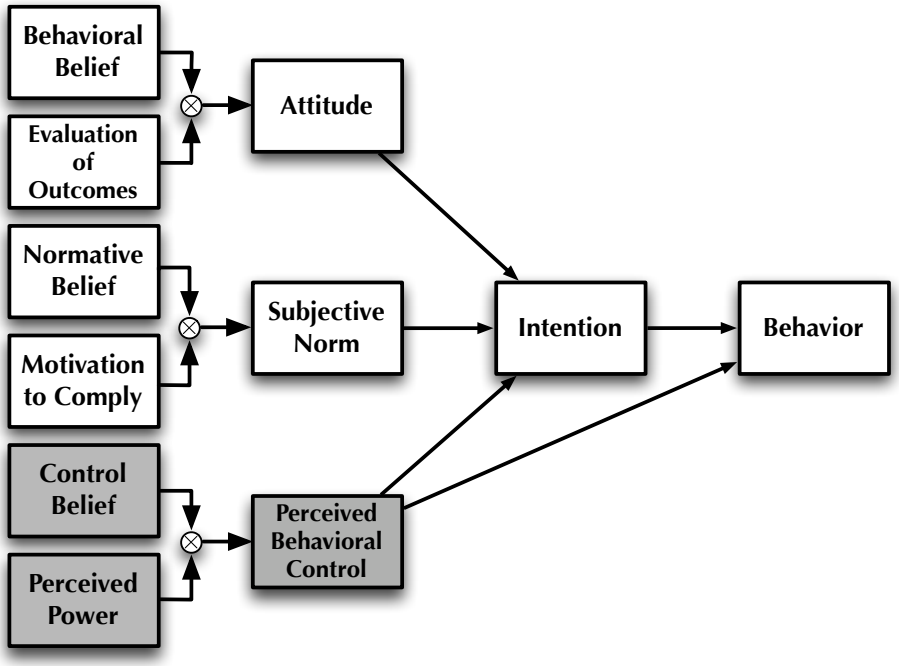

Figure 2.1: The path diagram for Theory of Planned Behavior (TPB). It includes three more constructs (shaded) in addition to the unshaded constructs original to the Theory of Reasoned Action (TRA).

Table 2.1: Tabulation of TPB constructs with corresponding definitions.

Constructs	Definition
Attitude (η_1)	Overall evaluation of the behavior
Subjective Norm (η_2)	Belief about whether most people approve or disapprove the behavior.
Perceived Behavioral Control (η_3)	Overall measure of the perceived control over the behavior.
Intention (η_4)	Perceived likelihood of performing the behavior
Behavioral Belief (b)	Belief that behavioral performance is associated with certain attributes or outcomes
Evaluation of Outomes (e)	Values attached to a behavioral outcome or attribute.
Normative Belief (n)	Belief about whether each referent approves or disapproves of the behavior.
Motivation to Comply (m)	Motivation to do what each referent thinks.
Control Belief (c)	Perceived likelihood of occurrence of each facilitating or constraining condition.
Perceived Power (p)	Perceived effect of each condition in making behavioral performance difficult or easy.

included in the framework which is led by the control belief weighted by their perceived power, as shown in the shaded box in Fig. 2.1. Since then, the conceptual framework in Fig. 2.1 has been accomplished and adopted in various behavioral interventions.

2.2.2 Dynamical TPB Model Development

Originating from the classical TPB diagram as shown in Fig. 2.1, the two TPB models for healthy eating and physical activity are described in this subsection. As we can see from the path diagram of the TPB model for healthy eating in Fig. 2.2, some limit constructs are included: limit attitude, limit subjective norm, limit perceived behavioral control, and limit intention. These are the additional measures of attitude, subjective norm, perceived behavioral control and intention towards not performing unhealthy eating behaviors. Including the additional measures of these constructs enables capturing the meaningful variances of these constructs more completely and further leads to more accurate predictions of connecting constructs. Similarly, when a questionnaire is designed to measure certain construct, the obtained measures would be more reliable and more valid by including more variables that can capture that construct more completely.

In the following, the TPB dynamic modeling development will be presented for both the healthy eating and physical activity side, starting from the static path diagram model to a dynamical systems model. First, the TPB for healthy eating represented as a structured equation model with a vector η of endogenous variables and a vector ζ of exogenous variables is expressed as follows:

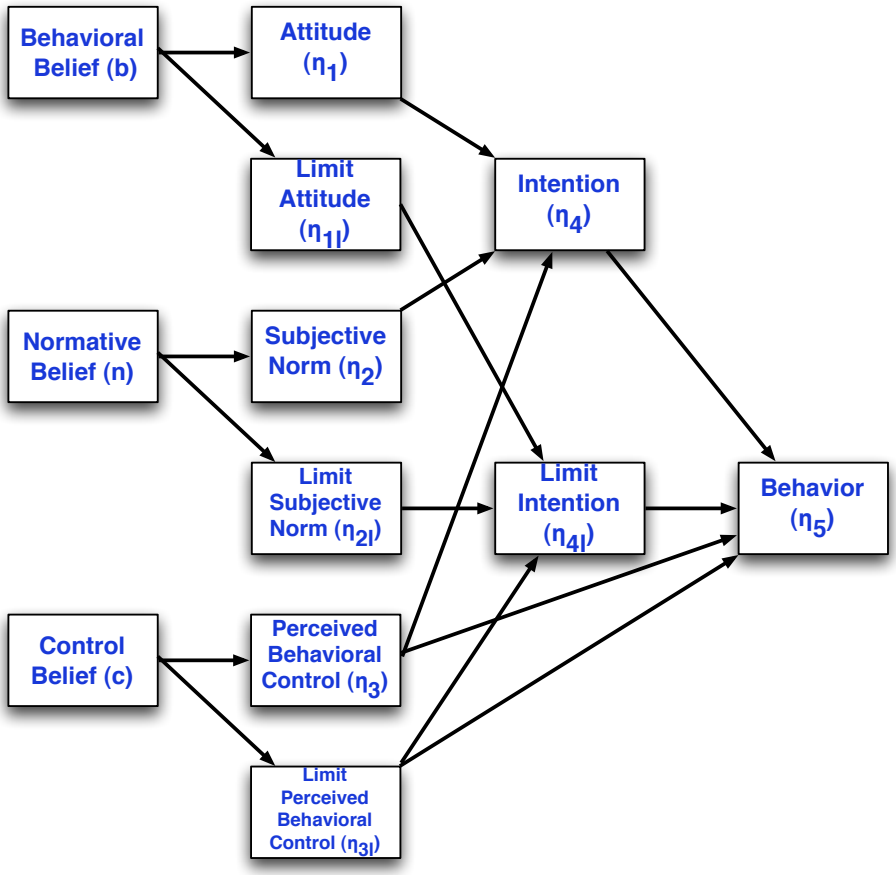

Figure 2.2: Theory of Planned Behavior (TPB) path diagram for healthy eating, including limit constructs.

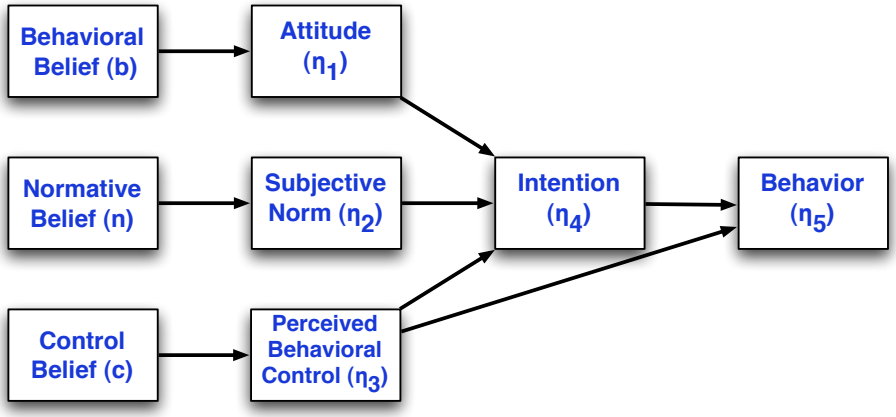

Figure 2.3: Theory of Planned Behavior (TPB) path diagram for physical activity.

$$
\overbrace{\begin{bmatrix} \eta_1 \\ \eta_{1l} \\ \eta_2 \\ \eta_{2l} \\ \eta_3 \\ \eta_{3l} \\ \eta_4 \\ \eta_{4l} \\ \eta_5 \end{bmatrix}}^{\eta}
=
\overbrace{\begin{bmatrix}
0 & 0 & 0 & 0 & 0 & 0 & 0 & 0 & 0 \\
0 & 0 & 0 & 0 & 0 & 0 & 0 & 0 & 0 \\
0 & 0 & 0 & 0 & 0 & 0 & 0 & 0 & 0 \\
0 & 0 & 0 & 0 & 0 & 0 & 0 & 0 & 0 \\
0 & 0 & 0 & 0 & 0 & 0 & 0 & 0 & 0 \\
0 & 0 & 0 & 0 & 0 & 0 & 0 & 0 & 0 \\
\beta_{41} & 0 & \beta_{42} & 0 & \beta_{43} & 0 & 0 & 0 & 0 \\
0 & \beta_{41l} & 0 & \beta_{42l} & 0 & \beta_{43l} & 0 & 0 & 0 \\
0 & 0 & 0 & 0 & \beta_{53} & \beta_{53l} & \beta_{54} & \beta_{54l} & 0
\end{bmatrix}}^{\Gamma}
\begin{bmatrix} \eta_1 \\ \eta_{1l} \\ \eta_2 \\ \eta_{2l} \\ \eta_3 \\ \eta_{3l} \\ \eta_4 \\ \eta_{4l} \\ \eta_5 \end{bmatrix}
+
\overbrace{\begin{bmatrix}
\gamma_{1b} & 0 & 0 \\
\gamma_{1lb} & 0 & 0 \\
0 & \gamma_{2n} & 0 \\
0 & \gamma_{2ln} & 0 \\
0 & 0 & \gamma_{3c} \\
0 & 0 & \gamma_{3lc} \\
0 & 0 & 0 \\
0 & 0 & 0 \\
0 & 0 & 0
\end{bmatrix}}^{B}
\begin{bmatrix} b \\ n \\ c \end{bmatrix}
+
\overbrace{\begin{bmatrix} \zeta_1 \\ \zeta_{1l} \\ \zeta_2 \\ \zeta_{2l} \\ \zeta_3 \\ \zeta_{3l} \\ \zeta_4 \\ \zeta_{4l} \\ \zeta_5 \end{bmatrix}}^{\zeta}
\tag{2.1}
$$

where Γ and B is a matrix of β_{ij} and γ_{ij} regression weights, respectively, and ζ is a vector of disturbance variables. Compared with the classical TPB model that is shown in Fig. 2.1, the evaluation of the outcome (e), the motivation to comply (m), and perceived power of the control factor (p) are treated as constants, which thereby are omitted in the equation here.

Equation (2.1) represents a static (*i.e.*, steady-state) system that does not capture any changing behavior over time. To expand the TPB model to include dynamic effects, we apply a fluid analogy that parallels the problem of inventory management in supply chains. A system of differential equations based on (2.1) can then be obtained:

$$\tau_1 \frac{d\eta_1}{dt} = \gamma_{1b}\ b(t-\theta_1) - \eta_1 + \zeta_1 \tag{2.2a}$$

$$\tau_{1l} \frac{d\eta_{1l}}{dt} = \gamma_{1lb}\ b(t-\theta_{1l}) - \eta_{1l} + \zeta_{1l} \tag{2.2b}$$

$$\tau_2 \frac{d\eta_2}{dt} = \gamma_{2n}\ n(t-\theta_2) - \eta_2 + \zeta_2 \tag{2.2c}$$

$$\tau_{2l} \frac{d\eta_{2l}}{dt} = \gamma_{2ln}\ n(t-\theta_{2l}) - \eta_{2l} + \zeta_{2l} \tag{2.2d}$$

$$\tau_3 \frac{d\eta_3}{dt} = \gamma_{3c}\ c(t--\theta_3) - \eta_3 + \zeta_3 \tag{2.2e}$$

$$\tau_{3l} \frac{d\eta_{3l}}{dt} = \gamma_{3lc}\ c(t--\theta_{3l}) - \eta_{3l} + \zeta_{3l} \tag{2.2f}$$

$$\tau_4 \frac{d\eta_4}{dt} = \beta_{41}\ \eta_1 + \beta_{42}\ \eta_2 + \beta_{43}\ \eta_3 - \eta_4 + \zeta_4 \tag{2.2g}$$

$$\tau_{4l} \frac{d\eta_{4l}}{dt} = \beta_{41l}\ \eta_{1l} + \beta_{42l}\ \eta_{2l} + \beta_{43l}\ \eta_{3l} - \eta_{4l} + \zeta_{4l} \tag{2.2h}$$

$$\tau_5 \frac{d\eta_5}{dt} = \beta_{53}\ \eta_3 + \beta_{53l}\ \eta_{3l} + \beta_{54}\ \eta_4 + \beta_{54l}\ \eta_{4l} - \eta_5 + \zeta_5 \tag{2.2i}$$

where τ_i are time constants, θ_i are pure time delays, and ζ_i are disturbances. At steady-state (*i.e.*, when $\frac{d\eta_i}{dt} = 0$), the dynamical model in (2.2) corresponds exactly to the TPB SEM in (2.1) without approximation.

In the remainder of the dissertation, the following assumptions are considered:

1. All the pure time delays will be considered to be zero; this is for simplicity and clarity of the results and is consistent with the data we have obtained.

2. Uncertainties ζ_i are represented as zero mean stochastic signals.

Under these two assumptions, the differential equations described above can be transformed to the following state space representations of the model.

$$\dot{x} = A(\phi)x(t) + B(\phi)u(t) + G(\phi)e(t) \tag{2.3a}$$

$$y = C(\phi)x(t) \tag{2.3b}$$

where:

$x = \begin{bmatrix} \eta_1 & \eta_{1l} & \eta_2 & \eta_{2l} & \eta_3 & \eta_{3l} & \eta_4 & \eta_{4l} & \eta_5 \end{bmatrix}^T$, which denotes a vector of $d_x = 9$ state variables;

$u = \begin{bmatrix} b & n & c \end{bmatrix}^T$, which denotes a vector of $d_u = 3$ input variables;

$y = \begin{bmatrix} \eta_1 & \eta_{1l} & \eta_2 & \eta_{2l} & \eta_3 & \eta_{3l} & \eta_4 & \eta_{4l} & \eta_5 \end{bmatrix}^T$, which denotes a vector of $d_y = 9$ output variables;

$e = \begin{bmatrix} \zeta_1 & \zeta_{1l} & \zeta_2 & \zeta_{2l} & \zeta_3 & \zeta_{3l} & \zeta_4 & \zeta_{4l} & \zeta_5 \end{bmatrix}^T$, which are uncertainties associated to each one of the states and outputs;

$\phi = [\tau_1,\ \tau_{1l},\ \tau_2,\ \tau_{2l},\ \tau_3,\ \tau_{3l},\ \tau_4,\ \tau_{4l},\ \tau_5,\ \gamma_{1b},\ \gamma_{1lb},\ \gamma_{2n},\ \gamma_{2ln},\ \gamma_{3c},\ \gamma_{3lc},\ \beta_{41},\ \beta_{42},\ \beta_{43},\ \beta_{41l},\ \beta_{42l},\ \beta_{43l},\ \beta_{53},\ \beta_{53l},\ \beta_{54},\ \beta_{54l}]^T$, which denotes a vector of $d_\phi = 25$ unknown model parameters;

$$A = \begin{bmatrix} -\frac{1}{\tau_1} & 0 & 0 & 0 & 0 & 0 & 0 & 0 & 0 \\ 0 & -\frac{1}{\tau_{1l}} & 0 & 0 & 0 & 0 & 0 & 0 & 0 \\ 0 & 0 & -\frac{1}{\tau_2} & 0 & 0 & 0 & 0 & 0 & 0 \\ 0 & 0 & 0 & -\frac{1}{\tau_{2l}} & 0 & 0 & 0 & 0 & 0 \\ 0 & 0 & 0 & 0 & -\frac{1}{\tau_3} & 0 & 0 & 0 & 0 \\ 0 & 0 & 0 & 0 & 0 & -\frac{1}{\tau_{3l}} & 0 & 0 & 0 \\ \frac{\beta_{41}}{\tau_4} & 0 & \frac{\beta_{42}}{\tau_4} & 0 & \frac{\beta_{43}}{\tau_4} & 0 & -\frac{1}{\tau_4} & 0 & 0 \\ 0 & \frac{\beta_{41l}}{\tau_{4l}} & 0 & \frac{\beta_{42l}}{\tau_{4l}} & 0 & \frac{\beta_{43l}}{\tau_{4l}} & 0 & -\frac{1}{\tau_{4l}} & 0 \\ 0 & 0 & 0 & 0 & \frac{\beta_{53}}{\tau_3} & \frac{\beta_{53l}}{\tau_{3l}} & \frac{\beta_{54}}{\tau_4} & \frac{\beta_{54l}}{\tau_{4l}} & -\frac{1}{\tau_5} \end{bmatrix};$$

$$B = \begin{bmatrix} \frac{\gamma_{1b}}{\tau_1} & 0 & 0 \\ \frac{\gamma_{1lb}}{\tau_{1l}} & 0 & 0 \\ 0 & \frac{\gamma_{2n}}{\tau_2} & 0 \\ 0 & \frac{\gamma_{2ln}}{\tau_{2l}} & 0 \\ 0 & 0 & \frac{\gamma_{3c}}{\tau_3} \\ 0 & 0 & \frac{\gamma_{3lc}}{\tau_{3l}} \\ 0 & 0 & 0 \\ 0 & 0 & 0 \\ 0 & 0 & 0 \end{bmatrix};$$

$$G = \begin{bmatrix} \frac{1}{\tau_1} & 0 & 0 & 0 & 0 & 0 & 0 & 0 & 0 \\ 0 & \frac{1}{\tau_{1l}} & 0 & 0 & 0 & 0 & 0 & 0 & 0 \\ 0 & 0 & \frac{1}{\tau_2} & 0 & 0 & 0 & 0 & 0 & 0 \\ 0 & 0 & 0 & \frac{1}{\tau_{2l}} & 0 & 0 & 0 & 0 & 0 \\ 0 & 0 & 0 & 0 & \frac{1}{\tau_3} & 0 & 0 & 0 & 0 \\ 0 & 0 & 0 & 0 & 0 & \frac{1}{\tau_{3l}} & 0 & 0 & 0 \\ 0 & 0 & 0 & 0 & 0 & 0 & \frac{1}{\tau_4} & 0 & 0 \\ 0 & 0 & 0 & 0 & 0 & 0 & 0 & \frac{1}{\tau_{4l}} & 0 \\ 0 & 0 & 0 & 0 & 0 & 0 & 0 & 0 & \frac{1}{\tau_5} \end{bmatrix};$$

$C = I$ (9×9).

The model per (2.2) represents a system of first-order differential equations, the capability of which to describe the dynamics is limited. If a more elaborate transient response is required, the left hand of the equation can be augmented to the second order. The dynamics of second order system with an inventory system can be conceptualized as being subject to self-regulation.

The development of the system of equations for TPB model on physical activity behaviors is similar to the system equations for TPB model that are used to describe healthy eating behaviors in (2.2), but with the limit constructs excluded as shown in the path diagram in Fig. 2.3. The TPB model on physical activity is simpler with less equations and state variables involved. If represented with a system of differential equations, we have

$$\tau_1 \frac{d\eta_1}{dt} = \gamma_{1b}\ b(t-\theta_1) - \eta_1 + \zeta_1 \tag{2.4a}$$

$$\tau_2 \frac{d\eta_2}{dt} = \gamma_{2n}\ n(t-\theta_2) - \eta_2 + \zeta_2 \tag{2.4b}$$

$$\tau_3 \frac{d\eta_3}{dt} = \gamma_{3c}\ c(t--\theta_3) - \eta_3 + \zeta_3 \tag{2.4c}$$

$$\tau_4 \frac{d\eta_4}{dt} = \beta_{41}\ \eta_1 + \beta_{42}\ \eta_2 + \beta_{43}\ \eta_3 - \eta_4 + \zeta_4 \tag{2.4d}$$

$$\tau_5 \frac{d\eta_5}{dt} = \beta_{53}\ \eta_3 + \beta_{54}\ \eta_4 - \eta_5 + \zeta_5 \tag{2.4e}$$

where τ_i are time constants, θ_i are pure time delays, and ζ_i are disturbances; same assump-

tions for delays and uncertainties hold. Similarly, (2.4) can be transformed to the following state space representations as,

$$\dot{x} = A(\phi)x(t) + B(\phi)u(t) + G(\phi)e(t) \tag{2.5a}$$

$$y = C(\phi)x(t) \tag{2.5b}$$

where:

$x = \begin{bmatrix} \eta_1 & \eta_2 & \eta_3 & \eta_4 & \eta_5 \end{bmatrix}^T$, which denotes a vector of $d_x = 5$ state variables;

$u = \begin{bmatrix} b & n & c \end{bmatrix}^T$, which denotes a vector of $d_u = 3$ input variables;

$y = \begin{bmatrix} \eta_1 & \eta_2 & \eta_3 & \eta_4 & \eta_5 \end{bmatrix}^T$, which denotes a vector of $d_y = 5$ output variables;

$e = \begin{bmatrix} \zeta_1 & \zeta_2 & \zeta_3 & \zeta_4 & \zeta_5 \end{bmatrix}^T$, which are uncertainties associated to each one of the states and outputs;

$\phi = [\tau_1,\ \tau_2,\ \tau_3,\ \tau_4,\ \tau_5,\ \gamma_{1b},\ \gamma_{2n},\ \gamma_{3c},\ \beta_{41},\ \beta_{42},\ \beta_{43},\ \beta_{53},\ \beta_{54}]^T$, which denotes a vector of $d_\phi = 13$ unknown model parameters;

$$A = \begin{bmatrix} -\frac{1}{\tau_1} & 0 & 0 & 0 & 0 \\ 0 & -\frac{1}{\tau_2} & 0 & 0 & 0 \\ 0 & 0 & -\frac{1}{\tau_3} & 0 & 0 \\ \frac{\beta_{41}}{\tau_4} & \frac{\beta_{42}}{\tau_4} & \frac{\beta_{43}}{\tau_4} & -\frac{1}{\tau_4} & 0 \\ 0 & 0 & \frac{\beta_{53}}{\tau_3} & \frac{\beta_{54}}{\tau_4} & -\frac{1}{\tau_5} \end{bmatrix};$$

$$B = \begin{bmatrix} \frac{\gamma_{1b}}{\tau_1} & 0 & 0 \\ 0 & \frac{\gamma_{2n}}{\tau_2} & 0 \\ 0 & 0 & \frac{\gamma_{3c}}{\tau_3} \\ 0 & 0 & 0 \\ 0 & 0 & 0 \end{bmatrix};$$

$$G = \begin{bmatrix} \frac{1}{\tau_1} & 0 & 0 & 0 & 0 \\ 0 & \frac{1}{\tau_2} & 0 & 0 & 0 \\ 0 & 0 & \frac{1}{\tau_3} & 0 & 0 \\ 0 & 0 & 0 & \frac{1}{\tau_4} & 0 \\ 0 & 0 & 0 & 0 & \frac{1}{\tau_5} \end{bmatrix};$$

$C = I\ (5 \times 5)$.

2.3 Intervention Delivery Dynamics

The models for intervention delivery dynamics relate the magnitude and frequency of intervention components to the input variables in the TPB models. Hence, it serves as a connection between the HMPC controller and the TPB model. The development of the model is similar to the TPB model, using the concept of fluid analogy and network of production inventory systems in supply management, and the details of modeling will be described in this section.

Intuitively, the model is supposed to use the magnitude of each intervention component as inputs and the belief variable (b, n, and c) in the TPB model as outputs. The intervention components as listed in Table 1.2, include education, goal setting, self-monitoring and active learning, among which the first three components are all included in the baseline intervention with no magnitude changes throughout the intervention, while active learning is not included at baseline intervention, but is given only if a step-up intervention is necessary. As needs for augmenting intervention dosages increase per Table 6.3, the number of step-ups for healthy eating/physical activity active learning (or stated as the intensities of active learning) can range from one to three respectively with one step-up at a time. Based on the different delivery features of these intervention components, the four components can be categorized and simplified into two inputs: one as baseline intervention ($base$), and one as intervention step up (up). Given the proposed two inputs and three outputs, a path diagram can be generated to illustrate the cross-relations among the model variables as shown in Fig. 2.4, based on which a system of differential equations can be obtained using the fluid analogy:

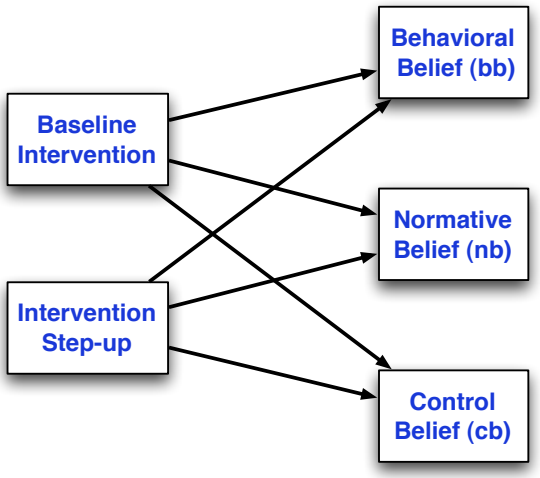

Figure 2.4: Path diagram for the model of intervention delivery dynamics using simplified inputs.

$$\tau_b \frac{db(t)}{dt} = \gamma_{11}\ base(t-\theta_{11}) + \gamma_{12}\ up(t-\theta_{12}) - b + \zeta_b \tag{2.6a}$$

$$\tau_n \frac{dn(t)}{dt} = \gamma_{21}\ base(t-\theta_{21}) + \gamma_{22}\ up(t-\theta_{22}) - n + \zeta_n \tag{2.6b}$$

$$\tau_c \frac{dc(t)}{dt} = \gamma_{31}\ base(t-\theta_{31}) + \gamma_{32}\ up(t-\theta_{32}) - c + \zeta_c \tag{2.6c}$$

where τ_i are time constants, θ_i are pure time delays, and ζ_i are disturbances. Same assumptions proposed for TPB model as zero delays and zero mean white noise signals for disturbances still hold for this intervention delivery dynamics model. The model per (2.6) represents a system of first-order differential equations. If a more elaborate transient response is required but cannot be described by the first-order systems, the left hand of the equation can be augmented to the second order. If (2.6) is transformed to the state space representations, it gives,

$$\dot{x} = A(\phi)x(t) + B(\phi)u(t) + G(\phi)e(t) \tag{2.7a}$$

$$y = C(\phi)x(t) \tag{2.7b}$$

where:

$x = \begin{bmatrix} b & n & c \end{bmatrix}^T$, which denotes a vector of $d_x = 3$ state variables;

$u = \begin{bmatrix} base & up \end{bmatrix}^T$, which denotes a vector of $d_u = 2$ input variables;

$y = \begin{bmatrix} b & n & c \end{bmatrix}^T$, which denotes a vector of $d_y = 3$ output variables;

$e = \begin{bmatrix} \zeta_b & \zeta_n & \zeta_c \end{bmatrix}^T$, which are uncertainties associated to each one of the states and outputs;

$\phi = [\tau_b,\ \tau_n,\ \tau_c,\ \gamma_{11},\ \gamma_{12},\ \gamma_{21},\ \gamma_{22},\ \gamma_{31},\ \gamma_{32}]^T$, which denotes a vector of $d_\phi = 9$ unknown model parameters;

$$A = \begin{bmatrix} -\frac{1}{\tau_b} & 0 & 0 \\ 0 & -\frac{1}{\tau_n} & 0 \\ 0 & 0 & -\frac{1}{\tau_c} \end{bmatrix};$$

$$B = \begin{bmatrix} \frac{\gamma_{11}}{\tau_b} & \frac{\gamma_{12}}{\tau_b} \\ \frac{\gamma_{21}}{\tau_n} & \frac{\gamma_{22}}{\tau_n} \\ \frac{\gamma_{31}}{\tau_c} & \frac{\gamma_{32}}{\tau_c} \end{bmatrix};$$

$$G = \begin{bmatrix} \frac{1}{\tau_b} & 0 & 0 \\ 0 & \frac{1}{\tau_n} & 0 \\ 0 & 0 & \frac{1}{\tau_c} \end{bmatrix};$$

$C = I\ (3 \times 3)$.

This developed model for intervention delivery dynamics by representations of either (2.6) or (2.7) can be applied to integrate with TPB models for both healthy eating and physical activity. The form of this delivery dynamics model and the TPB behavioral models is amenable in the design and analysis of GWG interventions and lends itself to system identification. Once the model parameters are identified and validated based on the collected data, a participant validated model can be formed by integrating these two models with the reformulated EB model, as will be presented in the next section. Based on the individualized comprehensive model, advanced decision algorithms such as HMPC can be designed using control engineering approaches to optimize the intervention intensities in response to individuals' specific needs. Hence, the customized intervention strategy that can adapt to individuals' unique needs can be realized.

2.4 Energy Balance Model

The basis for most of the work explored in this document relies on a closed-form EB model which is reformulated from a maternal EB model developed by Thomas *et al.* (2012). In this section, the original EB model will be reviewed, followed by a detailed description of the development of the reformulated EB model. For simplicity and clarity, the original EB model developed by Thomas *et al.* (2012) will be referred to as the initial EB model in the remainder of the document. Based on the initial model, we formulate a Multiple Input Single Output (MISO) dynamical system model in a closed form that is better suited for control purposes.

The initial EB model from Thomas *et al.* (2012) to predict gestational weight gain (GWG) based on gestational energy intake (EI) and energy expenditure (EE) relies on the principle of energy conservation, which can be expressed as

$$ES(t) = (1-g)EI(t) - EE(t) \tag{2.8}$$

where $ES(t)$ is the daily energy stored at time t. The parameter $g = 0.03$ is the nutrient partitioning constant. The excess energy is stored and converted into different body tissues (*e.g.* body fat and muscle tissue), leading to a weight change of different body compositions. Hence, ES can be constructed as a sum of the instantaneous rates of change of different energy storage compartments during pregnancy. Here, a two-compartment model which separates maternal materials into two components, fat free mass (FFM) and fat mass (FM) is applied. The sum of FFM and FM represents the total maternal body weight (W) as

$$W(t) = FFM(t) + FM(t) \tag{2.9}$$

Under this two-compartment model assumption, the ES term in (2.8) can be expanded into the sum of the instantaneous weight change of the two components of FM and FFM, multiplied by their respective energy densities λ_{FM} and λ_{FFM}, leading to

$$\lambda_{FFM}\frac{dFFM}{dt} + \lambda_{FM}\frac{dFM}{dt} = (1-g)EI(t) - EE(t) \tag{2.10}$$

where $\lambda_{FM} = 9500$ kcal/kg, $\lambda_{FFM} = 771$ kcal/kg. The resulting solution of the differential equation in (2.10) predicts FFM and FM as a function of time.

In this model from Thomas *et al.* (2012), EE is estimated with a regression-based function of maternal W. In the case of small W changes, the EE quantity remains relatively constant. Despite the effectiveness and simplicity in the use of EE estimation functions for weight gain predictions, this is not quite suited for an intervention application where individual levels of PA can be significantly increased or adapted as a result of intervention sessions, leading to a substantial change observed in total EE. This issue can also be described (as noted in Sabounchi *et al.* (2014)) that the initial EB model estimates EE as a monolithic quantity. Here modifications are made to compensate for limitations of the modeling in Thomas *et al.* (2012) that the different components of maternal EE cannot be adjusted individually.

EE is commonly considered to be composed of physical activity (PA), resting metabolic rate (RMR), and the thermic effect of food (TEF) (Ravussin and Bogardus, 1992). With commercially available accelerometers, PA can be easily measured. RMR is the minimal energy expenditure of a human at rest and is considered as dynamically changing throughout gestation. This quantity can be obtained through estimation, or by measurement with a metabolism device. TEF is usually expressed as a percentage of EI, ranging from 4.0% to 17.1% due to different diets (Westerterp, 2004). Regardless of intake nutrients, we assume it to be approximately 7% of daily EI as measured in Piers *et al.* (1995). Thus, EE can be expressed as,

$$EE(t) = PA(t) + RMR(t) + r_{TEF}EI(t) \tag{2.11}$$

where $r_{TEF} = 0.07$. Substituting (2.9) and (2.11) into (2.10) gives,

$$\lambda_{FFM}\frac{dFFM(t)}{dt} + \lambda_{FM}\frac{d(W(t) - FFM(t))}{dt} = (1 - g - r_{TEF})EI(t) - PA(t) - RMR(t) \tag{2.12}$$

Instead of keeping two differential terms in (2.12), FFM can be expressed to relate to W so that the derivative term is only with respect to W, and the equations become

much easier to solve. To begin with, FFM can be considered to be the sum of total body water (TBW), total body protein (TBP), and mass that stays constant during gestation (constant massCM); this latter quantity includes bone mass for example. This leads to,

$$FFM(t) = TBW(t) + TBP(t) + CM \tag{2.13}$$

where $CM = FFM(0) - TBW(0) - TBP(0)$. TBW and TBP are linear functions of simultaneously measured W based on a participant's BMI, which can be expressed in a generalized form as,

$$TBW(t) = a_W W(t) + b_W \tag{2.14a}$$

$$TBP(t) = a_P W(t) + b_P \tag{2.14b}$$

where a_W, b_W, a_P, b_P are the coefficients of the corresponding functions, the values of which can be found in Table 2.2. Note that TBP and W are expressed in kg, TBW in liters. Substituting (2.14) into (2.13) leads to,

$$FFM(t) = (a_W + a_P)W(t) + (b_W + b_P + CM) \tag{2.15}$$

which if substituted into (2.12) gives the differential equation expressed in terms of the derivative of W as,

$$\frac{dW(t)}{dt} = K_1 EI(t) + K_2 PA(t) + K_2 RMR(t) \tag{2.16}$$

where

$$K_1 = \frac{1 - g - r_{TEF}}{(a_W + a_P)\lambda_{FFM} + (1 - a_W - a_P)\lambda_{FM}} \tag{2.17a}$$

$$K_2 = \frac{-1}{(a_W + a_P)\lambda_{FFM} + (1 - a_W - a_P)\lambda_{FM}} \tag{2.17b}$$

K_1 and K_2 are system gain coefficients, expressed in kg/kcal/day. Table 2.3 shows the values of K_1 and K_2 for different categories of BMI. Equation (2.16) forms the basis of the work presented in this dissertation, from which we are able to predict the system output

Table 2.2: Tabulation of the coefficients for the linear functions of total body water (TBW) and total body protein (TBP) with respect to maternal weight (W).

BMI Category (kg/m^2)	Weight Range (kg)	a_W	b_W	a_P	b_P
Low BMI (≤ 19.8)	$W \leq 52$	0.489	3.875	-0.04762	9.28
	$52 < W \leq 57.7$			0.105263	1.33
	$W > 57.7$			0.075472	3.05
Normal BMI (19.8–26)	$W \leq 60.2$	0.4836	2.853	-0.667	47.533
	$60.2 < W \leq 65.1$			0.0204	6.17
	$W > 65.1$			0.0724	3.05
High BMI (≥ 26)	$W \leq 81.8$	0.503	4.885	-0.03226	10.4387
	$81.8 < W \leq 85.8$			0.1	0.38
	$W > 85.8$			0.098765	0.27407

W using the explicitly measurable inputs EI, PA and RMR. Written in discretized form for daily sampling time $T = 1$, the EB model can be expressed as,

$$GWG(k+1) = K_1 EI(k) + K_2 PA(k) + K_2 RMR(k) \tag{2.18}$$

where GWG is defined by $GWG(k+1) = W(k+1) - W(k)$. When written in deviation variables and using Laplace transforms, (2.16) gives,

$$\Delta W(s) = \frac{K_1}{s}\Delta EI(s) + \frac{K_2}{s}\Delta PA(s) + \frac{K_2}{s}\Delta RMR(s) \tag{2.19}$$

As seen here, the reformulated EB model for GWG can be represented in terms of a simple sum of integrators, each integrator defined by K_1 or K_2 (the system gain coefficients) with respect to the three inputs.

One can notice that the constant term CM cancels out when substituting (2.15) into (2.12) followed by the differentiation. In the case where FFM needs to be calculated using (2.15), CM can be expressed as

$$CM = FFM(0) - TBW(0) - TBP(0) \tag{2.20}$$

Table 2.3: System gain parameters K_1 and K_2 for low, normal and high BMI.

BMI Category (kg/m^2)	Weight Range (kg)	Gain $K_1 \times 10^4$ ($\frac{kg}{kcal \cdot day}$)	Gain $K_2 \times 10^4$ ($\frac{kg}{kcal \cdot day}$)
Low BMI (≤ 19.8)	$W \leq 52$	1.59	-1.77
	$52 < W \leq 57.7$	2.09	-2.32
	$W > 57.7$	1.97	-2.19
Normal BMI (19.8–26)	$W \leq 60.2$	0.81	-0.90
	$60.2 < W \leq 65.1$	1.76	-1.96
	$W > 65.1$	1.94	-2.15
High BMI (≥ 26)	$W \leq 81.8$	1.67	-1.85
	$81.8 < W \leq 85.8$	2.12	-2.36
	$W > 85.8$	2.12	-2.35

where day 0 indicates the pre-gravid state of the variables. $TPB(0)$ and $TPW(0)$ may be calculated using the functions in Table 2.2 based on the pre-gravid weight, $W(0)$; But it has to be noted that the functions in Table 2.2 might be less accurate when applied to pre-gravid calculations. $FFM(0)$ in (2.20) can be calculated from

$$FFM(0) = W(0) - FM(0) \tag{2.21}$$

where $FM(0)$ is obtained by solving (2.22) below. Here, *age* is expressed in years, *height* in cm, $W(0)$ and $FM(0)$ in kg.

$$\begin{aligned} W(0) = {} & 3.5 \times 10^{-7} \times FM(0)^4 - 0.187 \times 10^{-5} \times height \times FM(0)^3 + 0.2291 \times 10^{-3} \\ & \times FM(0)^3 + 0.332 \times 10^{-4} \times age \times FM(0)^2 + 0.2721 \times 10^{-3} \times height \times FM(0)^2 \\ & - 0.0390627 \times FM(0)^2 - 0.002296 \times age \times FM(0) - 0.013308 \times height \times FM(0) \\ & + 3.4837412 \times FM(0) - 0.038273 \times age + 0.6555023 \times height - 72.055453 \end{aligned} \tag{2.22}$$

Formula (2.22) for body composition is obtained using the data from the National Health and Nutrition Examination Survey (NHANES).

From the derivations described in these sections, a control-oriented energy balance model for gestational weight gain has been developed, starting from the first-principles model of Thomas *et al.* (2012). As will be shown in this dissertation, this reformulated model has been extremely useful in the intervention development and participant data analysis. With the use of this reformulated model, it is easier to predict the trajectory of maternal weights based on the longitudinal measurements of the model inputs (maternal EI, PA, and RMR). Comparing the model predictions with the trajectory of weight measurements, further analysis of the predictive model or measurement errors can be performed. This is how it leads us to the exploration into the issues observed in the self-reported data. In next section, the issue of energy intake underreporting will be described, and it will be clearly explained why it is problematic for intervention assessments as well as for the implementation of the closed-loop controller algorithms. Motivated from this need, a series of estimation approaches to correcting self-reports have been developed to address this issue. Further estimation related work is documented in Chapters 3 and 4.

2.5 Energy Intake Underreporting & Other Data Issues

2.5.1 Data Description

In this section, the reformulated energy balance model is evaluated against the actual participant data from both the Phase I and Phase II studies of the HMZ intervention. In the pilot HMZ intervention study (Phase I study), maternal EI, PA and W of 17 OW/OB pregnant women (age mean: 28.9, standard deviation (SD): 5.1, and pre-pregnancy body mass index (BMI) mean: 29.6, SD: 4.0) were measured for six weeks. For the measurement of W, participants weighed themselves daily using Aria Wifi smart digital scales. Participant EI was obtained from self-reports using two options: 1) A dietary intake phone app *MyFitnessPal (MFP)* at the frequency of three days a week and 2) a weekly online assessment through Automated Self-Administered 24-hour dietary recall system (ASA24, Subar *et al.* (2007)). The daily measurements of PA were obtained using both a waist-worn

activity monitor (ActiGraph wGT3X-BT) and a wrist-worn commercial monitor (Jawbone UP). For the sake of clarity, only the results of the wrist-worn monitor are presented in this work as they parallel those from the waist-worn device; another consideration about PA data is that the measurements from the wrist-worn device were obtained for the entire span of six weeks, while ActiGraph data were only available for two weeks. Likewise, only EI self-reports from the dietary intake phone app are presented due to their parallel values as ASA24. RMR was not measured in the pilot study, but was measured and objectively assessed over pregnancy in the full trial in Phase II study using *Breezing*, a commercial portable metabolism tracker device (Xian *et al.* (2015)). For both phases of the intervention, estimated RMR has been used extensively: a good estimate of gestational RMR can be provided with the quadratic function as shown below:

$$RMR = 0.1976W^2 - 13.424W + 1457.6 \tag{2.23}$$

where W is the maternal weight expressed in kg. This regression formula is originally proposed by Thomas (2009), who derived the equation by fitting the data from Butte *et al.* (2004). This equation captures the slight increase of RMR as women gain weight during gestation, and the values of the estimated RMR have been demonstrated to be comparable with the measured RMR. For simplicity and other computational benefits, the estimated RMR has been adopted for approach demonstration and other analysis instead of using the less frequently measured RMR.

In the full HMZ intervention study (Phase II study), maternal W, EI and PA of 27 OW/OB pregnant women (age mean: 30.6; SD: 3.0, and pre-pregnancy body mass index (BMI) mean: 31.6, SD: 7.1) were measured for 22-28 weeks. Similar as the Phase I study, participant W is self-monitored every day using Aria Wifi smart digital scales. Self-reported EI was obtained through MFP alone at the frequency of three days per week. This is based on the practical assessment from Phase I study that MFP shows parallel values as ASA24, and it is more user friendly and involves less participant burden. PA data were obtained from Jawbone UP and Actigraph on a daily basis, but Actigraph was only collected for

a couple of weeks. RMR was measured with *Breezing* on a weekly basis. As mentioned previously, estimated RMR has been used for algorithm demonstrations in this work.

Some special considerations or manipulations of the participant data taken in this dissertation are described here. The PA signal is considered as having negligible measurement noise for purposes of this work. Since PA signals are relatively stationary, mean replacement is employed to impute any missing data points for Phase II study: the mean of adjacent three weeks of PA measurements ($\pm$ 10 days) is used for missing data imputation. Note that due to the much shorter intervention span in Phase I study, linear interpolation of PA measurements is used for missing data replacement.

Considering the burden of recording their food consumption, participants are not required to report the energy intake every day. Because EI measurements were not obtained daily as measured PA and W, or estimated RMR, this leads to a substantial number of gaps in the self-reported EI. For any days when the self-reports are not available or missing, linear interpolation is one approach that can be used to impute the missing days so that simulations can be performed. This can also apply to missing data that occurs during the collection of participant W. The missingness rates for the measured EB variables are tabulated for some selected participants in Table 2.4.

Table 2.4: Rates of missing measurements for the self-monitored or self-reported EB variables for representative Phase II participants. Note: Missingness % is compute by $\frac{\text{Number of missing measurements (days)}}{\text{Total number of days for intervention}} \times 100\%$.

Participant	W	PA	EI
A	10%	11%	26%
B	16%	0%	59%
C	0%	1%	54%
D	26%	22%	55%
E	16%	1%	59%
F	11%	0%	No MFP

2.5.2 *Energy Intake Underreporting*

The energy balance model reformulated into the form of (2.16) is easier and more practical for use compared to the original energy balance model in Thomas *et al.* (2012). It can provide an accurate weight prediction based on the actual values of the major determinants of energy balance. In real life weight control interventions, however, it is difficult to assure accurate measures of a participant's actual energy intake, different energy expenditure components, and weight change from self-collected data. Among these, significant underreporting in the self-reported measures of energy intake from MFP is the most problematic issue of concerns that interferes with accurate weight predictions, and this has been observed for most participants.

Energy intake misreporting is prevalent in the general adult population, estimated at 40 to 50% for underreporting and 5 to 10% for overreporting (Johansson *et al.* (1998); Poslusna *et al.* (2009)); the extent of underreporting can be as much as 59% of their total caloric intake (Lichtman *et al.* (1992)). BMI has been found to be a significant independent predictor of EI underreporting: higher extent of underreporting is observed with increasing BMI (McGowan and McAuliffe (2012); Trabulsi and Schoeller (2001)). Hence, the participants in the HMZ Study as OW/OB pregnant women are more likely to underreport their EI. The high prevalence of EI underreporting among OW/OB pregnant women has also been previously reported in Moran *et al.* (2018), Nowicki *et al.* (2011) and Mullaney *et al.* (2014). Misreporting of EI may relate to participant education, age, psychological status such as depression or poor body image (Poslusna *et al.* (2009)). It also might be due to recall bias or memory lapses, poor awareness of quantities or types of foods eaten, inaccurate portion size estimation, or the inconvenience of reporting (Lutomski *et al.* (2011)). Thus, the measurement bias due to EI misreporting can be characterized as both systematic and random and remains a challenging issue for EB model predictions.

To illustrate underreporting in EI self-reports and their influence on weight predictions, Fig. 2.5 compares the measured weight from two representative participants from

Phase II study of the HMZ with the EB model simulated weight using their self-reported EI. Among this two selected participants, participant A (BMI = 28.6; age = 31; OW) is from the intervention group and participant B (BMI = 25.3; age = 37; OW) from the control group. The selection of these two participants aims to embrace the different characteristics or aspects of the two study groups.As shown in the figure, the discrepancies between the model predictions and weight measurements accumulate along the intervention weeks; similar observations also exist with other participant data that have been collected in the HMZ intervention. While multiple causes could explain this mismatch, the most significant is the accumulation of errors resulting from underreported EI, which increases substantially over time as a result of the integrating dynamics of the system. From a practical standpoint, self-reported or self-monitored measurements are convenient to obtain from free-living participants, yet found to contain bias and measurement noise, along with data missingness due to lack of participant compliance with the monitors or adherence to interventions. These issues with participant data all pose challenges to reliable model-based estimation and limit the assessment of intervention outcomes.

Motivated from this standpoint, a series of estimation approaches that can address measurement noise and measurement losses are developed in Chapter 3 and 4 to better understand the extent of energy intake underreporting. These include back-calculating energy intake from the EB model per (2.18) for gestational weight gain prediction, Kalman filtering-based approaches to recursively estimate energy intake from intermittent measurements in real time, and approaches based on semi-physical identification principles which features the capability of correcting future self-reported energy intake by parametrizing the extent of underreporting. The development of these estimation approaches enables the accurate weight control assessment, as well as the effective use of the EB model in an intervention setting. Please refer to those chapters for the details of each listed approach.

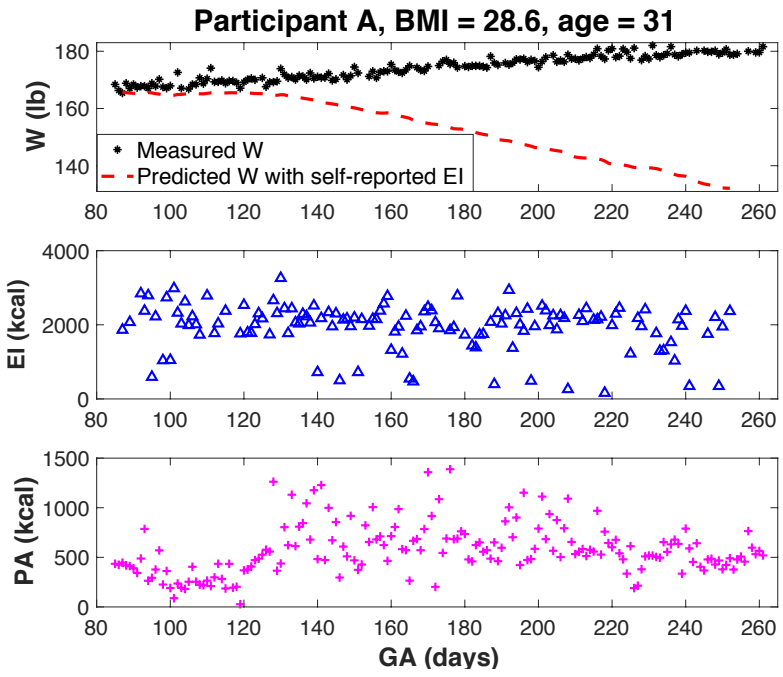

(a)

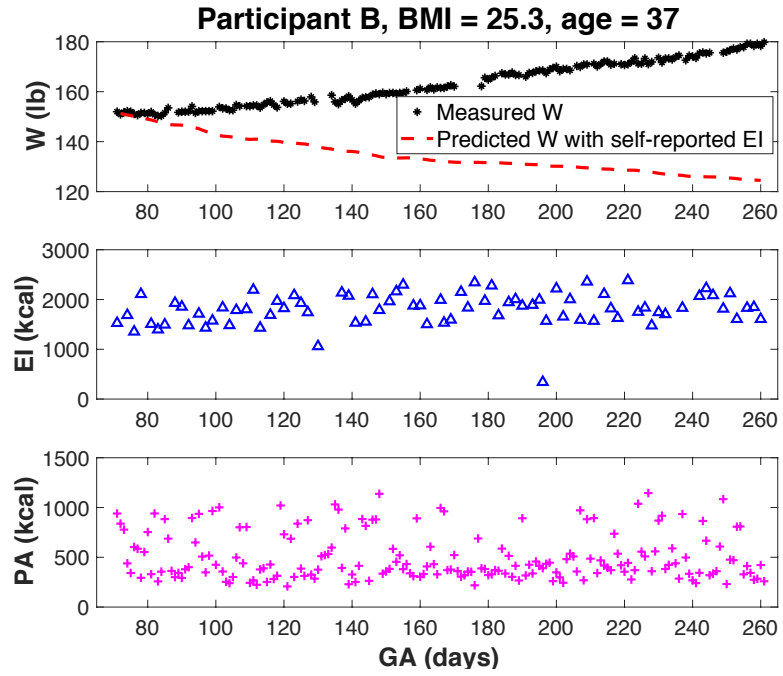

(b)

Figure 2.5: Weight predictions from the energy balance model according to (2.18) using data from two representative participants in the Phase II study of the HMZ intervention. These show evidence of significant underreporting of energy intake. Participant A is an OW woman from the intervention group and Participant B (OW) from the control group. The self-reported EI were obtained from a smartphone app (MyFitnessPal) and PA was objectively monitored with a wrist-worn accelerometer (Jawbone).

Chapter 3

ESTIMATION FOR UNDERREPORTING

As explained in Section 2.5.2, the use of the energy balance (EB) model per (2.18) for weight gain prediction can be compromised in intervention practice, due to biased or noise-corrupted input measurements; this has been found to be an issue of concern especially when using self-reported energy intake (EI) from the HMZ intervention study for maternal weight predictions. EI underreporting limits the use of EB model for accurate weight prediction, but also creates barriers and challenges for effective interventions. The literature shows that avoiding excessive maternal dietary intake is crucial for optimizing maternal and fetal outcomes during pregnancy (IOM (2005)). Misreporting of food consumed and dietary calories also makes it difficult for clinicians to determine if participants are meeting their energy intake goals, and prevents appropriate health counseling advice to be provided.

Thus it can be seen that the issue of EI underreporting calls for effective estimation/correction approaches to correct for participant misreports, and to effectively implement intervention. If participant energy intake can be accurately estimated/corrected, timely feedback can be provided to both participants and dietitians; consequently, nutrition counseling as well as suggestions regarding how to adjust physical activity behaviors can be tailored in order for intervention participants to manage their gestational weight gain in line with clinical recommendations. In this particular aspect, real-time estimation approaches that can address noise and measurement losses have significant appeal in real-world intervention settings. However, there is a scarcity of literature enabling such implementation, examining or identifying the characteristics of EI misreporting in pregnancy.

In this chapter, a series of estimation approaches are developed to better understand the issue of EI underreporting. One approach from the literature is to back-calculate EI from the EB model (Guo *et al.* (2016); Hall and Chow (2011)); this conventional approach,

while simple to implement, suffers from a number of inherent limitations. To address this problem, a Kalman filter-based approach that can estimate EI in real time from intermittent and noise-corrupted measurements is developed (Guo *et al.* (2017)). The EB model is the essential core for both these two approaches, and the implementations do not require participant self-reported EI to provide a reliable estimate. In Chapter 4, two semi-physical identification approaches that can systematically characterize the extent of underreporting will be presented as additional approaches to the problem. There, a functional relationship will be established between self-reported and actual EI. Once validated, it can be used to correct participant self-reports, independent of any other measurements involved in the EB model.

An important end-use application for EI estimation with any of the methods described above is to improve the effectiveness of closed-loop interventions using control engineering principles. A block diagram for a control system incorporating this functionality is shown in Fig. 3.1. Here a hybrid model predictive control (HMPC) algorithm, as will be described in Chapter 6, is used to specify the dosages of intervention components (e.g., healthy eating active learning, physical activity active learning, goal setting) based on the assessments of participant behavior outcomes in real time. EI, as an input to the internal controller EB model, is critical to determine the appropriate control actions; consequently biased EI self-reports will negatively influence controller performance. Therefore, estimated EI measurements described in this work are essential for adequate performance of the closed-loop control system for interventions.

3.1 Back-calculation Approach

As shown in Fig. 2.5, bias between the simulated and measured weight is mostly due to the substantial under-reported EI. To test this hypothesis, we back-calculate EI using the reformulated EB model based on the measured W, PA, and the estimated RMR. Numerically approximating the derivative term in (2.16) using the 2nd order centered difference formula and doing some algebra leads to the expression of the estimated EI (EI_{est}) as

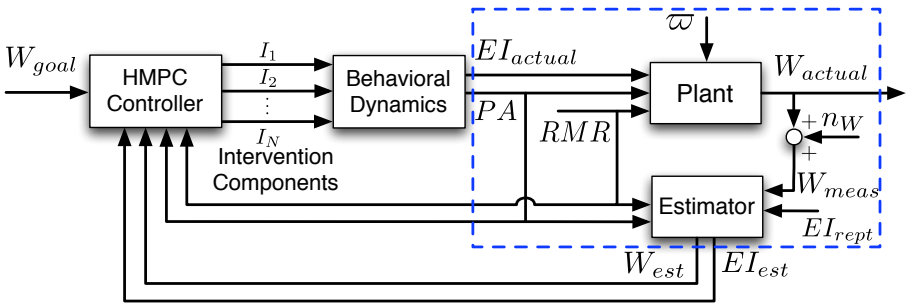

Figure 3.1: Block diagram depicting a closed-loop intervention for gestational weight gain, and how estimation approaches to energy intake as developed in this paper (indicated in the blue box) can be incorporated within the system. Energy intake estimates as well as the filtered weight measurements resulting from these estimators can be used by a hybrid model predictive control (HMPC) algorithm to determine optimized intervention dosages of intervention components.

shown below,

$$EI_{est}(k) = \frac{-W(k+2T) + 8W(k+T) - 8W(k-T) + W(k-2T)}{12\,TK_1} - \frac{K_2}{K_1}(PA(k) + RMR(k)) \tag{3.1}$$

T is the sampling time, in this case, $T = 1$ day. The variables are indexed by k with $k = 1, 2, ..., N$ corresponding to day 1 to day N. If written in the convention used in system identification, (3.2) can be represented as,

$$EI_{est}(k) = \frac{-W(k+2) + 8W(k+1) - 8W(k-1) + W(k-2)}{12\,K_1} - \frac{K_2}{K_1}(PA(k) + RMR(k)) \tag{3.2}$$

The noise in W is considered small relative to the total W; however the extent of this noise can significantly affect the numerical calculation of the rate of weight gain per day. Consequently, a 9-day ($\pm$ 4 days) moving average filter is used to smooth the measured W for Phase II participant data (for Phase I participant data, a 5-day ($\pm$ 2 days) moving average filter is used) before an estimate of the daily EI is obtained from (3.2). The selected length of the smoothing window is in agreement with the experience of behavioral scientists that a seven day window (or longer) is needed accurately reflect typical daily EI (Willett (1990)).

A 95% confidence interval of EI estimation can be calculated with Monte Carlo simulations or the technique of standard propagation of error, based on an assumed uncertainty

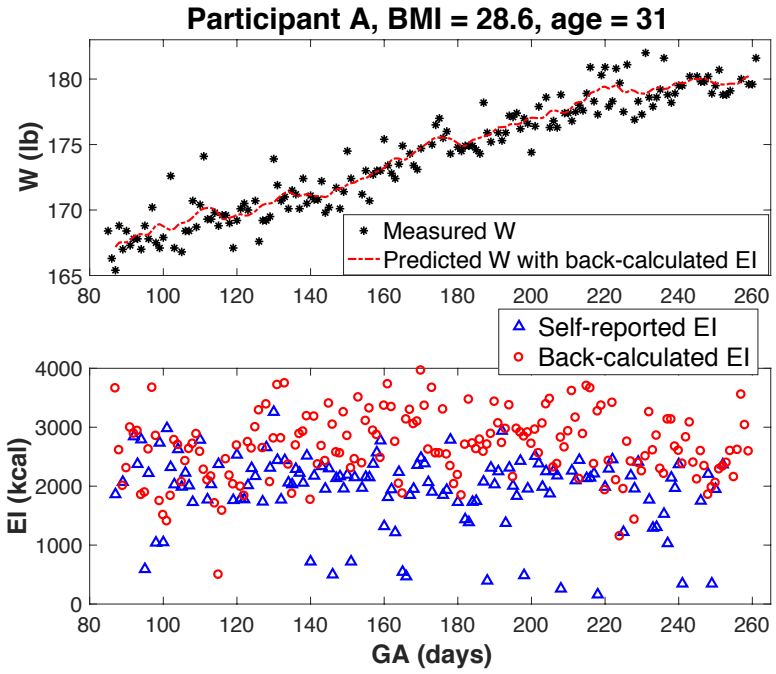

(a)

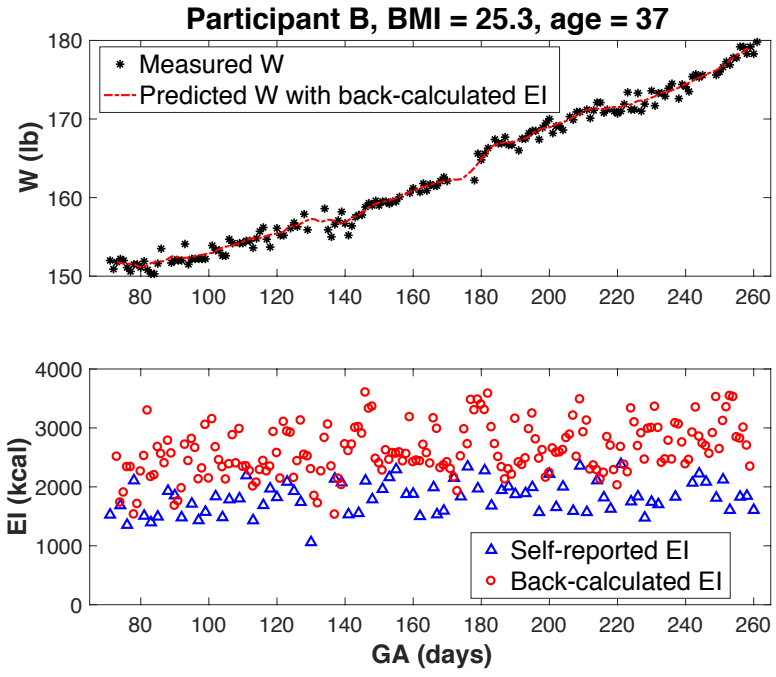

(b)

Figure 3.2: The *EI* back-calculation results for the two representative participants from the Phase II Study of the HMZ Intervention. The predicted W using back-calculated EI follows the trajectory of the measured W, which provides support for the validity of the EI estimates. BMI: body mass index; GA: gestational age.

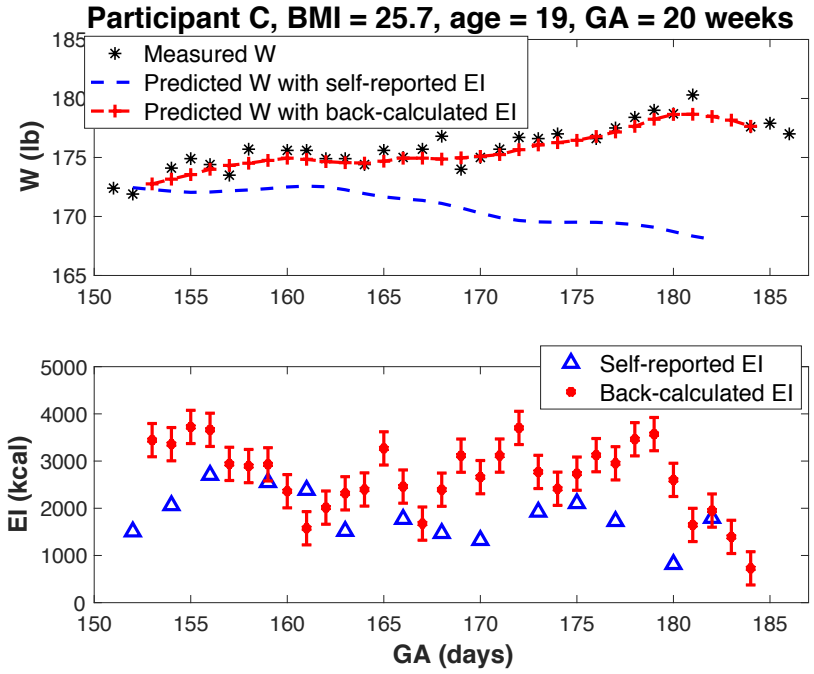

(a)

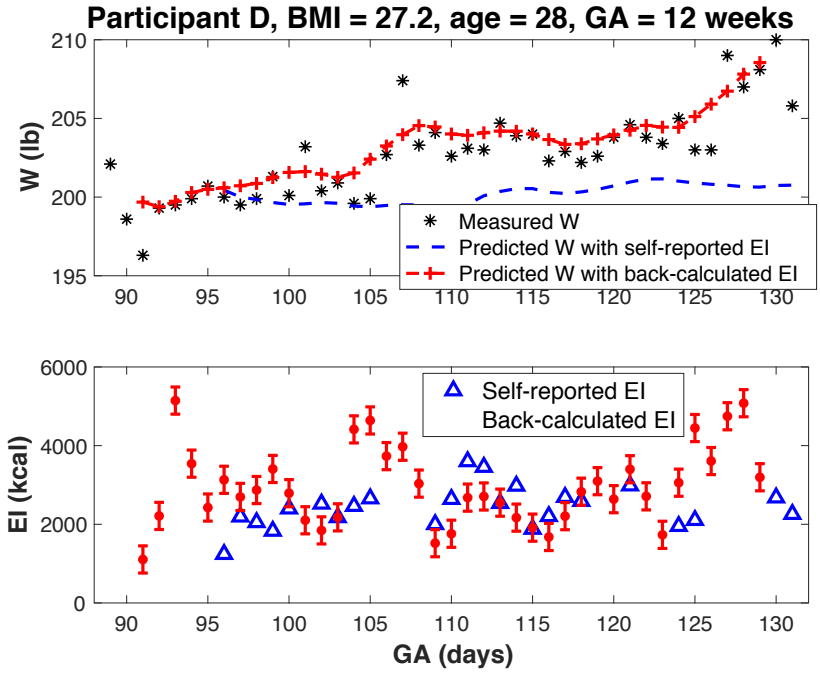

(b)

Figure 3.3: Simulations based on the reformulated EB model using self-reported and back-calculated EI for two representative participants in the Phase I Study of the HMZ, the accumulated bias between which is representative of the substantial EI underreporting in self-reported measures. The error bars represent the 95% confidence intervals of the estimates. BMI: body mass index; GA: gestational age at baseline.

perturbation in the smoothed W measurement and an uncertainty perturbation in the sum of PA and RMR. In this dissertation, we use the standard propagation of error technique to compute the confidence interval. Generally, for a function of $Q = f(x, y, z, ...)$ where x, y, z and any other variables involved in the function f are independent variables, the standard deviation of Q can be defined as,

$$s_f = \sqrt{(\frac{\partial f}{\partial x})^2 s_x^2 + (\frac{\partial f}{\partial y})^2 s_y^2 + (\frac{\partial f}{\partial z})^2 s_z^2 + ...} \tag{3.3}$$

where s_f, s_x, s_y, and s_z represent the standard deviation of Q, x, y and z, respectively. Applying this formula to (3.2) for EI back-calculation where EI_{est} is determined from multiple measurements of W and the sum of PA and RMR (which can be treated as a single variable with respect to energy expenditure in the unit of kcal), gives the standard deviation of estimated EI as,

$$EI_{std}(k) = \sqrt{\frac{\delta^2(W(k+2)^2 + W(k-2)^2) + 64\delta^2(W(k+1)^2 + W(k-1)^2)}{(12\,TK_1)^2} + (\frac{K_2}{K_1})^2\epsilon^2(PA(k) + RMR(k))^2} \tag{3.4}$$

where δ is the percentage uncertainty perturbation in W measurement, and ϵ is the uncertainty perturbation in the sum of PA and RMR. Note that the sum of PA and RMR is considered as a single variable in units of kcal in the calculation of the standard deviation in (3.4), thus incorporating the existence of errors in both the measurement of PA and in the estimation of RMR.

The back-calculation result is shown in Fig. 3.3 for the two Phase I participants and in Fig. 3.2 for the two Phase II participants. For clarity, in the first demonstration for Phase I participants where the set of measurements is relatively small, the confidence intervals are calculated based on the assumption that $\delta = 0.3\%$ and $\epsilon = 5\%$, that is, an error of 0.3 lb in a measured $W = 100$ lb, and 100 kcal perturbation for a measured energy expenditure in total of 2000 kcal. In these results, the backtracked EI is generally higher than the reported EI measurements. The difference between the back-calculated EI and the self-reported EI is quantified using the mean and its standard deviation (SD). The mean $\pm$ SD of the EI

estimate for participant A is 2787 ± 617 kcal; the mean ± SD for participant B is 3353 ± 1025 kcal. Similarly, the mean±SD of the EI estimate for participant C is 2660 ± 570 kcal and 2617 ± 434 kcal for participant D. One can also notice that the predicted W using the back-calculated EI follows closely with the measured W, which also provides support for the accuracy of the EI back-calculation from this method.

The method of using algebraic back-calculation for EI is the simplest and quickest approach to implement, and repeated EI estimates can be generated without requiring any EI measurements. Since estimation with this method is sensitive to noise in the weight measurements, pre-processing of measured weight data with techniques such as moving average filters is necessary to reduce variability in the estimates. It is also observed that, while the standard deviation can be significantly reduced by increasing length of the moving average window, the average of the estimates is not affected. The selection of the moving average window is an important adjustable parameter for smoothing, and needs to be determined based on the variance and length of the intervention.

3.2 Classical Kalman Filtering Approach for EI Estimation

Kalman filtering (KF) is an important approach to state estimation and is usually applied for estimating states that cannot be measured directly the majority of the time. A system state refers to a variable that can represent certain aspect of the dynamic characteristics of the system at any given time. By measuring the output instead, which is a function of the states but corrupted by noise, inference can be made about the dynamical system. Kalman filtering approach can produce states for linear dynamical systems in the presence of noise by propagating the mean and covariance of the probability distribution function of the model state in an optimal (minimum mean square error) manner (Chen (1995); Jazwinski (1970)). It is convenient and practical for use due to its property as a recursive filter. In the case where an estimate is required every time that a measurement is received, this recursive filtering approach can process the received data sequentially instead of per batch; hence it is not necessary to store the complete data set or to reprocess existing

data if a new measurement becomes available (Gordon (1996)). This property is beneficial in practice both from the point of view of storage costs as well as for rapid adaptation to changing signal characteristics (Arulampalam *et al.* (2002)).

As demonstrated in the previous subsection, back-calculation is simple to implement, but the variation in the estimates is largely due to the noise in the measured GWG (GWG_{meas}). In this section, we develop a recursive method based on KF to sequentially estimate EI in real time and filter out the noise in GWG_{meas} simultaneously. In this method, we do not need the self-reported EI measurements, but a state-space model that describes the dynamics of the system is required before the KF can be applied. The variable we aim to estimate, i.e., EI in this application, is viewed as the "state" of a system. To establish the model, we treat this "state" invariant in time but affected by noise, which leads to the state equation expressed as,

$$EI(k+1) = EI(k) + \varpi(k+1) \tag{3.5}$$

where the random variable $\varpi(k)$ represents the process noise. The discretized EB model equation in (2.18) is used as the measurement equation but with PA and RMR as system inputs. If the state of this system is denoted by $x = [EI]$, the input by $u = [PARMR]^T$ and the output $y = [GWG]$ respectively, we can write the dynamics of this discrete system by coupling (3.5) with (2.18) as,

$$x(k+1) = A\ x(k) + B\ u(k+1) + \varpi(k+1) \tag{3.6a}$$

$$y(k+1) = C\ x(k+1) + D\ u(k+1) + \nu(k+1) \tag{3.6b}$$

where $A = I$, $B = \mathbf{0}$, $C = [K_1]$, and $D = [K_2\ K_2]$. The random variable $\nu(k)$ represents the measurement noise.

As shown in the system equations per (3.6), both the model prediction and the measurement are subject to noise. We assume these two noise terms, $\varpi(k)$ and $\nu(k)$ are independent and identically distributed (*i.i.d.*) over time, zero mean Gaussian signals with variance ϑ^2 and σ^2 respectively, that is, $\varpi(k) \sim N(0, \vartheta^2)$ and $\nu(k) \sim N(0, \sigma^2)$ for all k.

Kalman filtering, or any other recursive filtering technique involves two steps: "Predict" and "Update". The "Predict" step generates the *a priori* estimates of the states based on the known system model, while the "Update" step makes modification to the priori estimates according to the latest measurement and gives a new estimate, called the *a posteriori* estimate. This correction step is also called the innovation process. The detailed KF algorithm is described below, where "hat" denotes the estimate, P the error covariance, and K the Kalman gain.

1. **Initialize**:

   Set $\hat{x}(0|0) = EI_0$, $P(0|0) = I$. EI_0 is the initial value of EI, calculated using the regression formula which fits the baseline energy expenditure EE_0 data using the doubly labeled water (DLW) method from the IOM/National Academy of Sciences (NAS) database (IOM (2005)), as shown below,

   $$EI_0 = EE_0 = 0.278W_b^2 + 9.2893W_b + 1528.90 \tag{3.7}$$

2. **Predict**: The prediction stage is independent of the update stage and can be expressed as:

   $$\hat{x}(k+1|k) = A\hat{x}(k|k) + Bu(k+1); \tag{3.8}$$

   $$P(k+1|k) = AP(k|k)A' + Q(k+1); \tag{3.9}$$

3. **Update**: The model estimates from "Predict" step is corrected base on measurements:

   $$K(k+1) = P(k+1|k)C'[CP(k+1|k)C' + R(k+1)]^{-1}; \tag{3.10}$$

   $$\hat{x}(k+1|k+1) = \hat{x}(k+1|k) + K(k+1)[y(k+1) - \hat{y}(k+1|k)]; \tag{3.11}$$

   $$P(k+1|k+1) = (I - K(k+1)C)P(k+1|k). \tag{3.12}$$

where $Q(k+1)$ is the covariance for process noise $\varpi(k+1)$ with $Q(k+1) = \vartheta^2$; $R(k+1)$ is the covariance for measurement noise $\nu(k+1)$ with $R(k+1) = \sigma^2$. Q and R can be used as adjustable parameters to influence the performance of the KF estimation algorithm.

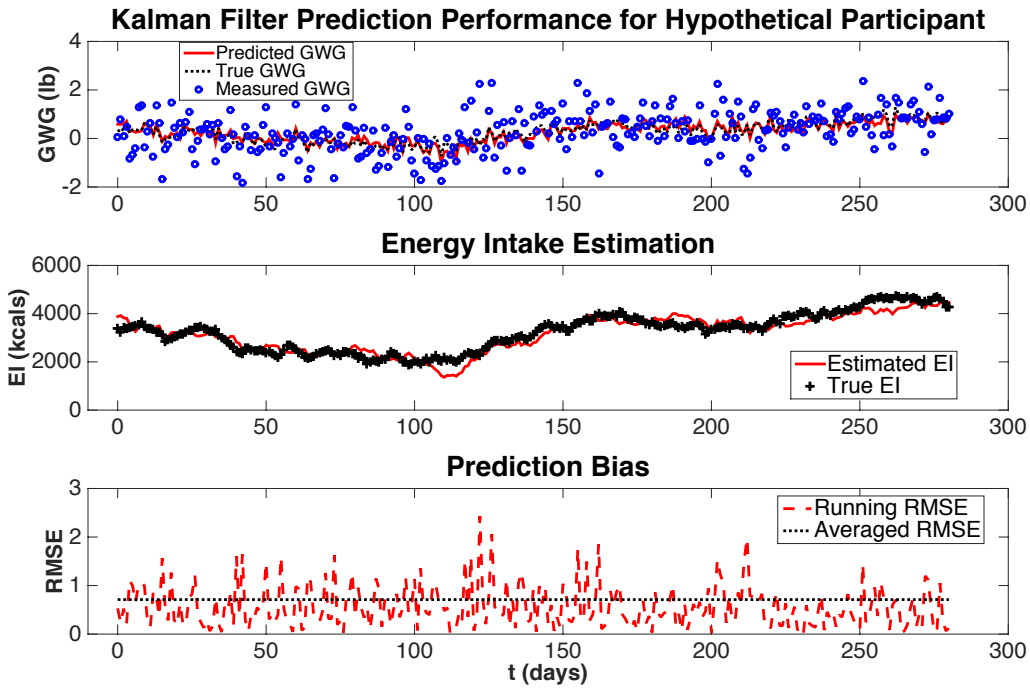

Figure 3.4: Performance of the KF algorithm, illustrated using a hypothetical participant. $RMSE$ stands for Root Mean Square Error.

For performance evaluation, we use the Root Mean Square Error ($RMSE$) as the metric, which is defined as,

$$RMSE = \sqrt{\frac{1}{T_{span}} \sum_{k=1}^{T_{span}} (\hat{y}(k) - y(k))^2} \tag{3.13}$$

$T_{span} = 1$ when calculating the running $RMSE$.

To test the performance of the algorithm, we create the input data, output data, as well as noise with known statistics for a hypothetical participant. A simulation result using the hypothetical data is presented in Fig. 3.4; $Q = \vartheta^2 = 10000$, $R = \sigma^2 = 0.1$. It can be seen that the EI "adapts" from a given initial value and keeps tracking the true EI closely despite the presence of noise during the KF algorithm. The algorithm also produces better weight gain predictions than the noise corrupted measurements.

The results of the two simulations using actual participant data from Phase I Study are presented in Fig. 3.5, where $Q = \vartheta^2 = 100000$, $R = \sigma^2 = 0.2$ are set for both participants. It can be seen that the estimates of the true EI using this algorithm lie above the self-reported

measures of EI, which is consistent with what we find using the two estimation approaches presented in the preceding sections. From the simulation result, the $ME \pm SD$ of the EI estimate is 2711 $\pm$ 568 kcal for participant A, and 3198 $\pm$ 784 kcal for participant B.

For these two estimation methods, we are assuming both the measured physical activity and the estimated resting metabolic rate are accurate, so they can serve as inputs in the KF model per (3.6). While the measurements of energy intake from self-reports are usually more biased from the actual values and uncertain due to the considerable noise, the measurements of resting metabolic rate and physical activity are also subject to measurement error or noise. This can be caused, for example, by occasional misuse of the *Breezing* device against the correct protocol, or overreporting physical activity by recording the movement of the arms only with a wrist accelerometer. Hence, a KF algorithm that can filter out the noise in either or both of the other key determinants of the energy balance model will be useful in real-life weight control interventions.

Motivated from this standpoint, some extensions of the KF approach are demonstrated below for the application of multiple state estimation during weight interventions. To include more than one state in the systems model, we re-write our systems equations in the form of (3.6) by reallocating the states to estimate and the state matrices. For two-state systems, EI remains as the first state to be estimated, and either RMR or PA can be used as the second state that needs to be estimated from noisy measurements. For the case of estimating EI and RMR from noise-corrupted measurement of GWG and RMR, the system can be written as: $x = [EI\ RMR]^T$, $y = [GWG\ RMR]^T$, $u = [PA]$, where PA measurement can be treated as a noise-free input; For estimating EI and PA from uncertain measurement of GWG and PA and noiseless measurement of RMR, the system is $x = [EI\ PA]^T$, $y = [GWG\ PA]^T$, $u = [RMR]$. That is, one of the two signals of RMR and PA is used as a noise-corrupted output, while the other used as a noise-free input. For either of these two models, system matrices can be derived as: $C = \begin{bmatrix} K_1 & K_2 \\ 1 & 0 \end{bmatrix}$, $A = I$.

With the established models, standard KF algorithm can be applied to these systems to

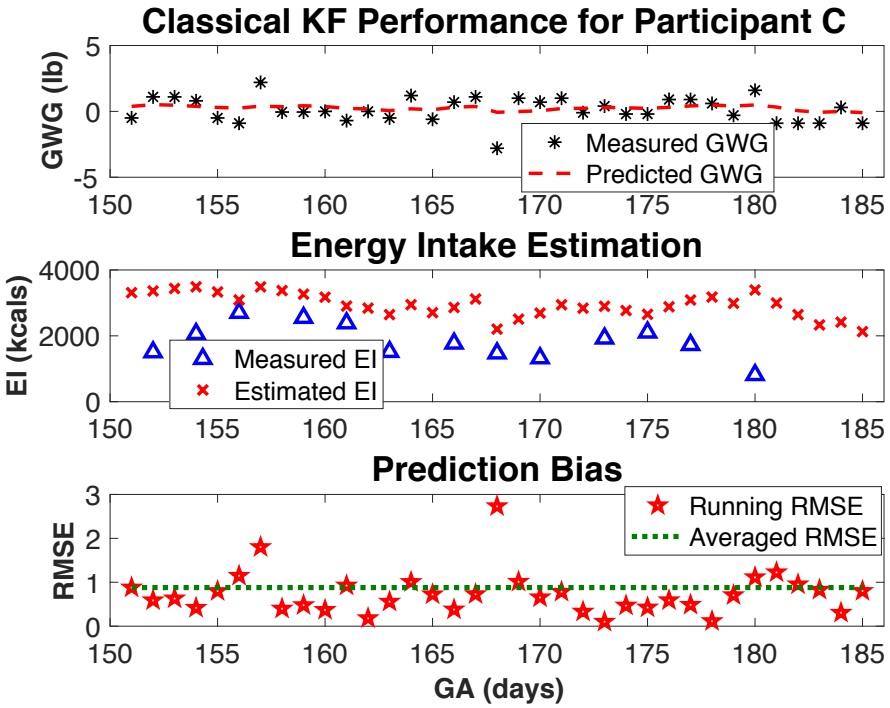

(a)

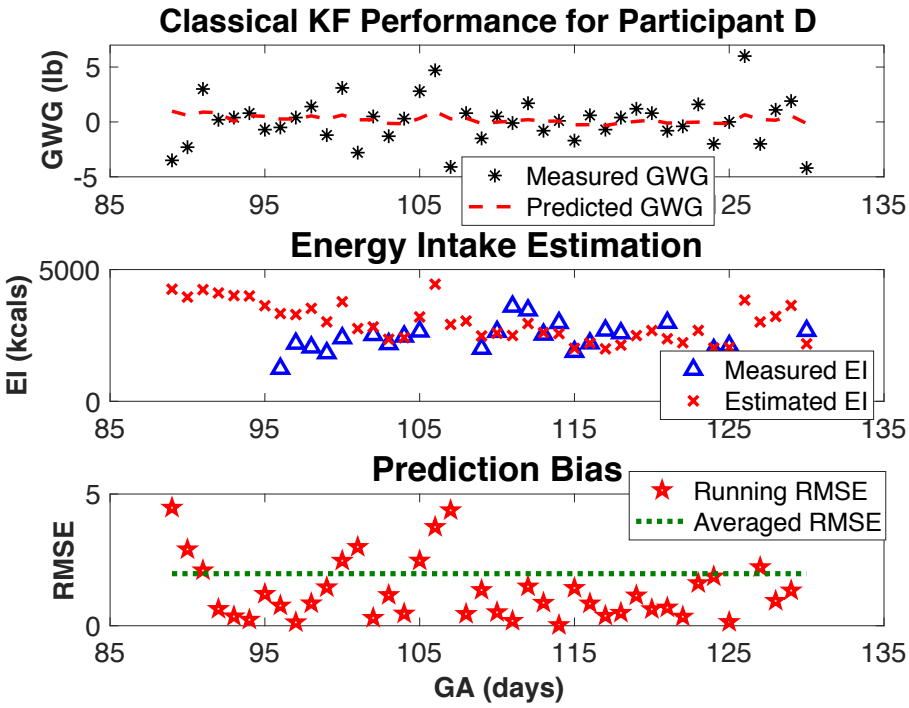

(b)

Figure 3.5: Performance of the KF algorithm for estimating *EI* evaluated using two participants from the Phase I Study of the HMZ.

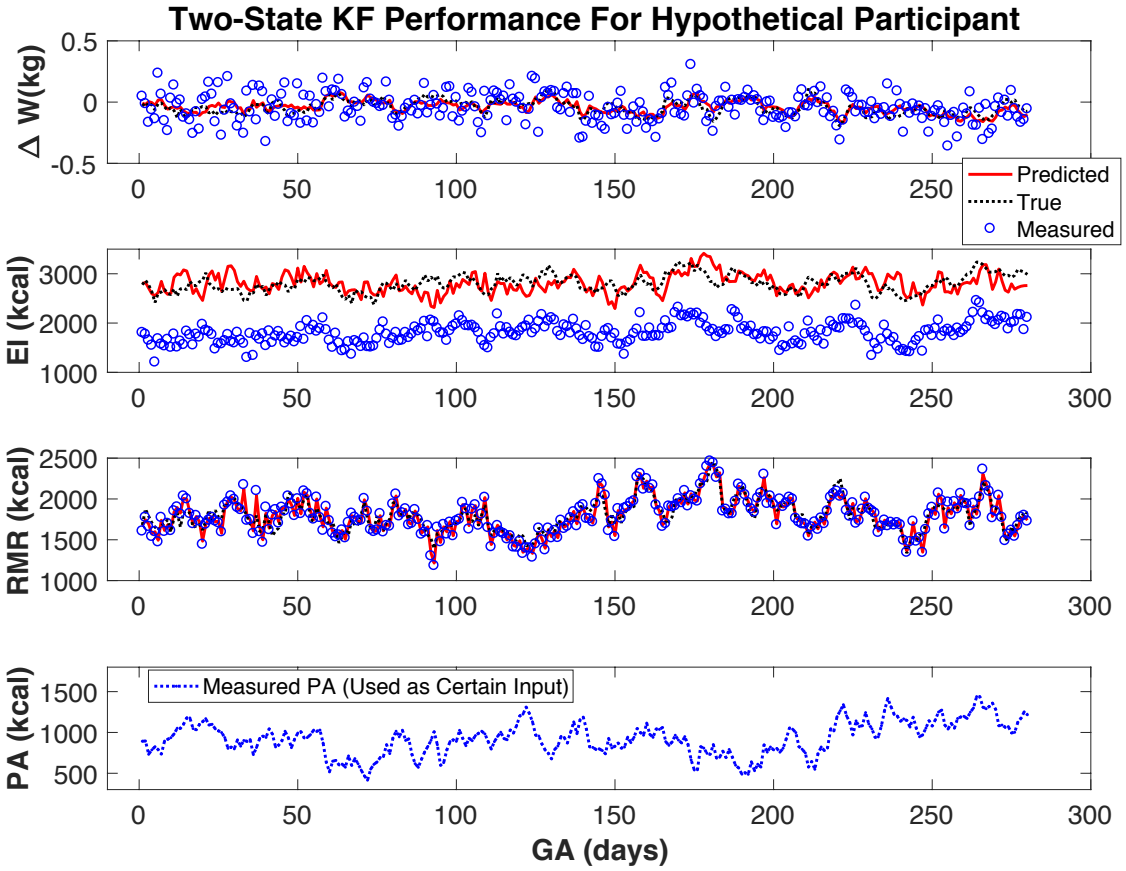

Figure 3.6: The performance of the KF algorithm for the two-state system ($x = [EI\ RMR]^T$ with noise-free input of PA) illustrated using hypothetical data.

realize state estimation. Here, hypothetical participant data with averaged EI underreporting of 1000 kcal is used for performance demonstration. For this hypothetical participant who has the same system gains as Participant A ($K_1 = 1.94\times10^{-4}$ and $K_2 = -2.15\times10^{-4}$), two simulation examples based on the listed two models are shown in Fig. 3.6 and 3.7 respectively. All the measurements are assumed to be obtained daily. For both the two cases, it is assumed that $Q = \begin{bmatrix} 10000 & 0 \\ 0 & 10000 \end{bmatrix}$, $R = \begin{bmatrix} 0.01 & 0 \\ 0 & 10000 \end{bmatrix}$. As we can see from the results, KF algorithm can successfully filter out the noise in the measurement of the outputs and return a good estimation of the EI regardless of the underreporting in the energy intake.

For three-state systems, both the RMR and PA are treated as states in addition to EI. The corresponding system is formulated as $x = [EI\ RMR\ PA]^T$, $y = [GWG\ RMR\ PA]^T$

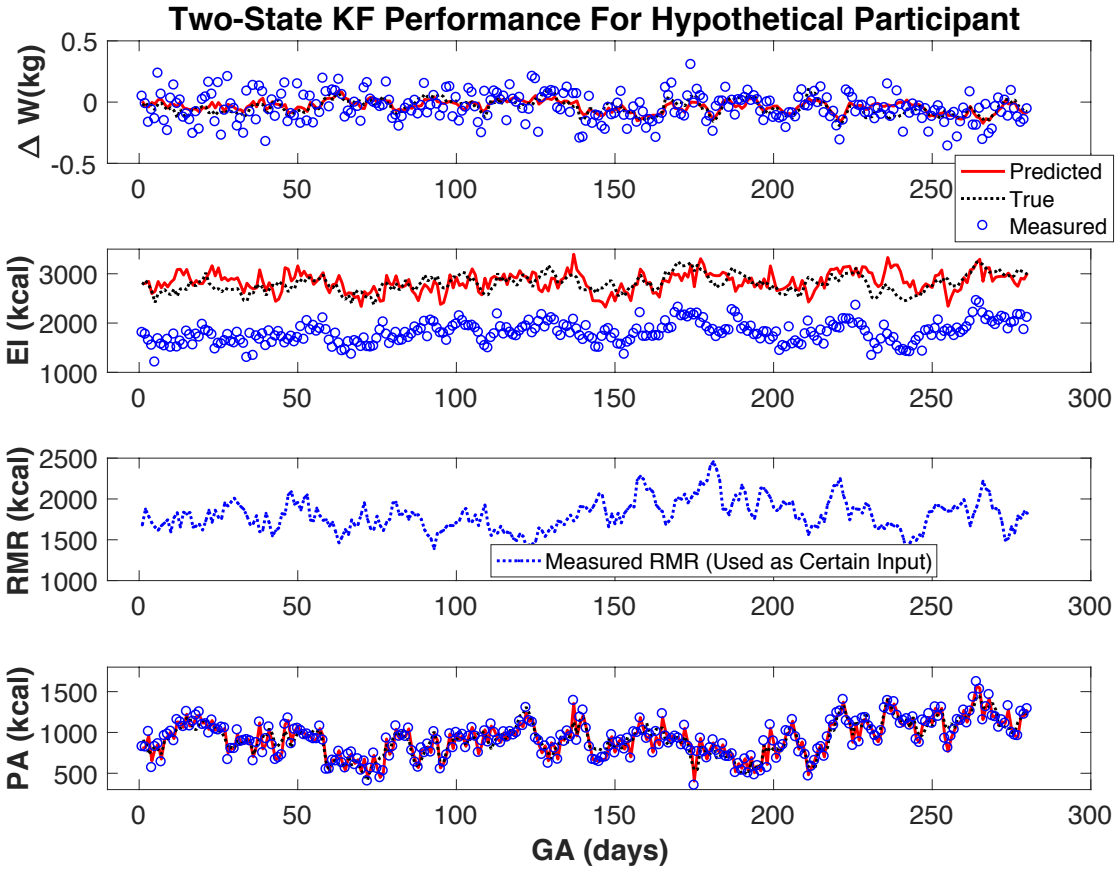

Figure 3.7: The performance of the KF algorithm for the two-state system ($x = [EI\ PA]^T$ with noise-free input of RMR) illustrated using hypothetical data.

with $C = \begin{bmatrix} K_1 & K_2 & K_2 \\ 0 & 1 & 0 \\ 0 & 0 & 1 \end{bmatrix}$, $A = I$, where all the measurements of GWG, RMR, and PA are assumed to be noisy. Standard KF algorithm can be applied to this three-state system, and the performance is demonstrated with the same hypothetical data that is used to illustrate the two-state systems. With $Q = \begin{bmatrix} 10000 & 0 & 0 \\ 0 & 10000 & 0 \\ 0 & 0 & 10000 \end{bmatrix}$, $R = \begin{bmatrix} 0.01 & 0 & 0 \\ 0 & 10000 & 0 \\ 0 & 0 & 10000 \end{bmatrix}$, the estimation results are simulated and shown in Fig. 3.8. It can seen that computational error arises from the estimation with the state estimates diverging from the true values.

To explain the errors, observability analysis is re-examined. Observability refers to the property of the system that is used to determine whether the states of the system can be inferred based on the measured output. In order to be able to use Kalman filter for

state estimation, the model set up for the KF algorithm has to be observable, which can be determined by examining whether the rank of the observability matrix of the model $\mathcal{O} = [C^T \ A^T C^T \ \cdots \ (A^T)^{(n-1)} C^T]$ equal to n, where n is the number of estimated states. In the state space model for EI estimation with Kalman filtering algorithm per (3.6), for example, it is easy to confirm that the rank of the observability gramian matrix $\mathcal{O} = [K_1]$ equals 1, which corresponds to the number of the estimated system states. Thus, the model is fully observable and applicable for Kalman filtering.

For the three-state system, the observability matrix can be obtained as below,

$$\mathcal{O} = \begin{bmatrix} K_1 & 1 & 0 & K_1 & 1 & 0 & K_1 & 1 & 0 \\ K_2 & 1 & 0 & K_2 & 1 & 0 & K_2 & 1 & 0 \\ K_2 & 0 & 1 & K_2 & 0 & 1 & K_2 & 0 & 1 \end{bmatrix} \tag{3.14}$$

With the pre-determined system gains $K_1 = 1.94 \times 10^{-4}$ and $K_2 = -2.15 \times 10^{-4}$, this observability matrix has a rank of 3 but condition number of 5154.6. The condition number should ideally be close to unit. Hence, with technically full rank, $\mathcal{O}$ is an ill-conditioned matrix due to the small values of K_1 and K_2. Once this kind of model is applied with the KF algorithm, it is likely to result in computation error as show in Fig. 3.8 where the system cannot converge. To overcome the observability issue, EI has to be set as one of the outputs for the three-state system, reformulating the system as $x = [EI \ RMR \ PA]^T$, $y = [GWG \ EI \ RMR \ PA]^T$. This means, the measurement of EI is required for the implementation of the algorithm and cannot be significantly biased/underreporting from the true EI, assuming there is only noise existed in the EI measures.

Therefore, due to the inherent observability problem of the model, one needs to be careful when setting up the system for the KF approach to be applied. For the current maternal energy balance model for gestational weight gain interventions, estimation of EI underreporting is only possible for the one/two-state system, while three-state system requires un-biased EI measures. If more than two variables need to be estimated simultaneously, EI measurement needs to be unbiased so that it can be used as one of the outputs in order for KF estimation to be implemented.

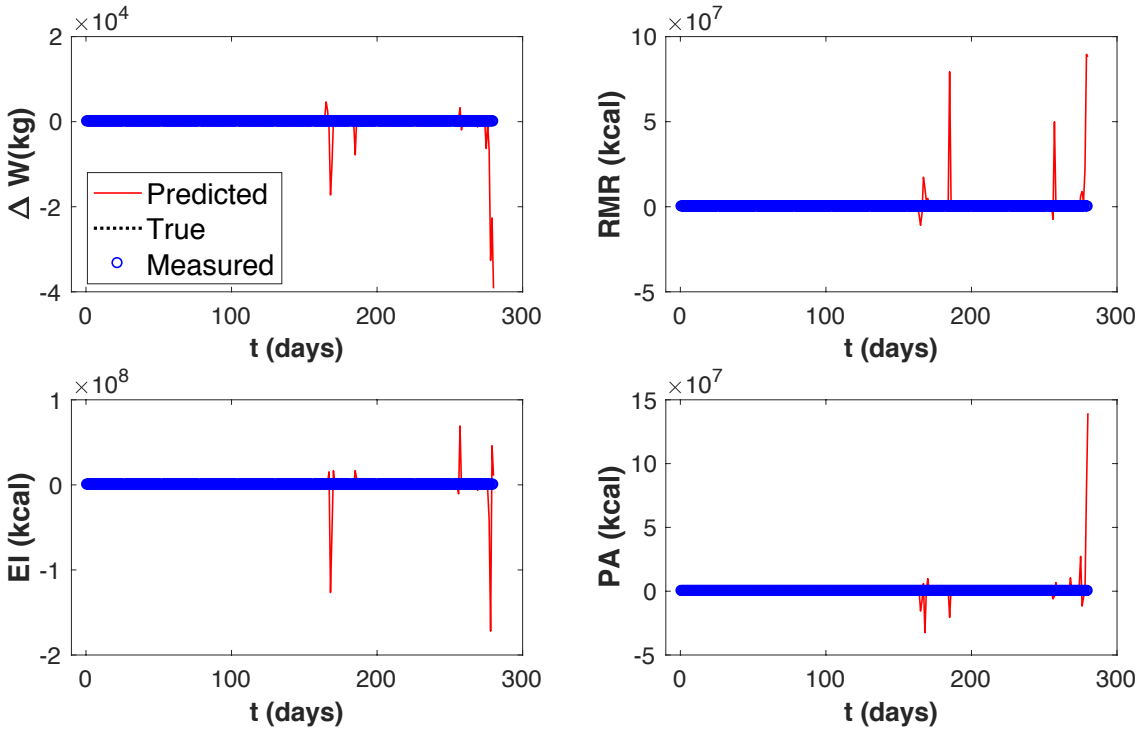

Figure 3.8: The performance of the KF algorithm for the three-state ill-conditioned system illustrated using hypothetical data.

Note that data missingness is not considered in this section. In real-life weight interventions, however, measurement loss is common in data collection. An inevitable partial or complete loss of measurements may also occur when a participant forgets to take any of those self-measures occasionally. For example, a participant might forget to record W and EI on a certain day, while PA is still recorded by wearing the tracking device. This is more common with long-duration interventions, in which the measurements can be lost in a random fashion. Also note that, if one component is not measured on a given day, the measurements of other components are likely to be missing for that same day as well. So the probability of measurement loss for individual components may be correlated with each other. All these flaws in the measured data can impact the accurate assessment of the effectiveness of the intervention, especially when a quantitative energy balance model is involved. Hence, an on-line algorithm that can address the issue of missing data to realize real-time estimation can be useful for the success of weight interventions. In next section,

a Kalman filter-based algorithm for intermittent measurements is developed and demonstrates significant potential for real-time use. The observability analysis for the current maternal energy balance model will be useful for the system set-up when illustrating the algorithm with numerical examples.

3.3 Kalman Filtering Approach Under Partial Measurement Losses

It has been pointed out in the previous section that data imputation techniques, such as linear interpolation, are still required to address the issue of missing data during the implementation of the classical Kalman filtering approach. In real-life behavior weight management interventions, however, the data available for modeling and estimation is corrupted not only by measurement noise, but also with possible missingness. If a measurement is determined to be physiological implausible due to significant error, it has to be discarded for assessment, resulting in additional data missingness. The classical Kalman filtering approach is technically not realizable for on-line estimation at the presence of data missingness. Based on the nature of this problem, an optimal recursive estimator that allows on-line estimation in the presence of inevitable random measurement losses would be the most suitable option for this application.

In this section, we present a filtering approach with time-varying Kalman gains to cope with intermittent observations. The problem of Kalman filtering with intermittent measurements has been examined in many recent papers. In the study by Sinopoli *et al.* (2004), the random arrival of measurements is modeled as a Bernoulli process, which is characterized by an independent probability parameter λ (bounded between 0 and 1). Compared to the classical Kalman filtering formula, the Algebraic Riccati Equation (ARE) used for the iteration of the error covariance matrix becomes stochastic due to the random observation losses. The boundness of the convergence of the iteration proves to be ensured if λ is greater than the critical arrival rate λ_c. The results in Sinopoli *et al.* (2004) are based on the assumption that each set of measurements at a sampling time is either obtained in full or lost completely. Liu and Goldsmith (2004) generalize the analysis by allowing partial loss

of observations, where the measurement loss of each output element needs to be considered separately. However, the derivation of the Kalman filter updates with partial measurement losses in Liu and Goldsmith (2004) is limited to a system with only two output elements. In weight interventions, there are at least three key energy balance components that can be measured separately (W, EI and EE related terms as shown in (2.16)), and sometimes even more than three if any of the components is divided into and measured in multiple sub-components, such as EE being divided into PA, RMR and TEF as noted in Chapter 2. Thus, a general formula of the recursive algorithm needs to be developed to accommodate an arbitrary system with multiple output elements. Additionally, the analysis in Liu and Goldsmith (2004) assumes the probability distributions of the measurement losses to be independent with each other, that is, the intermittent measurements are described with two *i.i.d.* Bernoulli variables. In this work, the observation losses among different components can be mutually correlated instead of independent. For example, if one component is not measured on a given day, the measurements of other components are likely to be missing for that same day also. So the probability of measurement loss for individual components may be correlated with each other. Consequently, the correlation of observation losses needs to be incorporated in the problem formulation and can be reflected with the joint probability density functions. Such settings have been established and studied by Deshmukh *et al.* (2014), where the convergence can also be ensured and the bounds on λ_c can also be computed by adding constraints from the joint probability density functions. In addition to the work mentioned above, similar derivation and analysis recently have been extended to non-linear systems for which the extended Kalman filtering with intermittent observations is investigated (Ahmad and Namerikawa (2013); Hu *et al.* (2012)).

Inspired from these papers, we develop a recursive algorithm based on Kalman filtering with correlated measurement losses as an extension to the two element study in Liu and Goldsmith (2004), and also provide an EKF-based algorithm to enable a broader application. Such exploration has been published in Guo *et al.* (2017). The presented algorithms

differ from the classical KF mainly by defining stochastic updates of the innovation process which is dependent on the random arrivals of measurements. The random measurement loss is modeled as a Bernoulli process with binary sequences taking values of 0 or 1. When it comes to a missing data point, the estimator treats it as receiving a measurement consisting of noise alone. Partial data loss is considered in the derivation of the Kalman filter updates where the availability of measurements of individual components is modeled separately. In practice of long-duration interventions, it is common that the participant may forget to complete measures of a single or multiple determinants of the EB model on the same day occasionally. For example, a participant might forget to record W and EI on a certain day, while PA is still recorded by wearing the tracking device. Hence, partial random data loss is considered and incorporated in the formulation of the algorithm for enhancement. Simulation studies are presented to illustrate the performance of the algorithms and the potential benefits of this technique in real-life interventions.

3.3.1 Linear System With Measurement Losses

Algorithm

The detailed development of this Kalman filter-based algorithm for intermittent measurements based on linear systems is elaborated in this section. Consider a multiple-input multiple-output (MIMO) discrete time linear system model with three output elements. The state and measurement equations of the system are defined as follows:

$$x_{k+1} = A\ x_k + B\ u_k + \varpi_k \tag{3.15a}$$

$$\underbrace{\begin{bmatrix} y_{1,k} \\ y_{2,k} \\ y_{3,k} \end{bmatrix}}_{y_k} = \underbrace{\begin{bmatrix} C_1 \\ C_2 \\ C_3 \end{bmatrix}}_{C} x_k + \underbrace{\begin{bmatrix} \nu_{1,k} \\ \nu_{2,k} \\ \nu_{3,k} \end{bmatrix}}_{\nu_k} \tag{3.15b}$$

where k is the sampling time; $x_k, \varpi_k \in \mathbb{R}^n$ are the state and noise of the system, respectively; $u_k \in \mathbb{R}^p$ is the system input; $y_k, \nu_k \in \mathbb{R}^{\Sigma_{i=1}^{3} m_i}$ are the measurement and measurement noise

with elements $y_{i,k}, \nu_{i,k} \in \mathbb{R}^{m_i}$, respectively; A, B, and C are the system matrices with appropriate dimensions. We assume that ϖ_k and $\nu_{i,k}$ are uncorrelated zero-mean Gaussian white noise with covariances of $Q \geq 0$ and $R_{ii} > 0$, respectively, that is $\varpi_k \sim \mathcal{N}(0, Q)$ and $\nu_{i,k} \sim \mathcal{N}(0, R_{ii})$; R is the block-diagonal covariance matrix for ν_k with the matrices R_{ii} on the diagonal, written as $R = diag\{R_{11}, R_{22}, R_{33}\}$. For the system described per (3.15), we also assume that (A, B) is completely stabilizable and (A, C) completely detectable so that the error covariance of Kalman filter converges to a unique value in case of no measurement loss.

To incorporate measurement loss in the algorithm, we use the Bernoulli variable $\gamma_{i,k}$ to model the random arrivals of the measurements: $\gamma_{i,k}$ taking the value of 1 indicates the measurement of the corresponding element, $y_{i,k}$, has been successfully received at time k, whereas its value of 0 indicates a measurement loss. $\gamma_{i,k}$ is assumed to have known probability distributions. Here, in order to simulate real-life intervention conditions, we assume correlation exists among $\gamma_{1,k}$, $\gamma_{2,k}$, and $\gamma_{3,k}$. Thus, the joint probability density function of $\Pr(\gamma_{1,k}, \gamma_{2,k}, \gamma_{3,k})$ is used. Note that $\gamma_{i,k}$ assumes to be independent of $\gamma_{j,l}$ if $k \neq l$.

The loss of a measurement can be treated equivalently as receiving a measurement with infinite noise variance. In the presence of measurement loss, the statistical characteristics of measurement noise will change accordingly and cannot be fully described with $\nu_{i,k}$ in (3.15b). Thus, a second measurement noise term $\nu'_{i,k}$ is introduced and defined with $\nu'_{i,k} \sim \mathcal{N}(0, R'_{ii})$, with $R'_{ii} \to \infty$. $\nu'_{i,k}$ has the same structure and dimensions as $\nu_{i,k}$. Similarly, we have $\nu'_k = [{\nu'_{1,k}}^T \; {\nu'_{2,k}}^T \; {\nu'_{3,k}}^T]^T \sim \mathcal{N}(0, R')$ with $R' = diag\{R'_{11}, R'_{22}, R'_{33}\}$.

With the augmentation of the variables $\gamma_{i,k}$ and $\nu'_{i,k}$, the measurement equation per

(3.15b) can be redefined for a general case with observation losses as

$$\begin{bmatrix} y_{1,k} \\ y_{2,k} \\ y_{3,k} \end{bmatrix} = \begin{bmatrix} \gamma_{1,k}(C_1 x_k + \nu_{1,k}) \\ \gamma_{2,k}(C_2 x_k + \nu_{2,k}) \\ \gamma_{3,k}(C_3 x_k + \nu_{3,k}) \end{bmatrix} + \begin{bmatrix} (1-\gamma_{1,k})\nu'_{1,k} \\ (1-\gamma_{2,k})\nu'_{2,k} \\ (1-\gamma_{3,k})\nu'_{3,k} \end{bmatrix}$$

$$= \underbrace{\begin{bmatrix} \gamma_{1,k}C_1 \\ \gamma_{2,k}C_2 \\ \gamma_{3,k}C_3 \end{bmatrix}}_{\widetilde{C}_k} x_k + \underbrace{\begin{bmatrix} \gamma_{1,k}\nu_{1,k} + (1-\gamma_{1,k})\nu'_{1,k} \\ \gamma_{2,k}\nu_{2,k} + (1-\gamma_{2,k})\nu'_{2,k} \\ \gamma_{3,k}\nu_{3,k} + (1-\gamma_{3,k})\nu'_{3,k} \end{bmatrix}}_{\widetilde{\nu}_k} \tag{3.16}$$

Note that the measurement equation per (3.16) now becomes time-varying and stochastic in nature, due to the time-varying matrix $\widetilde{C}_k$ being a function of the random variables $\gamma_{i,k}$. The elements of the new noise vector follow $\widetilde{\nu}_{i,k} \sim \mathcal{N}(0, \widetilde{R}_{ii})$ with $\widetilde{R}_{ii} = \gamma_{i,k}R_{ii} + (1-\gamma_{i,k})R'_{ii}$, leading to $\widetilde{\nu}_k \sim \mathcal{N}(0, \widetilde{R})$ with $\widetilde{R} = diag\{\widetilde{R}_{11}, \widetilde{R}_{22}, \widetilde{R}_{33}\}$. From here, we re-derive the Kalman filter algorithm based on the time-varying system as described per (3.15a) and (3.16).

Following the Kalman filtering approach, we define,

$$\begin{aligned} \hat{x}_{k|k} &\triangleq \mathbb{E}\left[x_k |\ y_0^k, u_0^k, \gamma_0^k\right] \\ P_{k|k} &\triangleq \mathbb{E}\left[(x_k - \hat{x}_{k|k})(x_k - \hat{x}_{k|k})^T |\ y_0^k, u_0^k, \gamma_0^k\right] \\ \hat{x}_{k+1|k} &\triangleq \mathbb{E}\left[x_{k+1} |\ y_0^k, u_0^k, \gamma_0^k\right] \\ P_{k+1|k} &\triangleq \mathbb{E}\left[(x_{k+1} - \hat{x}_{k+1|k})(x_{k+1} - \hat{x}_{k+1|k})^T |\ y_0^k, u_0^k, \gamma_0^k\right] \end{aligned} \tag{3.17}$$

where x_k, $\hat{x}_{k|k}$, and $\hat{x}_{k+1|k}$ represent the true state, the *a posteriori* and *a priori* state estimate; $\hat{P}_{k|k}$ and $\hat{P}_{k+1|k}$ denotes the *a posteriori* and *a priori* error covariance matrix; $\gamma_k = [\gamma_{1,k}\ \gamma_{2,k}\ \gamma_{3,k}]^T$, $\gamma_0^k = \{\gamma_0, \cdots, \gamma_k\}$, and $y_0^k = \{y_0, \cdots, y_k\}$.

The prediction step of this KF based algorithm to compute $\hat{x}_{k+1}$ and $P_{k+1|k}$ uses the information from the state equation only, so it remains deterministic as in the classical

Kalman filter:

$$\begin{aligned} \hat{x}_{k+1|k} &= A\ \hat{x}_{k|k} + B\ u_k + \varpi_k \\ P_{k+1|k} &= A\hat{P}_{k|k}A^T + Q \end{aligned} \tag{3.18}$$

However, the correction step becomes stochastic due to its dependence on the observation process:

$$\begin{aligned} \hat{x}_{k+1|k+1} &= \hat{x}_{k+1|k} + K_{k+1}(y_{k+1} - \widetilde{C}_{k+1}\hat{x}_{k+1|k}) \\ P_{k+1|k+1} &= P_{k+1|k} - K_{k+1}\widetilde{C}_{k+1}P_{k+1|k} \end{aligned} \tag{3.19}$$

where $K_{k+1} = P_{k+1|k}\widetilde{C}_{k+1}^T(\widetilde{C}_{k+1}P_{k+1|k}\widetilde{C}_{k+1}^T + \widetilde{R})^{-1}$ is the optimal Kalman gain computed by minimizing $P_{k+1|k+1}$, that is, K_{k+1} given by the solution to the following equation:

$$\frac{\partial P_{k+1|k+1}}{\partial K_{k+1}} = 0 \tag{3.20}$$

Given the random set of γ_k at each sampling time k, we can expect that there exists $2^3 = 8$ possible scenarios for measurement loss: Specifically, the number of missing elements can range from 0 to 3, with 0 as the measurement set being completely received and 3 indicating completely lost. The probability of each combination can be calculated from the joint probability function $\Pr(\gamma_{1,k}, \gamma_{2,k}, \gamma_{3,k})$. In the following, the Kalman filter update equations based on four possible scenarios is discussed.

Scenario 1: No Observation Loss

This is the case where $\gamma_k = [1\ 1\ 1]^T$. The measurement equation per (3.16) becomes the same as (3.15b) with $\widetilde{C}_k = C$ and $\widetilde{\nu}_k = \nu_k$, so the system becomes completely observable with the measurement noise covariance of R. Hence, the corrector equations remain the same as in the standard Kalman filter formulation, expressed as:

$$\begin{aligned} \hat{x}_{k+1|k+1} &= \hat{x}_{k+1|k} + P_{k+1|k}C^T(CP_{k+1|k}C^T + R)^{-1} \times (y_{k+1} - C\hat{x}_{k+1|k}) \\ P_{k+1|k+1} &= P_{k+1|k} - P_{k+1|k}C^T(CP_{k+1|k}C^T + R)^{-1}\ \times CP_{k+1|k} \end{aligned} \tag{3.21}$$

Scenario 2: Complete Observation Loss

The complete observation loss is mathematically modeled by $\gamma_k = [0\ 0\ 0]^T$, leading to the description of the system per (3.16) simplified as $y_k = \nu'_k$. The corrector equations are equivalent to (3.21) by assigning $C = \mathbf{0}$ and replacing R with $R' \to \infty$, which gives

$$\begin{aligned} \hat{x}_{k+1|k+1} &= \hat{x}_{k+1|k} \\ P_{k+1|k+1} &= P_{k+1|k} \end{aligned} \tag{3.22}$$

Equation (3.22) shows that the corrector updates the state estimate by directly propagating the *a priori* estimate when the system is completely unobservable.

Scenario 3: Single Observation Loss

There are three possible cases to be discussed when a single observation is lost. Because of space limitations, only the derivation for the case of $\gamma_{1,k} = 0, \gamma_{2,k} = \gamma_{3,k} = 1$ is described in detail here. Before using (3.19), note that the following holds:

$$\begin{aligned} & \widetilde{C}_k^T (\widetilde{C}_k P_{k+1|k} \widetilde{C}_k^T + \widetilde{R})^{-1} \widetilde{C}_k \\ = \ & \widetilde{C}_k^T (\widetilde{C}_k P_{k+1|k} \widetilde{C}_k^T + R + diag\{(R'_{11} - R_{11}), 0, 0\})^{-1} \widetilde{C}_k \\ = \ & \widetilde{C}_k^T \begin{bmatrix} 0 & 0 & 0 \\ 0 & \mathcal{M}_{22} - \mathcal{M}_{21}\mathcal{M}_{11}^{-1}\mathcal{M}_{12} & \mathcal{M}_{23} - \mathcal{M}_{21}\mathcal{M}_{11}^{-1}\mathcal{M}_{13} \\ 0 & \mathcal{M}_{32} - \mathcal{M}_{31}\mathcal{M}_{11}^{-1}\mathcal{M}_{12} & \mathcal{M}_{33} - \mathcal{M}_{31}\mathcal{M}_{11}^{-1}\mathcal{M}_{13} \end{bmatrix} \widetilde{C}_k \\ = \ & \widetilde{C}_k^T \begin{bmatrix} 0 & 0 \\ 0 & \left(\begin{bmatrix} C_2 \\ C_3 \end{bmatrix} P_{k+1|k} \begin{bmatrix} C_2 \\ C_3 \end{bmatrix}^T + \begin{bmatrix} R_{22} & 0 \\ 0 & R_{33} \end{bmatrix} \right)^{-1} \end{bmatrix} \widetilde{C}_k \\ = \ & \begin{bmatrix} C_2 \\ C_3 \end{bmatrix}^T \left(\begin{bmatrix} C_2 \\ C_3 \end{bmatrix} P_{k+1|k} \begin{bmatrix} C_2 \\ C_3 \end{bmatrix}^T + \begin{bmatrix} R_{22} & 0 \\ 0 & R_{33} \end{bmatrix} \right)^{-1} \begin{bmatrix} C_2 \\ C_3 \end{bmatrix} \end{aligned} \tag{3.23}$$

where $(\widetilde{C}_k P_{k+1|k} \widetilde{C}_k^T + R)^{-1} = \begin{bmatrix} \mathcal{M}_{11} & \mathcal{M}_{12} & \mathcal{M}_{13} \\ \mathcal{M}_{21} & \mathcal{M}_{22} & \mathcal{M}_{23} \\ \mathcal{M}_{31} & \mathcal{M}_{32} & \mathcal{M}_{33} \end{bmatrix}$. By combining (3.23) with (3.19), the update step for this case becomes

$$\begin{aligned} \hat{x}_{k+1|k+1} &= \hat{x}_{k+1|k} + P_{k+1|k} \begin{bmatrix} C_2 \\ C_3 \end{bmatrix}^T \Big(\begin{bmatrix} C_2 \\ C_3 \end{bmatrix} P_{k+1|k} \begin{bmatrix} C_2 \\ C_3 \end{bmatrix}^T + \begin{bmatrix} R_{22} & 0 \\ 0 & R_{33} \end{bmatrix} \Big)^{-1} \Big(\begin{bmatrix} y_{2,k} \\ y_{3,k} \end{bmatrix} + \begin{bmatrix} C_2 \\ C_3 \end{bmatrix} \hat{x}_{k+1|k} \Big) \\ P_{k+1|k+1} &= P_{k+1|k} - P_{k+1|k} \begin{bmatrix} C_2 \\ C_3 \end{bmatrix}^T \Big(\begin{bmatrix} C_2 \\ C_3 \end{bmatrix} P_{k+1|k} \begin{bmatrix} C_2 \\ C_3 \end{bmatrix}^T + \begin{bmatrix} R_{22} & 0 \\ 0 & R_{33} \end{bmatrix} \Big)^{-1} \begin{bmatrix} C_2 \\ C_3 \end{bmatrix} P_{k+1|k} \end{aligned} \tag{3.24}$$

The mathematical analysis for the other two cases is quite similar. For an arbitrary case of single observation loss, the update step can be generalized as:

$$\begin{aligned} \hat{x}_{k+1|k+1} &= \hat{x}_{k+1|k} + P_{k+1|k} \begin{bmatrix} C_j \\ C_l \end{bmatrix}^T \Big(\begin{bmatrix} C_j \\ C_l \end{bmatrix} P_{k+1|k} \begin{bmatrix} C_j \\ C_l \end{bmatrix}^T + \begin{bmatrix} R_{jj} & 0 \\ 0 & R_{ll} \end{bmatrix} \Big)^{-1} \Big(\begin{bmatrix} y_{j,k} \\ y_{l,k} \end{bmatrix} + \begin{bmatrix} C_j \\ C_l \end{bmatrix} \hat{x}_{k+1|k} \Big) \\ P_{k+1|k+1} &= P_{k+1|k} - P_{k+1|k} \begin{bmatrix} C_j \\ C_l \end{bmatrix}^T \Big(\begin{bmatrix} C_j \\ C_l \end{bmatrix} P_{k+1|k} \begin{bmatrix} C_j \\ C_l \end{bmatrix}^T + \begin{bmatrix} R_{jj} & 0 \\ 0 & R_{ll} \end{bmatrix} \Big)^{-1} \begin{bmatrix} C_j \\ C_l \end{bmatrix} P_{k+1|k} \end{aligned} \tag{3.25}$$

Scenario 4: Two Observation Losses

Similar derivation of the correction step for this scenario can be listed as shown in (3.23), leading to the update equations below,

$$\begin{aligned} \hat{x}_{k+1|k+1} &= \hat{x}_{k+1|k} + P_{k+1|k} C_i^T (C_i P_{k+1|k} C_i^T + R_{ii})^{-1} \times (y_{i,k+1} - C_i \hat{x}_{k+1|k}) \\ P_{k+1|k+1} &= P_{k+1|k} - P_{k+1|k} C_i^T (C_i P_{k+1|k} C_i^T + R_{ii})^{-1} \times C_i P_{k+1|k} \end{aligned} \tag{3.26}$$

Generalized Formulation for an Arbitrary System

Based on the detailed derivations of this Kalman filter based algorithm for a three-sensor system, it is possible to extend it to an arbitrary MIMO system with q separate output

sensors, as described below:

$$x_{k+1} = A\ x_k + B\ u_k + \varpi_k \tag{3.27a}$$

$$\underbrace{\begin{bmatrix} y_{1,k} \\ y_{2,k} \\ \vdots \\ y_{q,k} \end{bmatrix}}_{y_k} = \underbrace{\begin{bmatrix} \gamma_{1,k}C_1 \\ \gamma_{2,k}C_2 \\ \vdots \\ \gamma_{q,k}C_q \end{bmatrix}}_{\widetilde{C}_k} x_k + \underbrace{\begin{bmatrix} \gamma_{1,k}\nu_{1,k} + (1-\gamma_{1,k})\nu'_{1,k} \\ \gamma_{2,k}\nu_{2,k} + (1-\gamma_{2,k})\nu'_{2,k} \\ \vdots \\ \gamma_{q,k}\nu_{q,k} + (1-\gamma_{q,k})\nu'_{q,k} \end{bmatrix}}_{\widetilde{\nu}_k} \tag{3.27b}$$

where $\widetilde{\nu}_k \sim \mathcal{N}(0, \widetilde{R})$ with $\widetilde{R} = diag\{\widetilde{R}_{ii} = \gamma_{i,k}R_{ii} + (1-\gamma_{i,k})R'_{ii}, i = 1, 2, \cdots, q\}$. The hypothesis of (A, B) being completely stabilizable and (A, C) completely detectable still holds for this system. It can be expected that there are 2^q possible scenarios for observation loss. Here, we define a notation of $X^-_{\mathbb{Z}_1,\mathbb{Z}_2}$ as a sub-matrix of $X \in \mathbb{R}^{q_1 \times q_2}$ by deleting the rows of X as indexed in $\mathbb{Z}_1$ and the columns indexed in $\mathbb{Z}_2$, respectively. For an arbitrary sequence of measurements defined by $\mathbb{Z} = \{n_1, n_2, \cdots\}\ or\ \{\phi\}$, where $n_1, n_2, \cdots \in \{1, 2, \cdots, q\}$, the generalized formulation for the update equations is expressed as below,

$$\begin{aligned} \hat{x}_{k+1|k+1} &= \hat{x}_{k+1|k} + P_{k+1|k}\{C^-_{\mathbb{Z},\phi}\}^T(\{C^-_{\mathbb{Z},\phi}\}P_{k+1|k}\{C^-_{\mathbb{Z},\phi}\}^T \\ &\quad + R^-_{\mathbb{Z},\mathbb{Z}})^{-1}(\{y_{k+1}\}^-_{\mathbb{Z},\phi} - \{C^-_{\mathbb{Z},\phi}\}\hat{x}_{k+1|k}) \\ P_{k+1|k+1} &= P_{k+1|k} - P_{k+1|k}\{C^-_{\mathbb{Z},\phi}\}^T(\{C^-_{\mathbb{Z},\phi}\}P_{k+1|k}\{C^-_{\mathbb{Z},\phi}\}^T \\ &\quad + R^-_{\mathbb{Z},\mathbb{Z}})^{-1}\{C^-_{\mathbb{Z},\phi}\}P_{k+1|k} \end{aligned} \tag{3.28}$$

Numerical Examples

To illustrate the KF-based algorithm with intermittent measurements, two simulation studies using hypothetical participant data are presented in this section. The first example is based on the reformulated energy balance model which has been used in the HMZ study for maternal weight gain prediction. This example aims to test how the algorithm works for gestational weight gain interventions. To demonstrate the potential of the algorithm to be used for general weight interventions, the energy balance model which is designed in

Thomas *et al.* (2009) to predict weight change for general populations is used for purpose of broader applications. The algorithm shows good performance in both simulation studies, and can be potentially used in actual intervention therapies.

Simulation Based on Maternal Energy Balance Model

Based on the reformulated maternal energy balance per (2.16), a system for algorithm implementation can be set up. Due to the inherent observability problem of the model as illustrated in previous section, we cannot test for the three-state estimation unless unbiased EI measurement is available. Instead, a two-state estimation case is presented in a hypothetical context similar to the HMZ intervention. For a hypothetical participant with pre-pregnancy weight of 75 kg and BMI of 21.5 kg/m^2, the gains according to Table 2.3 are $K_1 = 1.92 \times 10^{-4}$, $K_2 = -2.15 \times 10^{-4}$. It is assumed that the measurement of W and PA is obtained daily but corrupted with noise; since RMR is relatively stable, it can be measured less frequently as a weekly variable using a portable sensing device (*Breezing*, Xian *et al.* (2015)). As a result of the relatively high accuracy of *Breezing* device, RMR can be defined as a noise-free input with zero-order hold performed between weekly measures. To estimate the underreporting of EI from the noise-corrupted measures of W and PA, a two-state system can be configured as: $x = [EI\ PA]^T$, $y = [GWG\ PA]^T$, $u = [RMR]$. The corresponding system matrices for the state space representation is $A = \begin{bmatrix} 1 & 0 \\ 0 & 1 \end{bmatrix}$; $B = \mathbf{0}$; $C = \begin{bmatrix} K_1 & K_2 \\ 0 & 1 \end{bmatrix}$; $D = \begin{bmatrix} K_2 \\ 0 \end{bmatrix}$. (A, B) and (A, C) are checked to confirm stabilizability and detectability respectively in case of no observation losses.

A simulation example based on the proposed system is presented in Fig. 3.9 with the hypothetical data to test the performance of the algorithm. Here, the noise covariances is predetermined as $Q = \begin{bmatrix} 10000 & 0 \\ 0 & 10000 \end{bmatrix}$, $R = \begin{bmatrix} 0.01 & 0 \\ 0 & 10000 \end{bmatrix}$. The arrival rates of the output measurements are defined with the joint probability function as shown in Table 3.1, where γ_1 and γ_2 indicate the arrivals of the measurements for GWG and PA, respectively. It can be seen from the results that the state estimation of PA and EI follows the true values

closely despite the presence of noise and missing data with the developed KF algorithm. Compared with the noise corrupted measurement of GWG, an accurate prediction of weight gain is obtained from the algorithm as well. Underreporting of EI can be well identified from the estimation results.

Table 3.1: The joint probabilities of the measurement loss for a hypothetical participant used for the illustration based on maternal energy balance model. γ_1 and γ_2 indicate the arrivals of the measurements for ΔW and PA, respectively.

Scenarios	$\gamma_2 = 0$	$\gamma_2 = 1$
$\gamma_1 = 0$	0.1	0.05
$\gamma_1 = 1$	0.05	0.8

To extend the evaluation of the effectiveness of this method in real applications, intervention participant data with under-reported EI measures from the HMZ study is used. A real-time estimation of EI can be performed despite the presence of missing data. The results for the four representative participants used in back-calculation are shown in Fig.3.10 and 3.11, where the prediction bias is demonstrated with root mean square error ($RMSE$). For these participants, $Q = [100000]$ and $R = [0.5]$ are used for obtaining the presented results. It can be seen from the results that state estimation of EI generally keeps above the self-reported EI despite the presence of noise and missing data. When missingness in the measured output GWG_{meas} occurs repeatedly, bias in EI_{est} is inevitably observed, since it is propagated from the previous measurement available. Compared with the noise corrupted GWG_{meas}, an accurate prediction of GWG is obtained from the algorithm as well. Underreporting of EI can be well identified from the estimation results. The mean$\pm SD$ of the EI estimate for Phase II participant A is 2721 $\pm$ 911 kcal; the mean$\pm SD$ for participant B is 2676 $\pm$ 997 kcal. For Phase I participants, the mean$\pm SD$ of the EI estimate for participant C is 2701 $\pm$ 711 kcal; the mean$\pm SD$ for participant D is 3126 $\pm$ 797 kcal.The estimated EI is comparable to back-calculation approach while pre-processing of data to remove missingness or reduce noise is not required. A comparison between the back-calculation method and the Kalman filtering approach based on the estimation results for the two representa-

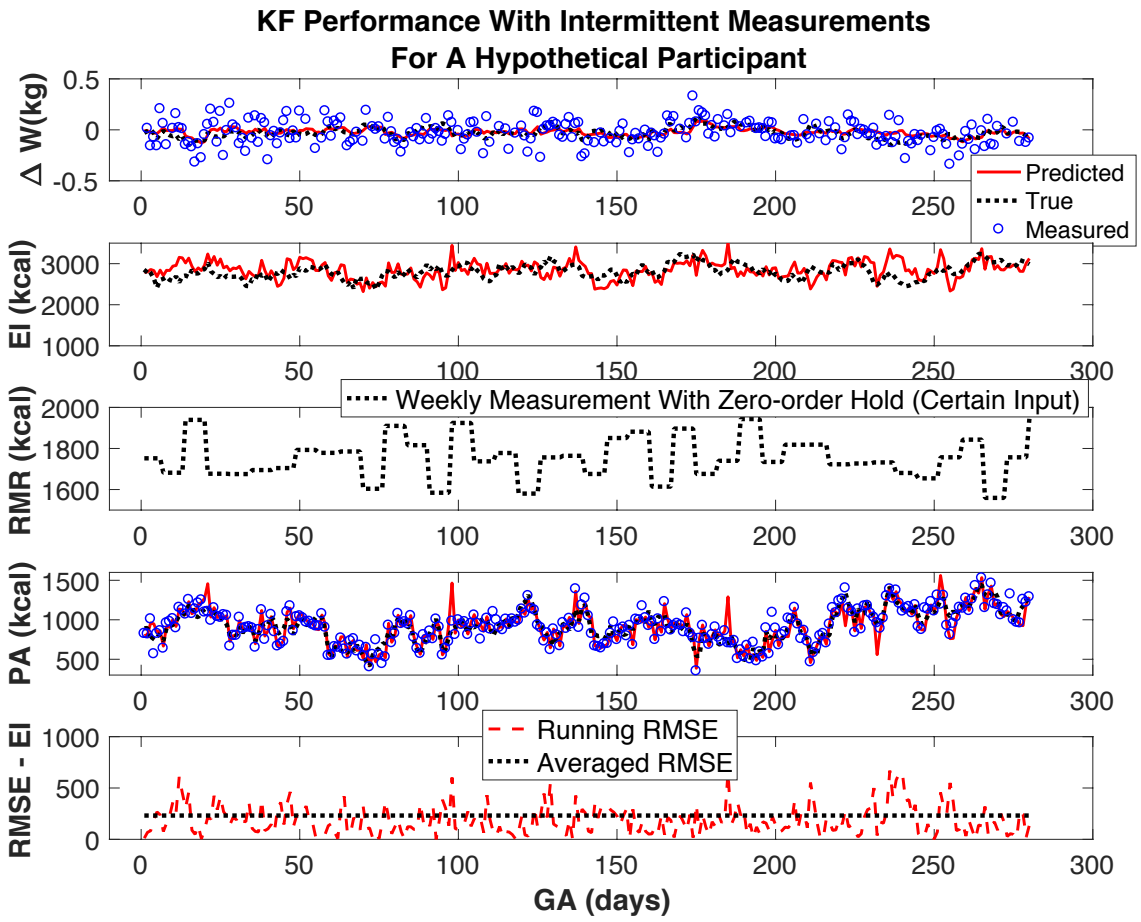

Figure 3.9: Performance of the KF algorithm illustrated using a hypothetical participant with correlated partial measurement losses during a gestational weight control intervention. $RMSE$ stands for the root mean square error.

tive participants is tabulated in Table 3.2, where it can be seen that the back-tracked EI is similar for the two approaches.

In addition, this approach can be applied to the alternative system models proposed in previous section if necessary. An example of the two state estimation with the data from Participant B is presented below where the PA measurements are considered to be noise-corrupted and need to be estimated in addition to the EI. The results are shown in Fig. 3.12 where the selected covariance matrices are $Q = \begin{bmatrix} 100000 & 0 \\ 0 & 100000 \end{bmatrix}$, $R = \begin{bmatrix} 0.5 & 0 \\ 0 & 1000000 \end{bmatrix}$. The mean $\pm SD$ of the EI estimate for participant B is 2323 $\pm$ 434 kcal, while the PA

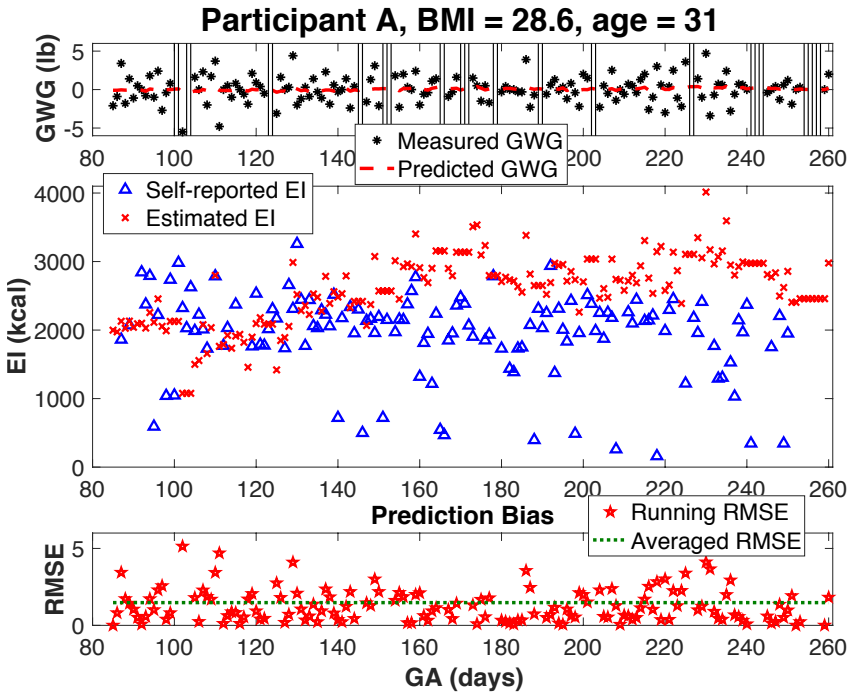

(a)

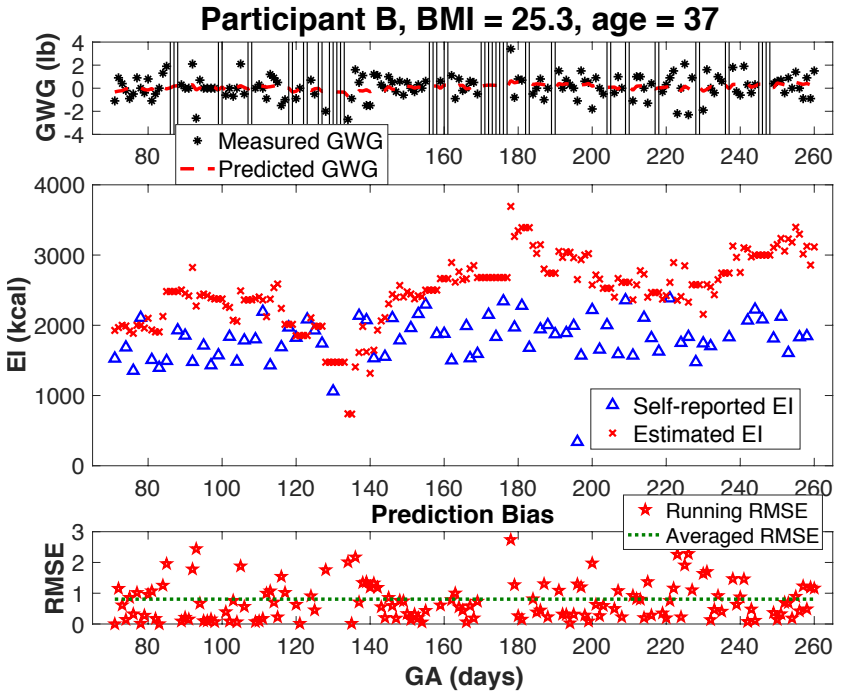

(b)

Figure 3.10: Results of estimating the EI using Kalman filtering for two HMZ Phase II participants. The results indicate that underreporting of EI can be identified for most of the time; however, estimates accuracy is compromised when the weight measurement is missing for multiple consecutive days. The prediction bias is indicated with root mean square error ($RMSE$). Vertical black lines in the GWG plot indicate the days of missing GWG measurements.

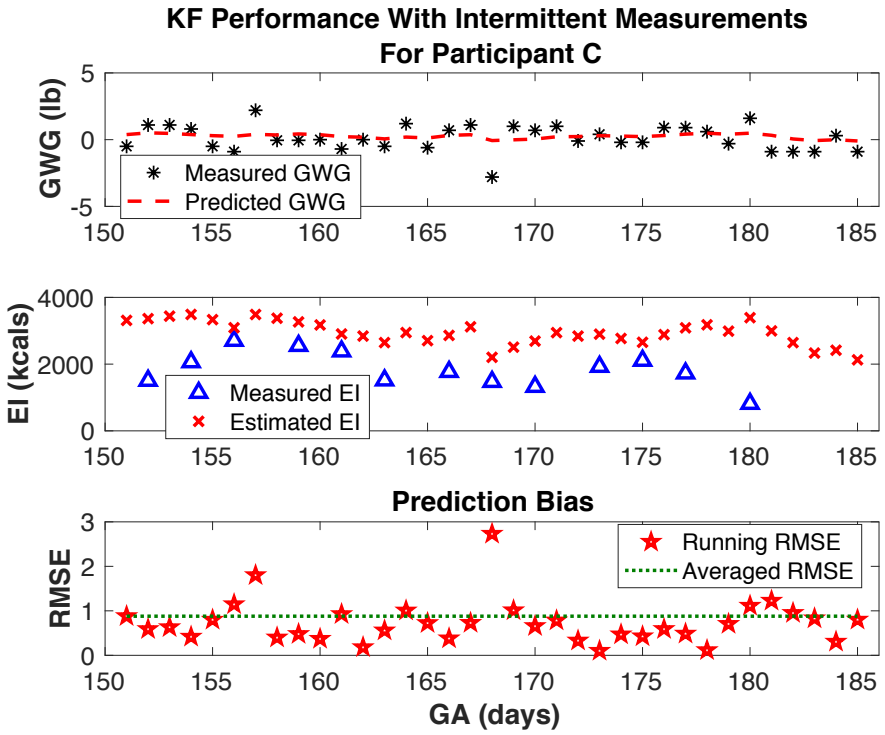

(a)

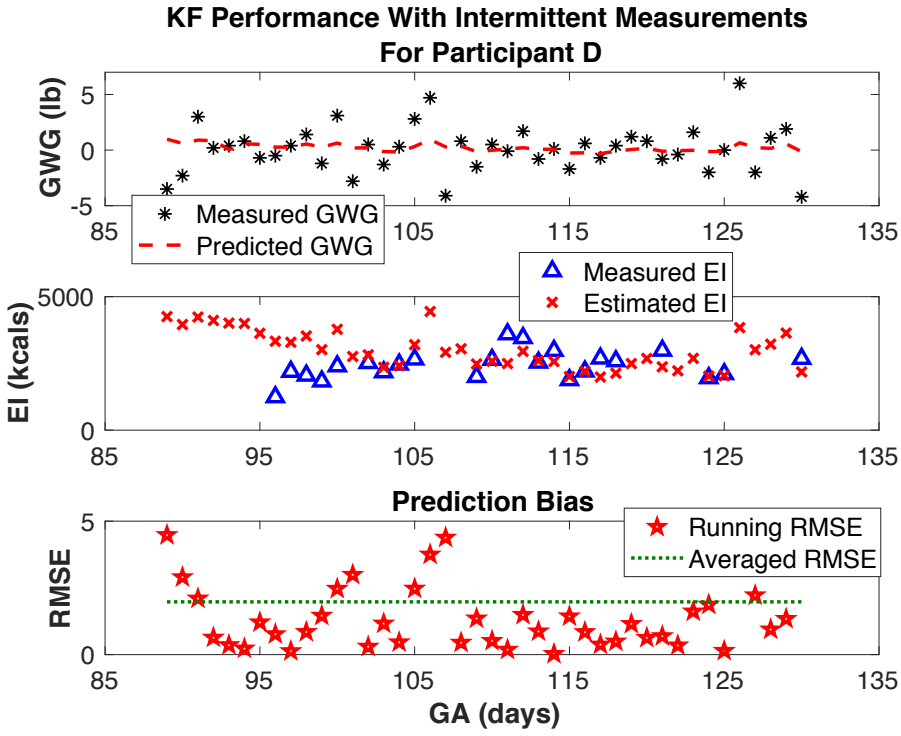

(b)

Figure 3.11: The performance of the KF algorithm with intermittent measurements for estimating *EI* evaluated using two intervention participants from the Phase I Study of the HMZ.

Table 3.2: Estimation results of EI for Participant A and B with back-calculation method and Kalman filtering approach.

		EI_{est} (kcal)	
Phase	Participant	Back-calculation	Kalman filtering
I	A	2677±607	2721±911
	B	2611±443	2676±997
II	C	2787±617	2701±711
	D	3353±1025	3126±797

estimates are 165.5 ± 55 kcal. It has to be noted that for more than one state estimation, convergence is a common issue if multiple variables are missing at the same time continuously, leading to instability. Since there is no missing data in PA measurements for this participant, instability issue is not a concern here. Otherwise, data imputation such as linear interpolation can be employed to mitigate missingness. Similar analysis can be extended to three state estimation cases, for example, including both PA and RMR as states to be estimated. However, one needs to be careful about system observability when applying Kalman filtering in this case.

Simulation Based on Energy Balance Model For General Population

Another simulation study to illustrate the KF-based algorithm with hypothetical data is presented based on an energy balance model for a general population. The energy balance model is based on the work in Thomas *et al.* (2009), and is designed to predict weight change for a general population. We reformulate the model into the form as following:

$$\Delta W_k = K_1 EI_k + K_2 PA_k + K_2 RMR_k \tag{3.29}$$

where ΔW is the body weight change; EI is the energy intake; PA is the physical activity; RMR is the resting metabolic rate; K_1 and K_2 are the system gain parameters, the values of which can vary by gender and other factors. Here, all participants are assumed to be

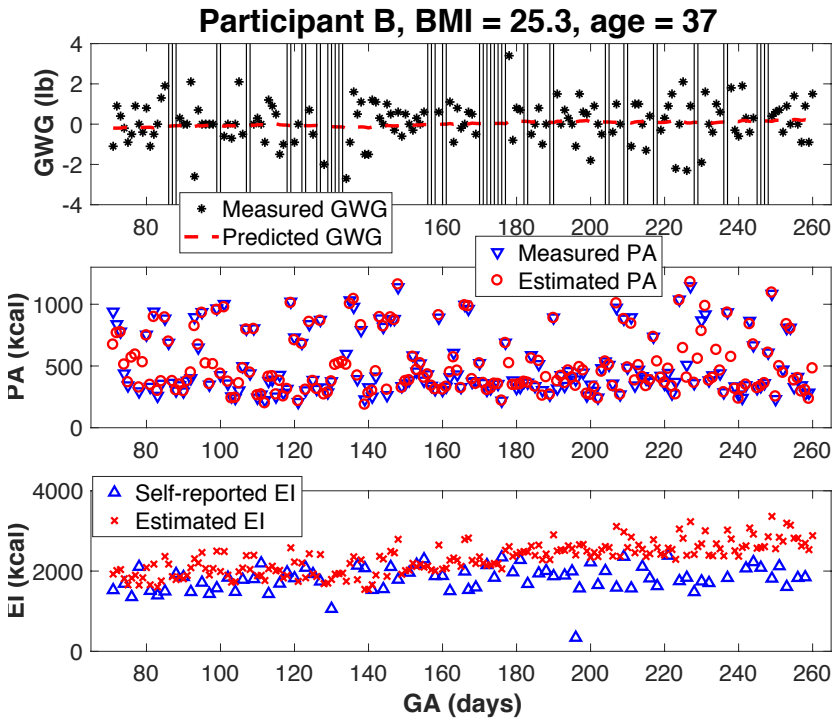

Figure 3.12: KF performance for Participant B from Phase II study for two-state estimation. In this case, the estimation of the EI is implemented simultaneously with noise filtering for the PA measurements. Vertical black lines in the GWG plot indicate the days of missing GWG measurements. $RMSE$ stands for root mean square error.

females, leading to $K_1 = 1.67 \times 10^{-4}$ and $K_2 = -1.8 \times 10^{-4}$. The derivation for the values of the two gain parameters is similar as in Section 2.4 in Chapter 2, but applied to the general female population. The details of the derivation are elaborated below.

The main differential equation for the two-compartment energy balance model from Thomas *et al.* (2009) is expressed as

$$\lambda_{FFM}\ p_{FFM} \frac{dFFM(t)}{dt} + \lambda_{FM} \frac{dFM(t)}{dt} = EI(t) - EE(t) \tag{3.30}$$

where EE is the energy expenditure; FFM and FM represent the fat free mass and fat mass, respectively; these two body mass compositions have their respective energy densities of $\lambda_{FFM} = 955.384$ kcals/kg and $\lambda_{FM} = 7165$ kcals/kg; p_{FFM} is the proportion of $FFM(t)$ being muscle tissue available for energy reserve, ranging from 0.3 to 0.5. Here, we pick the value of p_{FFM} as 0.4. A linear approximation of the relationship between total body weight (W) and FM was given in Thomas *et al.* (2009), where $W = \alpha\ FM + \beta$ with $\alpha = 1.32$ for

female. Combining this relationship with $W = FFM + FM$ and substituting into (3.30) gives an expression of the model with respect to W alone, as shown below:

$$K\frac{dW(t)}{dt} = EI(t) + EE(t) \tag{3.31}$$

where $K = \frac{\lambda_{FM}+\lambda_{FFM}\ p_{FFM}(\alpha-1)}{\alpha}$. We consider EE comprised of three major components: physical activity (PA), resting metabolic rate (RMR), and thermic effect of food (TEF), with $TEF = \delta EI$, $\delta = 0.08$. Then EE can be represented as $EE = PA + RMR + \delta\ EI$, if combined with the original energy balance model per (3.31), leading to the reformulated model as:

$$\frac{dW(t)}{dt} = K_1 EI(t) + K_2 PA(t) + K_2 RMR(t) \tag{3.32}$$

where $K_1 = 1.67 \times 10^{-4}$ and $K_2 = -1.8 \times 10^{-4}$. Discretizing (3.32) gives the equation in (3.29). Note that the non-volitional physical activity in the original energy balance model is neglected here for simplicity.

With this model, a Kalman filtering problem with correlated partial measurement losses is formulated for an intervention designed for a general female population. In this hypothetical intervention, all the measurements are assumed to be self-reported or self-monitored. For the measurement of ΔW, it is assumed that the participants weigh themselves daily using smart digital scales. The measurement of EI is obtained daily from self-reported questionnaires: Automated Self-Administered 24-Hour Dietary Recall (ASA-24), where EI underreporting is present. PA is measured daily with a wrist-worn accelerometer (*Jawbone*). RMR is measured daily with an affordable device subject to significant noise. Compared to other variables, PA measurement is more accurate and can be used as a noise-free input. This can accommodate a situation where the measurement noise in PA can be neglected, while the noise and data missingness in RMR measurement is more significant. With these assumptions, W and RMR are set as system outputs while PA as the noise-free input; EI and RMR are defined as the states to be estimated. For this case, the state space representation of the system can be formulated with $A = \begin{bmatrix} 1 & 0 \\ 0 & 1 \end{bmatrix}$, $B = \mathbf{0}$, $C = \begin{bmatrix} K_1 & K_2 \\ 0 & 1 \end{bmatrix}$ and

$D = \begin{bmatrix} K_2 \\ 0 \end{bmatrix}$.

To test the algorithm on a hypothetical participant with frequent measurement losses, it is assumed that the output measurements for this participant are missing for one fifth of the intervention (80% availability only); Correlation exists in the loss of data as shown by the pre-defined arrival rates of the two output measurements (Table 3.3). The steps for the KF-based algorithm are summarized as below:

1. **Initialize**: Set $\hat{x}(0|0) = [EI_0 \ RMR_0]^T$, $P(0|0) = I$. EI_0 and RMR_0 are baseline measurements.

2. **Predict**: The prediction stage is independent of the update stage and can be expressed as:

$$\hat{x}_{k+1|k} = A\hat{x}_{k|k}; \tag{3.33}$$

$$P_{k+1|k} = AP_{k|k}A' + Q; \tag{3.34}$$

3. **Update**: The model estimates from "Predict" step is corrected base on measurements:

$$\begin{aligned} \hat{x}_{k+1|k+1} &= \hat{x}_{k+1|k} + P_{k+1|k}\{C^-_{\mathbb{Z},\phi}\}^T \times (\{C^-_{\mathbb{Z},\phi}\}P_{k+1|k}\{C^-_{\mathbb{Z},\phi}\}^T + R^-_{\mathbb{Z},\mathbb{Z}})^{-1} \\ &\quad (\{y_{k+1}\}^-_{\mathbb{Z},\phi} - \{C^-_{\mathbb{Z},\phi}\}\hat{x}_{k+1|k}) \\ P_{k+1|k+1} &= P_{k+1|k} - P_{k+1|k}\{C^-_{\mathbb{Z},\phi}\}^T(\{C^-_{\mathbb{Z},\phi}\}P_{k+1|k} \times \{C^-_{\mathbb{Z},\phi}\}^T + R^-_{\mathbb{Z},\mathbb{Z}})^{-1}\{C^-_{\mathbb{Z},\phi}\}P_{k+1|k} \end{aligned} \tag{3.35}$$

With pre-determined noise covariances as $Q = \begin{bmatrix} 10000 & 0 \\ 0 & 10000 \end{bmatrix}$, $R = \begin{bmatrix} 0.01 & 0 \\ 0 & 10000 \end{bmatrix}$, the performance of the algorithm for this hypothetical participant is presented in Fig. 3.13, where good estimates of EI and RMR are provided based on data with noise and missingness. Underreporting of EI can be calculate from the estimation as well. The algorithm also produces good weight gain predictions compared with the noise corrupted measurements. Note that the high arrival rates are required for the estimation error to remain bounded,

which is illustrated using the root mean square error ($RMSE$) for EI estimates as shown by the bottom plot in Fig. 3.13. With a low arrival rate, the boundedness of the error cannot be guaranteed, resulting in the estimation error to be divergent (shown in Fig. 3.14).

Table 3.3: The joint probabilities of the measurement loss for a hypothetical participant used for the illustration based on the energy balance model for general populations. γ_1 and γ_2 indicate the arrivals of the measurements for ΔW and RMR, respectively.

Scenarios	$\gamma_2 = 0$	$\gamma_2 = 1$
$\gamma_1 = 0$	0.05	0.05
$\gamma_1 = 1$	0.1	0.8

3.3.2 Extended Kalman Filtering With Partial Measurement Losses

Algorithm

In case of a non-linear system, the extended Kalman filter needs to be considered. Here, we define a MIMO non-linear discrete-time system with q output sensors as described with the following equations:

$$x_{k+1} = f(x_k, u_k) + \varpi_k \tag{3.36a}$$

$$\underbrace{\begin{bmatrix} y_{1,k} \\ y_{2,k} \\ \vdots \\ y_{q,k} \end{bmatrix}}_{y_k} = \underbrace{\begin{bmatrix} g_1(x_k, u_k) \\ g_2(x_k, u_k) \\ \vdots \\ g_q(x_k, u_k) \end{bmatrix}}_{g(x_k, u_k)} + \underbrace{\begin{bmatrix} \nu_{1,k} \\ \nu_{2,k} \\ \vdots \\ \nu_{q,k} \end{bmatrix}}_{\nu_k} \tag{3.36b}$$

where the deterministic nonlinear functions $f(x_k, u_k) : \mathbb{R}^n, \mathbb{R}^p \to \mathbb{R}^n$, and $h(x_k, u_k) : \mathbb{R}^n, \mathbb{R}^p \to \mathbb{R}^q$ are continuously differentiable at every x_k and u_k. Linearizing the model in (3.36) gives $A_k = \frac{\partial f(x_k, u_k)}{\partial x_k}|_{\hat{x}_{k-1|k-1}, u_k}$, and $C_k = \frac{\partial g(x_k, u_k)}{\partial x_k}|_{\hat{x}_{k|k-1}, u_k}$. For this system, (A_k, Q) is completely stabilizable and (A_k, C_k) completely detectable. The prediction step

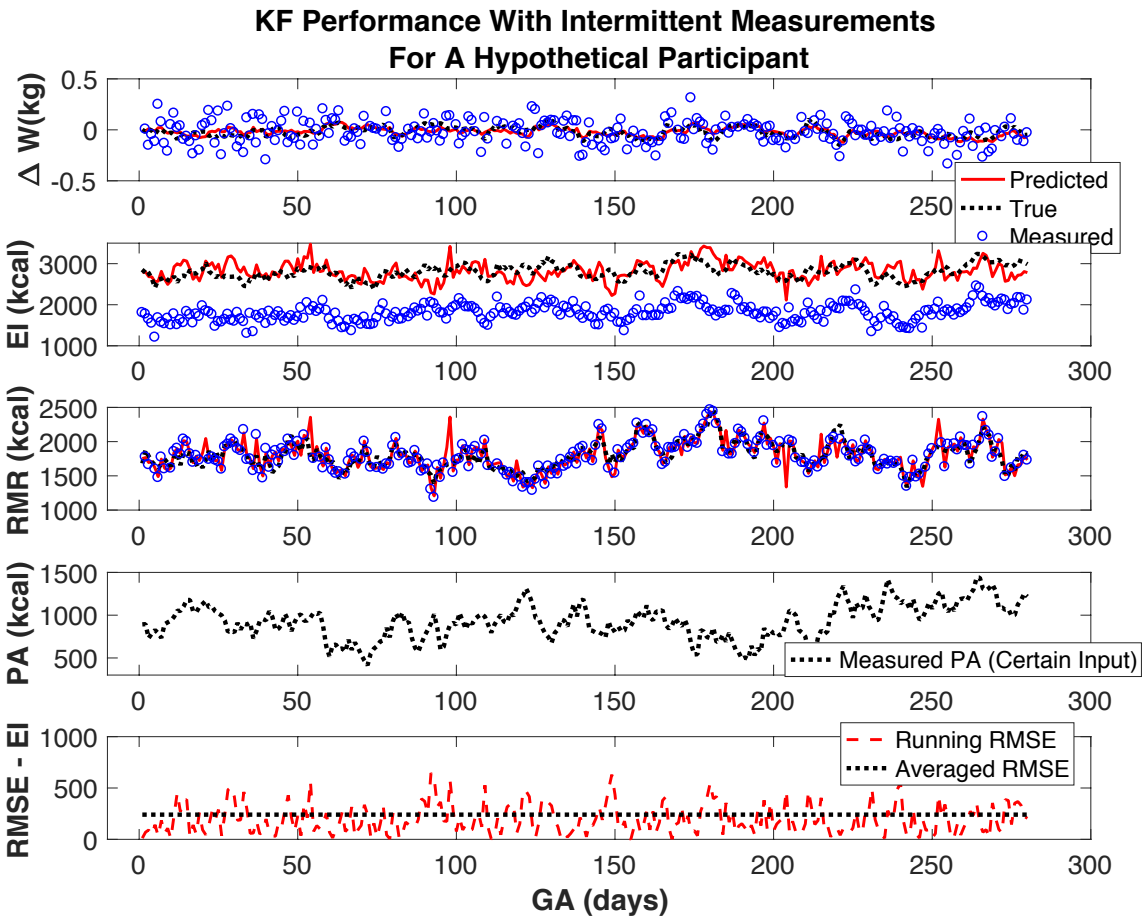

Figure 3.13: Performance of the KF algorithm illustrated using the hypothetical data with correlated partial measurement losses during a general weight control intervention. The arrival rates of the output measurements are high enough to ensure the boundness of the estimation error. $RMSE$ stands for the root mean square error.

is the same as in the classical EKF:

$$\begin{aligned} \hat{x}_{k+1|k} &= f(\hat{x}_{k|k}, u_k) \\ P_{k+1|k} &= A_k \hat{P}_{k|k} A_k^T + Q \end{aligned} \tag{3.37}$$

There are 2^q possible scenarios for observation losses. For an arbitrary sequence of measurement losses defined by $\mathbb{Z} = \{n_1, n_2, \cdots\}$ *or* $\{\phi\}$, where $n_1, n_2, \cdots \in \{1, 2, \cdots, q\}$, the generalized formulation for the EKF updates can be derived and it is described as

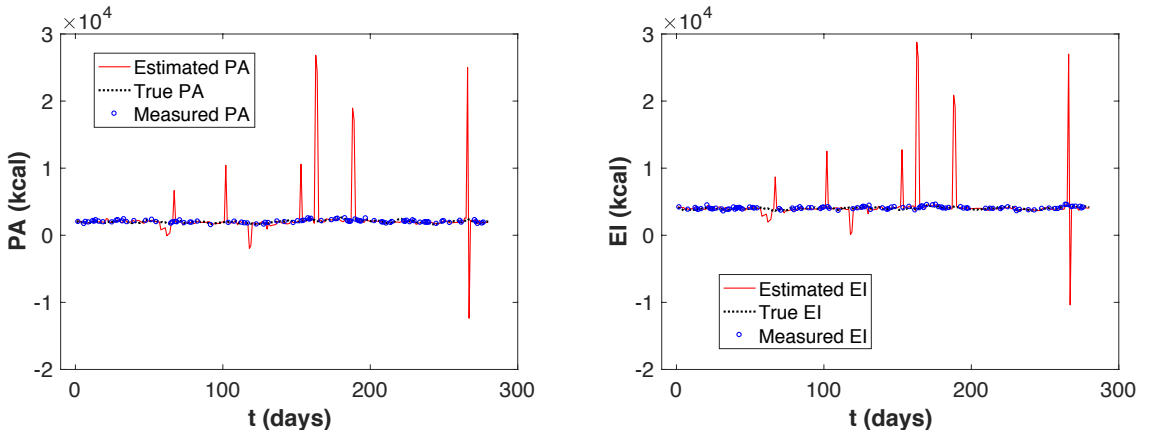

Figure 3.14: Simulation results with low arrival rates are shown to be divergent and stable.

follows,

$$\begin{aligned}\hat{x}_{k+1|k+1} &= \hat{x}_{k+1|k} + P_{k+1|k}\{C^-_{k_{\mathbb{Z},\phi}}\}^T(\{C^-_{k_{\mathbb{Z},\phi}}\}P_{k+1|k}\{C^-_{k_{\mathbb{Z},\phi}}\}^T \\ &\quad + R^-_{\mathbb{Z},\mathbb{Z}})^{-1}(\{y_{k+1}\}^-_{k_{\mathbb{Z},\phi}} - \{C^-_{k_{\mathbb{Z},\phi}}\}\hat{x}_{k+1|k}) \\ P_{k+1|k+1} &= P_{k+1|k} - P_{k+1|k}\{C^-_{k_{\mathbb{Z},\phi}}\}^T(\{C^-_{k_{\mathbb{Z},\phi}}\}P_{k+1|k}\{C^-_{k_{\mathbb{Z},\phi}}\}^T \\ &\quad + R^-_{\mathbb{Z},\mathbb{Z}})^{-1}\{C^-_{k_{\mathbb{Z},\phi}}\}P_{k+1|k}\end{aligned} \tag{3.38}$$

This is the same as (3.28) except for matrix C replaced with C_k. With this generalized formulation, state estimation based on an arbitrary non-linear system is enabled in the presence of intermittent measurements.

Numerical Example

To illustrate the performance of the EKF-based algorithm, an example based on the re-formulated maternal energy balance model per (2.16) is presented. The reformulation of the model and the derivation for the system gain coefficients K_1 and K_2 has been shown in Chapter 2 where K_1 and K_2 are categorized by maternal BMI and weight. Here, we assume a participant with pre-pregnancy weight of 95 kg and BMI of 31 kg/m^2. For this participant, the gains according to Table 2.3 are $K_1 = 2.119 \times 10^{-4}$, $K_2 = -2.35 \times 10^{-4}$. To generate hypothetical data, it is assumed that physical activity and maternal weight are self-monitored, and energy intake measurement is unbiased. Considering the cost and par-

ticipant burdens for measuring RMR, a quadratic regression formula proposed in Thomas (2009) to dynamically model RMR as a function of W is used throughout the intervention. The empirical function is written as:

$$RMR_k = aW_k^2 + bW_k + c \tag{3.39}$$

where $a = 0.1976$; $b = -13.424$; $c = 1457.6$. This quadratic function fits the data from the study in Butte *et al.* (2004) and it brings non-linearities into the energy balance model if combined with (3.39). Note that (3.39) uses total weight $W(k)$ instead of weight change $\Delta W(k)$. Defining $\Delta W(k) = W(k) - W(k-1)$, the nonlinear model by combining the discretized maternal EB in the form as shown in (3.29) with the equation of RMR in (3.39) is described as below,

$$x_{k+1} = \begin{bmatrix} f_1(x_k, u_k) \\ f_2(x_k, u_k) \end{bmatrix} + \varpi_k \tag{3.40a}$$

$$y_k = x_k + \nu_k \tag{3.40b}$$

where $x = [W \ EI]^T$; $y = x$; $u = [PA + c]$;

$$\begin{aligned} f_1(x_k, u_k) &= K_2 a x_{1,k}^2 + (K_2 b + 1)x_{1,k} + K_1 x_{2,k} + K_2 u \\ f_2(x_k, u_k) &= x_{2,k} \end{aligned} \tag{3.41}$$

After the linearization of the model, the algorithm specified in Section 3.3.2 can be applied. Baseline weight and energy intake are used for initialization. Simulation results are presented in Fig. 3.15 to test the performance of the algorithm, where $Q = \begin{bmatrix} 0.1 & 0 \\ 0 & 10000 \end{bmatrix}$, $R = \begin{bmatrix} 0.1 & 0 \\ 0 & 10000 \end{bmatrix}$. It can be seen that given the probability of arrival for EI is 0.5, the state estimation of EI keeps tracking the true values closely despite the presence of noise and measurement loss with the EKF-based algorithm. Note that the estimation error remains bounded for the high arrival rate as shown in Fig. 3.15.

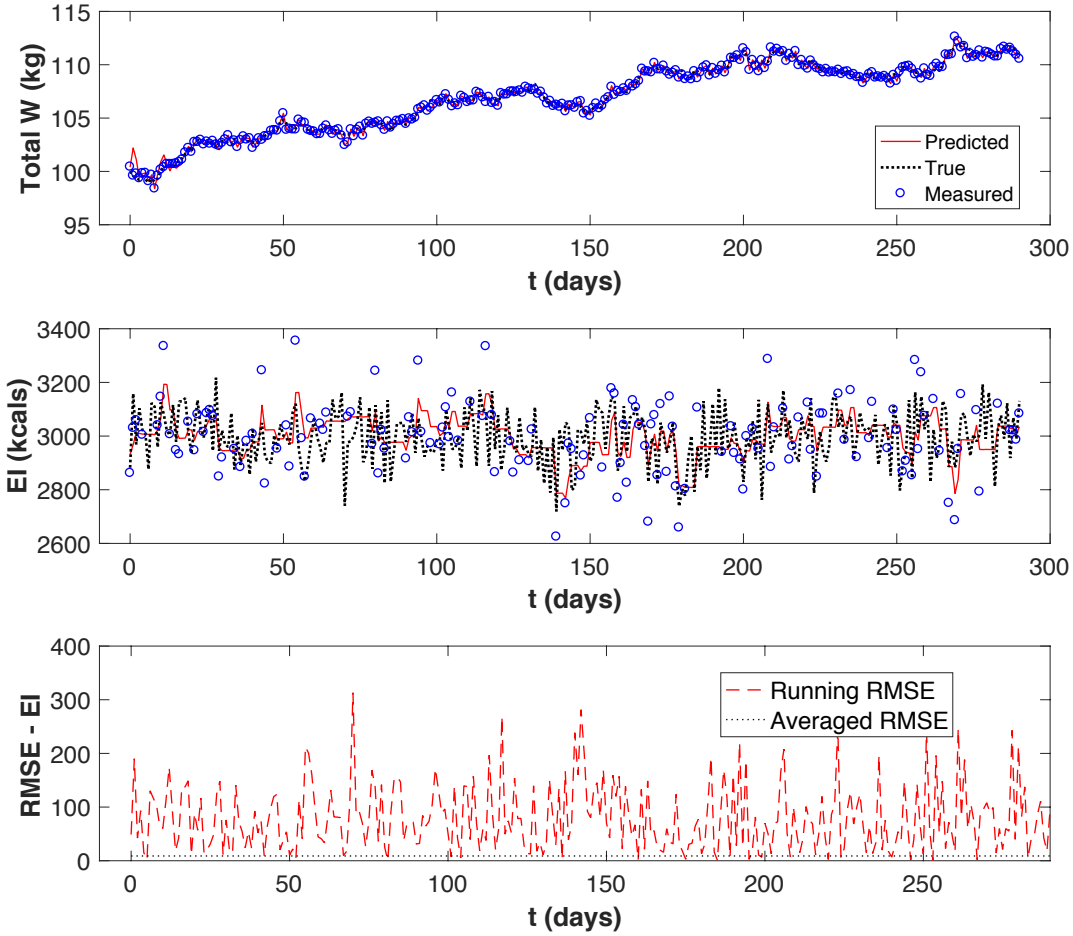

Figure 3.15: Performance of the EKF-based algorithm illustrated using a hypothetical participant in a pregnancy intervention.

3.4 Summary of Proposed Estimation Approaches

In this chapter, energy intake is estimated with a back-calculation method, followed by a Kalman filtering approach which can provide real-time estimation while addressing the problem of measurement noise and data missingness simultaneously. From the literature and HMZ pilot data, it has been clearly shown that misreporting is commonly observed in self-reported measures, especially significant in self-reported energy intake. To better characterize reporting accuracy for individual participant, we developed two model-based approaches originating from state estimation techniques to estimate the actual energy intake

based on measured W, PA and estimated RMR. Methods were demonstrated with both hypothetical participants and actual intervention participants from the Phase I and II study to validate their effectiveness. In this section, a summary of the advantages and disadvantages of these two methods are provided for the purpose of comparison; some limitations in our modeling and estimation work are also listed for the guidance of future applications.

The first approach of algebraic back-calculating EI from the EB model is the easiest to implement and understand compared to the other approaches, and may be favored by users seeking low computational complexity. With this method, intensive EI estimates can be generated without requiring any EI measurement; confidence intervals can be computed from standard error propagation methods or Monte Carlo simulations. However, it requires *a priori* data smoothing and imputation or interpolation approaches to address data missingness. Specifically, due to the intrinsic property of this approach, the estimation with this method is sensitive to the noise in weight measurements; thus, pre-processing of measured weight data with techniques such as moving average filter is necessary to reduce the variation in the estimates. It has been observed that the average of the estimates is not affected by the selected moving average window, while the standard deviation is significantly affected, which produces an adjustable parameter for this method.

The second category of approaches based on Kalman filtering enables real-time estimation of EI in the absence/presence of missing data, without demanding *a priori* smoothing. The time-varying Kalman filter gains can accommodate missing data in the output, giving more flexibility than the classical Kalman filtering method. These Kalman filter based estimates can be interpreted as a refined way of back-calculating EI, which improves the model-predicted estimates by filtering out the noise in the intermittent weight measurements; confidence intervals can be calculated from the covariance matrix. It must be noted that the estimation results will depend on the values of the covariance parameters, Q and R, which may be viewed as adjustable parameters. In this work, the conventional approach for specifying Q and R is used for simplicity. However, algorithms that can adaptively

adjust Q and R may be used to improve filtering performance; such methods have been explored in Akhlaghi *et al.* (2017). Alternatively, a time-varying Kalman filter that includes an auxiliary state estimator (so-called double Kalman filtering) is also a possible option to adjust noise covariance based on the change in the system dynamics (Johansen and Fossen, 2016). Yet, the performance of these algorithms under intermittent measurements remains unclear and needs to be examined; this remains a topic for future research that is worth further exploration.

To enable the use of any of these estimation methods, linear interpolation of weight and physical activity measurements is required to replace any missing data; for the missing data beyond the available data points for measured physical activity, mean replacement is performed. It should be noted that the data imputation might introduce errors into the estimation.

It also should be pointed out that, the simulation and the results of energy intake estimation demonstrated in this chapter are based on the assumption that the theoretical energy balance model is built accurately with reliable model parameters. The system gains of the energy balance model are categorized by maternal pre-pregnancy BMI, which takes into account the distinction between underweight, normal-weight, overweight or obese pregnant populations; nevertheless, it still lacks adaption to individual differences. In addition, both methods rely on the assumption that the measured physical activity and estimated resting metabolic rate are without noise or bias in order to realize the estimation of energy intake. But in real-life settings, the measurement or empirical estimation of physical activity and resting metabolic rate are inevitably subject to noise and bias. These all form the limitations of the use of the model. Therefore, when applying the proposed estimation methods in actual intervention, researchers should be aware of these assumptions and be careful in the analysis of the estimates.

Another issue that can be examined in the future is the stability analysis. In the current demonstration of the algorithms, we only use an example to show that low arrival rates of

the output measurement can result in divergence in the estimates (Fig. 3.14). However, systematic stability analysis is not performed yet to prove our observations. Hence, it can be proposed as one of the future research directions for further examination. In addition, approaches that can deal with the observability problem resulted from ill-conditioned systems is also an interesting topic for future work.

Chapter 4

CORRECTION FOR UNDERREPORTING THROUGH SEMI-PHYSICAL IDENTIFICATION

As highlighted in previous chapters, energy intake underreporting is a widespread problem for interventions relying on self-reported measures of EI; this is reflected in our experience from the *Healthy Mom Zone* intervention. To address this issue in the context of a gestational weight control intervention, a series of estimation approaches that address measurement noise and measurement losses were developed in Chapter 3. These include back-calculating energy intake from the reformulated energy balance model and a variety of Kalman filtering-based approaches to recursively estimate energy intake from interpolated or intermittent measurements. Evaluated with hypothetical data or actual participant data obtained through the HMZ intervention study, these approaches have demonstrated the potential to promote the success of weight control. We have analyzed the pros and cons of the presented approaches to provide insights for users in future applications.

It is important to note that the back-calculation method and those Kalman filtering-based estimates are capable of providing estimates of EI only when the measures/estimation of W, PA and RMR are available. This means that, repeated data collection of W and PA is always necessary for these estimation approaches to be implemented. In this chapter, we aim to develop a method that can systematically characterize the extent of energy intake underreporting. The idea behind this method is to enable the correction of future self-reported EI that contains potential misreporting, but without the need to require for intensive data collection of W and energy expenditure terms (PA and/or RMR). Such goal can be realized by building models that can describe the quantitative relationships between the actual energy intake (EI_{actual}) and the EI self-reports ($\widetilde{EI}_{rept}$, or other input variables if absolutely necessary, such as participant weight (W_{actual})). When a self-report

is available, the model is able to predict EI_{actual}. Fig. 4.1 depicts such relationships for modeling purposes, where EI_{actual} is a function of $\widetilde{EI}_{rept}$ and W_{actual}, denoted as

$$EI_{actual} = f(\widetilde{EI}_{rept}, W_{actual}) \tag{4.1}$$

Here the functional relationship f can be structured differently at the users' request. For simplicity, we only focus on linear or quadratic relationships in this work. However, f is allowed to be time-invariant (fixed) or dynamically changing with respect to time due to the characteristics of the data. To obtain a time-invariant f, a global modeling approach based on semi-physical identification principles (linear regression from past collected data) is developed to parametrize the extent of underreporting for future self-reports adjustment. As a counterpoint for this global estimation approach, a local modeling technique based on the concept of Model-on-Demand is applied to identify time-varying parameters for the correction models; as will be demonstrated, comparable performance can be achieved with less engineering effort and *a priori* information required. Cross-validation procedures are applied to test the performance of both approaches, and the resulting performance is relied on for selecting parsimonious yet accurate models with good predictive ability. The established model is useful to further understand the percentage of EI that is systematically under-reported, enabling health providers to deliver informative health guidance for participants.

This chapter is organized as below: a global modeling approach is developed in Section 4.1, where the results and model selection using cross-validation is presented and followed by a prediction error analysis. In Section 4.2, the Model-on-Demand approach to estimating the energy intake from the self-reports is developed and compared with the global method. Section 4.3 gives a summary of our conclusions. As will be shown, the proposed approaches for estimating energy intake are helpful for accurate intervention assessment, and also promote

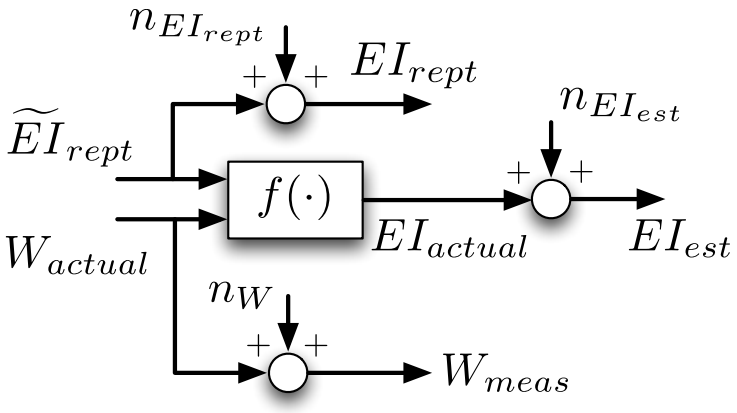

Figure 4.1: Block diagram of the regression model used for the development of the semi-physical identification approach. n_W, $n_{EI_{rept}}$ and $n_{EI_{est}}$ indicate the noise in the measured W, self-reported EI, and estimated EI, respectively.

the success of weight control.

4.1 Semi-Physical Estimation

In this section, a semi-physical identification approach based on linear regression from past collected data is developed to obtain the functional relationship f as indicated in Fig. 4.1. Since EI self-reports or weight measurements are usually corrupted by noise, the data used as inputs are noise-corrupted signals: EI_{rept} and measured weight (W_{meas}). Accurately estimated EI (EI_{est}) from either back-calculation or Kalman filtering can be used to approximate EI_{actual} and to serve as regression outputs. Once the model is identified, it can be used to to adjust future self-reports. The effectiveness of this approach is assessed with participant data evaluated on multiple model structures, demonstrating the ability of correcting biased EI_{rept} in the future.

4.1.1 Method Description

A variety of model structures can be proposed to predict the actual EI from self-reported EI, that is, to correct the self-reported EI from misreporting. For example, a linear formula can be assumed to describe the relationship between EI_{actual} (model output) and $\widetilde{EI}_{rept}$

(model input); this follows according to (4.2).

$$EI_{actual}(k) = \alpha_1 \, \widetilde{EI}_{rept}(k) + \xi \tag{4.2}$$

For clarification, $\widetilde{EI}_{rept}$ represents the nominal values of self-reported EI without noise corruption. This linear relationship describes the deterministic portion of underreporting, which tends to be systematically observed in one's behaviors. For example, an individual may mistake a 320 kcal bagel to be 250 kcal, or repeatedly forgets to report calories from snacks. This consistent behavioral pattern is the target that the proposed relationship tries to capture and model. A challenging aspect of underreporting is associated with possible random variations in the EI self-reports. The effect of such variations can be treated as an input noise signal ($n_{EI_{rept}}$) added to $\widetilde{EI}_{rept}$:

$$EI_{rept}(k) = \widetilde{EI}_{rept}(k) + n_{EI_{rept}}(k) \tag{4.3}$$

where EI_{rept} is the reported EI from the smartphone app; $n_{EI_{rept}} \sim \mathcal{N}(0, \sigma^2_{n_{EI_{rept}}})$ and $\sigma^2_{n_{EI_{rept}}}$ is the variance of the white noise $n_{EI_{rept}}$ in self-reports. To form the output of the regression problem, $EI_{actual}(k)$ can be approximated from the model-based back-calculation or Kalman filtering approaches described in Chapter 3. For simplicity, $EI_{actual}(k)$ values computed directly from the EB model in (2.18) are used here, leading to,

$$EI_{actual}(k) \cong \frac{(GWG(k+1) - K_2(PA(k) + RMR(k)))}{K_1} \tag{4.4}$$

In the HMZ intervention study, all measurements/estimates are subject to noise, but the noise in GWG_{meas} (n_{GWG}) is relatively more predominant than in other signals, considering daily weight changes that result from the individuals' varying hydration status. Hence, n_{GWG} cannot be neglected and its presence corrupts the model-based estimates of EI_{actual},

leading to the expression of EI_{est} as,

$$\begin{aligned} EI_{est}(k) &= \frac{GWG_{meas}(k+1) - K_2(PA(k) + RMR(k))}{K_1} \\ &= \frac{GWG(k+1) - K_2(PA(k) + RMR(k))}{K_1} + \frac{n_{GWG}(k+1)}{K_1} \\ &= EI_{actual}(k) + n_{GWG}(k+1)/K_1 \\ &= EI_{actual}(k) + n_{EI_{est}} \end{aligned} \tag{4.5}$$

where $n_{GWG} \sim \mathcal{N}(0, \sigma^2_{n_{GWG}})$. Since the magnitude of the noise term $\frac{n_{GWG}(k)}{K_1}$ tends to be quite large compared to EI_{est}, smoothing techniques can be used to reduce variability in the estimation.

With the constructed input and output of the correction model, the model parameters α_1 and ξ in (4.2) can be estimated by solving a regression problem formulated based on measurements as shown below,

$$\begin{array}{ccc} \mathcal{Z} & = & \mathcal{R} \qquad\quad \theta \\ \begin{bmatrix} EI_{est}(k_1) \\ EI_{est}(k_2) \\ \vdots \\ EI_{est}(k_N) \end{bmatrix} & = & \begin{bmatrix} EI_{rept}(k_1) & 1 \\ EI_{rept}(k_2) & 1 \\ \vdots & \vdots \\ EI_{rept}(k_N) & 1 \end{bmatrix} \begin{bmatrix} \alpha_1 \\ \xi \end{bmatrix} \end{array} \tag{4.6}$$

where $\mathcal{Z} \in \mathbb{R}^N$ is the output vector based on EI_{est} obtained from (4.5); $\mathcal{R} \in \mathbb{R}^{N\times 2}$ is the regressor that stores input measurements; $\theta \in \mathbb{R}^2$ is the parameter vector that needs to be estimated; k_1, k_2,..., k_N are the intermittent days at which the involved measurements are taken. Since EI_{rept} is not obtained daily (in order to minimize participant burden during intervention), the time index of the measurements involved in the regressor is not necessarily consecutive in terms of gestational age (days).

To identify the parameter vector θ, a least squares cost function is considered:

$$J(k) = \min_{\hat{\theta}} \left\{ \frac{1}{2} \left[\mathcal{Z} - \mathcal{R}\hat{\theta} \right]^2 \right\} \tag{4.7}$$

Table 4.1: Summary of the proposed structures to correct self-reported EI. Each structure is characterized by the number of model parameters and the number of pieces of required information (longitudinal measurements of EB variables). The estimator corresponding to each regression model is a subset of $[\alpha_1, \xi, \alpha_2, \beta]$.

Model Structure		Para #	Info #
A	$EI_{est}(k) = \quad \xi$	1	0
B	$EI_{est}(k) = \quad \alpha_1 \ EI_{rept}(k)$	1	1
C	$EI_{est}(k) = \quad \xi + \ \alpha_1 \ EI_{rept}(k)$	2	1
D	$EI_{est}(k) = \quad \alpha_1 \ EI_{rept}(k) + \ \alpha_2 \ EI_{rept}(k)^2$	2	1
E	$EI_{est}(k) = \quad \xi + \ \alpha_1 \ EI_{rept}(k) + \ \alpha_2 \ EI_{rept}(k)^2$	3	1
F	$EI_{est}(k) = \quad \xi + \ \alpha_1 \ EI_{rept}(k) + \ \beta \ W_{meas}(k)$	3	2
G	$EI_{est}(k) = \quad \xi + \ \alpha_1 \ EI_{rept}(k) + \ \alpha_2 \ EI_{rept}(k)^2 + \ \beta \ W_{meas}(k)$	4	2

Identification of this model will give the estimates of θ, from which α_1 and ξ, the coefficients used to model the under-reported EI in (4.2) can be calculated. This allows us to estimate the actual EI from the EI_{rept} as shown below,

$$\hat{EI}_{est}(k) = \hat{\alpha}_1 \ EI_{rept}(k) + \hat{\xi} \tag{4.8}$$

where "hat" denotes the estimate. Besides the linear structure as shown in (4.2), other structures that directly relates the EI_{rept} with the output of regression model, EI_{est}, can be considered. These structures may involve different number of parameters or different polynomial orders. Table 4.1 summarizes all the evaluated structures in this paper for this approach. For each model structure, the regressor $\mathcal{R}$ and the estimator θ should change accordingly. As seen from this table, nonlinear aspects are incorporated by including quadratic terms with respect to EI_{rept}, while computational complexity is not elevated by maintaining a linear regression solution. It might be noted that, structure F and G use maternal weight as one of the system inputs. During pregnancy, intervention compliance might change as gestation advances to a later stage. Hence, a gestational time dependency or maternal weight dependency might be a potential factor to improve the prediction of women's underreporting behaviors.

Models A to G in Table 4.1 involve increasing number of model parameters, as well as requiring additional pieces of information relevant to the EB model. For example, Model G contains four parameters to be identified, and once estimated, participant weight measurement is required in addition to the EI_{rept}. In comparison, Model A, with one parameter to be identified, needs no measurements. The comparison of how different structures perform in terms of their predictive ability will be discussed in the next section.

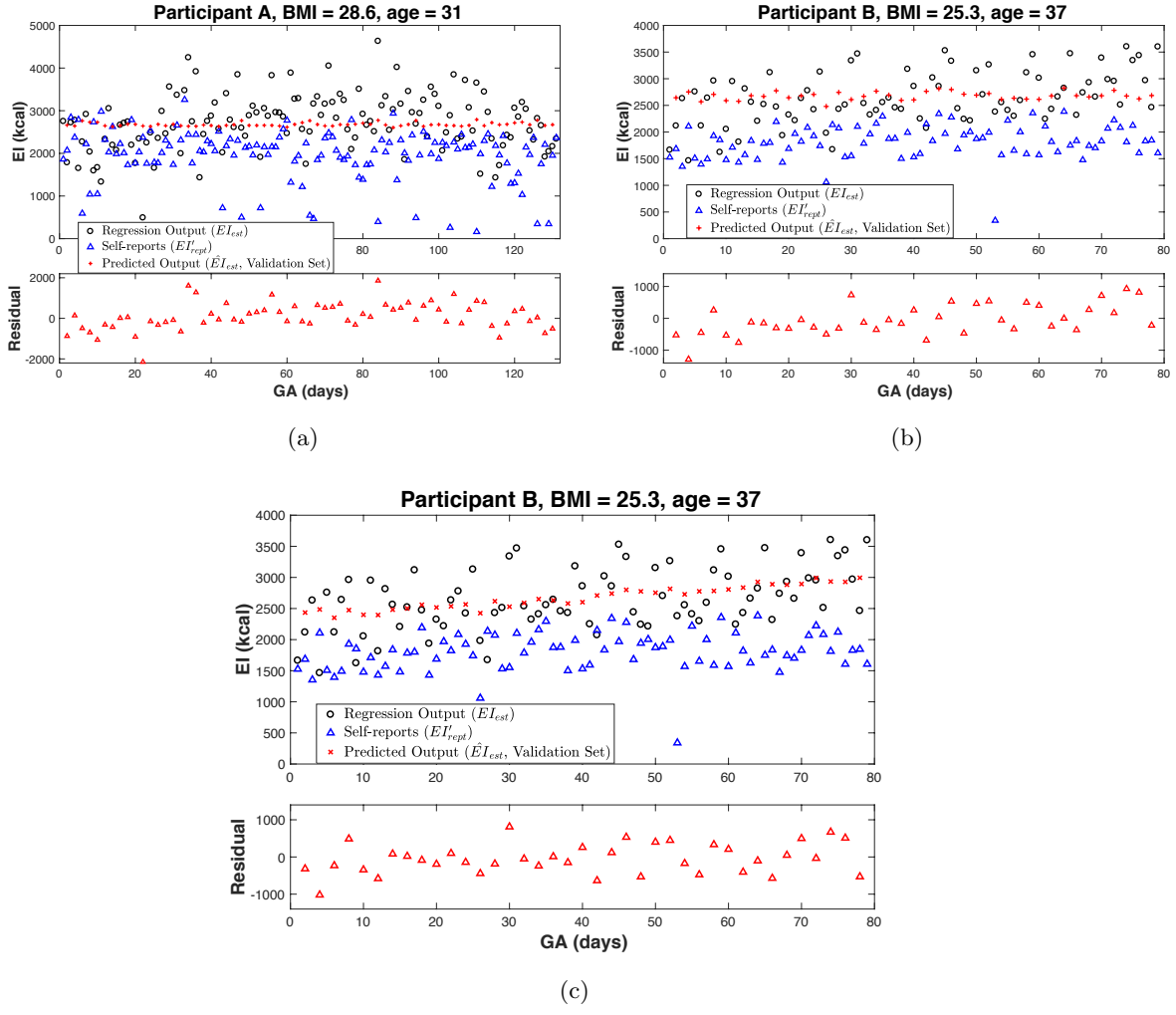

Figure 4.2: Results of semi-physical identification approach for two HMZ participants. (a) Estimation results based on Model C for an intervention Participant A on validation data set only. (b) Results for a control Participant B based on Model C (residual demonstrating non-stationarity). (c) Results based on Model F for the control Participant B (non-stationary trend in the residuals is successfully removed).

4.1.2 Results From Cross-Validation

In this section, the semi-physical approach is evaluated against participant data from the HMZ intervention study, and cross-validation techniques are used to test their performance. Cross-validation is a common test procedure in system identification to examine how accurately this predictive model performs on an independent data set. Different procedures for assigning data to estimation and validation sets can be used. Considering the characteristics of the data collected during gestation intervention, an interspersed way of data partitioning is applied by choosing one data point for estimation and every other point for validation. In this manner, the estimation and validation data sets each occupy half of the entire data set respectively, but are spread out uniformly over the intervention span.

For each model structure, estimation based on the assigned data set is performed followed by the validation on the remaining independent data set. To evaluate the performance of model prediction, multiple criteria are examined, including comparing the $\hat{EI}_{est}$ and analyzing the residual from regression. Specifically, the mean and SD of $\hat{EI}_{est}$ as well as the root mean square (RMS) of the residuals are used for analysis. Based on these evaluation criteria, the best model with a good fit can be selected while maintaining a parsimonious structure with minimum inputs. Other measures, such as the Akaike Information Theoretic Criterion (AIC) or Rissanen's minimum description length (MDL) principle can also be considered but are not as critical in this case where a cross-validation data set is available.

In Figs. 4.2a and 4.2b, the results of $\hat{EI}_{est}$ calculated for the two representative study participants are presented based on the model structure C. For Participant A, the residuals remain random and stationary while an increasing drift in the residuals is observed for Participant B. This is caused by the substantial increase observed in the regression output EI_{est} towards late pregnancy due to the increasing rate of maternal weight change. While the increase in the regression output is observed, the regression input EI_{rept} does not reflect such trend of increase but remains stationary. This issue is also found among some of the other participants from the control group, for whom substantial maternal weight gains are

observed along with a causal substantial increase in their dietary intake. If this is the case, the relationship between EI_{rept} and EI_{est} cannot be described as linear without introducing other variables. The literature also provides evidence of the time-varying characteristics of EI underreporting status across pregnancy: The level of under reporting was higher in late pregnancy in comparison to early pregnancy Moran *et al.* (2018). For participants with such characteristics, a time-dependent input such as gestational age or maternal weight, as shown in model structures F and G, will improve the estimates significantly. Fig. 4.2c shows the estimation results for Participant B using Model F, where the non-stationary trend in the residuals are successfully removed. However, this additional input does not change the results as much for the participants for whom such discrepancy in the increase of EI_{est} and EI_{rept} is not observed.

The estimated results for the two participants using different model structures are tabulated in Table 4.2. From analyzing the $\hat{EI}_{est}$ time series and the RMS of the residuals (on estimation and validation data sets), the best model for each individual participant can be selected. It should be noted that moderate variation in $\hat{EI}_{est}$ is preferred, as opposed to stationary/"static" estimates. Among all the examined model structures, Model A is the most parsimonious but with the most stationary estimates, while Model B gives the most variable yet least reliable estimates. Therefore, Model C to G are among the best informative models, with a fair balance between the residual RMS and the number of parameters. Estimates from Model C and E show similar RMS magnitudes, but Model C only involves two parameters instead of Model G with three. Hence, Model C is preferred over E. Similarly, Model F produces comparable RMS as Model G but using less parameters, so Model F is preferable to G. This analysis concludes that Model C and F are the best two options for the majority of participants, without overparametrizing the model structures. Depending on the data characteristics for individual participants, these two models can be selected one over the other based on whichever minimizes the averaged RMS. It can be concluded from the results that when there is no substantial increase in the EI_{est}, the 1st

Table 4.2: Estimation Results for Participants A and B using the global semi-physical approach for all the proposed model structures (A to G in Table 4.1). RMS represents the root mean square of the residuals.

Model Structure	Participant A				Participant B			
	Estimation		Validation		Estimation		Validation	
	$\hat{EI}_{est}$	RMS	$\hat{EI}_{est}$	RMS	$\hat{EI}_{est}$	RMS	$\hat{EI}_{est}$	RMS
A	2665±3E-12	654	2665±3E-12	675	2671±1E-12	503	2671±1E-12	483
B	2455±699	1008	2257±771	1160	2592±500	648	2628±410	577
C	2665±39	653	2676±43	673	2671±90	495	2677±74	477
D	2594±457	769	2540±536	938	2646±289	549	2680±98	470
E	2665±91	648	2677±69	687	2671±90	495	2677±79	478
F	2665±50	652	2674±50	665	2671±198	463	2674±183	409
G	2665±95	647	2675±74	680	2671±203	460	2678±189	406

order model with two parameters and the 2nd order model with three parameters provide the best (and comparable) estimation results. When substantial increases in the estimates are observed due to dramatic gestational weight gain (e.g., Participant B), the dynamics in the energy intake cannot be fully captured with correction models that are only dependent on EI_{rept} Augmentation of a time-dependent variable in the models, e.g., gestational age or weight, will significantly improve the predictive performance as shown in the residual analysis. It is important to note that the noise (as shown in Fig. 4.1) poses a challenge for this estimation problem due to the errors-in-variables problem Söderström (2012, 2018). This issue is part of current research and will be elaborated in the next section.

4.1.3 Prediction Error Analysis For Semi-physical Estimation

Semi-physical identification approach can estimate the extent of systematic underreporting and can be used for the prediction and correction of individuals' underreporting.

Table 4.3: Estimated parameters and energy intake under different scenarios. Note: % error is compute by $\frac{\text{(True Value - Estimated Value)}}{\text{True Value}} \times 100\%$.

	Scenarios							
$\mu_{\widetilde{EI}_{rept}}$	2500 kcal				4500 kcal			
$\frac{\sigma^2_{n_{EI_{rept}}}}{\sigma^2_{n_{\widetilde{EI}_{rept}}}}$	$\frac{1}{9}$		$\frac{9}{1}$		$\frac{1}{9}$		$\frac{9}{1}$	
	True	Estimated	True	Estimated	True	Estimated	True	Estimated
θ_1 (α_1)	1.1	0.1 (-90%)	1.1	1.0 (-10%)	1.1	0.1 (-90%)	1.1	1.0 (-10%)
θ_2 (ξ)	400	2875 (619%)	400	675 (69%)	400	4854 (1114%)	400	895 (124%)
EI (kcal)	3150±110	3150±35	3150±330	3150±313	5350±110	5350±35	5350±330	5350±313

The method requires EI_{rept}, leading to point-wise estimates available only at the days with EI self-reports. From the structure of the regression model in Fig. 4.1, it can be seen that both the input and output signals are corrupted by noise. Traditional system identification considers only noise in the output, treating the input signals as perfectly known and noiseless. The model that we are trying to identify here, however, corresponds to an errors-in-variables (EIV) problem with both uncertain output and input, the noise in the input being unknown and unneglectable.

This estimation can be further understood with the prediction error analysis in the frequency domain. For the example of Model C, the prediction error in time domain can be written as,

$$\begin{aligned} e_{pred}(t) =& \frac{GWG_{meas}(t) - K_2(PA(t) + RMR(t))}{K_1} - \hat{EI}_{est}(t|t-1) \\ =& (\theta_1 - \hat{\theta}_1)\widetilde{EI}_{rept}(t) + (\theta_2 - \hat{\theta}_2) - \hat{\theta}_1 n_{EI_{rept}}(t) + \frac{n_{GWG}(t)}{K_1} \end{aligned} \tag{4.9}$$

where the estimated parameters α_1 and ξ are represented as θ_1 and θ_2 for simplicity. From Parseval's theorem, the following relationship between the variance of the prediction error and its power spectrum can be obtained.

$$\lim_{N\to\infty} \sum_{i=0}^{N} e^2_{pred}(t) = \frac{1}{2\pi} \int_{-\pi}^{\pi} \Phi_e(\omega) d\omega \tag{4.10}$$

Suppose $\widetilde{EI}_{rept} \sim \mathcal{N}(\mu_{EI_{rept}}, \sigma^2_{n_{\widetilde{EI}_{rept}}})$ by assuming $\widetilde{EI}_{rept}$ being a stationary signal composed of a mean ($\mu_{\widetilde{EI}_{rept}}$) and an additive white noise ($n_{\widetilde{EI}_{rept}}$) with variances $\sigma^2_{n_{\widetilde{EI}_{rept}}}$.

$\Phi_e(\omega)$ can then be derived as,

$$\begin{aligned}\Phi_e(\omega) =&|\theta_1-\hat{\theta}_1|^2\Phi_{\widetilde{EI}_{rept}}(\omega)+|\hat{\theta}_1|^2\sigma^2_{n_{EI_{rept}}}+|\theta_2-\hat{\theta}_2|^2+2Re\{(\theta_1-\hat{\theta}_1)(\theta_2-\hat{\theta}_2)^*\mu_{\widetilde{EI}_{rept}}\}\\&+\frac{\sigma^2_{n_{GWG}}}{K_1^2}\\=&\Phi_{\widetilde{EI}_{rept}}(\omega)(|\theta_1-\hat{\theta}_1|^2+|\hat{\theta}_1|^2\frac{\sigma^2_{n_{EI_{rept}}}}{\Phi_{\widetilde{EI}_{rept}}(\omega)})+\frac{\sigma^2_{n_{GWG}}}{K_1^2}+2Re\{(\theta_1-\hat{\theta}_1)(\theta_2-\hat{\theta}_2)^*\mu_{\widetilde{EI}_{rept}}\}\\&+|\theta_2-\hat{\theta}_2|^2\end{aligned} \tag{4.11}$$

where $\Phi_{\widetilde{EI}_{rept}}(\omega)=\mu^2_{\widetilde{EI}_{rept}}+\sigma^2_{n_{\widetilde{EI}_{rept}}}$. The detailed derivation for (4.11) is presented below. Given (4.9), the covariance of the prediction error can be derived as,

$$\begin{aligned}R_{e_{pred}} =&\bar{E}\{e_{pred}(t)^2\}\\=&\bar{E}\{((\theta_1-\hat{\theta}_1)\widetilde{EI}_{rept}(t)+(\theta_2-\hat{\theta}_2)-\hat{\theta}_1 n_{EI_{rept}}(t)+\frac{n_{GWG}(t)}{K_1})^2\}\\=&\bar{E}\{(\theta_1-\hat{\theta}_1)^2EI^2_{rept}(t)+2(\theta_2-\hat{\theta}_2)\frac{n_{GWG}(t)}{K_1}+2(\theta_1-\hat{\theta}_1)(\theta_2-\hat{\theta}_2)\widetilde{EI}_{rept}(t)\\&-2\hat{\theta}_1(\theta_1-\hat{\theta}_1)\widetilde{EI}_{rept}(t)n_{EI_{rept}}(t)+(\theta_2-\hat{\theta}_2)^2+2(\theta_1-\hat{\theta}_1)\widetilde{EI}_{rept}(t)\frac{n_{GWG}(t)}{K_1}\\&-2\hat{\theta}_1 n_{EI_{rept}}(t)\frac{n_{GWG}(t)}{K_1}-2\hat{\theta}_1(\theta_2-\hat{\theta}_2)n_{EI_{rept}}(t)+\frac{n^2_{GWG}(t)}{K_1^2}+\hat{\theta}_1^2 n^2_{EI_{rept}}(t)\}\end{aligned} \tag{4.12}$$

from which the power spectrum analysis of the prediction error can be derived below,

$$\begin{aligned}\Phi_e(\omega) =&|\theta_1-\hat{\theta}_1|^2\Phi_{\widetilde{EI}_{rept}}(\omega)+|\theta_2-\hat{\theta}_2|^2+|\hat{\theta}_1|^2\sigma^2_{n_{EI_{rept}}}+\frac{\sigma^2_{n_{GWG}}}{K_1^2}\\&+2Re\{(\theta_1-\hat{\theta}_1)(\theta_2-\hat{\theta}_2)^*\mu_{EI_{rept}}\}+2Re\{(\theta_1-\hat{\theta}_1)(-\hat{\theta}_1)^*\mu_{\widetilde{EI}_{rept}}\mu_{n_{EI_{rept}}}\}\\&+2Re\{(\theta_1-\hat{\theta}_1)\mu_{\widetilde{EI}_{rept}}\mu_{n_{GWG}}/K_1\}+2Re\{(\theta_2-\hat{\theta}_2)\mu_{n_{GWG}}/K_1\}\\&+2Re\{-\hat{\theta}_1\mu_{n_{EI_{rept}}}\mu_{n_{GWG}}/K_1\}+2Re\{(\theta_2-\hat{\theta}_2)(-\hat{\theta}_1)^*\mu_{n_{EI_{rept}}}\}\\\\=&|\theta_1-\hat{\theta}_1|^2\Phi_{\widetilde{EI}_{rept}}(\omega)+|\theta_2-\hat{\theta}_2|^2+|\hat{\theta}_1|^2\sigma^2_{n_{EI_{rept}}}+2Re\{(\theta_1-\hat{\theta}_1)(\theta_2-\hat{\theta}_2)^*\mu_{\widetilde{EI}_{rept}}\}\\&+\frac{\sigma^2_{n_{GWG}}}{K_1^2}\end{aligned} \tag{4.13}$$

This is the final expression as shown in (4.11) under the assumption that all the signals are uncorrelated with noise terms being zero mean, and θ_1 and θ_2 are independently parameterized. Note that $n_{\widetilde{EI}_{rept}}$ indicates the variations in the noiseless signal of $\widetilde{EI}_{rept}$, while $n_{EI_{rept}}$ corresponds to the noise and random errors in EI_{rept}. The variance of the prior is expressed with $\sigma^2_{n_{\widetilde{EI}_{rept}}}$ and the latter with $\sigma^2_{n_{EI_{rept}}}$.

As shown in (4.11), the estimated parameters are affected by multiple coefficients that are determined by the mean and variance of the signals involved. In the case of the $\widetilde{EI}_{rept}$ signal being zero mean, that is, when $\mu_{\widetilde{EI}_{rept}} = 0$, the expression of $\Phi_e(\omega)$ simplifies to,

$$\Phi_e(\omega) = \sigma^2_{n_{\widetilde{EI}_{rept}}}(\omega)(|\theta_1 - \hat{\theta}_1|^2 + |\hat{\theta}_1|^2 \frac{\sigma^2_{n_{EI_{rept}}}}{\sigma^2_{n_{\widetilde{EI}_{rept}}}}) + |\theta_2 - \hat{\theta}_2|^2 + \frac{\sigma^2_{n_{GWG}}}{K_1^2} \tag{4.14}$$

which shows that the presence of bias in θ_1 is influenced by the ratio of $\frac{\sigma^2_{n_{EI_{rept}}}}{\sigma^2_{n_{\widetilde{EI}_{rept}}}}$, while the estimates of θ_2 should be unbiased. When $\frac{\sigma^2_{n_{EI_{rept}}}}{\sigma^2_{n_{\widetilde{EI}_{rept}}}} \gg 1$, the bias in the estimate of θ_1 will be negligible. For the case of $\widetilde{EI}_{rept}$ with non-zero mean (which corresponds to real life conditions), bias in the estimation of both parameters can be observed and is affected by the magnitude of the mean and the variance of the signals involved. Despite knowing the fact that removing the mean in EI_{rept} can reduce the bias in θ_2, the strategy of mean removal is difficult to implement in real data, because most of the model structures proposed in this paper contain a constant term, ξ. Removing the mean of $\widetilde{EI}_{rept}$ results in the removal of one of the to-be-estimated parameters.

In support of this error analysis, simulations with hypothetical yet representative data are run under the condition of 10^7 samples to test against such observations in asymptotic condition. Stationary $\widetilde{EI}_{rept}$ signals are generated with mean $\mu_{\widetilde{EI}_{rept}}$ and additive white noise signals $n_{\widetilde{EI}_{rept}}$ with variances of $\sigma^2_{n_{\widetilde{EI}_{rept}}}$. Four different scenarios are created by adjusting the ratio of $\frac{\sigma^2_{n_{EI_{rept}}}}{\sigma^2_{n_{\widetilde{EI}_{rept}}}}$ and $\mu_{\widetilde{EI}_{rept}}$. Specifically, two representative $\mu_{\widetilde{EI}_{rept}}$ are selected to simulate the real-life conditions: 2500 kcal and 4500 respectively; the ratio of $\frac{\sigma^2_{n_{EI_{rept}}}}{\sigma^2_{n_{\widetilde{EI}_{rept}}}}$ are manipulated to be 1/9 or 9/1 with $\sigma^2_{n_{\widetilde{EI}_{rept}}}$ to be 100 or 900. The estimated parameters

under different conditions are tabulated in Tables 4.3.

It is shown from the simulated cases that bias in the estimation of parameter θ_1 always exists, but the extent of the bias can be manipulated by the ratio of $\frac{\sigma^2_{n_{EI_{rept}}}}{\sigma^2_{n_{\widetilde{EI}_{rept}}}}$. When the ratio decreases to 1/9, bias in θ_1 is negligible. On the other hand, bias in the estimation of the other parameter θ_2 is readily observed and affected by the magnitude of the mean and the variance of the signals involved, largely dependent on the magnitude of the mean of $\widetilde{EI}_{rept}$. The bias in θ_2 decreases with a lower $\mu_{\widetilde{EI}_{rept}}$, while increasing $\mu_{\widetilde{EI}_{rept}}$ makes the bias in θ_2 more significant. This is also consistent with the prediction error analysis. Even though bias can be observed in both estimated parameters θ_1 and θ_2 regardless of the ratio of the noise variances, the mean of the estimated EI remains unbiased, indicating that the $\hat{E}I_{est}$ obtained from this semi-physical approach is reliable. The standard deviation of the estimates will vary and is dependent on the ratio of the variances, but as long as the ratio is modest, the variability in the estimates is close to the true signals.

Considering the EIV problem inherent to this system, pursuing approaches developed for EIV model identification is appealing. Unfortunately, the traditional maximum-likelihood approach (or a maximum-likelihood approach with Gaussian latent variables) is not effective for solving the proposed EI correction model, as large errors will result from the estimation Risuleo (KTH Royal Institute of Technology, Sweden) (2017). The problem lies in that the relationship between intake and gestational weight gain is modeled as instantaneous, leading to one effective measurement for each unknown value; for any additional data point, there is an additional parameter to be estimated. As noted in Söderström (2012, 2018), such static errors-in-variables models are among the most difficult to solve. Other approaches, such as Total Least Squares, require the noise variance ratio between the input and output measurements to be known *a priori*, or the availability of multiple experiments from the same participant; these are challenging experimental conditions that are not experienced in our study.

4.2 Model-on-Demand Approach

The semi-physical approach described previously was illustrated on a variety of model structures that are characterized by different inputs or polynomial orders; confidence intervals for the estimates are possible by bootstrapping the residues. The accuracy of this approach suffers from the intrinsic errors-in-variables problem due to input noise, but a simulation study showed that when the variance of the input noise is modest, this semi-physical approach is still accurate and reliable in terms of estimating the EI.

This semi-physical identification approach falls in the category of global parametric modeling methods, where all the available data points are used for batch estimation, leading to a single estimator for every operating condition. The model obtained with this global approach is assumed to be valid over the entire regressor space. Considering the dynamical changes in both physiological and psychological status during gestation, it may not be sensible to use a fixed model to describe the maternal energy intake behaviors by averaging the data collected in different gestational stages. Hence, the usefulness of this approach is limited.

Alternatively, local modeling techniques such as the Model-on-Demand (MoD) predictor use only portions of the data, relevant to the region of interest, to determine a model as needed (Braun *et al.*, 2001). In MoD estimation all observations are stored on a database, and a local regression is performed using an "on demand" linear or quadratic model to estimate the system output at each time step. Hence, a model/prediction is obtained "on demand" and the data used for every iteration is selected independently, making this estimator capable of coping with nonlinearities presented in the model. This data-centric, nonlinear estimation method substantially enhances the classical local modeling problem. Since the MoD technique is data-driven, the user can dedicate less time making decisions regarding model structure; the requirement, however, is an informative database.

4.2.1 Method Description

Consider a SISO system with nonlinear ARX structure

$$y(t) = m(\varphi(t)) + e(t) \tag{4.15}$$

where $m(\cdot)$ is an unknown nonlinear mapping and e is an error term modelled as i.i.d. random variables with zero mean. The regressor space $\varphi(t)$ is of the same form as an ARX model:

$$\varphi(t) = [y(t-1), \cdots, y(t-n_a), u(t-n_k), \cdots, u(t-n_b-n_k)]^T \tag{4.16}$$

where n_a, n_b and n_k denote the number of previous outputs, inputs and delays in the model. The MoD algorithm is designed to provide an estimate of $\hat{y}(t)$ based on local neighborhood of $\varphi(t)$, denoted as $\varphi(k)$. Considering computation complexity and efficiency, a local linear or quadratic relationship is proposed to approximate $m(\cdot)$ for further optimization. For example, a local linear structure with respect to estimator $\beta = [\beta_0, \beta_1]$ can be assumed as below,

$$\hat{m}(\varphi(k), \hat{\beta}) = \hat{\beta}_0 + \hat{\beta}_1^T(\varphi(k) - \varphi(t)) \tag{4.17}$$

The estimates of β is computed from the following objective function:

$$\hat{\beta} = \min_{\hat{\beta}} \sum_{k=1}^{N} \ell(\hat{y}(k) - \hat{m}(\varphi(k), \hat{\beta}))\, W\left(\frac{||\varphi(k) - \varphi(t)||_M}{h}\right)$$

where $\ell(\cdot)$ is the function for computing quadratic norm; $||u||_M$ is a scaled distance function, defined as $||u||_M = \sqrt{uM^Tu}$. The bandwidth parameter h is used to control the size of the local neighborhood and is computed adaptively for each prediction with a localized version of the Akaike Information Criterion (AIC) method. The selection of the bandwidth reflects the trade-off between the bias and variance of the estimate errors. $W(\cdot)$ is the kernel function to assign weights to every data point within the selected neighborhood window. The weight for each point is determined based on its distance from the operating condition with the goal of minimizing the point-wise mean square error of the estimate. Specifically,

a tricube window function is used in lieu of the typical bell-shaped function, to improve computational tractability (Braun *et al.*, 2001).

In contrast to the global semi-physical identification approach which leads to a fixed estimator from batch estimation, the MoD algorithms re-perform the optimization problem for each operating condition with newly computed weighting values. These iterations provide dynamically changing estimators/predictions corresponding to the local data characteristics. In a user-friendly MoD software package [1] , the only user decision required is the choice of regressor vector parameters n_a, n_b and n_k, local model order (linear or quadratic), and a lower bound on the number of data the bandwidth selector can use (readily determined by validation in a few iterations). This greatly enhances ease of use and acceptance of the technique.

From our experience from the global semi-physical approach, the output, y, of the MoD predictor corresponds to EI_{actual} in the semi-physical model while $\hat{y}$ corresponds to EI_{est}. The input to the predictor u can be combinations of the signals EI_{rept}, EI^2_{rept}, and W_{meas} (per Table 4.1). To construct the regressor, $n_a = 0$, $n_b = 1$, and $n_k = 0$.

4.2.2 Estimation Results Compared With Semi-physical Approach

In this section, the MOD approach will be evaluated against the same HMZ participant data (participant A and B) used for the global method. Similarly, cross-validation techniques with intersperse data partitioning are used to test the performance of the models. The examined criteria for analyzing the performance of model prediction are the same, including the mean and standard deviation of $\hat{EI}_{est}$ as well as the computed root mean square (RMS) of the residuals from regression.

In Fig. 4.3 and 4.4, the results of EI_{est} calculated for the two representative study participants (A and B) using the MoD approach are presented and compared with the best model structures, *e.g.*, Model C and F in the global approach. The mean and SD of the

[1] http://csel.asu.edu/MoDMPCtoolbox

estimates as well as the RMS of the residuals using MoD approach is tabulated in Table 4.4. The horizontal comparison between the two approaches can be found in Table 4.5 for cases with different number of inputs and model structures.

As demonstrated in previous section, the residuals for participant B using both Model C and F in global method remain random and stationary. With an additional input in Model F, the model prediction does not improve significantly compared with Model C, and the estimates for both structures are quite static with low variances. Model B gives more variable estimates with an expense of increasing residuals. On the other hand, the MoD approach can provide good estimates for this participant with lower residuals and moderate variances. To be parallel with the semi-physical approach, one input case with the MoD approach is compared with the one-input structures in Model B and C as shown in Fig. 4.4.

The analysis for participant A is even more interesting. Section 4.1.2 has described an increasing drift observed in the residuals for this participant when using Model C. This is due to the significant increase in EI_{est} towards late pregnancy while the model input signals (self-reports) remaining stationary synchronously. Such observations in maternal weight gains can lead to a nonlinear relationship between EI_{rept} and EI_{est}. For participants with such characteristics, a time-dependent input such as gestational age or maternal weight (as shown in Model Structure F) can improve the estimates significantly. MoD approach can successfully remove the drift in the residuals by capturing the unmodeled dynamics without requiring any extra piece of time-dependent information, as seen from Fig. 4.3. For a parallel comparison, one input case with the MoD approach is compared with the one-input structure in Model C, while two-input case in MoD is used to compare with the two-input Model F. Furthermore, Table 4.5 shows that MoD approach can achieve better prediction by requiring less pieces of information/measurements from participants by comparing the RMS for each estimator. This advantage from MoD approach can reduce participant burdens and contribute to the success of future intervention.

In summary, when significant increases in self-reports are observed due to dramatic

Table 4.4: Estimation Results for Participants A and B using Model-on-Demand (MoD).

Inputs	Participant A				Participant B			
	Estimation		Validation		Estimation		Validation	
	$\hat{EI}_{est}$	RMS	$\hat{EI}_{est}$	RMS	$\hat{EI}_{est}$	RMS	$\hat{EI}_{est}$	RMS
$[EI_{rept}]$	2666±172	642	2696±203	671	2699±144	458	2678±147	404
$[EI_{rept},\ EI^2_{rept}]$	2648±210	610	2696±246	709	2718±183	447	2747±246	449
$[EI_{rept},\ W_{meas}]$	2696±203	671	2659±235	616	2681±211	440	2654±239	389
$[EI_{rept},\ EI^2_{rept}]$ $W_{meas}]$	2625±145	614	2666±156	674	2704±199	436	2704±237	380

weight gain (e.g., Participant A), the dynamics in the energy intake cannot be fully captured with correction models that are only dependent on EI_{rept} (which are usually being stationary signals). Augmentation of a time-dependent variable in the models, e.g., gestational age or weight, will improve the predictive performance as shown in the residual analysis. The MoD approach, on the other hand, can achieve comparable and even better prediction performance, while requiring less information of the energy balance system from participants, as well as involving reduced engineering effort. When there is no significant increase in EI_{rept}, the MoD approach can still achieve comparable or better estimation results (in terms of residuals) compared with the best model options in the global approach. In addition, the MoD estimates are showing more variances than the ones from the global approach.

Above all, both approaches described here can correct for future participant self-reported energy intake which contains potential underreporting. The estimated models are useful in determining the portion of energy intake that is systematically underreported, enabling health providers to deliver informative health guidance for participants, and allowing energy balance models to be more accurately used in intervention settings.

Table 4.5: Comparison of estimation results for the two approaches for Participants A and B. Note: model structure A of the semi-physical approach is not included in the comparison.

Participant A				Participant B		
MoD Method		Semi-physical Approach			MoD Method	
Inputs	RMS	RMS	Model Structure	RMS	RMS	Inputs
$[EI_{rept}]$	671	1160	B	577	404	$[EI_{rept}]$
		673	C	478		
$[EI_{rept},\ EI^2_{rept}]$	709	938	D	470	449	$[EI_{rept},\ EI^2_{rept}]$
		687	E	478		
$[EI_{rept},\ W_{meas}]$	616	665	F	409	389)	$[EI_{rept},\ W_{meas}]$
$[EI_{rept},\ EI^2_{rept},\ W_{meas}]$	674	680	G	406	380	$[EI_{rept},\ EI^2_{rept},\ W_{meas}]$

4.3 Summary of Proposed Correction Approaches

From past literature and our experience from HMZ, it is evident that misreporting is a common problem in self-reported measures, and especially significant in self-reported energy intake. To address this issue, we extended our exploration in the estimation approaches and developed another category of estimating methods in this chapter, which is based on system identification principles to correct biased self-reported measurements of EI in the future. Specifically, efforts have been made to obtain a functional relationship between actual EI and self-reports, leading to two approaches that both feature the ability to parametrize the extent of EI underreporting: a global estimation approach and a local non-linear estimator based on "Model-on-Demand" concept.

If compared between these two semi-physical methods, they feature different pros and cons. The identified model from the global semi-physical approach remains fixed over the entire span of interest. It may be good to use the fixed model to average the dynamics of the underreporting behaviors, especially in weight control interventions for general populations,

but the fixed model may not be accurate enough to describe the potentially time-varying functional relationships between actual EI and self-reports for pregnant women in different stages during gestation. In addition, the global approach has to require *a priori* information to make sensible decisions of model structures. Nevertheless, this method can still generate moderate estimates with less computational effort.

In contrast, the Model-on-Demand approach can obtain time-varying models that capture nonlinearities observed in the data, and it can achieve comparable and even better prediction performance, while requiring less information of the energy balance system from participants, as well as involving reduced engineering effort. Even though this local method requires reduced engineering effort from users and can be implemented via user-friendly software, it still involves higher complexity in the computation. When applying these illustrated approaches in various settings, the features of each method need to be considered and examined carefully for the interests of different applications. As a future research direction, it may be worthwhile to explore the contributions of certain maternal psychological factors to the underreporting correction models from either approach by using the longitudinal measurements of maternal depression, anxiety, visual perception of body image in pregnancy as model inputs.

In contrast with the estimation approaches developed in Chapter 3, intensive measurements of the EB variables (W, PA and RMR) may not be necessary for these two methods once a correction model is estimated. With this being said, less information from participant measurements is required to realize future estimation. However, unlike the estimation approaches in Chapter 3, these methods do require self-reported EI, leading to point-wise estimates available only at EI measurements. It is also important to note that the input noise poses a challenge for both estimation methods due to the problem of errors-in-variables, as shown in Fig. 4.1. Usually, the system identification problems only consider the noise in the output, treating the input signals as perfectly known and noiseless. The model that we are trying to identify in this chapter, however, is a model with both uncertain output and

input, with the noise in the input unknown and unneglectable. The models of this kind is categorized as the errors-in-variables (EIV) models, which are more complicated to identify than the models subject to output noise only. It requires additional assumptions on the noise in the input measurements or the input signal itself in order to be able to identify this class of models; otherwise, the EIV is intrinsically unidentifiable. The EIV problem has been a growing interest in recent research and multiple estimation approaches have been developed with different levels of computation efforts and complicity. Further exploration on this topic can be interesting for future work.

So far, we have demonstrated a diverse set of approaches for energy intake estimation that feature varying levels of complexity, novelty, and usefulness. Each approach has pros and cons, and features advantages over the other approaches based on user requirements or data characteristics; decisions of which approach to be used need to be made carefully considering different circumstances. Ultimately, approaches presented in this work have played (and will continue to play) an important role in *Healthy Mom Zone*, and related weight control interventions resulting from this research that require judicious determination of energy intake.

In the following chapters, the use of the Hybrid Model Predictive Control (HMPC) schemes based on participant validated models will be demonstrated to show how the individually tailored intervention strategies developed for the HMZ Study are implemented and superior to the traditional "If-Then" rules. Since participant energy intake serves as one of the tailoring variables that the HMPC algorithm uses to determine the optimized intervention dosages, the accuracy of the assessments of this element is crucial. As pointed out in previous contents, substantially biased EI self-reports will deter the purpose of the controller design. Therefore, the estimation approaches developed in the current and previous chapters is necessary for the good performance of the closed-loop control system for interventions. Chapter 5 describes how the participant validated models are obtained, and Chapter 6 details the HMPC controller design and feedback strategy of the intervention.

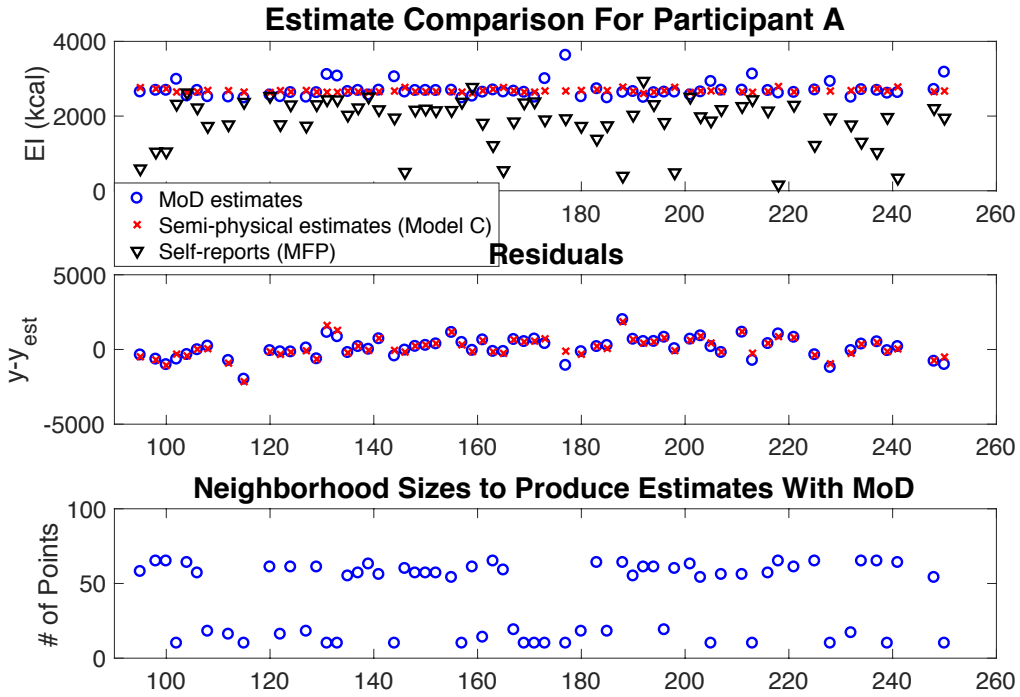

(a)

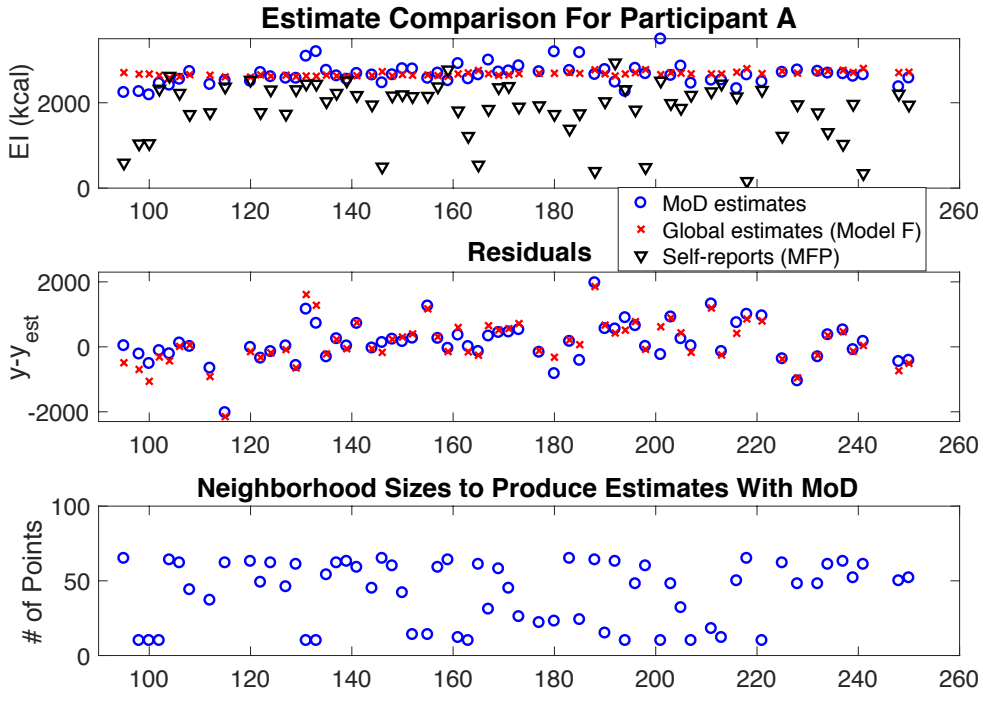

(b)

Figure 4.3: Estimate comparison on validation data set with the two approaches for Participant A (an intervention participant) from HMZ Study. One input case was used for MoD approach in Figure (a), where Model structure C (also using one input) was used with the semi-physical approach. Figure (b) compares the two input case with MoD approach (EI_{rept} and W_{meas}) and Model F (two inputs as well) with the semi-physical approach.

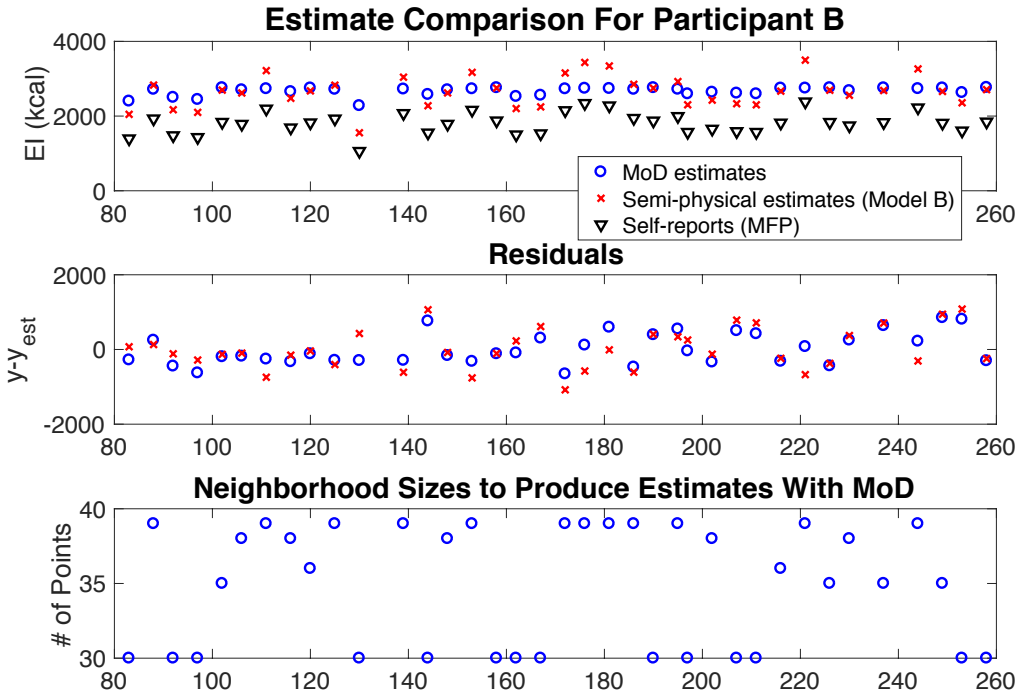

(a)

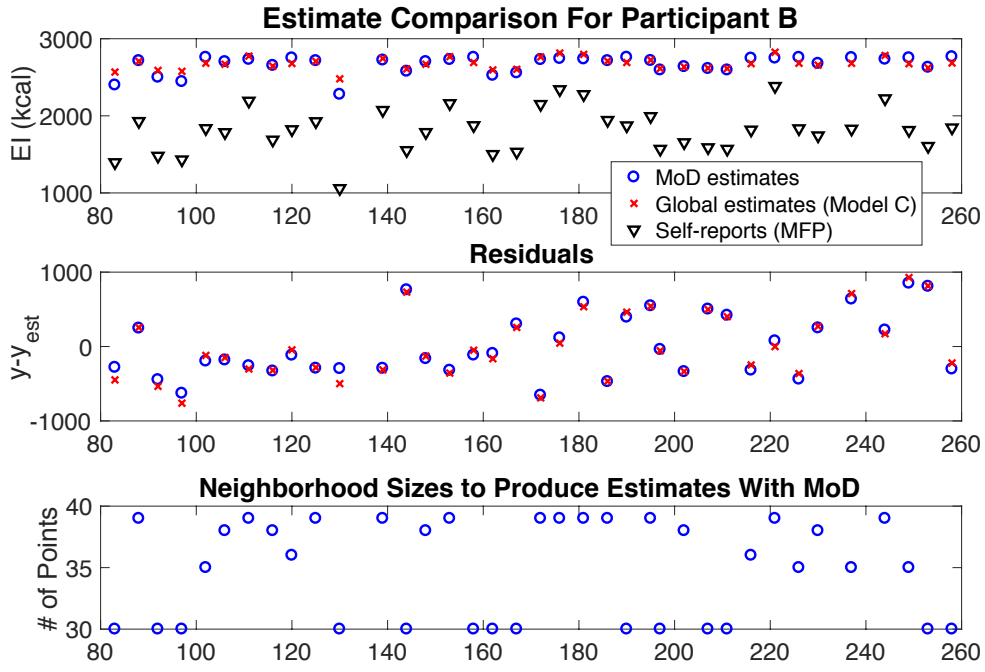

(b)

Figure 4.4: Estimate comparison on validation data set with the two approaches for Participant B (a control participant) from HMZ Study. One input case was used for MoD approach in both figures, while Model B and C (both using one input) from the semi-physical approach were used in Figure (a) and (b) respectively.

Chapter 5

SEMI-PHYSICAL IDENTIFICATION OF PARTICIPANT VALIDATED MODELS

The individually tailored and intensively adaptive intervention approach developed for the *Healthy Mom Zone* study considers a closed-loop design that can be achieved with either IF–THEN decision rules or the Hybrid Model Predictive Control (HMPC). HMPC decision policies can assign optimized intervention dosages based on real-time measures of participant weight gain and energy intake. In this way, a customized intervention that can adapt to individuals' unique needs can be provided for each participant, and the effectiveness of any intervention efforts can be maximized.

Considering HMPC being a model-based control algorithm, the accuracy of the models that HMPC uses for the prediction of participant behaviors and behavioral outcomes (maternal weight gain) is crucial in the optimization of the intervention dosages. As shown in Fig. 1.2, output of the HMPC controller is the magnitude and frequency of intervention components determined based on participant responses in real-time. How the different intervention components dictated by HMPC eventually affect participant behaviors/behavioral outcomes need to be accurately described in order for a good performance of the HMPC controller. In Chapter 2, the development of a behavioral model based on the Theory of Planned Behavior (TPB), an energy balance model for maternal weight prediction and a model for intervention delivery dynamics have been presented. Once integrated, these three models comprise a comprehensive model that can be used for the implementation of the HMPC. The first-principles energy balance model has been well-developed with categorical system gains that are accurate enough to predict maternal weight gain for women with different levels of BMI/weights. However, the TPB model and the intervention delivery dynamics are only provided with model structures, leaving the model parameters undetermined. In the HMZ study, measurements of the variables in the TPB models have been

collected for individual participants, hence can be used to obtain and individualize the model parameters for HMPC implementation.

The goal of the work presented in this chapter is to obtain participant-validated models that can be used for control purposes, as will be shown in Chapter 6. Semi-physical identification techniques will be used to estimate the model parameters involved in the TPB model. Results based on the small data sets collected in the feasibility study in Phase I will be used to inform Phase II study. However, clinical constraints such as participant burden and compliance need to be considered in the design or modification of the intervention/measurement protocols. These constraints limit the size of the collected data sets, and further limit the identification work based on the data available. More details will be provided in ensuing sections. Despite the challenges proposed by the issues in participant data, this work still provides an informative insight for related intervention design in the future.

5.1 Modeling and Measures

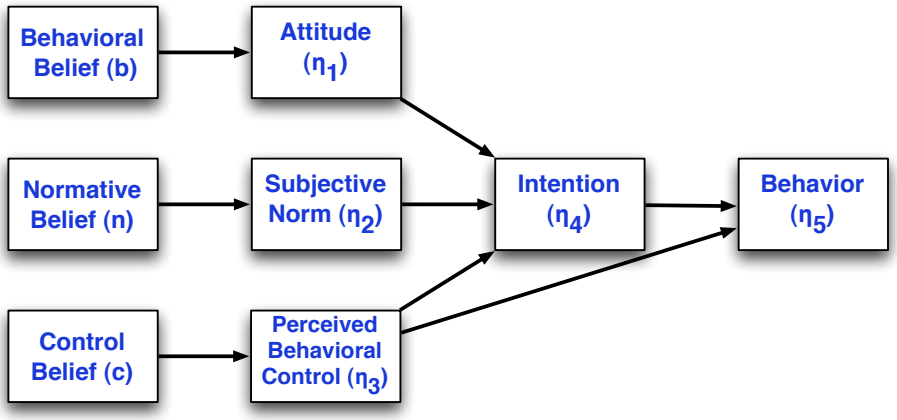

Figure 5.1: Standard Theory of Planned Behavior (TPB) path diagram for physical activity.

The parameters in the comprehensive model that need to be estimated include the TPB behavioral model and the model for intervention delivery dynamics. The TPB model that includes two independent modules to dynamically model physical activity (PA) and healthy eating (HE) behaviors has been developed in Chapter 2. The path diagrams for the two

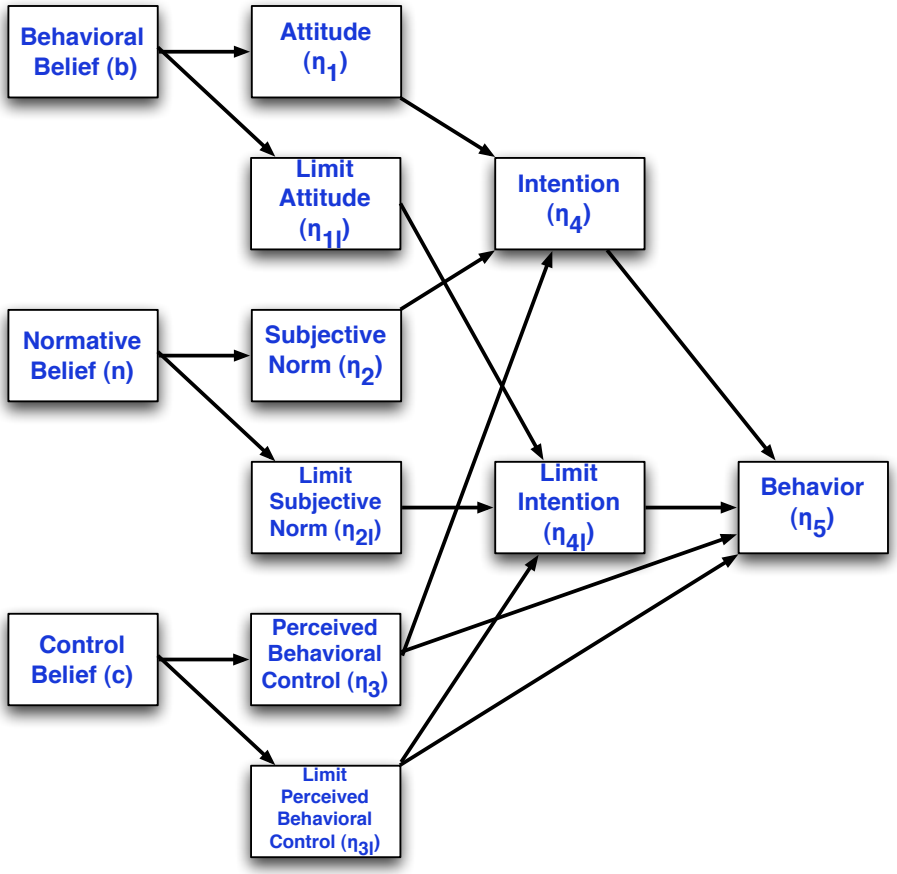

Figure 5.2: TPB path diagram for healthy eating, including limit constructs.

modules with the variable representation for each construct are shown in Fig. 5.1 and 5.2, from which two sets of differential equations for the behavioral system are established. The system of differential equations used to describe the PA module is expressed below,

$$\tau_1 \frac{d\eta_1(t)}{dt} = \gamma_{1b}\, b(t) - \eta_1(t) \tag{5.1a}$$

$$\tau_2 \frac{d\eta_2(t)}{dt} = \gamma_{2n}\, n(t) - \eta_2(t) \tag{5.1b}$$

$$\tau_3 \frac{d\eta_3(t)}{dt} = \gamma_{3c}\, c(t) - \eta_3(t) \tag{5.1c}$$

$$\tau_4 \frac{d\eta_4(t)}{dt} = \beta_{41}\eta_1(t) + \beta_{42}\eta_2(t) + \beta_{43}\eta_3(t) - \eta_4(t) \tag{5.1d}$$

$$\tau_5 \frac{d\eta_5(t)}{dt} = \beta_{54}\eta_4(t) + \beta_{53}\eta_3 - \eta_5(t) \tag{5.1e}$$

The differential equations described above can be transformed to the following state space

representations of the TPB model on PA.

$$\dot{x} = A(\phi)x(t) + B(\phi)u(t) \tag{5.2a}$$

$$y = C(\phi)x(t) \tag{5.2b}$$

where: $x = \begin{bmatrix} \eta_1 & \eta_2 & \eta_3 & \eta_4 & \eta_5 \end{bmatrix}^T$, which denotes a vector of $d_x = 5$ state variables;

$u = \begin{bmatrix} b & n & c \end{bmatrix}^T$, which denotes a vector of $d_u = 3$ input variables;

$y = \begin{bmatrix} \eta_1 & \eta_2 & \eta_3 & \eta_4 & \eta_5 \end{bmatrix}^T$, which denotes a vector of $d_y = 5$ output variables;

$\phi = [\tau_1\ \tau_2\ \tau_3\ \tau_4\ \tau_5\ \gamma_{1b}\ \gamma_{2n}\ \gamma_{3c}\ \beta_{41}\ \beta_{42}\ \beta_{43}\ \beta_{53}\ \beta_{54}]^T$, which denotes a vector of $d_\phi = 13$ unknown model parameters;

$$A = \begin{bmatrix} -\frac{1}{\tau_1} & 0 & 0 & 0 & 0 \\ 0 & -\frac{1}{\tau_2} & 0 & 0 & 0 \\ 0 & 0 & -\frac{1}{\tau_3} & 0 & 0 \\ \frac{\beta_{41}}{\tau_4} & \frac{\beta_{42}}{\tau_4} & \frac{\beta_{43}}{\tau_4} & -\frac{1}{\tau_4} & 0 \\ 0 & 0 & \frac{\beta_{53}}{\tau_3} & \frac{\beta_{54}}{\tau_4} & -\frac{1}{\tau_5} \end{bmatrix};$$

$$B = \begin{bmatrix} \frac{\gamma_{1b}}{\tau_1} & 0 & 0 \\ 0 & \frac{\gamma_{2n}}{\tau_2} & 0 \\ 0 & 0 & \frac{\gamma_{3c}}{\tau_3} \\ 0 & 0 & 0 \\ 0 & 0 & 0 \end{bmatrix};$$

$C = I\ (9 \times 9)$.

The system of differential equations for the HE module with limit constructs are shown

in (5.3).

$$\tau_1 \frac{d\eta_1(t)}{dt} = \gamma_{1b} b(t) - \eta_1(t) \tag{5.3a}$$
$$\tau_{1l} \frac{d\eta_{1l}(t)}{dt} = \gamma_{1lb} b(t) - \eta_{1l}(t) \tag{5.3b}$$
$$\tau_2 \frac{d\eta_2(t)}{dt} = \gamma_{2n} n(t) - \eta_2(t) \tag{5.3c}$$
$$\tau_{2l} \frac{d\eta_{2l}(t)}{dt} = \gamma_{2ln} n(t) - \eta_{2l}(t) \tag{5.3d}$$
$$\tau_3 \frac{d\eta_3(t)}{dt} = \gamma_{3c} c(t) - \eta_3(t) \tag{5.3e}$$
$$\tau_{3l} \frac{d\eta_{3l}(t)}{dt} = \gamma_{3lc} c(t) - \eta_{3l}(t) \tag{5.3f}$$
$$\tau_4 \frac{d\eta_4(t)}{dt} = \beta_{41}\eta_1(t) + \beta_{42}\eta_2(t) + \beta_{43}\eta_3(t) - \eta_4(t) \tag{5.3g}$$
$$\tau_{4l} \frac{d\eta_{4l}(t)}{dt} = \beta_{41l}\eta_{1l}(t) + \beta_{42l}\eta_{2l}(t) + \beta_{43l}\eta_{3l}(t) - \eta_{4l}(t) \tag{5.3h}$$
$$\tau_5 \frac{d\eta_5(t)}{dt} = \beta_{54}\eta_4(t) + \beta_{54l}\eta_{4l}(t) + \beta_{53}\eta_3(t) + \beta_{53l}\eta_{3l}(t) - \eta_5(t) \tag{5.3i}$$

The differential equations described above can be transformed to the following state space representations of the TPB model on HE.

$$\dot{x} = A(\phi)x(t) + B(\phi)u(t) \tag{5.4a}$$
$$y = C(\phi)x(t) \tag{5.4b}$$

where: $x = \begin{bmatrix} \eta_1 & \eta_{1l} & \eta_2 & \eta_{2l} & \eta_3 & \eta_{3l} & \eta_4 & \eta_{4l} & \eta_5 \end{bmatrix}^T$, which denotes a vector of $d_x = 9$ state variables;

$u = \begin{bmatrix} b & n & c \end{bmatrix}^T$, which denotes a vector of $d_u = 3$ input variables;

$y = \begin{bmatrix} \eta_1 & \eta_{1l} & \eta_2 & \eta_{2l} & \eta_3 & \eta_{3l} & \eta_4 & \eta_{4l} & \eta_5 \end{bmatrix}^T$, which denotes a vector of $d_y = 9$ output variables;

$\phi = [\tau_1,\ \tau_{1l},\ \tau_2,\ \tau_{2l},\ \tau_3,\ \tau_{3l},\ \tau_4,\ \tau_{4l},\ \tau_5,\ \gamma_{1b},\ \gamma_{1lb},\ \gamma_{2n},\ \gamma_{2ln},\ \gamma_{3c},\ \gamma_{3lc},\ \beta_{41},\ \beta_{42},\ \beta_{43},\ \beta_{41l},\ \beta_{42l},\ \beta_{43l},\ \beta_{53},\ \beta_{53l},\ \beta_{54},\ \beta_{54l}]^T$, which denotes a vector of $d_\phi = 25$ unknown model parameters;

$$A = \begin{bmatrix} -\frac{1}{\tau_1} & 0 & 0 & 0 & 0 & 0 & 0 & 0 & 0 \\ 0 & -\frac{1}{\tau_{1l}} & 0 & 0 & 0 & 0 & 0 & 0 & 0 \\ 0 & 0 & -\frac{1}{\tau_2} & 0 & 0 & 0 & 0 & 0 & 0 \\ 0 & 0 & 0 & -\frac{1}{\tau_{2l}} & 0 & 0 & 0 & 0 & 0 \\ 0 & 0 & 0 & 0 & -\frac{1}{\tau_3} & 0 & 0 & 0 & 0 \\ 0 & 0 & 0 & 0 & 0 & -\frac{1}{\tau_{3l}} & 0 & 0 & 0 \\ \frac{\beta_{41}}{\tau_4} & 0 & \frac{\beta_{42}}{\tau_4} & 0 & \frac{\beta_{43}}{\tau_4} & 0 & -\frac{1}{\tau_4} & 0 & 0 \\ 0 & \frac{\beta_{41l}}{\tau_{4l}} & 0 & \frac{\beta_{42l}}{\tau_{4l}} & 0 & \frac{\beta_{43l}}{\tau_{4l}} & 0 & -\frac{1}{\tau_{4l}} & 0 \\ 0 & 0 & 0 & 0 & \frac{\beta_{53}}{\tau_3} & \frac{\beta_{53l}}{\tau_{3l}} & \frac{\beta_{54}}{\tau_4} & \frac{\beta_{54l}}{\tau_{4l}} & -\frac{1}{\tau_5} \end{bmatrix};$$

$$B = \begin{bmatrix} \frac{\gamma_{1b}}{\tau_1} & 0 & 0 \\ \frac{\gamma_{1lb}}{\tau_{1l}} & 0 & 0 \\ 0 & \frac{\gamma_{2n}}{\tau_2} & 0 \\ 0 & \frac{\gamma_{2ln}}{\tau_{2l}} & 0 \\ 0 & 0 & \frac{\gamma_{3c}}{\tau_3} \\ 0 & 0 & \frac{\gamma_{3lc}}{\tau_{3l}} \\ 0 & 0 & 0 \\ 0 & 0 & 0 \\ 0 & 0 & 0 \end{bmatrix};$$

$C = I\ (9 \times 9)$.

The path diagram for the model for intervention delivery dynamics is shown in Fig. 5.3 and if represented using a systems of differential equations, the system can be written as:

$$\tau_b \frac{db(t)}{dt} = \gamma_{11} base(t) + \gamma_{12} up(t) - b \tag{5.5a}$$

$$\tau_n \frac{dn(t)}{dt} = \gamma_{21} base(t) + \gamma_{22} up(t) - n \tag{5.5b}$$

$$\tau_c \frac{dc(t)}{dt} = \gamma_{31} base(t) + \gamma_{32} up(t) - c \tag{5.5c}$$

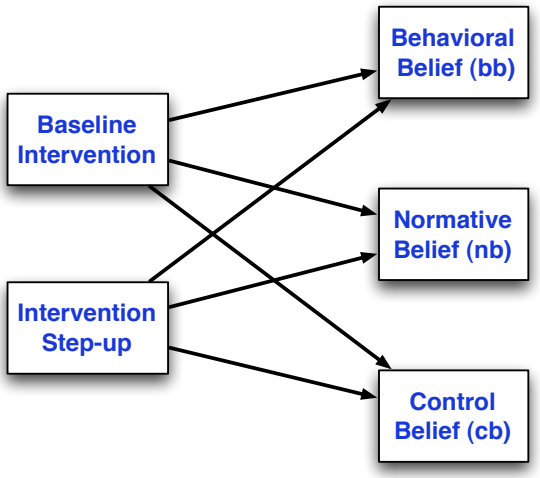

Figure 5.3: Path diagram for the model of intervention delivery dynamics using simplified inputs.

and if transformed to the state space representations gives,

$$\dot{x} = A(\phi)x(t) + B(\phi)u(t) \tag{5.6a}$$

$$y = C(\phi)x(t) \tag{5.6b}$$

where:

$x = \begin{bmatrix} b & n & c \end{bmatrix}^T$, which denotes a vector of $d_x = 3$ state variables;

$u = \begin{bmatrix} base & up \end{bmatrix}^T$, which denotes a vector of $d_u = 2$ input variables;

$y = \begin{bmatrix} b & n & c \end{bmatrix}^T$, which denotes a vector of $d_y = 3$ output variables;

$\phi = [\tau_b,\ \tau_n,\ \tau_c,\ \gamma_{11},\ \gamma_{12},\ \gamma_{21},\ \gamma_{22},\ \gamma_{31},\ \gamma_{32}]^T$, which denotes a vector of $d_\phi = 9$ unknown model parameters;

$$A = \begin{bmatrix} -\frac{1}{\tau_b} & 0 & 0 \\ 0 & -\frac{1}{\tau_n} & 0 \\ 0 & 0 & -\frac{1}{\tau_c} \end{bmatrix};$$

$$B = \begin{bmatrix} \frac{\gamma_{11}}{\tau_b} & \frac{\gamma_{12}}{\tau_b} \\ \frac{\gamma_{21}}{\tau_n} & \frac{\gamma_{22}}{\tau_n} \\ \frac{\gamma_{31}}{\tau_c} & \frac{\gamma_{32}}{\tau_c} \end{bmatrix};$$

$C = I\ (3 \times 3)$.

In (5.1), (5.3) and (5.5), τ_i are time constants; γ_i and β_i are system gains. For simplicity, no pure time delays or parameter uncertainties are considered in the equations.

The data used to identify the parameters of the behavioral model are measured from the HMZ study. The behavioral constructs involved in the model are self-reported by participants using a well-designed questionnaire on a weekly basis. Each construct is evaluated based on 3 to 10 questions; the score of each question is scaled from 1 to 7, with 1 as the lowest intensity and 7 as the highest; the final score of each construct is computed from the average score of the set of the questions. The PA behavior is measured daily with *Jawbone* device as mentioned in Chapter 3; when used with the weekly behavioral data for semi-physical identification, the average of the PA data from Jawbone is computed per week to represent the PA behaviors. The HE behavior is represented with the weekly average of energy intake; since significant under-reporting of EI is identified in the self-measurements from MFP, the weekly average of EI back-calculated with the back-calculation method in Chapter 3 is used instead.

It has to be noted that the HMZ involves two longitudinal studies: a Phase I which is designed as a feasibility test, followed by a Phase II study designed for proof of concept. The Phase I study, as a trial study of the interventions, aims to establish the feasibility of the intervention dosages and the intensive measurement protocols. Hence, the intervention is designed for a shorter period of time: each participant is only subject to a six-week intervention between the 2nd and the 3rd trimester of gestation, resulting in six measurements of behavioral variables. Despite the small sample being a strong limitation for the identification work, some insights can still be gained on the dynamical characteristics of the behavioral variables, as well as improvements on the identification techniques. The findings from Phase I study can be used to inform any necessary modifications on the intervention design for Phase II.

The Phase II study is to establish proof of concept of the fully adaptive intervention, including the criterion rule for making adaptive decisions. In the Phase II study, the inter-

vention is delivered for a longer period of time: Participants are recruited into the program from the 6∼12 weeks gestation (1st trimester), and are engaged in the intervention until 37 weeks towards the delivery. The data is collected and monitored along the 26∼31 weeks of intervention. Hence, more data is possible from Phase II study which is beneficial for model identification work. However, efforts still need to be made to minimize the burden for participants in order to improve their adherence. We need to modify the frequency of the measurements based on our conclusions from Phase I study and selectively increase the measurement frequency of the more significant constructs.

In the following sections, the results of our proof-of-concept identification work are presented based on the data from the Phase I or II Studies, from which we learned some lessons that can be used to modify the intervention and measurement protocols. Any other improvements for Phase II Study will also be summarized from the results in Phase I study in Section 5.2. The results based on the data from the on-going Phase II study will be presented in Section 5.3.

5.2 Results From Phase I Study

The measured data from individual participants of the Phase I study (17 participants) are used to individually estimate the model parameters from the theoretical TPB model structure. The model parameters are estimated by a grey-box system identification procedure which relies on two sources of information: prior knowledge of the system (i.e., the TPB dynamical model), and the measured data. In this data-based analysis, the purpose is to explain the effects of three inputs over six (or nine) outputs in the context of the TPB model as shown in the path diagrams in Fig. 5.1 and 5.2. The search of parameters will keep the defined model structure. The number of data points is limited to six in Phase I study due to the measurements of behavior variables on a weekly basis over the period of six weeks of the intervention. For any missing data, mean replacement is performed to maintain enough data for identification.

Based on the dynamic characteristics of the measured behavioral variables and other

model limitations, we made several changes to the semi-physical identification procedures as described in the following.

Variable Scaling:

The final output of our model is behavioral kcal, that is the average weekly physical activity (kcal) measured by *Jawbone*, or energy intake (kcal) estimated using the first method (back-calculation method) in Chapter 3. These final outputs of behaviors in kcal are scaled to similar magnitudes as behavioral variables, which can give better fit between the estimated and real data. All constructs including "Beh (kcal)" plot in the figures are mean subtracted for identification purposes.

Model Reduction:

To ensure that the data, especially the data as input or intermediate constructs that was used for identification shows enough variation, we checked the coefficient of variation (COV) of the data from Phase I study. COV, also known as relative standard deviation, is a standardized measure of dispersion of a probability distribution or frequency distribution. It shows the extent of variability in relation to the mean of the data. It is often expressed as a percentage, and is defined as the ratio of the standard deviation of the data to the mean. As shown in the tabulated COV of the constructs for four selective participants in Table 5.1, belief variables generally show less variation within the span of the intervention. Therefore, we decide to collect the belief variables on a monthly basis for Phase II Study, as well as eliminate from our identification framework. In addition, the relative importance of attitudes, subjective norms and perceived behavioral control in terms of intentions can vary for different behaviors of interest and for different population. Attitude is showing less significance in the context of the HMZ study. Further analysis is performed to remove Attitude from the framework, due to the high burden in the measurement of that variable. Similar model reduction is adopted for TPB models on both PA and HE side, with TPB for HE behaviors further reduced by removing non-limit constructs from the structure. Non-limit constructs in the TPB model for HE behaviors demonstrate similar dynamics as the

limit constructs, while the limit constructs also favor more variations in the collected data.

Based on this analysis, a decision to change the measurement protocols was made to favor the identification work: the measurement frequency for the constructs that remain in the reduced model structures will be increased to a weekly basis. In this way, the size of the data sets used for semi-physical identification will be increased, ranging from 20 to 30 data points available. The measurements of the constructs that are removed from identification will be collected on a monthly basis, to ensure that the participant burden will not be substantially increased. Since the change of measurement protocols occurred after the start of Phase II study, two participants have completed the intervention using the old measurement protocols. As a result, a smaller data set with 7 data points is available for their analysis. Six participants went through the transitions between two measurement frequencies. The number of data points for these six participants is slightly higher, but the resulted data are severely subject to the issues of unevenly spaced sampling time, hence unfavored by identification protocols.

With such changes in the TPB model, the model for intervention delivery dynamics need to be changed accordingly: instead of connecting with the three belief variables in the full TPB model, the outputs for intervention delivery dynamics are changed to subjective norm (SN) and perceived behavioral control (PBC) in order to connect with TPB model on PA, and changed to limit SN and lim PBC for HE. The resulted path diagrams are shown in Fig. 5.4.

Constraints:

Initially, constraints were only added on the time constants of the model. With further analysis of the model, it was recognized that constraints may also be added to the paths leading from subjective norm, perceived behavioral control towards intention. This is because the change in the former two constructs can be expected to be in the same direction as the change in intention in general. For example, an increase in the attitude measurement means the overall evaluation of a participant's behavior is elevated, an increase of the

Table 5.1: The coefficient of variation (COV) of the measured TPB constructs collected for the four representative participants in Phase I Study.

Constructs	COV				
	PID1010	PID1013	PID1019	PID1041	Average
PA_BB	0%	6%	1%	4%	3%
HE_BB	0%	3%	1%	8%	3%
PA_NB	0%	5%	14%	7%	7%
HE_NB	0%	5%	3%	4%	3%
PA_CB	13%	14%	15%	14%	14%
HE_CB	21%	6%	13%	14%	13%
PA_ATT	0%	3%	3%	17%	6%
HE_ATT	2%	6%	3%	8%	5%
HE_LIM_ATT	1%	6%	6%	15%	7%
PA_SN	0%	15%	4%	8%	7%
HE_SN	0%	13%	2%	7%	5%
HE_LIM_SN	0%	19%	4%	10%	8%
PA_PBC	2%	14%	14%	14%	11%
HE_PBC	3%	25%	5%	9%	11%
HE_LIM_PBC	6%	23%	8%	9%	11%
PA_INT	1%	10%	18%	28%	14%
HE_INT	2%	10%	6%	12%	7%
HE_LIM_INT	2%	9%	9%	19%	10%

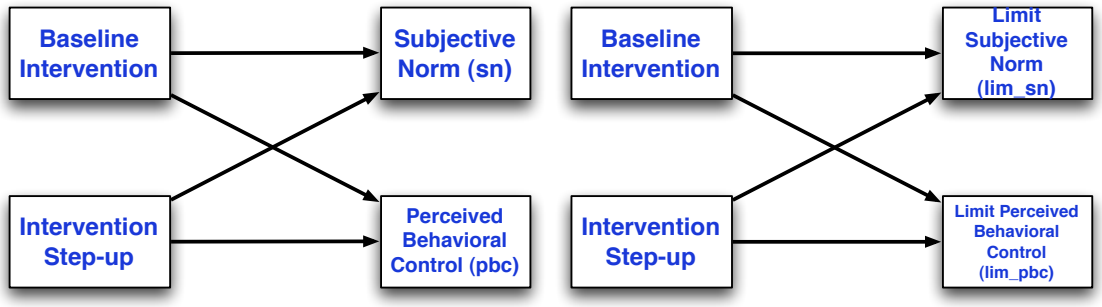

(a) (b)

Figure 5.4: Updated path diagrams for intervention delivery dynamics to integrate with reduced TPB models (left: to integrate with TPB model for PA; right: for HE).

perceived likelihood of performing that behavior is more likely occur, with less possibility to see the opposite. In this way, the identified parameters can be more physically meaningful. Similarly for the gains in the intervention delivery dynamics, where an increase of the attitude or other TPB variables will be expected following an augmentation of intervention dosage.

However, such decisions for adding constraints are subject to scrutiny. It is possible that increasing the dosages or an increase in one of the TPB constructs might not necessarily lead to a positive gain in the connected constructs, but possibly in a contradicting way. For example, requesting participants to exercise more by adding a 30 min physical activity session on site that a participant does not like might lead to a decrease in the intention for PA. Such adverse intervention outcomes might also result in a decrease of participant compliance, reflected as more data missingness in the following measurements. Therefore, such negative gains and corresponding dynamics need to be forecasted by the model, in which case any unnecessary constraints on gains should be removed. Based on this consideration, constraints or partial constraints on the gain parameters will be evaluated with intervention participants, but will not be added in the estimation of participant-validated models used for closed-loop implementation.

An illustration of using the partial constraints added for the semi-physical identification on TPB for PA behaviors is shown in Fig. 5.5, where we have positive ("+") constraint

for subjective norm (SN) and perceived behavioral control (PBC) to intention (INT), but no constraint on CB/INT/PBC to Behavior. Similarly in Fig. 5.6 for TPB model on HE behaviors, it shows that constraints for limit subject norm, limit perceived behavioral control to limit intention are imposed.

Model Order Augmentation:

The model per (5.1) or (5.3) consists of a system of first-order differential equations, but to describe a more elaborate transient response (such as overdamped, critically damped or underdamped responses), a second order system could be used (Navarro-Barrientos *et al.* (2011)). If second order dynamics are present, these can be conceptualized as being part of an inventory system that is subject to self-regulation. This will be illustrated with an example considering only one inventory as a reference: To represent behavior kcal (η_5) as a system with two poles, the equation with respect to η_5 in (5.3) can be rewritten as:

$$\tau_5^2 \frac{d^2\eta_5}{dt^2} + 2\zeta\tau_5 \frac{d\eta_5}{dt} = \beta_{54}\ \eta_4 + \beta_{54l}\ \eta_{4l} + \beta_{53}\ \eta_3 + \beta_{53l}\ \eta_{3l} - \eta_5 \tag{5.7}$$

which yields to the transfer function:

$$\eta_5(s) = \frac{\beta_{54}\ \eta_4(s) + \beta_{54l}\ \eta_{4l}(s) + \beta_{53}\ \eta_3(s) + \beta_{53l}\ \eta_{3l}(s)}{(\tau_5^2 s^2 + 2\zeta\tau_5 s + 1)} \tag{5.8}$$

For simplicity in the semi-physical identification on reduced TPB models, only the equation to describe the dynamic behaviors for η_5 is augmented to second order, while the other output of η_4 remains first order. The model structure with constraints that is adopted for semi-physical identification framework is shown in Fig. 5.5 and 5.6, where the most significant inputs in terms of input variation and the contribution of input dynamics to output are included. After examining the variation in the dynamics of the TPB constructs, it was decided to increase the measurement frequency of SN, PBC, and INT from monthly to weekly for Phase II Study.

With model structure reduction and order augmentation, the differential equations for

the TPB model on PA side can be re-written as,

$$\tau_4^2 \frac{d^2\eta_4(t)}{dt^2} + 2\zeta_4\tau_4 \frac{d\eta_4(t)}{dt} = \beta_{42}\ \eta_2(t) + \beta_{43}\ \eta_3(t) - \eta_4(t) \tag{5.9a}$$

$$\tau_5^2 \frac{d^2\eta_5(t)}{dt^2} + 2\zeta_5\tau_5 \frac{d\eta_5(t)}{dt} = \beta_{53}\ \eta_3(t) + \beta_{54}\ \eta_4(t) - \eta_5(t) \tag{5.9b}$$

The differential equations described above can be transformed to the following state space representations of the TPB model on PA.

$$\dot{x} = A(\phi)x(t) + B(\phi)u(t) \tag{5.10a}$$

$$y = C(\phi)x(t) \tag{5.10b}$$

where: $x = \begin{bmatrix} \eta_4 & \eta_5 & \frac{d\eta_5}{dt} \end{bmatrix}^T$, which denotes a vector of $d_x = 3$ state variables;

$u = \begin{bmatrix} \eta_2 & \eta_3 \end{bmatrix}^T$, which denotes a vector of $d_u = 2$ input variables;

$y = \begin{bmatrix} \eta_4 & \eta_5 \end{bmatrix}^T$, which denotes a vector of $d_y = 2$ output variables;

$\phi = [\tau_4\ \tau_5\ \beta_{42}\ \beta_{43}\ \beta_{53}\ \beta_{54}\ \zeta_5]^T$, which denotes a vector of $d_\phi = 7$ unknown model parameters;

$$A = \begin{bmatrix} -\frac{1}{\tau_4} & 0 & 0 \\ 0 & 0 & 1 \\ -\frac{\beta_{54}}{\tau_5^2} & -\frac{1}{\tau_5^2} & -\frac{2\zeta}{\tau_5} \end{bmatrix};$$

$$B = \begin{bmatrix} \beta_{42} & \beta_{43} \\ 0 & 0 \\ \frac{\beta_{53}}{\tau_5^2} & 0 \end{bmatrix};$$

$$C = \begin{bmatrix} 1 & 0 & 0 \\ 0 & 1 & 0 \end{bmatrix}.$$

Similarly, the system of differential equations with order augmentation for the TPB model for HE can be written as,

$$\tau_{4l}^2 \frac{d^2\eta_{4l}(t)}{dt^2} + 2\zeta_{4l}\tau_{4l} \frac{d\eta_{4l}(t)}{dt} = \beta_{4l2l}\eta_{2l}(t) + \beta_{4l3l}\eta_{3l}(t) - \eta_{4l}(t) \tag{5.11a}$$

$$\tau_{5l}^2 \frac{d^2\eta_{5l}(t)}{dt^2} + 2\zeta_{5l}\tau_{5l} \frac{d\eta_{5l}(t)}{dt} = \beta_{5l3l}\eta_{3l}(t) + \beta_{5l4l}\eta_{4l}(t) - \eta_{5l}(t) \tag{5.11b}$$

and the state-space representation for (5.11) can be rewritten with,

$x = \begin{bmatrix} \eta_{4l} & \eta_5 & \frac{d\eta_5}{dt} \end{bmatrix}^T$, which denotes a vector of $d_x = 3$ state variables;

$u = \begin{bmatrix} \eta_{2l} & \eta_{3l} \end{bmatrix}^T$, which denotes a vector of $d_u = 2$ input variables;

$y = \begin{bmatrix} \eta_{4l} & \eta_5 \end{bmatrix}^T$, which denotes a vector of $d_y = 2$ output variables;

$\phi = [\tau_{4l}\ \tau_5\ \beta_{4l2l}\ \beta_{4l3l}\ \beta_{53l}\ \beta_{54l}\ \zeta_5]^T$, which denotes a vector of $d_\phi = 7$ unknown model parameters;

$$A = \begin{bmatrix} -\frac{1}{\tau_{4l}} & 0 & 0 \\ 0 & 0 & 1 \\ -\frac{\beta_{54l}}{\tau_5^2} & -\frac{1}{\tau_5^2} & -\frac{2\zeta}{\tau_5} \end{bmatrix};$$

$$B = \begin{bmatrix} \beta_{4l2l} & \beta_{4l3l} \\ 0 & 0 \\ \frac{\beta_{53l}}{\tau_5^2} & 0 \end{bmatrix};$$

$$C = \begin{bmatrix} 1 & 0 & 0 \\ 0 & 1 & 0 \end{bmatrix};$$

All the parameters to be estimated are incorporated in the variable ϕ_e. To estimate ϕ_e, the well-known prediction-error identification methods (PEM) will be used. The prediction error of the system is:

$$\varepsilon(t, \phi_e) = y(t) - \hat{y}(t, \phi_e) \tag{5.12}$$

where $\hat{y}(t, \phi_e)$ is the estimated output.

Computations are executed in MATLAB using the commands *idgrey* and *greyest* from the System Identification Toolbox based on PEM methods. One criterion to evaluate the results from semi-physical identification is to compute and compare the goodness of fit for system outputs. The percentage of fit between the measured signal and model prediction is calculated using the following formula:

$$\text{fit } \% = 100 \left(1 - \frac{\|y - \hat{y}\|_2}{\|y - \bar{y}\|_2} \right) \tag{5.13}$$

where $\bar{y}$ represents the mean of the measured signal. The goodness of fit can be significantly

improved by adjusting the initial conditions of the models or by trying higher order models with more parameters involved.

Phase I participants are randomly assigned to six dosages with baseline only or baseline plus different levels of intervention steps-up. Due to the short span of intervention and the resulted small data sets, only the identification for the TPB model will be tested and presented. The identification results on TPB model for PA behaviors for two selected participants are shown in Fig. 5.7 and 5.8. The identification results on TPB model for HE behaviors for two selected participants are shown in Fig. 5.9 and 5.10. The identified parameters are tabulated in Table 5.2 and 5.3. Seen from the results, the goodness of fit is significantly improved by the modification we made to the models. However, it is important to note that with only six weeks of data points for the TPB variables and no validation data, the estimation of the model parameters is limited. The more comprehensive modeling procedure requires more data points. The goodness of fit is generally not bad with the simplified model in this case, but more data points are needed to validate predictive ability of the identified models for individual participants.

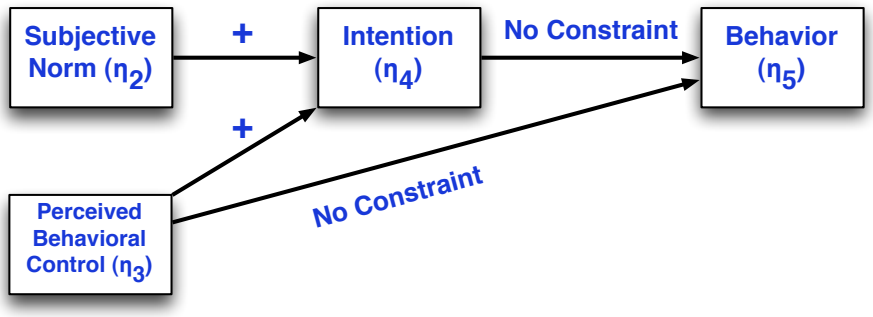

Figure 5.5: A constrained and simplified structure of the TPB model for PA behaviors for identification purpose.

5.3 Results From Phase II Study

In this section, the results for three representative Phase II participants will be presented and discussed. The first two participants are the ones recruited at the beginning of Phase

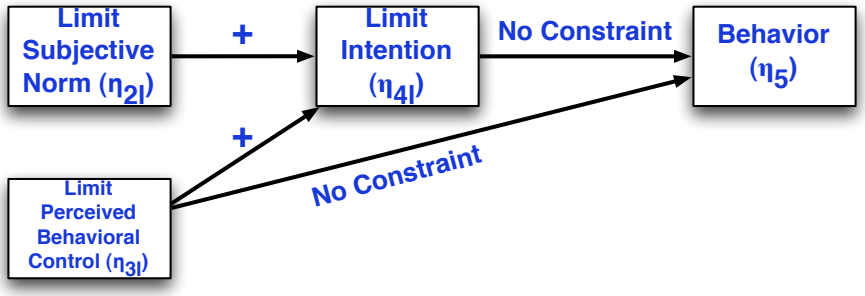

Figure 5.6: A constrained and simplified structure of the TPB model for HE behaviors for identification purpose.

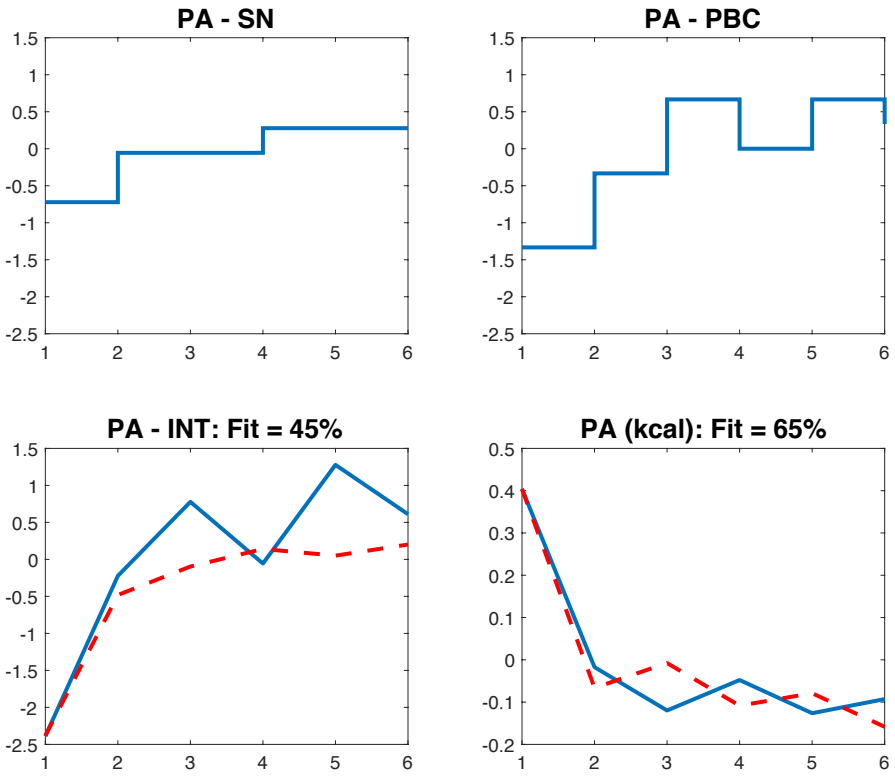

Figure 5.7: Identification results with the goodness of fit for PID 1041 based on the reduced TPB model for PA behaviors. Solid line: measured data; Dashed line: model prediction.

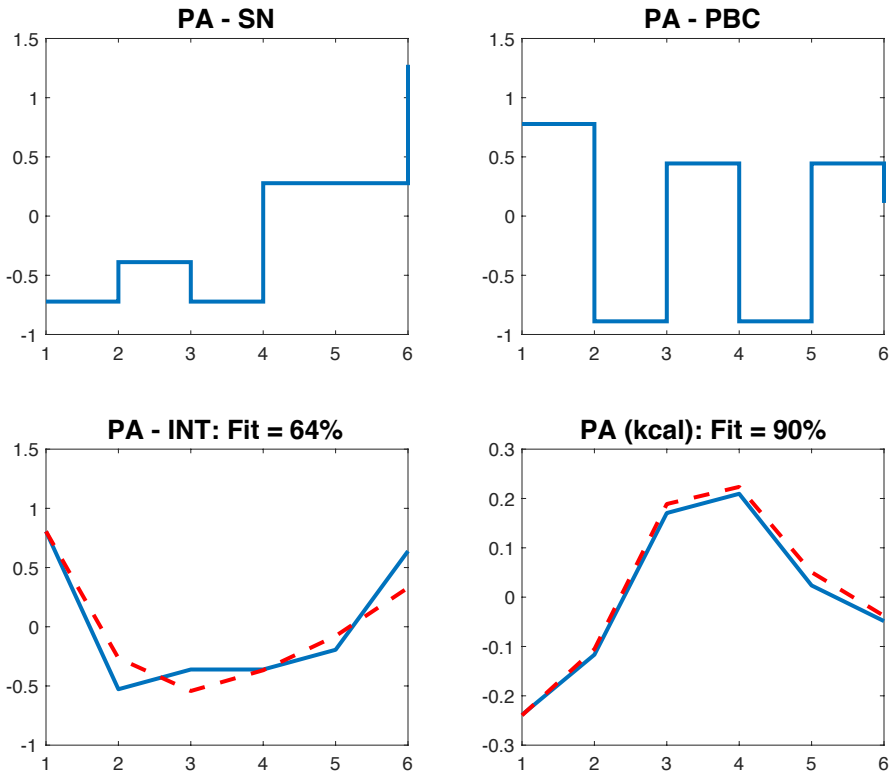

Figure 5.8: Identification results with the goodness of fit for PID 1013 based on the reduced TPB model for PA behaviors. Solid line: measured data; Dashed line: model prediction.

Table 5.2: The identified parameters for the reduced TPB model on PA behaviors for the two illustrative participants (PID 1041 and 1013) collected in Phase I Study.

TPB model on PA		
PID	1041	1013
τ_4	0.2623	1.00E-12
τ_5	0.05277	0.7048
ζ	35.74	0.08519
β_{42}	0.1754	0.6965
β_{43}	0.2335	3.06E-01
β_{53}	-0.694	-0.3959
β_{54}	0.2541	0.03992

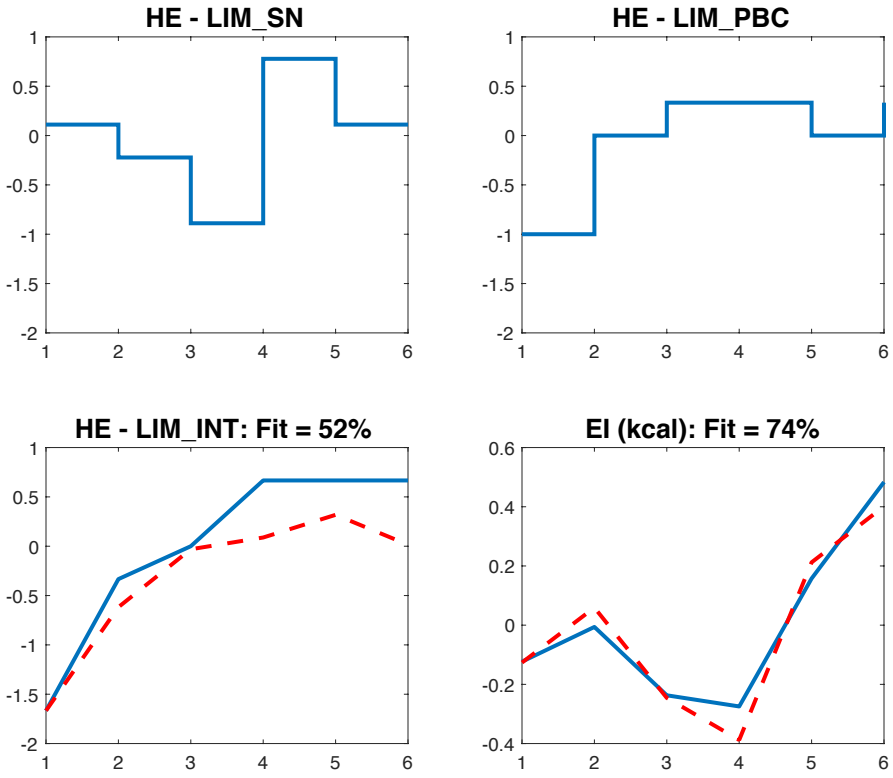

Figure 5.9: Identification results with the goodness of fit for PID 1041 based on the reduced TPB model for HE behaviors. Solid line: measured data; Dashed line: model prediction.

Table 5.3: The identified parameters for the reduced TPB model on HE behaviors for Participants 1041 and 1013 collected in Phase I Study.

TPB model on HE		
PID	1041	1019
τ_{4l}	1.00E-12	1.00E-12
τ_5	0.9412	1.193
ζ	1.614	0.2878
β_{4l2l}	0.1379	0.8015
β_{4l3l}	0.6328	1.00E-12
β_{53l}	-6.126	0.8456
β_{54l}	14.25	-1.427

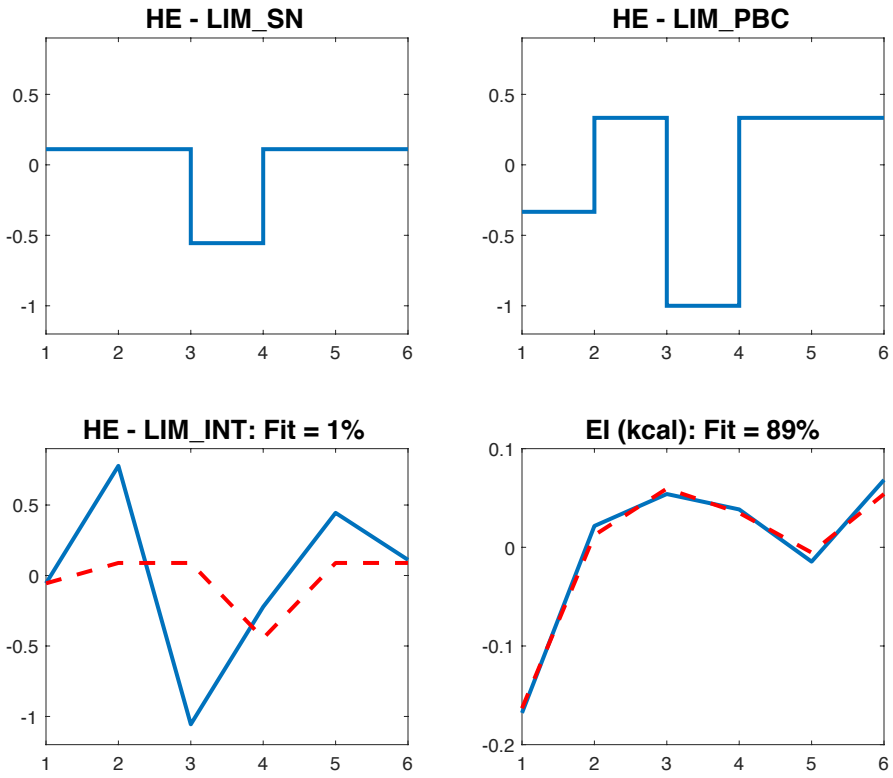

Figure 5.10: Identification results with the goodness of fit for PID 1019 based on the reduced TPB model for HE behaviors. Solid line: measured data; Dashed line: model prediction.

II study. The data of these two participants can be used to validate the characteristics of the participant data or other lessons that we have learned from Phase I participants. Once their intervention was completed and their data was cleaned and available for analysis, any changes of measurement protocols can be finalized and given to other Phase II participants. The third participant for analysis in this document is an intervention participant from later stage of Phase II study. The data from this participant is more consistent and shows least data missingness.

For the two participants (one from the control group, the other from the intervention group) before protocol changes, their measurements of the constructs of SN, PBC, and INT were obtained monthly, leading to 7 measurements for each construct available for individual participant. COV among all the constructs in the original TPB model are checked, with

results shown in Table 5.4. As we can see from the COV analysis, the constructs that we eliminated from the model structure are showing low COV, indicating less variation in the data dynamics, while higher COV are observed in the constructs that are determined to keep. This analysis of the COV on Phase II data supports our decision on the identification work. The identification results for these two participants on the TPB model in PA/HE sides are shown from Fig. 5.11 through 5.14, with the corresponding identified parameters tabulated in Table 5.5.

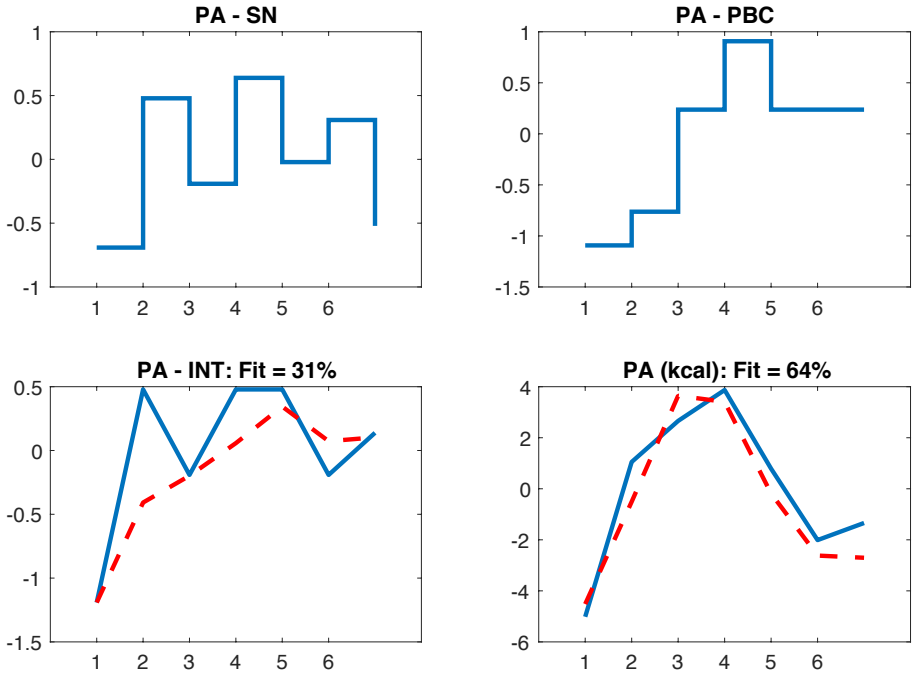

Figure 5.11: Identification results for TPB model for PA behaviors for PID 2002.

The third participant is from the intervention group who was given two steps-up based on the measured weight gain during intervention. As described in the previous section, the modifications on the identification procedures as well as on the measurement protocol were adopted. All the measurements of TPB variables were collected on a weekly basis. From initial identification results and other consideration for HMPC implementation, some further manipulations that might improve the identification results are provided.

Add Time-Dependent Input:

Table 5.4: Tabulation of the coefficient of variation (COV) for the TPB constructs for Participant 2002 and 2005 collected in Phase II Study.

Constructs	COV		
	Intervention Participant	Control Participant	Average
PA_BB	7%	8%	7%
HE_BB	8%	7%	7%
PA_NB	3%	3%	3%
HE_NB	5%	5%	5%
PA_CB	5%	7%	6%
HE_CB	4%	5%	5%
PA_ATT	4%	4%	4%
HE_ATT	5%	4%	5%
HE_LIM_ATT	4%	4%	4%
PA_SN	8%	8%	8%
HE_SN	5%	9%	7%
HE_LIM_SN	6%	8%	7%
PA_PBC	13%	15%	14%
HE_PBC	12%	11%	12%
HE_LIM_PBC	11%	10%	11%
PA_INT	9%	11%	10%
HE_INT	6%	3%	5%
HE_LIM_INT	11%	13%	12%

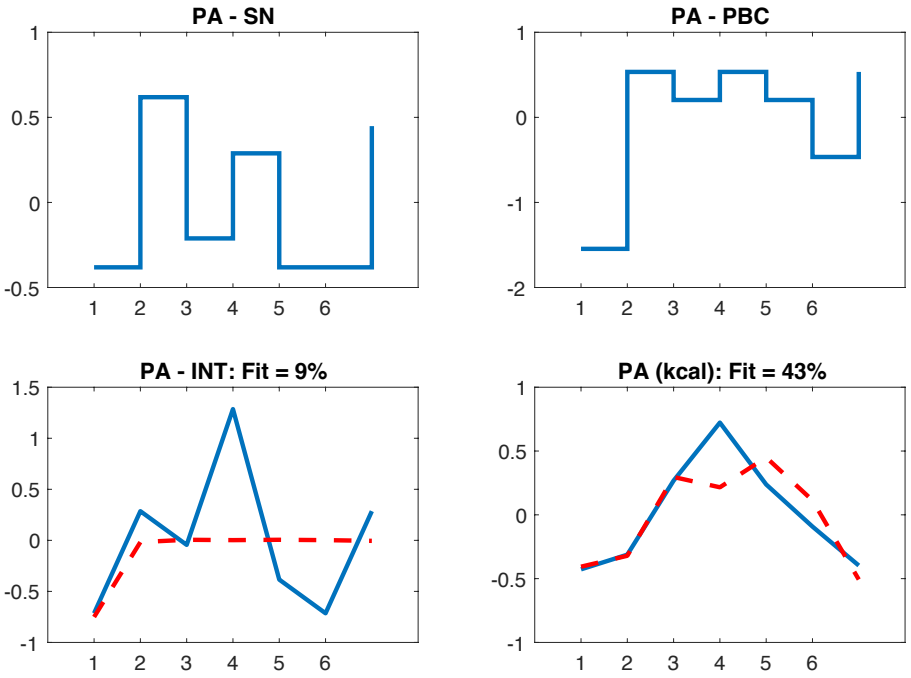

Figure 5.12: Identification results for TPB model for PA behaviors for PID 2005

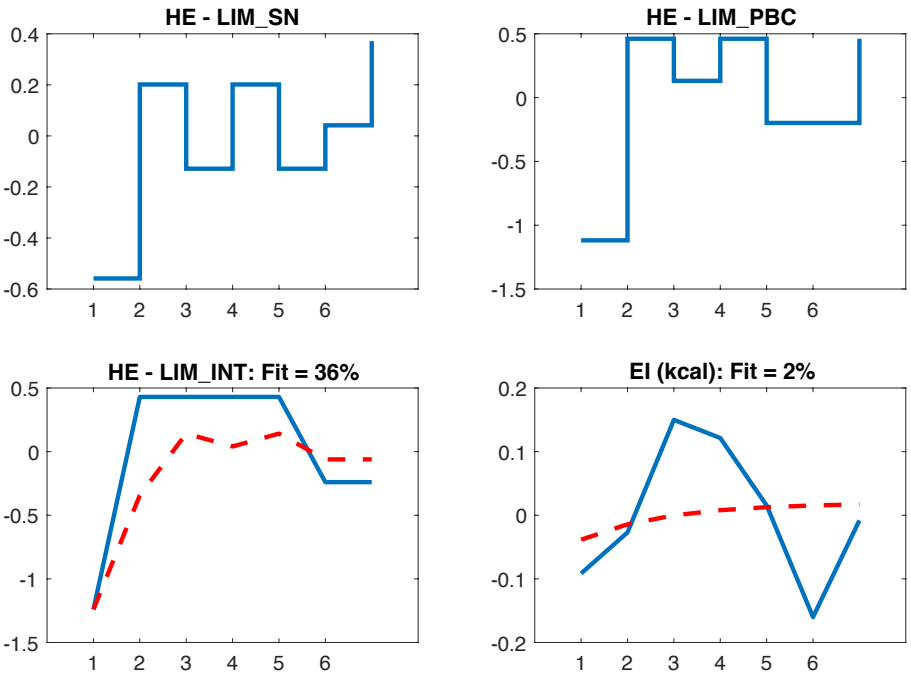

Figure 5.13: Identification results for TPB model for HE behaviors for PID 2002.

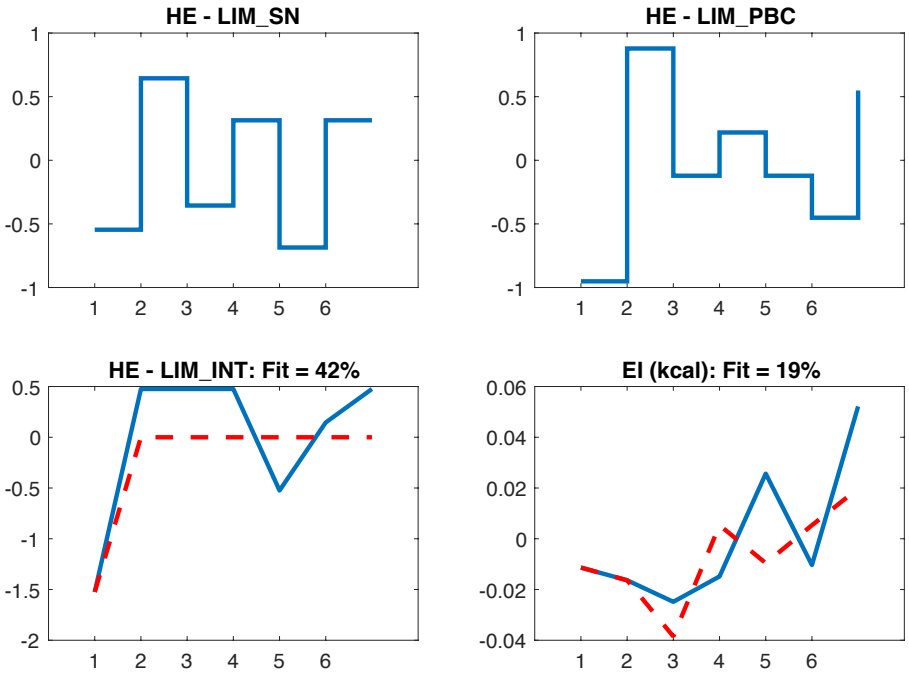

Figure 5.14: Identification results for TPB model for HE behaviors for PID 2005.

Table 5.5: Tabulation of the identified parameters for Participant 2002 and 2005 collected in Phase II Study.

TPB model on PA			TPB model on HE		
τ_4	10^{-12}	0.1482	τ_{4l}	10^{-12}	10^{-12}
τ_5	0.1851	0.2281	τ_5	3.861×10^6	0.08999
ζ	0.05375	0.2499	ζ	1.05×10^6	0.6396
β_{42}	0.09055	10^{-12}	β_{4l2l}	10^{-12}	10^{-12}
β_{43}	0.316	0.01046	β_{4l3l}	0.3073	10^{-12}
β_{53}	-5.018	0.7387	β_{53l}	5.406×10^5	-0.04388
β_{54}	6.41	4.598	β_{54l}	-9.688×10^5	3.172

A decrease in SN/PBC was observed in this participant as she advanced into later gestational stages. Similar decreases have also been found for some of other participants in SN and/or PBC, especially the ones who need augmentation of intervention dosages. If the relationship between such decreases in SN/PBC and the dosage increases (from baseline to one or more steps-up) is modeled using the structures proposed in Fig. 5.4, the gains for the step-up input (up) will be very likely to be negative. Mathematically, these negative gains are reflected as negative effects of the intervention components (HE/PA active learning) on the corresponding TPB constructs, which does not make sense physically. As a matter of fact, such decreases are more likely to be caused by advanced gestation instead of by intervention components, hence the effects of increasing gestational age on the TPB variables need to be factored out before the real effects of any intervention component can be accurately described or analyzed. Based on this consideration, one possible way to separate this decreasing trend is to introduce an additional input that is preferably to be time-dependent. Once introduced, we might be able to attribute the decrease tail in the output to this time-dependent input, and to leave the gains for intervention inputs being positive, or at least largely reduce the negativities of those gains.

For this purpose, the gestational trimester can be used and formulated as a step input to the model for intervention delivery dynamics, or using gestational age in term of days as a ramp input (preferred). To give the time-dependent input a magnitude comparable to other inputs, the slope for the ramp is given as 3/280, so that at the end of gestation, the gains for this input (gestational age, represented as ga) reaches 3. If using a step input with gestational trimesters, each trimester advance introduced as a step change is assigned to be 1. The gains for the additional time-dependent input (always being unconstrained regardless of the constraints for other gains) are more likely to be negative at the presence of prominent decrease in model outputs (SN/PBC), as will be shown later for PID 2072. With the additional time-dependent input, the negative gains previously obtained for intervention components are relaxed with smaller absolute values (i.e., moving towards positive direction)

or even become positive.

Integrating Models Before Identification:

Since the goodness of fit into TPB model outputs (for example the behavior variables of EI/PA kcal) is not 100%, the daily weight gain predicted from the model output EI/PA kcal cannot be exact as the actual daily weight gain, resulting in prediction errors for energy balance model. Similar modeling errors might be introduced when using the outputs from the model for intervention delivery dynamics to introduce into the TPB models. It can be easily envisioned that such errors will accumulate and become worse when integrating the two models that were identified separately. Hence, it is more efficient to integrate the dynamics from the two separate models and form a single comprehensive model before performing the semi-physical identification. The path diagrams of the integrated models are presented in Fig. 5.15 and 5.16. The resulted model uses intervention treatment (*base*, *up* and time-dependent variable *ga*) as inputs and participant behaviors of EI/PA kcal (η_5) as output. The system of differential equations for the integrated model can be written as below,

$$\tau_1 \frac{d\eta_2(t)}{dt} = \gamma_{11}\ base(t) + \gamma_{12} up(t) + \gamma_{13} ga(t) - \eta_2(t) \tag{5.14a}$$

$$\tau_2 \frac{d\eta_3(t)}{dt} = \gamma_{21}\ base(t) + \gamma_{22} up(t) + \gamma_{23} ga(t) - \eta_3(t) \tag{5.14b}$$

$$\tau_3 \frac{d\eta_4(t)}{dt} = \gamma_{31}\eta_2(t) + \gamma_{32}\eta_3(t) - \eta_4(t) \tag{5.14c}$$

$$\tau_4 \frac{d\eta_5(t)}{dt} = \gamma_{42}\eta_3(t) + \gamma_{43}\eta_4(t) - \eta_5(t) \tag{5.14d}$$

The differential equations described above can be transformed to the following state space representations:

$$\dot{x} = A(\phi)x(t) + B(\phi)u(t) \tag{5.15a}$$

$$y = C(\phi)x(t) \tag{5.15b}$$

where: $x = \begin{bmatrix} \eta_2 & \eta_3 & \eta_4 & \eta_5 \end{bmatrix}^T$, which denotes a vector of $d_x = 4$ state variables;

$u = \begin{bmatrix} base & up & ga \end{bmatrix}^T$, which denotes a vector of $d_u = 3$ input variables;

$y = \begin{bmatrix} \eta_2 & \eta_3 & \eta_4 & \eta_5 \end{bmatrix}^T$, which denotes a vector of $d_y = 4$ output variables;

$\phi = [\tau_1\ \tau_2\ \tau_3\ \tau_4\ \gamma_{11}\ \gamma_{12}\ \gamma_{21}\ \gamma_{22}\ \gamma_{31}\ \gamma_{32}\ \gamma_{42}\ \gamma_{43}]^T$, which denotes a vector of $d_\phi = 12$ unknown model parameters;

$$A = \begin{bmatrix} -\frac{1}{\tau_1} & 0 & 0 & 0 \\ 0 & -\frac{1}{\tau_2} & 0 & 0 \\ \frac{\gamma_{31}}{\tau_3} & \frac{\gamma_{32}}{\tau_3} & -\frac{1}{\tau_3} & 0 \\ 0 & \frac{\beta_{42}}{\tau_4} & \frac{\beta_{43}}{\tau_4} & -\frac{1}{\tau_4} \end{bmatrix};$$

$$B = \begin{bmatrix} \frac{\gamma_{11}}{\tau_1} & \frac{\gamma_{12}}{\tau_1} & \frac{\gamma_{13}}{\tau_1} \\ \frac{\gamma_{21}}{\tau_2} & \frac{\gamma_{21}}{\tau_2} & \frac{\gamma_{23}}{\tau_2} \\ 0 & 0 & 0 \\ 0 & 0 & 0 \end{bmatrix};$$

$C = I\ (4 \times 4)$.

The identification results based on the listed model representations with the first order structure is presented in this work. Higher orders of model can also be structured if necessary. It is also noted that the PA behaviors seem quite stationary/static for some participants. In order to avoid overfit into noise, a smoothing window of 10 data points is used to filter the measurements before the identification is implemented. With such modification, the results from semi-physical identification by integrating the two models are shown in Fig. 5.17, with the corresponding identified parameters tabulated in Table 5.6. For the purpose of complete demonstration, identification results for another participant can be found in Fig. 5.18, with identified parameters tabulated in Table 5.7.

The individual-parametrized model for each participant can be used for the design of the closed-loop control algorithm, and will significantly increase the accuracy of the model prediction and further enhance the performance of the controller. This is addressed in the work of Chapter 6. However, a few limitations in the identification work need to be noted and they are summarized below:

1. *Uneven sampling of the data*:

All the questionnaires used to collect the TPB data are completed by individual partici-

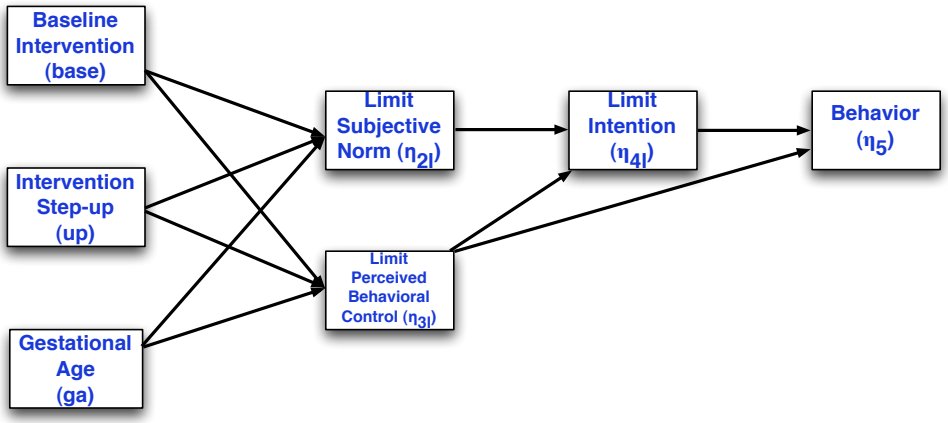

Figure 5.15: Path diagram for integrating the model for intervention delivery dynamics with reduced TPB model for HE.

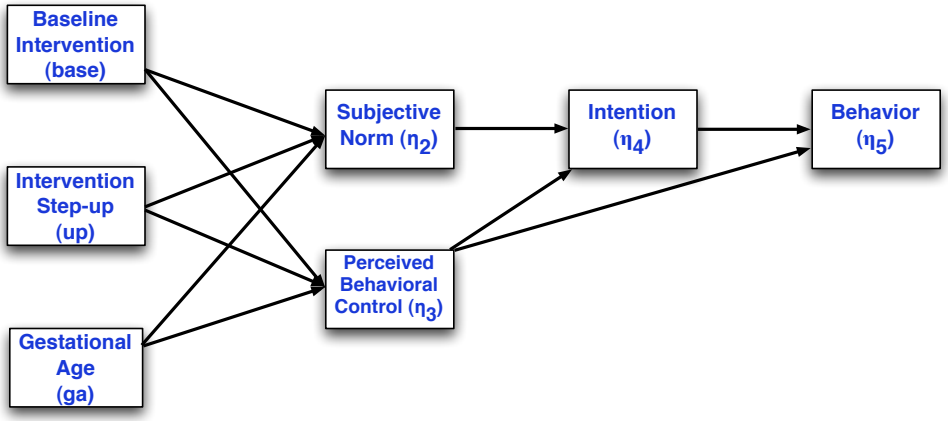

Figure 5.16: Path diagram for integrating the model for intervention delivery dynamics with reduced TPB model for PA.

Table 5.6: Tabulation of the identified parameters for the integrated model based on the models of intervention delivery dynamics and the TPB models for Phase II participant 2072.

Integrated model for PA				Integrated model for HE			
τ_1	9.74E+05	γ_{21}	0.3589	τ_1	1.00E-12	γ_{21}	-0.2844
τ_2	1.00E-12	γ_{22}	0.4358	τ_2	1.228	γ_{22}	0.2568
τ_3	1.00E-12	γ_{23}	-0.8444	τ_3	3.49	γ_{23}	-0.1818
τ_4	1.00E-12	γ_{31}	0.1364	τ_4	1.00E-12	γ_{31}	0.9092
γ_{11}	0.3347	γ_{32}	0.3325	γ_{11}	0.3125	γ_{32}	0.203
γ_{12}	-0.2413	γ_{42}	0.4358	γ_{12}	0.03866	γ_{42}	-0.9465
γ_{13}	0.5278	γ_{43}	6.609	γ_{13}	0.3549	γ_{43}	0.5715

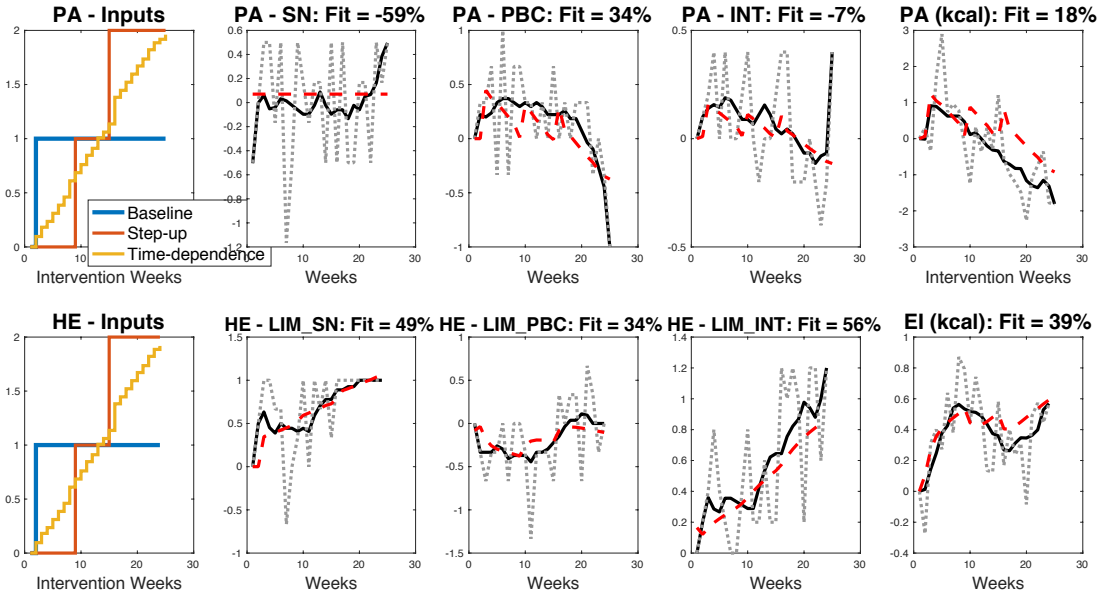

Figure 5.17: Identification results for integrating the models for the intervention delivery dynamics and the TPB model for PID 2072.

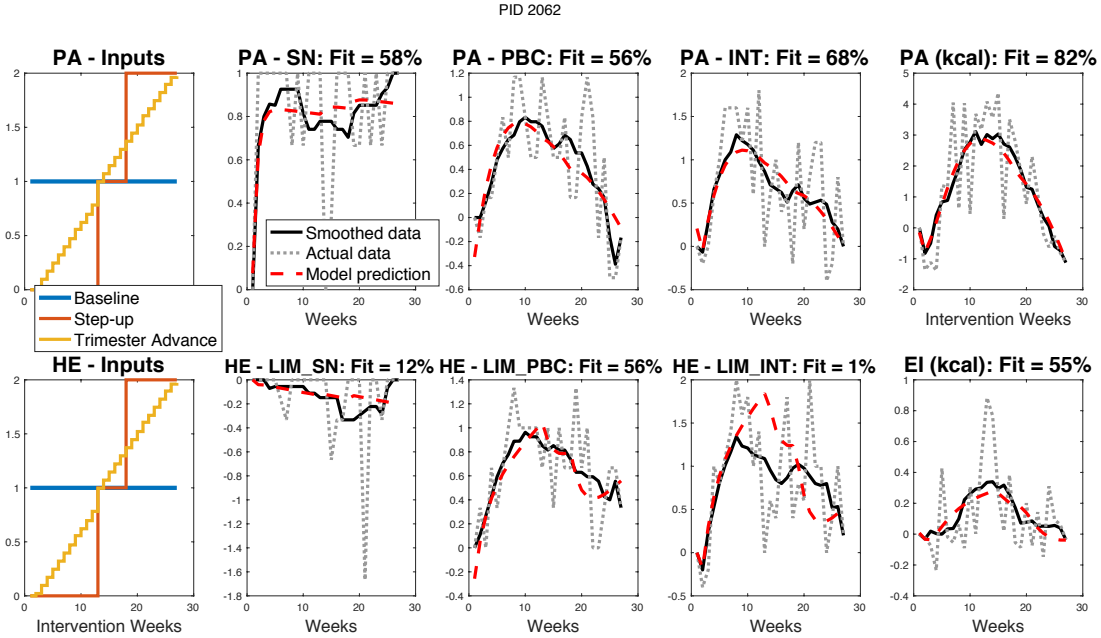

Figure 5.18: Identification results for integrating the models for the intervention delivery dynamics and the TPB model for PID 2062.

Table 5.7: Tabulation of the identified parameters for the integrated model based on the models of intervention delivery dynamics and the TPB models for Phase II participant 2062.

Integrated model for PA				Integrated model for HE			
τ_1	0.7922	γ_{21}	1.511	τ_1	1.00E-12	γ_{21}	0.6091
τ_2	5.298	γ_{22}	0.3936	τ_2	2.226	γ_{22}	-0.6566
τ_3	0.2961	γ_{23}	-1.417	τ_3	0.3265	γ_{23}	0.681
τ_4	4.448	γ_{31}	0.111	τ_4	1.681	γ_{31}	3.516
γ_{11}	0.8424	γ_{32}	1.294	γ_{11}	-0.04014	γ_{32}	2.242
γ_{12}	0.04916	γ_{42}	33	γ_{12}	0.03474	γ_{42}	-0.435
γ_{13}	-0.04248	γ_{43}	-20.1	γ_{13}	-0.1174	γ_{43}	0.4044

pants during an on-site intervention session. Even though the TPB data for each participant is designed to be collected weekly/monthly, it is hard to schedule the on-site appointment on the exact dates with even intervals between every two measurements. For example of PID 2072, the sample intervals observed in the measurements of this participant range from 3 to 23 days. This is a common issue for both Phase I and Phase II participants. Such uneven spaced measurements will result in inaccurate identified models for future predictions. Semi-physical identification with uneven sampling of the data is an interesting topic that has been extensively examined in the literature. Approaches to address this issue can be examined further in the future study.

2. *Lack of validation data set*:

In order to accurately assess each construct of the TPB models, multiple questions for each construct are designed and have to answered completely. This creates a significant burden for the participants in real practice. Considering the feasibility of the intervention and measurement protocols, limited number of data points are available. With the weekly measurement in Phase I and the monthly measurement in Phase II, only 6 to 7 data points are available for TPB identification. This is a huge barrier for the identification analysis, without validation data set.

3. *Different options for model estimation*:

Variables used in estimation process are usually in a deviation form. Deviation can be generated by subtracting baseline or mean of the data set. This will lead to different sets of identified parameters, and the corresponding goodness of fit varies across participants. Both ways of generating deviation variables can be tried for individual participants before deciding the best option. Similarly, the options for using the gestational trimester as a ramp or step input can lead to different results. For the selected participants, the goodness of fit into the measured data and the signs of the gains for this additional input are comparable/same, so we only show the results for ramp inputs in this document.

Chapter 6

HYBRID MODEL PREDICTIVE CONTROL IN OPTIMIZING INTERVENTION DOSAGES

The *Healthy Mom Zone* study for maternal weight gain management features individually tailored and intensively adaptive behavioral interventions that are time-varying in terms of the frequency or intensity of intervention dosages in order to better respond to individual's real-time need (Symons Downs *et al.*, 2018). Conceptually, this can be automated with a closed-loop framework using an appropriate decision algorithm. For example, a decision for dosage change can be made based on whether the participant stays within or exceeds the IOM guidelines for weight gain or energy intake: if she goes above the guidelines, intuitively dosages need to be augmented, otherwise decremented or kept the same. Such simple "IF–THEN" rules do not account for individual dynamics, usually resulting in delayed or aggressive interventions that lead to undesired or suboptimal participant responses. Such circumstances from the simple intervention schemes can be improved by adding a model-based controller that can optimize behavioral-related responses with participant-validated model as developed in previous chapter. However, multiple clinical constraints need to be considered for actual implementations.

In behavioral medicine settings, intervention components cannot be given arbitrarily. For example, some components need to be introduced to participants before or after the others have been given, or certain intensities of one intervention component cannot be changed until the intensity of the other has reached certain levels. Such requirements necessitate a formulation of decision rule that dictates the proper dosage sequence in which the order for component augmentations or decrements are specified. In addition, patient-friendly adaptive interventions in clinical settings require no more than one component to be altered at each intervention decision.

Other considerations or constraints also include the fixed time frame between decision making (can be interpreted as the intervals between participant visits to clinics), and the upper and lower bounds for assigned dosages and other behavior variables. The simple IF–THEN rules or simplistic control algorithms apparently cannot guarantee a good system response while satisfying all of these listed constraints.

Motivated by such needs, Mixed Logical Dynamical (MLD) framework-based Hybrid Model Predictive Control (HMPC) schemes have been developed in prior work (Dong *et al.* (2013); Dong (2014)), to address the discrete dosage inputs while enabling sequential decision framework for adaptive interventions and accounting for other clinical constraints. This control algorithm makes use of feedback and feedforward control action by online optimization of a cost function using a receding horizon strategy. This is the same as how conventional MPC works except for operating on a linear hybrid system (Borrelli *et al.* (2017)). This novel and appealing framework allows the user to have greater flexibility in the specification of different requirements in real-life clinical trials, and to generate the sequential decision policies with time-dependent relationships on manipulated variables, which are usually addressed by temporal logic specification in the control engineering.

In this chapter, the HMPC framework for sequential decision policies under other clinical requirements will be explained, and simulations using such HMPC-based algorithm with participant-validated models for individual participants will be presented and compared with results relying on simple IF–THEN decision rules. Specifically, a set of standard IF–THEN rules based on the same decision logics and time frame as the HMPC will be used. In addition, the set of IF–THEN rules as used in the HMZ study will be evaluated and compared with HMPC to examine the performance of HMPC in real-life settings.

6.1 Hybrid Model Predictive Control Formulations

Model Predictive control (MPC, Camacho and Bordons Alba (2013)) is an advanced control algorithm in which the optimization of the manipulated variables (closed-loop inputs) is not only computed for the current time point, but expanded over a finite time

horizon to take into account the prediction of future responses. A predetermined system model with exactly known parameters is required to solve the optimization problem for optimal control moves. The MPC controller is implemented by recursively determining the optimal control action at each time point by keeping shifting the prediction horizon forward; due to the feature of this strategy, MPC is also called a receding horizon control as illustrated in Fig. 1.1.

In behavioral medicine problem settings, the intervention components are usually delivered in pre-determined categorical (i.e., discrete) doses, and the decision is made in a discrete manner, which requires us to consider the use of hybrid system. A hybrid dynamical system considers discrete and continuous events simultaneously and the description of its dynamics consists of both differential equations and logical conditions (categorical/binary). A system of this kind is referred to as Mixed Logical Dynamical (MLD, Bemporad and Morari (1999); Borrelli *et al.* (2017)) systems (relying on which the HMPC controller can incorporate the constraints into the problem formulation). A hybrid linear system with real and integer states, inputs and constraints can be described with a MLD representation with the following linear relations. as:

$$x(k+1) = Ax(k) + B_1 u(k) + B_2 \delta(k) + B_3 z(k) + B_d d(k) \tag{6.1a}$$

$$y(k+1) = Cx(k+1) + d'(k+1) + v(k+1) \tag{6.1b}$$

$$E_2 \delta(k) + E_3 z(k) \leq E_5 + E_4 y(k) + E_1 u(k) - E_d d(k) \tag{6.1c}$$

where the system state is $x = [x_c^T \ x_d^T]^T$, with continuous state $x_c \in R^{n_x^c}$ and discrete state $x_d \in \{0,\ 1\}^{n_x^d}$; the system input is $u = [u_c^T \ u_d^T]^T$ with continuous element $u_c \in R^{n_u^c}$ and discrete element $u_d \in \{0, 1\}^{n_u^d}$; y is the system output; d, d_0 and v represent measured disturbances, unmeasured disturbances and measurement noise signals, respectively. $\delta \in \{0, 1\}$ and $z \in R^{n_z^c}$ are discrete and continuous auxiliary variables that are introduced in order to convert logical/discrete decisions into their equivalent linear inequality constraints. A, B_1, B_2, B_3, B_d, C, E_1, E_2, E_3, E_4, E_5 and E_d are the matrices used to describe the MLD system; particularly, the logical constraints incorporated into the system are manipulated

through E matrices. The dimension of these auxiliary variables and the number of linear constraints in (6.1c) depend on the specific character of the discrete logical/discrete decisions that would be enforced in the particular hybrid system.

With the system represented in MLD form per (6.1c), the HMPC problem can be formulated to optimize the sequence of control actions $u(k), \cdots, u(k+m-1)$, $\delta(k), \cdots, \delta(k+p-1)$ and $z(k), \cdots, z(k+p-1)$. The objective is to minimize the cost function J as shown below,

$$\min_{\Theta} \; J = \sum_{i=1}^{p} \|y(k+i) - y^r\|^2_{Q_y} + \sum_{i=0}^{m-1} \|\Delta u(k+i)\|^2_{Q_{\Delta u}} + \sum_{i=0}^{m-1} \|u(k+i) - u^r\|^2_{Q_u} \tag{6.2}$$

$$+ \sum_{i=0}^{p-1} \|\delta(k+i) - \delta^r\|^2_{Q_\delta} + \sum_{i=0}^{p-1} \|z(k+i) - z^r\|^2_{Q_z} \tag{6.3}$$

subject to the mixed integer constraints described in (6.1c) and various process constraints:

$$y_{min} \leq y(k+i) \leq y^{max} \;, \quad 1 \leq i \leq p \tag{6.4a}$$

$$u_{min} \leq u(k+i) \leq u^{max} \;, \quad 0 \leq i \leq m-1 \tag{6.4b}$$

$$\Delta u_{min} \leq \Delta u(k+i) \leq \Delta u^{max} \;, \quad 0 \leq \; i \leq \; m-1 \tag{6.4c}$$

Here, $\Theta = \{[u(k+i)]_{i=0}^{m-1}, [\delta(k+i)]_{i=0}^{p-1}, [z(k+i)]_{i=0}^{p-1}\}$; p is the prediction horizon and m is the control horizon; y^r, u^r, δ^r, and z^r are the references for output, input, discrete and continuous auxiliary variables respectively; Q_y, $Q_{\Delta u}$, Q_u, Q_δ and Q_z are penalty weights on the control error, move size, control signal, auxiliary binary variables and auxiliary continuous variables, respectively. The first term in the cost function J is used to minimize the prediction error; the second term is the move suppression, the third to the fifth terms are to keep control signal, auxiliary binary variables and auxiliary continuous variables at their setpoint, respectively. Details of the controller formulation can be found in Nandola and Rivera (2013). Based on the objective in (6.3) and the constraints in (6.4c), the MPC problem can be defined into a standard mixed integer quadratic program (miqp) problem, and solvers, such as the IMB™ILOG™CPLEX optimization studio can be used to solve the

resulting miqp optimization problem. The following sections will mainly focus on the design procedure for how to handle the logical specifications associated with sequential decision policies and other clinical constraints relying on MLD structure.

The aim of the adaptive intervention is to prevent excessive gestational weight gain (GWG) among the OW/OBPW. Therefore, GWG is the primary controlled variable in addition to energy intake (EI) in this design problem. The overall goal is to support the participant to meet the IOM guidelines for GWG and EI(setpoints) by appropriately adjusting the intensities of the intervention components (manipulated variables). The adaptive intervention of the HMZ study features multiple intervention components which can be used to influence health eating (HE) and physical activity (PA) behaviors. Hence, the intensity of the intervention dosage can be adjusted by augmenting or reducing the components on healthy eating or physical activity active learning (u_2 for PA and HE). The decision rules used in the HMPC formulations for changing or maintaining the dosage level are shown in Table 6.1. For example, u_2^{PA} will be augmented from its base dose only after u_2^{HE} reaches its maximum doses, while u_2^{HE} will not be reduced from full dosage until u_2^{PA} returns back to its base dose (augmentation and reduction sequence above baseline). Such dosage sequences can also be illustrated with the following: single meal replacement is designed to be a more intense component on HE, and if necessary, can be provided on certain number of days during intervention in addition to the regular healthy eating demonstration; on-site instructed PA training session is an example of the intense physical activity active learning strategies, only provided for higher dosages.

Such clinically designed sequence rules have to be incorporated in the controller design for correct decision policies. These sequential decision policies restrict how the dosages of intervention components can change over time. The underlying logical specification can be converted into linear inequalities relying on the generation of a sequence table. Table 6.1 is the sequence table derived from pre-determined augmentation/reduction rules. It summarizes the proposed dosage sequence according to the earlier description, which

specifies how the dosages will change during the intervention. For instance, if the participant is currently receiving the intervention with dosage sequence 2, then in the next decision point (two weeks later), there are three intervention options for this participant: (1) it can be augmented to sequence 3, 4, or 5 based on the move size $\Delta u_2^{HE}(k)$; (2) it can get reduced to sequence 1 or 0 according to the move size $\Delta u_1(k)$; or (3) it can remain unchanged. The HMPC controller should be able to determine the optimized discrete dosages according to the participant's response and the user-specified objective function, and subject to the general process constraints and the clinical constraints associated with the dosage sequence.

With the help of information in Table 6.1, the following logical conditions are generated and embedded into the dynamical model using binary variables ($\delta(k)$) in MLD model, so that only the dosage combinations in Table 6.1 are selected,

$$\begin{aligned}\Omega = \quad & (\delta_1 \wedge \delta_5 \wedge \delta_{10}) \oplus (\delta_1 \wedge \delta_5 \wedge \delta_{11}) \oplus (\delta_2 \wedge \delta_5 \wedge \delta_{11}) \oplus \\ & (\delta_2 \wedge \delta_6 \wedge \delta_{11}) \oplus (\delta_3 \wedge \delta_6 \wedge \delta_{11}) \oplus (\delta_4 \wedge \delta_6 \wedge \delta_{11}) \oplus \\ & (\delta_4 \wedge \delta_7 \wedge \delta_{11}) \oplus (\delta_4 \wedge \delta_8 \wedge \delta_{11}) \end{aligned} \tag{6.5}$$

where $(\delta_1 \wedge \delta_5 \wedge \delta_{10})$ stands for dosage sequence 0 in Table 6.1 ($u_1 = u_2^{HE} = u_2^{PA} = 0$), in which $\delta_1 = 1$ means $u_2^{HE} = 0$ is selected, $\delta_5 = 1$ means $u_2^{PA} = 0$, and $\delta_{10} = 1$ means $u_1 = 0$; $(\delta_1 \wedge \delta_5 \wedge \delta_{11})$ represents dosage sequence 1 in Table 6.1; $(\delta_2 \wedge \delta_5 \wedge \delta_{11})$ represents dosage sequence 2 in Table 6.1; and the like. The 8 combinations in (6.5) above are the 8 dosage sequences in Table 6.1. Ω in (6.5) can be expressed in the linear inequalities in (6.1c). This limits the possibilities of the dosage combinations to 8 instead of a possible $\binom{4}{1} \times \binom{4}{1} \times \binom{2}{1} = 32$ combinations. For problems with larger dimensions than those shown in this example, the generation of Table 6.1 and its corresponding logical conditions in (6.5) can be efficiently automated.

It has to be pointed out that in prior work (Dong, 2014), the start of intervention not only contains baseline intervention, but also includes first augmentation of active learning for both HE and PA (Dosage 3 in Table 6.1). When the participant responds favorably during the intervention, the intervention can also be reduced from Dosage 3, with u_2^{PA} first,

Table 6.1: Dosage sequence table employed by HMPC for adaptive GWG intervention.

Dosage	**Active Learning**		**Baseline**	**Description**	**Propositional**
Sequence	$\mathbf{u_2^{HE}}$	$\mathbf{u_2^{PA}}$	$\mathbf{u_1}$		**Logic**
0	0	0	0	Initialized	$\delta_1 \wedge \delta_5 \wedge \delta_{10}$
1	0	0	1	Baseline Intervention	$\delta_1 \wedge \delta_5 \wedge \delta_{11}$
2	1	0	1	1^{st} augmentation of u_2^{HE}	$\delta_2 \wedge \delta_5 \wedge \delta_{11}$
3	1	1	1	1^{st} augmentation of u_2^{PA}	$\delta_2 \wedge \delta_6 \wedge \delta_{11}$
4	2	1	1	2^{nd} augmentation of u_2^{HE}	$\delta_3 \wedge \delta_6 \wedge \delta_{11}$
5	3	1	1	3^{rd} augmentation of u_2^{HE}	$\delta_4 \wedge \delta_6 \wedge \delta_{11}$
6	3	2	1	2^{nd} augmentation of u_2^{PA}	$\delta_4 \wedge \delta_7 \wedge \delta_{11}$
7	3	3	1	3^{rd} augmentation of u_2^{PA}	$\delta_4 \wedge \delta_8 \wedge \delta_{11}$

followed by u_2^{HE} and baseline u_1 and it allows for Dosage 0; the augmentation sequence for the components will be in the opposite order, with u_1 added first, followed by u_2^{HE} and u_2^{PA}. But in the HMZ study, active learning components (u_2^{HE} and u_2^{PA}) serve as step-up for intervention, only available after baseline intervention has been assigned. The minimum dosage level once the intervention start is Dosage 1 in Table 6.1, with baseline alway kept during intervention. In addition, the highest intensity for PA active learning is 3 in the HMZ study instead of 4 from prior work.

6.1.1 Selection of Single Input in Multi-Input Scenario

In adaptive interventions, at each decision point, there is usually only one component being altered due to patient-friendly requirement and the change of the selected component cannot be too aggressive. This is necessary, because it can prevent the participant from being uncomfortable due to any dramatic intervention adaptation and hence unable to follow up with the pace of the intervention. This basically implies that the controller can choose only one input among all and incur only one step change of the selected input at each

decision point, and this change also has to follow the logic in the sequential decision policies described earlier. Such constraints can be enforced by the use of move size constraints, and the high and low limits on manipulated variables. The move size constraints for individual components can be expressed as

$$-1 \leq \Delta u_j(k) \leq 1, \quad j \in \{1, 2\} \tag{6.6}$$

For reasons of simplicity and easy implementation, constraints in (6.7) or (6.8) are used to handle logic specification associated with sequential decision policies under the assumption that the dosage change can take place only one step at a time (Dong *et al.* (2013)).

$$\Delta u_1(k)^2 + \Delta u_2^{HE}(k)^2 + \Delta u_2^{PA}(k)^2 \leq 1 \tag{6.7}$$

$$| \Delta u_1(k) | + | \Delta u_2^{HE}(k) | + | \Delta u_2^{PA}(k) | \leq 1 \tag{6.8}$$

In order to incorporate these constraints into the problem formulation, additional binary variables ρ and its associated logical specifications are introduced to the MLD equation to generate corresponding constraints on the basis of the sequence table. They are converted into linear inequalities, and are implemented by either appending them to (6.1c) or by overwriting the move size constraints in (6.4c). The number of the additional binary variables corresponds to the number of the manipulated inputs.

In the GWG intervention illustrated above, three binary variables (ρ_1, ρ_2 and ρ_3) are augmented into the vector of binary variables δ in (6.4c). The selection of one input change

can be logically expressed as follows,

$$\rho_1(k) = 1 \Leftrightarrow \begin{cases} \mid \Delta u_1(k) \mid > 0, \\ \Delta u_2^{HE}(k) \ = \Delta u_2^{PA}(k) = 0 \end{cases} \tag{6.9}$$

$$\rho_2^{HE}(k) = 1 \Leftrightarrow \begin{cases} \mid \Delta u_2^{HE}(k) \mid > 0, \\ \Delta u_1(k) \ = \Delta u_2^{PA}(k) = 0 \end{cases} \tag{6.10}$$

$$\rho_2^{PA}(k) = 1 \Leftrightarrow \begin{cases} \mid \Delta u_2^{PA}(k) \mid > 0, \\ \Delta u_1(k) \ = \Delta u_2^{HE}(k) = 0 \end{cases} \tag{6.11}$$

$$\rho(k) \odot \Delta u(k)_{\min} \leq \Delta u(k) \leq \rho(k) \odot \Delta u(k)^{\max} \tag{6.12}$$

$$\rho_1(k) + \rho_2^{HE}(k) + \rho_2^{PA}(k) \leq 1 \tag{6.13}$$

$$\text{where } \rho(k) = [\rho_1(k) \quad \rho_2^{HE}(k) \quad \rho_2^{PA}(k)]^T \tag{6.14}$$

$$\Delta u(k) = [\Delta u_1(k) \quad \Delta u_2^{HE}(k) \quad \Delta u_2^{PA}(k)]^T \tag{6.15}$$

$$\Delta u(k)^{\max} = [\Delta u_1(k)^{\max} \quad \Delta u_2^{HE}(k)^{\max} \quad \Delta u_2^{PA}(k)^{\max}]^T \tag{6.16}$$

$$\Delta u(k)_{\min} = [\Delta u_1(k)_{\min} \quad \Delta u_2^{HE}(k)_{\min} \quad \Delta u_2^{PA}(k)_{\min}]^T \tag{6.17}$$

and $\odot$ is the Hadamard product, k is the sampling time. In (6.9), the selection of $\rho_1(k)$ means $u_1(k)$ will be altered, while $u_2^{HE}(k)$ and $u_2^{PA}(k)$ remain unchanged; (6.10) and (6.11) have the similar logical meaning. (6.12) redefines the move size constraints at each decision point, and (6.13) makes sure that only one binary variable from $\rho_1(k)$, $\rho_2^{HE}(k)$ and $\rho_2^{PA}(k)$ will be selected if it is necessary. The logical specifications in (6.9) - (6.12) can be expressed as linear inequalities related with initial control effort $u(k_0)$, $u(k)$ over the m control horizon, and $\rho(k)$ over the p prediction horizon; (6.13) is augmented after the linear inequalities of binary variables $\delta(k)$ in (6.4c) over the p prediction horizon. Please note that the move size constraints in (6.16) and (6.17) are defined as time-varying vectors in order to maintain generality, and this can also help address the fact that the decision to assign the dosage is made on a bi-weekly basis versus the daily sampling time of output measurement through self-monitoring process, which is to be discussed in the ensuing subsection.

6.1.2 *Fixed Time Frame For Decision Making*

Due to clinical and resource considerations, it is often desirable to make decisions at frequencies other than the regular sampling interval. For example the participant visits the clinic on a weekly basis, and however the measurements are still taken on a daily basis. Therefore, it is necessary for the controller to understand at which point the intervention can be adapted, and at which time frame the intervention has to stay the course. In other words, the control decisions are required to be made at an *a priori* known integer multiple T_D (time frame for decision; for example, 14 in case of making decisions every two weeks) of the system sample time T_{s} in addition to the previously discussed constraints. This can be achieved by enforcing control move size constraints $\Delta u(k)$ to be zero over the control horizon except when decisions have to be made. This leads to another set of time-dependent linear equality constraints: $A_{T_{\mathrm{D}}}(k)u(k) = 0, i \in \{0,\ 1,\ \ldots\ ,\ m-1\}$. The matrix $A_{T_{\mathrm{sw}}}(k)$ has a block-diagonal structure, for example,

$$\begin{bmatrix} \star & & & & & & & & \\ \star\ \star & & & & & & & & \\ \star\ \ \star & & & & & & & & \\ & \mathbf{0} & & & & & & & \\ & & \star\ \star & & & & & & \\ & & \star\ \ \star & & & & & & \\ & & \star\ \ \ \ \star & & & & & & \\ & & & \ddots & & & & & \\ & & & & \mathbf{0} & & & & \\ & & & & & \star\ \star & & & \\ & & & & & \star\ \ \star & & & \end{bmatrix} \begin{bmatrix} u(k) \\ u(k+1) \\ \vdots \\ u(k+m-1) \end{bmatrix} = \begin{bmatrix} \star \\ 0 \\ \vdots \\ 0 \end{bmatrix} \tag{6.18}$$

where rows with $\star$ entries and $\mathbf{0}$ are assigned by the algorithm. The rest of the entries in the matrix are zero. This matrix is generated dynamically at each sampling instant k using the following steps:

1. Given the control horizon m and the time frame for decision $T_{\mathrm{D}}(\leq m)$, calculate the number of blocks $\texttt{numblocks} = \lfloor \frac{m-1}{T_{\mathrm{sw}}} \rfloor + 1$. If the $\texttt{numblocks} \geq 3$, define number of block excluding the first and last block: $\texttt{midblocks} = \texttt{numblocks} - 2$. The control is allowed to change its value only at the time points for decisions, which are the integer multiples of T_{sw}, i.e., $\texttt{iff rem}(\frac{k}{T_{\mathrm{sw}}}) = 0$, where $\texttt{rem}$ is the remainder.

2. The matrix $A_{T_{\mathrm{D}}}(k)$ is populated by $0, 1$ or -1 to implement the move size restriction, and its size is determined by length of control horizon and size of $\texttt{numblocks}$: $A_{T_{\mathrm{sw}}}(k) \in \mathbb{R}^{(T_{\mathrm{sw}}+\texttt{midblocks}\times(T_{\mathrm{sw}}-1)+\texttt{rem}(\frac{m-1}{T_{\mathrm{sw}}})+1)\times m}$.

3. The rows in $A_{T_{\mathrm{sw}}}(k)$ corresponding to decision time points will be set to zero; otherwise the rows will be populated to implement $\Delta u(k+i) = 0$.

4. Finally, the first sample $u(k)$ is assigned the previously calculated optimal value i.e. $u(k) = u^*$ when k is not at the time points allowed for decisions (as per the receding horizon framework).

6.1.3 Three Degree of Freedom (3 DoF)

The developed HMPC framework uses three-degree-of-freedom (3 DoF) approach to tune the controller, which is illustrated in Fig. 6.1. It allows the user to adjust the speed of setpoint tracking, measured and unmeasured disturbance rejection independently (Nandola and Rivera (2013)) in the closed-loop system by varying parameters α_r, α_d and f_a respectively. These parameters can be adjusted between values 0 and 1, and they in turn alter the response of the Type I ($f^1(q, \alpha_{r,d})$) or Type II filter ($f^2(q, \alpha_{r,d})$) in (6.19) - (6.22) which supplies a filtered signal to the controller for setpoint tracking and measured disturbance rejection,

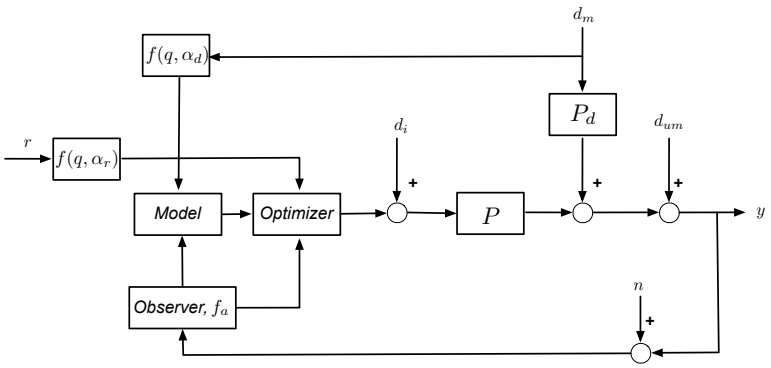

Figure 6.1: Three-Degree-of-Freedom (3 DoF) controller formulation of MPC (Nandola and Rivera, 2013).

$$f^1(q, \alpha_r) = \frac{(1-\alpha_r)q}{q-\alpha_r} \tag{6.19}$$

$$f^2(q, \alpha_d) = (\beta_0 + \beta_1 q^{-1} + \cdots + \beta_\omega q^{-\omega}) \times \frac{(1-\alpha_d)q}{q-\alpha_d} \tag{6.20}$$

$$\beta_k = \frac{-6k\alpha_d}{(1-\alpha_d)\omega(\omega+1)(2\omega+1)} \tag{6.21}$$

$$\beta_0 = 1 - (\beta_1 + \cdots + \beta_\omega) \tag{6.22}$$

or adjust the observer gain for unmeasured disturbance rejection as $K_f = [0 \quad (f_a)^2 \quad f_a]^T$ (Type I) or $K_f = [0 \quad (f_a)^2/(2-f_a) \quad f_a]^T$ (Type II). This 3 DoF tuning adjustment is more intuitive and convenient than the traditional MPC tuning rules which are determined by prediction horizon, control horizon and move suppression weights in the objective function that directly affect the manipulate variables and consequently, the effect on a specific controlled variable response is more difficult to predict.

6.2 HMPC With Participant-Validated Models

The previous section introduces three specific concepts: the generation of a sequence table, selection of one-at-a-time inputs in a multi-input scenario and a fixed time frame for decision making. In the context of an intervention, the control design problem can be formulated based on practical operational constraints and clinical considerations. The intervention components are delivered in pre-determined discrete doses, with HE active

learning (u_2^{HE}) in {0, 1, 2, 3}, PA active learning (u_2^{PA}) in {0, 1, 2, 3}, and other baseline components (u_1) in {0, 1}. With the participant validated models obtained in Chapter 5, the HMPC algorithm can be applied to determine the optimal categorical dosages of the intervention components based on participant behaviors (EI kcal)/behavioral outcomes (GWG) in real-time, and the assigned dosage sequence should be proper as described above in Table 6.1.

The obtained participant validated models in Chapter 5 can be used to describe individual behavioral dynamics in response to dosage changes. Once integrated with the reformulated energy balance model as developed in Chapter 2, a comprehensive model that relates dosage inputs to weight changes can be formed for individuals. To test the accuracy of the comprehensive model that integrates the different modules together, Fig. 6.2 shows the model predicted responses using as inputs the actual dosage changes assigned to this participant during HMZ intervention. The blue markers are the actual participant data and the black dashed curve is the model prediction. Note that the errors in the identified parameters for behavioral dynamics will result in a bias between the measured behavioral kcal and the model prediction using the actual intervention dosages given in the HMZ study. Due to the integrating dynamics from the energy balance module, the bias due to modeling errors will accumulate over time. Hence, the prediction from the participant validated models using the actual intervention components assigned during interventions will not agree with the measured weight/behaviors. Since the extent of the bias shown in the figure is moderate and acceptable, this participant-validated model will be used for the HMPC demonstration as will be shown later in this section.

To assess how adaptive interventions with sequential decision policies using HMPC framework assign the optimized dosages with the changes following the proposed dosage sequence, the illustrations of HMPC-based interventions will be presented and compared with adaptive interventions using other simple decision rules, for example, the IF–THEN rules. Considering the modeling errors as shown in Fig. 6.2, the results using the HMPC controller

as decision policies will not be compared directly with the actual measured weight/behaviors for Phase II participants, but will be compared with model predicted weight and EI/PA kcal using other decision rules.

6.2.1 HMPC versus Standard IF–THEN Rules

A standard IF–THEN rule follows the same dosage augmentation sequence as HMPC (shown in Table 6.1). Specifically, if the participant exceeds the upper bound of the IOM guidelines for weight gain, a more intensive dosage to increase the potency of the intervention is necessary for this participant; if her weight gain is below the IOM lower bound, the dosage should be decremented; or otherwise, the intervention dosage will be sustained. This can be mathematically represented as below,

$$Decision(\Delta u(k)) = \begin{cases} +1, & \text{if} \quad GWG > GWG^{IOM-high} \\ -1, & \text{if} \quad GWG < GWG_{IOM-low} \\ 0, & \text{otherwise} \end{cases}$$

where standard IF–THEN rules assign values to the decision for dosage change based on participant GWG; values of +1, -1 and 0 indicate a dosage augmentation, decrement and unchanged, respectively. In addition, the time interval between decision making using IF–THEN rules are set the same as the HMPC formulation of two weeks. In the following section, HMPC results under different scenarios will be presented and compared with such IF–THEN rules. The participant-validated model for PID 2072 from Chapter 5 will be used for detailed demonstration first, followed by demonstration using model for PID 2062.

Scenario 1: Fastest Responses

Since IF–THEN rules only use weight gain signals for decision making, we only add weights on controlled variable of weight gain (GWG) and assign zero weight to energy intake (EI) in this scenario, i.e., penalty weight $Q_y = [Q_{EI},\ Q_{GWG}]$ where $Q_{EI} = 0$. Only noise-free signals were included: neither measurement noise or unmeasured signals. In addition, α_r

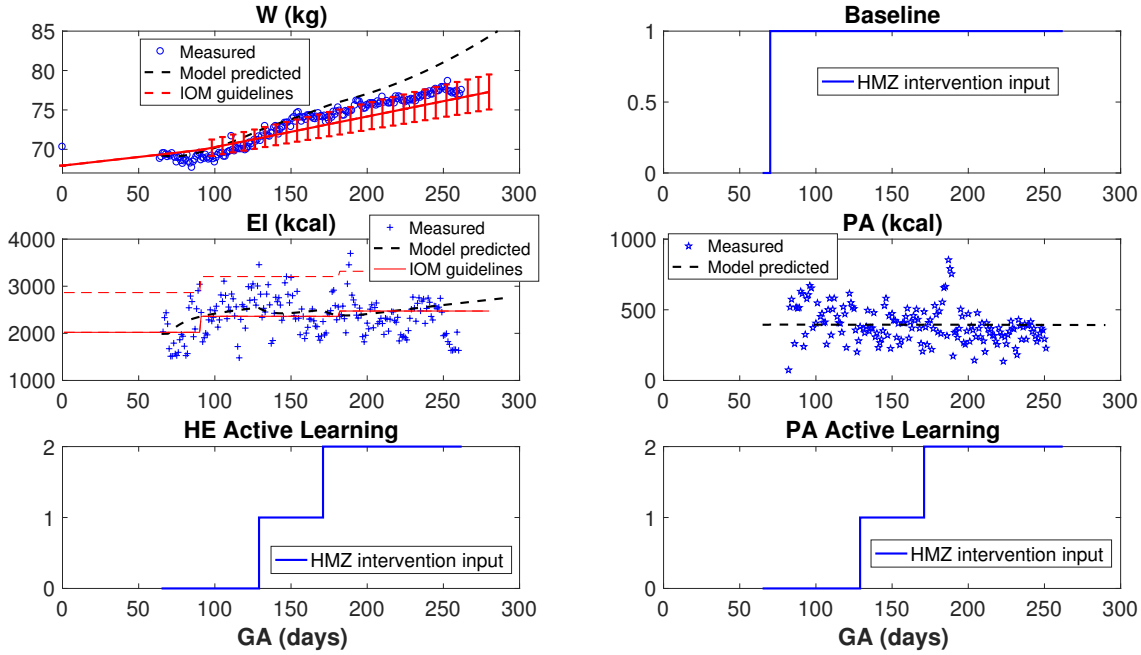

(a)

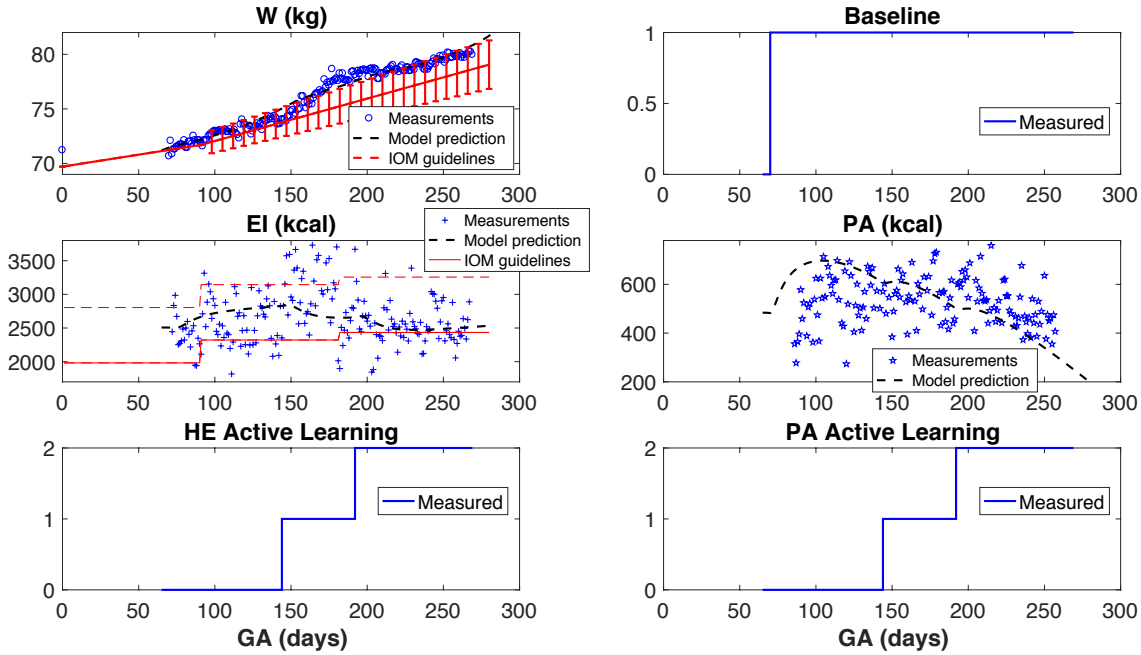

(b)

Figure 6.2: Prediction from estimated models using actual intervention dosages as inputs is compared with measured data for participant 2072 in (a) and 2062 in (b).

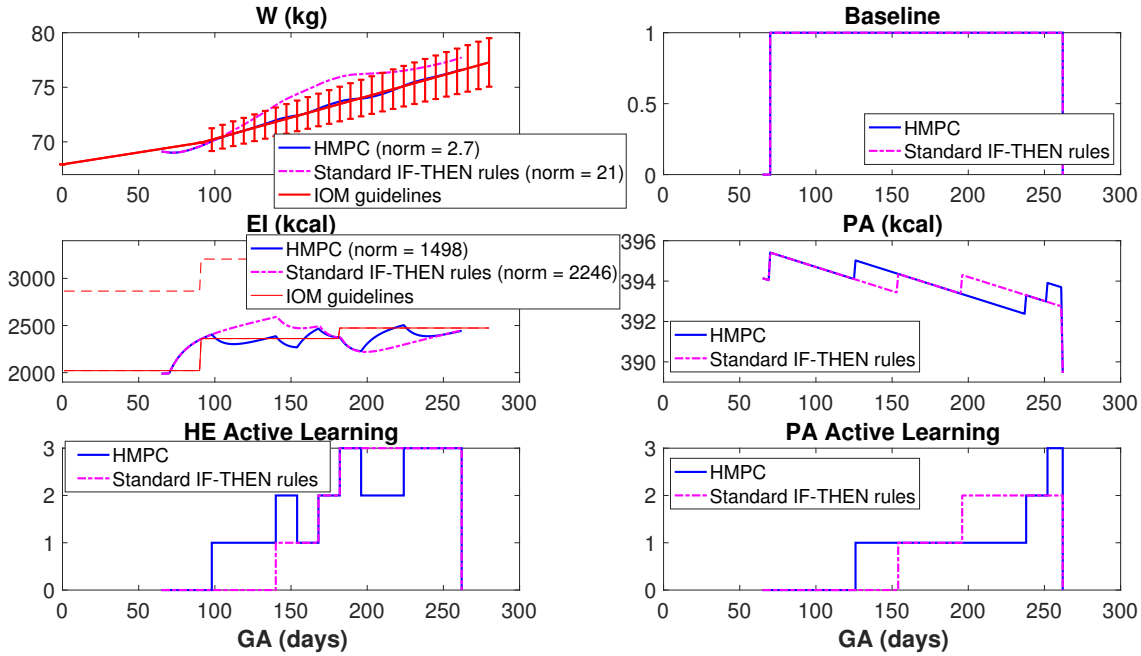

Figure 6.3: HMPC results comparison with standard IF–THEN rules for PID 2072 from Phase II study. (HMPC: noise-free signals only; $Q_y = [0,\ 10]$; $\alpha_r = \alpha_d = 0$; $f_a = 1$; $p = 25$, $m = 20$.

and α_d was set to 0 indicating fastest set point tracking, and fastest measured disturbance rejection. The HMPC results compared with standard IF–THEN rules for PID 2072 are presented in Fig. 6.3, where HMPC exhibits superior performance than standard IF–THEN rules. Despite $Q_{EI} = 0$, the response of EI is still within acceptable ranges given by the IOM guidelines. As seen later in Fig. 6.4 where weights are assigned to both controlled variables, the errors between predicted EI and the guidelines are reduced, but with a trade-off that predicted weight diverges from the nominal values of the guidelines. Considering it is more critical for participants to follow the weight guidelines and also more beneficial for maternal health during gestation, weights assigned to EI will be kept as zero for the subsequent scenarios.

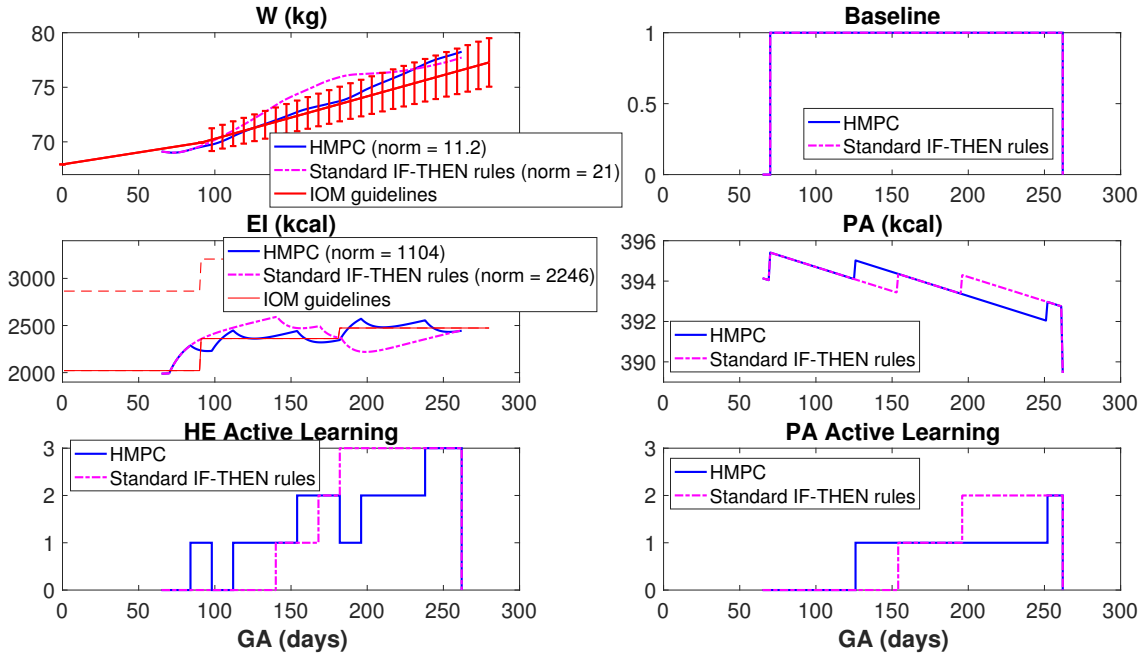

Figure 6.4: HMPC results comparison with standard IF–THEN rules for PID 2072 from Phase II study. (HMPC: noise-free signals only; $Q_y = [0.1,\ 10]$; $\alpha_r = \alpha_d = 0$; $f_a = 1$; $p = 25$, $m = 20$.

Scenario 2: Slow Setpoint Tracking

Similar as Scenario 1, weights on controlled variable of GWG only; only noise-free signal were included; α_d is set to 0 indicating fastest measured disturbance rejection. But α_r is set to 0.7 for slow set point tracking. The results of comparison with standard IF–THEN rules for the same participant PID 2072 are shown in Fig. 6.5, where a slow set-point tracking setting will not evidently affect the controller performance.

Scenario 3: Slow Measured Disturbance Rejection

The measured disturbance signals play an important role in the GWG intervention system and cannot be neglected. If not well addressed, it will significantly affect the control performance. The measured disturbance signal for EI output is mostly attributed from the time-dependent input (u_3) in the model of intervention delivery dynamics. Since this input cannot be manipulated or changed by the intervention, it is not included in the two-

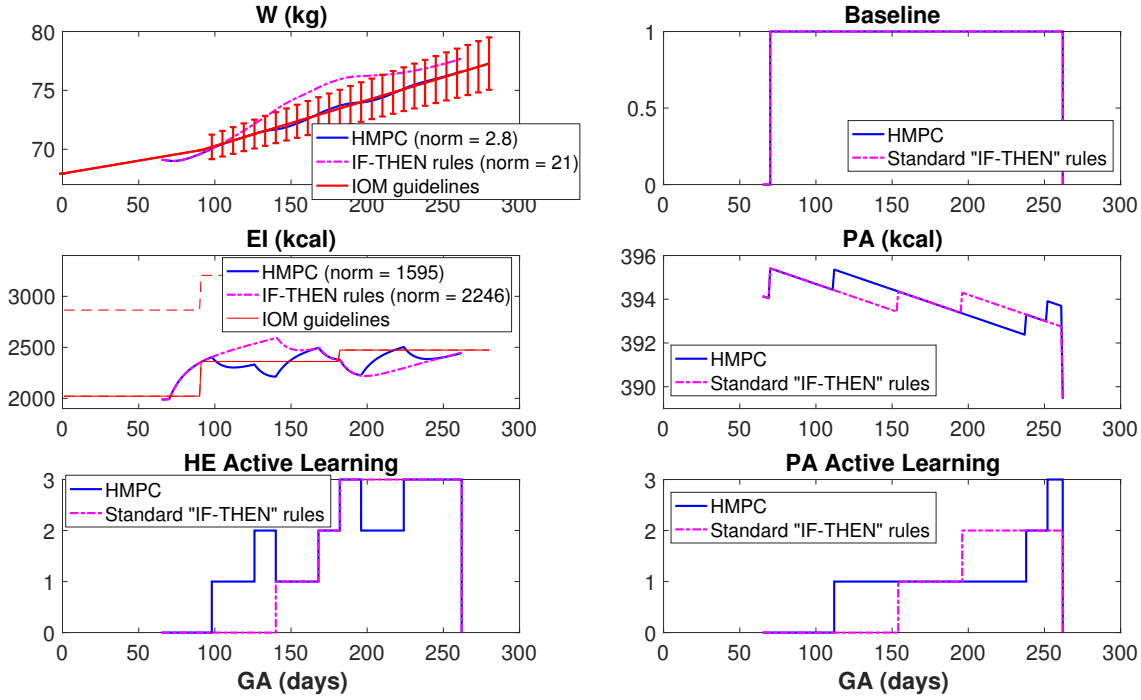

Figure 6.5: HMPC results comparison with standard IF–THEN rules for PID 2072 from Phase II study. (HMPC: noise-free signals only; $Q_y = [0,\ 10]$; $\alpha_r = 0.7$; $\alpha_d = 0$; $f_a = 1$; $p = 25$, $m = 20$.

input comprehensive participant-validated models that are used for control implementation. However, the effects of this input on system outputs need to be accounted before comparing the controlled outputs with the reference signals. The dynamical responses of EI resulted from u_3 can be forecasted using the identified model parameters and used as a feed forward signal introduced into HMPC.

The measured disturbance for GWG is a somewhat subtle. The reference signal used for the control system is the daily maternal weight gain, GWG, which is the first derivative of maternal weight. However, the controlled output provided by the integrated participant validated model is the change of GWG (ΔGWG), that is, the second derivative of weight. Therefore, before compared with the set-point, the actual model output in terms of ΔGWG needs to be added with the baseline GWG that incurs without the presence of the intervention. This is resulted from the baseline EI, PA and instantaneous RMR.

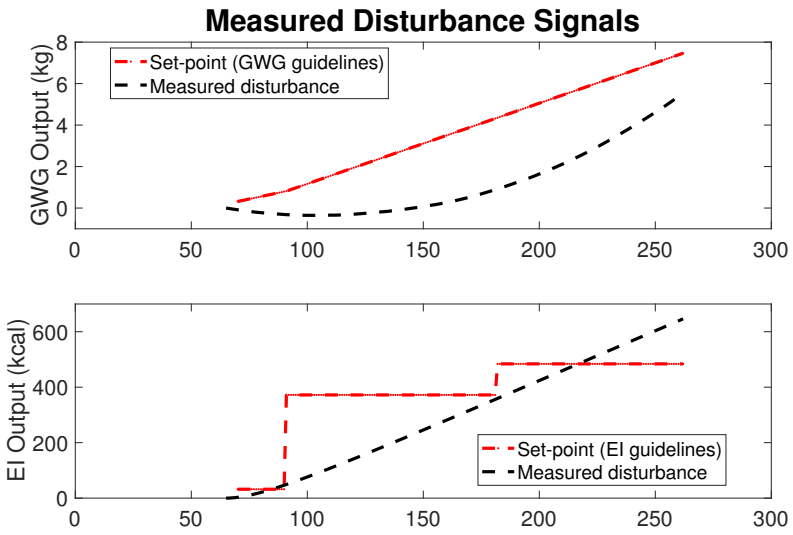

Figure 6.6: Measured disturbance signals in the controlled outputs that will be introduced in feedforward fashion into the HMPC (for PID 2072).

In addition, the changes in EI and PA kcal resulted from u_3 also need to be taken into account here. Once these kcal values are introduced into the energy balance model, they will lead to an weight gain accumulated over time. This accumulated weight gain and the EI change that is mentioned earlier due to u_3 are plotted for PID 2072 from Phase II study in Fig. 6.6 and will be used as measured disturbance signals to improve the HMPC performance. The measured disturbance signals are varying across different participants. Hence, the signals demonstrated in Fig. 6.6 will only be used for PID 2072 when applying closed-loop implementation with HMPC specifically for this participant.

For the case in Scenario 3, all the adjustable parameters are set to the same values as in Scenario 1, except for α_d set to 0.9, indicating slow measured disturbance rejection. The results of comparing HMPC with standard IF–THEN rules for PID 2072 are shown in Fig. 6.7.

Note that the disturbance signal for weight gain output does not become ramp until mid stage of gestation (around day 150). Hence, Type I filter is adequate for good disturbance rejection until day 150, after which the filter is still good enough for the purpose despite a small bias from the target as can be seen from the results. The performance of Type II filer

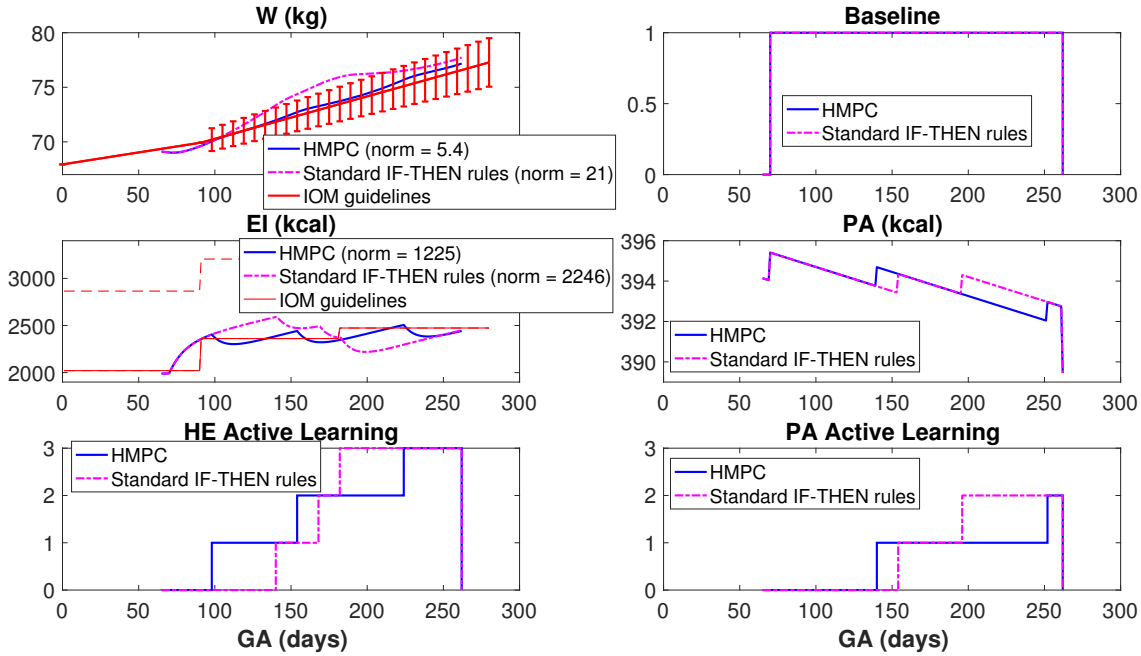

Figure 6.7: HMPC results comparison with standard IF–THEN rules for PID 2072 from Phase II study. (HMPC: noise-free signals only; $Q_y = [0,\ 10]$; $\alpha_r = 0$; $\alpha_d = 0.9$, Type I filter for measured disturbance rejection; $f_a = 1$; $p = 25$, $m = 20$.

($\alpha_d = 0.9$ and $\omega = 10$) for disturbance rejection for PID 2072 is shown in Fig. 6.8 where it gives better performance than Type I with no offset.

Scenario 4: Unmeasured Disturbance Rejection

In this case, measurement noise in weight will be manually introduced to simulate a practical setting. The performance of the controller will be affected by adjusting the tuning parameter f_a as described in 6.1.3, which ranges from 0 to 1. The controller performance compared to standard IF–THEN rules with $f_a = 1,\ 0.1$ for PID 2072 are presented in Fig. 6.9 and 6.10 respectively. Here, the covariance of the white noise signal is set to 0.5 and the same seed for noise signals is used in Fig. 6.9 and 6.10.

As seen from the results, the HMPC reacts to the participant intervention outcomes much faster than standard IF–THEN rules to successfully control the weight within the guidelines, while the decision of stepping up the dosages from standard IF–THEN is appar-

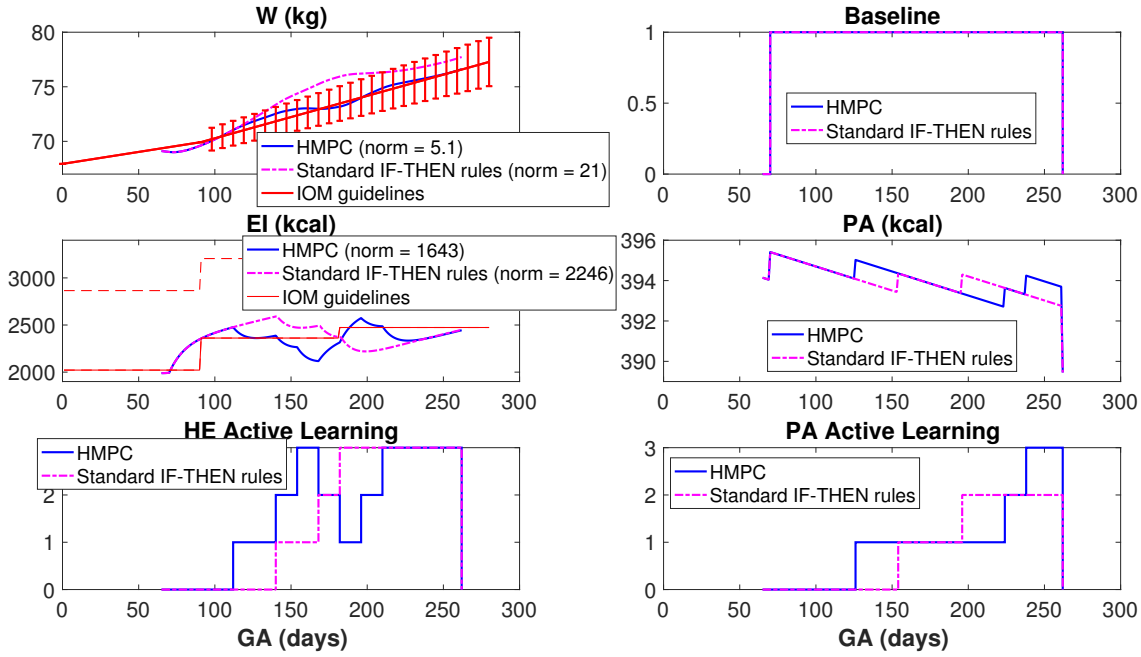

Figure 6.8: HMPC results comparison with standard IF–THEN rules for PID 2072 from Phase II study. (HMPC: noise-free signals only; $Q_y = [0,\ 10]$; $\alpha_r = 0$; $\alpha_d = 0.9$; $\omega = 10$, Type II filer for measured disturbance rejection; $f_a = 1$; $p = 25$, $m = 20$.

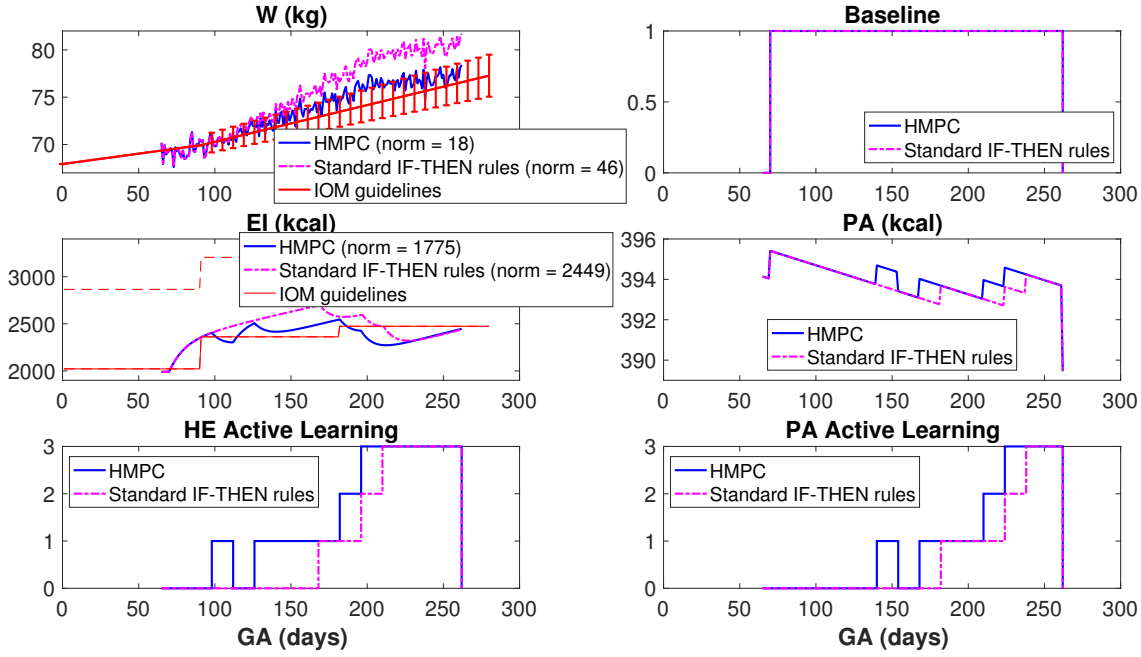

Figure 6.9: HMPC results comparison with standard IF–THEN rules for PID 2072 from Phase II study. (HMPC: noise signal included (covariance $R = 0.5$); $Q_y = [0,\ 10]$; $\alpha_r = \alpha_d = 0$; Type I filer for measured disturbance rejection; $f_a = 1$; $p = 25$, $m = 20$.

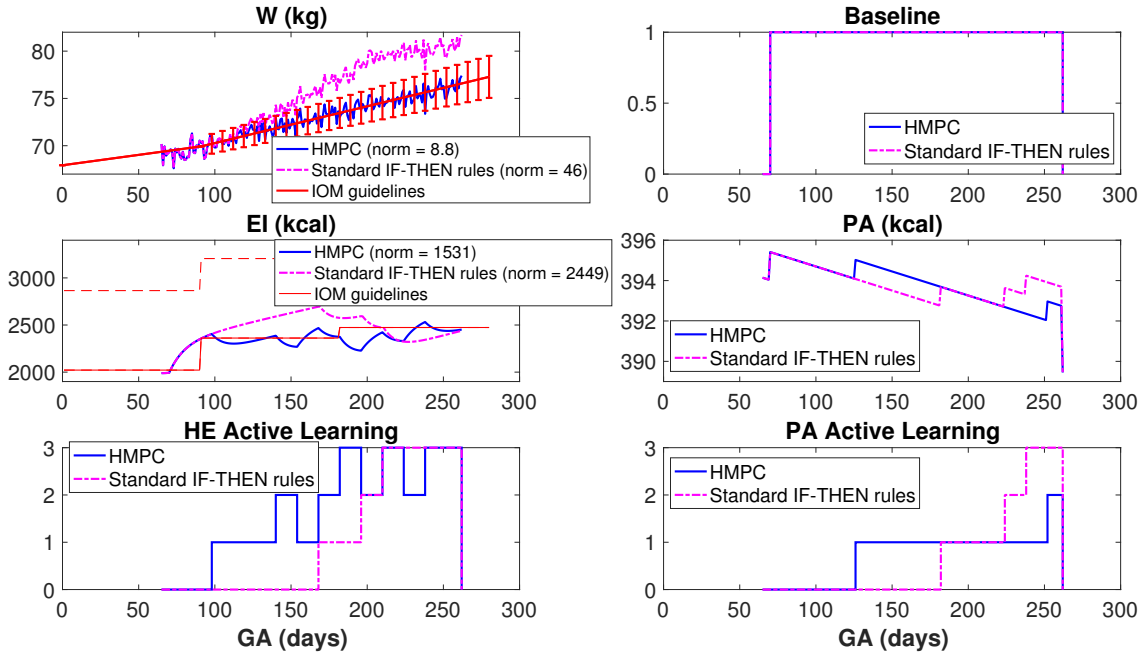

Figure 6.10: HMPC results comparison with standard IF–THEN rules for PID 2072 from Phase II study. (HMPC: noise signal included (covariance $R = 0.5$); $Q_y = [0,\ 10]$; $\alpha_r = \alpha_d = 0$; Type I filer for measured disturbance rejection; $f_a = 0.1$; $p = 25$, $m = 20$.

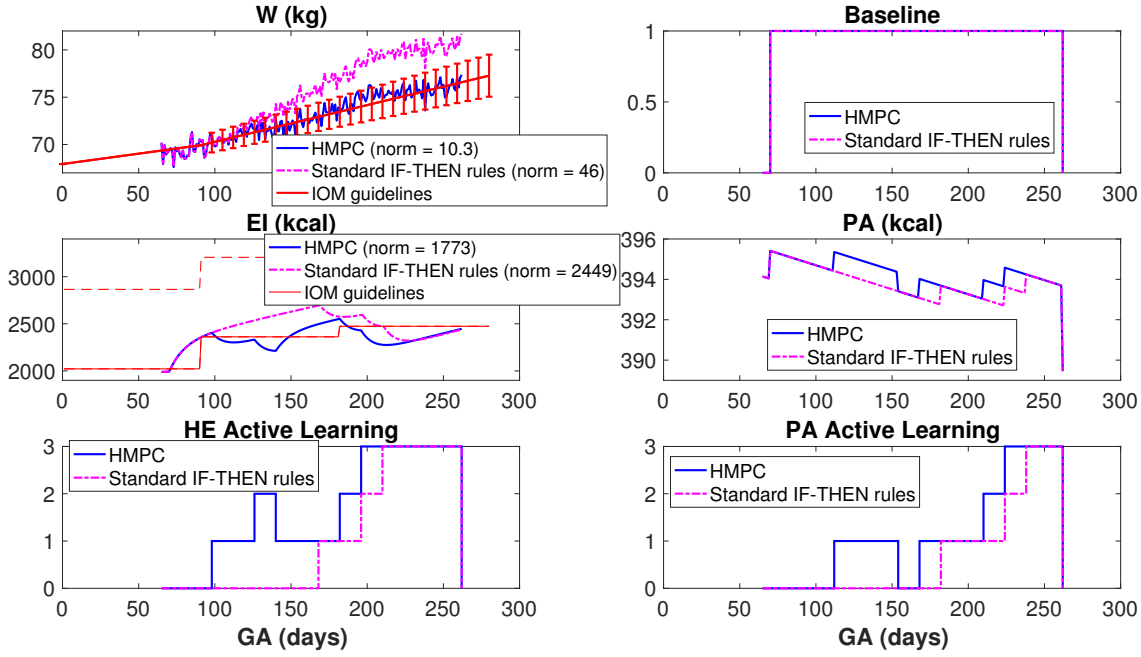

Figure 6.11: HMPC results comparison with standard IF–THEN rules for PID 2072 from Phase II study. (HMPC: noise signal included (covariance $R = 0.5$); $Q_y = [0,\ 10]$; $\alpha_r = 0.9$; $\alpha_d = 0$; Type I filer for measured disturbance rejection; $f_a = 1$; $p = 25$, $m = 20$.

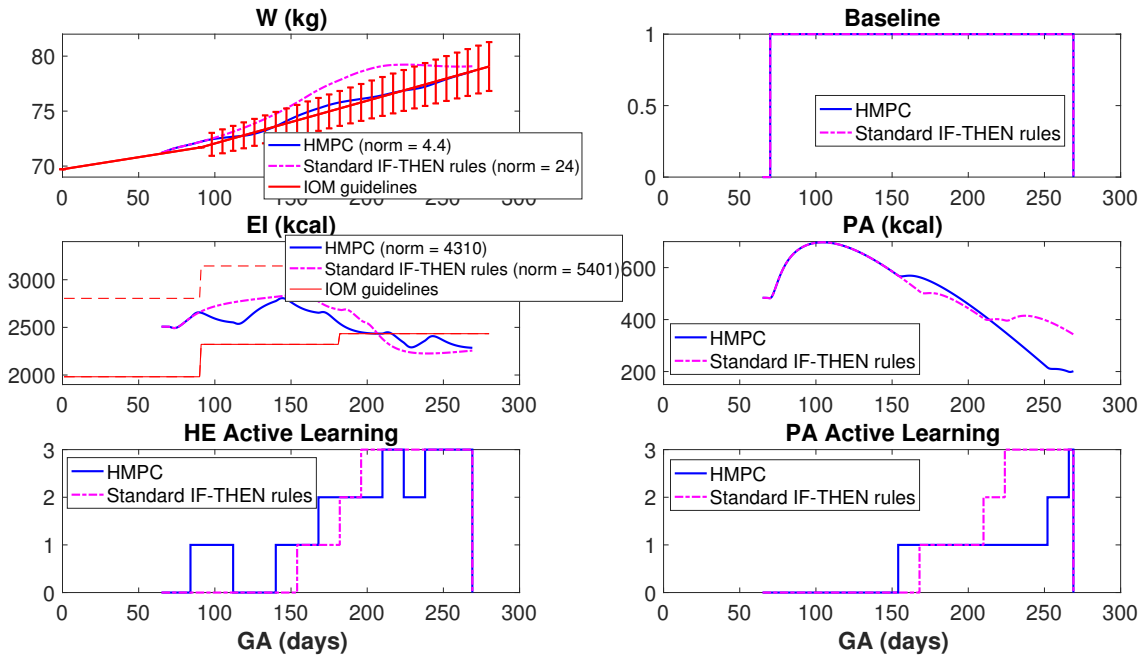

Figure 6.12: HMPC results comparison with standard IF–THEN rules for PID 2062 from Phase II study. (HMPC: noise-free signals only; $Q_y = [0,\ 10]$; $\alpha_r = 0.9$; $\alpha_d = 0.9$; Type I filer for measured disturbance rejection with; $f_a = 1$; $p = 28$, $m = 25$.

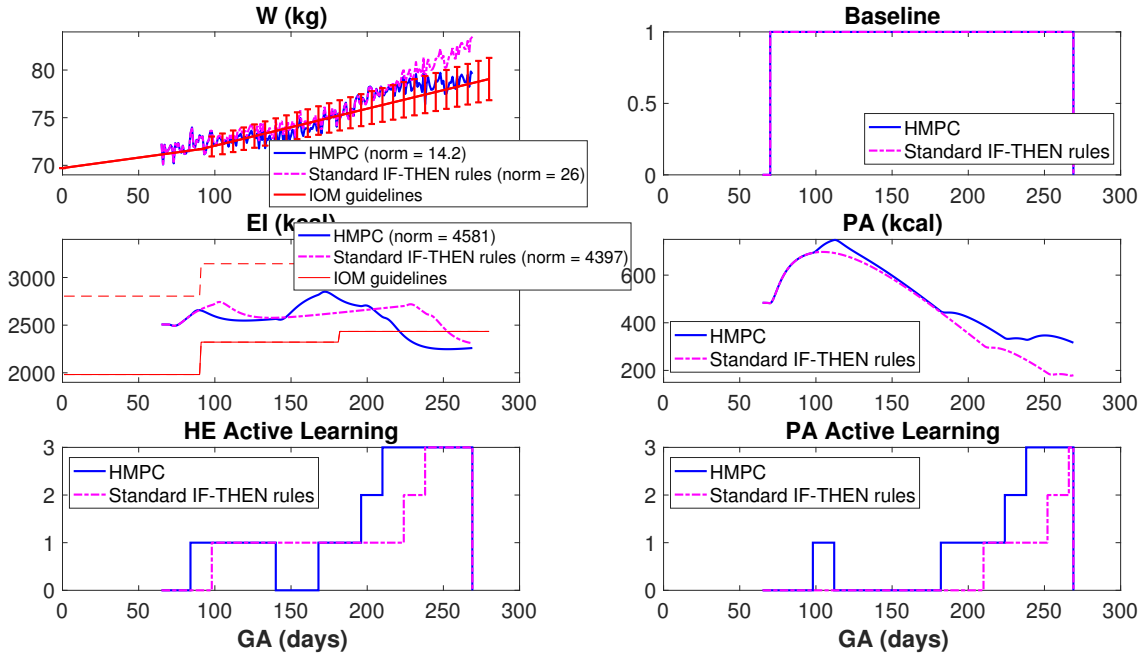

Figure 6.13: HMPC results comparison with standard IF–THEN rules for PID 2062 from Phase II study. (HMPC: noise signal included (covariance $R = 0.5$); $Q_y = [0,\ 10]$; $\alpha_r = 0.5$; $\alpha_d = 0.5$; Type I filer for measured disturbance rejection; $f_a = 0.5$; $p = 28$, $m = 25$.

ently too late to achieve the weight goal. The speed of unmeasured disturbance rejection is proportional to f_a. As f_a approaches zero, the state estimator increasingly ignores the prediction error correction, and the control solution is mainly determined by the deterministic model and the feedforward anticipation signal. On the other hand, the state estimator tries to compensate for all prediction error as f_a approaches 1, and consequently the controller might become extremely aggressive. Thus, by adjusting f_a, the user can directly influence unmeasured disturbance rejection, which is more intuitive than tuning with move suppression in the traditional MPC formulation. In Fig. 6.9 when $f_a = 1$, the controller relies more on measurements, leading to higher norm than using the same noise signals but with $f_a = 0.1$ as in Fig. 6.10. The performance of the HMPC with $f_a = 1$ can alternatively be improved by detuning the speed of reference tracking by increasing α_r to 0.9 as shown in Fig. 6.11.

Thus far, the comparison of HMPC versus standard IF–THEN has been illustrated with single participant-validated model for PID 2072. The norms from HMPC and IF–THEN rules for the scenarios discussed above are tabulated in Table 6.2, which clearly shows that the norm from standard IF–THEN is generally greater than HMPC. In Fig. 6.12 and 6.13, the participant-validated model for PID 2062 was used for further demonstration of these two closed-loop algorithms, where a noise-free case and a noise-corrupted scenario are shown respectively to illustrate that HMPC can achieve superior performance than simple IF–THEN rules.

6.2.2 HMPC versus HMZ IF–THEN Rules

The demonstration of the standard IF–THEN rules in previous section is mostly for the purpose of parallel comparison with HMPC decision rules. In the HMZ study, the IF–THEN rules that were used for actual interventions are different from the standard IF–THEN rules presented previously due to practical considerations. The differences in the two IF–THEN decision frameworks are reflected in the following aspects. First of all, HMZ intervention sessions were planned in a four-weeks cycle, during which dosage dosage changes were not

Table 6.2: Tabulation of adjustable parameters and norms from HMPC and norms from standard IF–THEN rules for different scenarios involved in Section 6.2.1.

		HMPC									IF–THEN	
PID	Noise $R = 0.5$	α_r	α_d	ω	f_a	p	m	Q_y	norm		norm	
									GWG	EI	GWG	EI
2072	N	0	0	–	1	25	20	[0,10]	2.7	1498	21	2246
		0	0	–	1	25	20	[0.1,10]	11.2	1104	21	2246
		0.7	0	–	1	25	20	[0,10]	2.8	1595	21	2246
		0	0.9	–	1	25	20	[0,10]	5.4	1225	21	2246
		0	0.9	10	1	25	20	[0,10]	5.1	1643	21	2246
	Y	0	0	–	1	25	20	[0,10]	18	1775	46	2449
		0	0	–	0.1	25	20	[0,10]	8.8	1531	46	2449
		0.9	0	–	1	25	20	[0,10]	10.3	1773	46	2449
2062	N	0.9	0.9	–	1	28	25	[0,10]	4.4	4310	24	5401
	Y	0.5	0.5	–	0.5	28	25	[0,10]	14.2	4581	26	4397

allowed once a decision had been given and delivered. This is different from the two-weeks timeframe for decision making employed in the standard IF-THEN. One reason for the HMZ intervention being set up with a four-weeks cycle is that some of the intervention components, for example, the active learning component for healthy eating was designed in modules that included four classes for each module; participants took one class every week when they visited the clinics. Hence, the active learning session cannot be completed in less than four weeks.

In addition, there was a one-week delay between decision making and actual implementation of dosage changes in the HMZ IF–THEN. If it is determined that a participant needs dosage increase and extra sessions accordingly, this would involve scheduling efforts between a participant and clinical staff (fitness instructors for example): the participant needs to coordinate time with instructors and adjust her schedules to accommodate for the

Table 6.3: Summary of dosage augmentations rules for HMZ intervention.

Options	Adaptation
Baseline	Base dose for all components
Step up 1	First augmentation of healthy eating and physical activity active learning
Step up 2	Second augmentation of healthy eating and physical activity active learning
Step up 3	Third augmentation of healthy eating and physical activity active learning

additional sessions. Hence, this needs to be planned ahead if an extra intervention session is necessary. Based on this consideration, decision making for dosage changes in the HMZ study is pushed back a week earlier before an actual implementation starts, i.e., the decision making occurs at the end of the third week to prepare for an implementation of any dosage changes for next intervention cycle.

Furthermore, the decision rules only allow for dosage augmentation without recommending decreasing intervention potency, which is different from the original HMPC setting and standard IF-THEN. It also needs to be noted that an augmentation of two components (u_2^{HE} and u_2^{PA}) is implemented at the same time in HMZ if a dosage increase is necessary. This leads to a new sequence table as shown in Table 6.3, which contrasts with the sequential rules that HMPC decision policy and standard IF–THEN rules follow (as specified in Table 6.1). The reduced speed in responding to intervention outcomes due to longer time frame for decisions in HMZ IF–THEN rules hopefully can be compensated by higher intervention intensities through two steps-up at the same time.

What also makes the two IF-THEN decision rules different is that HMZ IF–THEN incorporates anticipation of future weight gain into decision making. Participant GWG is evaluated weekly; if her weekly GWG from the past two weeks is over the IOM recommended weekly GWG at the time for decisions, the dosage will be augmented even if her total weight is still within upper bounds of the IOM recommended total weight.

All these intervention settings employed in the HMZ study, such as the delay between decision making and actual step-up implementation and other constraints are incorporated

in HMZ IF–THEN rules to ensure that it is representative of real cases. For the purpose of parallel comparison, the HMPC decision policy is slightly modified to only recommend dosage augmentations when compared with the HMZ IF–THEN rules. This indicates that, for scenarios in need of dosage reductions to achieve optimal responses, the intervention components remain unchanged for HMPC simulations in stead of getting decremented. Hence, a decrease in controller performance will be expected if compared to the original HMPC formulation. The "augmentation only" setting for HMPC can be implemented by modifying the move-size constraints to $0 \leq \Delta u_j(k) \leq 1$ for $j \in \{1, 2\}$. Other constraints in the HMPC formulations are kept the same: these include the two-weeks time frame for decisions and using the same sequential decision rules following Table 6.1.

The results of comparing HMPC with HMZ IF–THEN decision rules for PID 2072 are presented in Fig. 6.14 to Fig. 6.19: Fig. 6.14 shows the results with noise-free signals, while the other figures present the results with measurement noise added in GWG output to simulate real-life setting (covariance of GWG noise $R = 0.5$). Note that the noise sequence is the same in Fig. 6.15 and 6.16, while Fig. 6.17, 6.18 and 6.19 use a different realization of noise signal.

Fig. 6.15 and 6.16 compare the HMPC results using different values of adjustable parameters. The performance of HMPC in Fig. 6.15 with $f_a = 1$ can be improved by detuning f_a and other parameters as shown in Fig. 6.16. To examine the performances of these two decision rules under different uncertainties, another set of noise sequence is introduced and the results are shown in Fig. 6.17, 6.18 and 6.19.

From comparing the HMPC and HMZ IF–THEN under different circumstances, it should be noted that, the HMPC provides a good performance at the early stage of intervention, but it is likely to observe accumulated control errors at the end (more often to observe simulated weight lower than guidelines). This is because the HMPC optimizes control actions in response to real-time need by augmenting dosages at the beginning, but when dosage reductions are needed in later stage, it is not implementable due to the fact

that the controller has been modified to only allow for dosage augmentations. It inevitably results in accumulated control errors. This can be interpreted in a more intuitive way: when participant actual GWG has met the recommended GWG, she no longer needs such intense interventions. If the intervention intensity is still kept at a high level, her weight gain is low, leading to a total weight below guidelines.

Alternatively, detuning the controller by slowing down the speed of set-point tracking and disturbance rejections would be a good solution for this situation. Slowing down the response of the controller to the need of more intense interventions from the beginning of the intervention can push back dosage augmentations, which significantly reduce the accumulated errors and improve the performance. The benefits from controller detuning is more significant when using the participant-validated model obtained for PID 2062, the second participant demonstration in Chapter 5.

Fig. 6.20 and 6.21 compare the fastest response and the detuned actions from HMPC implementation using noise-free signals respectively, where the norm in W was brought down from 15 to 5.1 by pushing back the first augmentation of PA active learning by 6 decision cycles (12 weeks). For the cases with the addition of noise as shown in Fig. 6.22 and 6.23, detuning the controller successfully improves the closed-loop performance by delaying the augmentations of both HE and PA active learning.

From Fig. 6.20 to 6.23, one might also question the superiority of HMPC over HMZ IF–THEN from the presented closed-loop responses for this participant, because the norm from HMPC is not necessarily as low as HMZ IF-THEN but seems to be completely depending on the tuning of the controller. However, Fig. 6.20 where another realization of noise sequence is used for simulation clearly shows that the HMZ IF–THEN cannot ensure a good performance under certain circumstances while HMPC is absolutely more stable.

The tabulation of the adjustable parameters and the norm from HMPC and the norm from HMZ IF–THEN rules can be found in Table 6.5. From the demonstrations above, it can be concluded that HMPC can achieve better intervention outcomes than HMZ IF–THEN

Table 6.4: Summary of dosage augmentations rules for HMZ intervention.

Options	Adaptation
Baseline	Base dose for all components
Step up 1	First augmentation of healthy eating and physical activity active learning
Step up 2	Second augmentation of healthy eating and physical activity active learning
Step up 3	Third augmentation of healthy eating and physical activity active learning

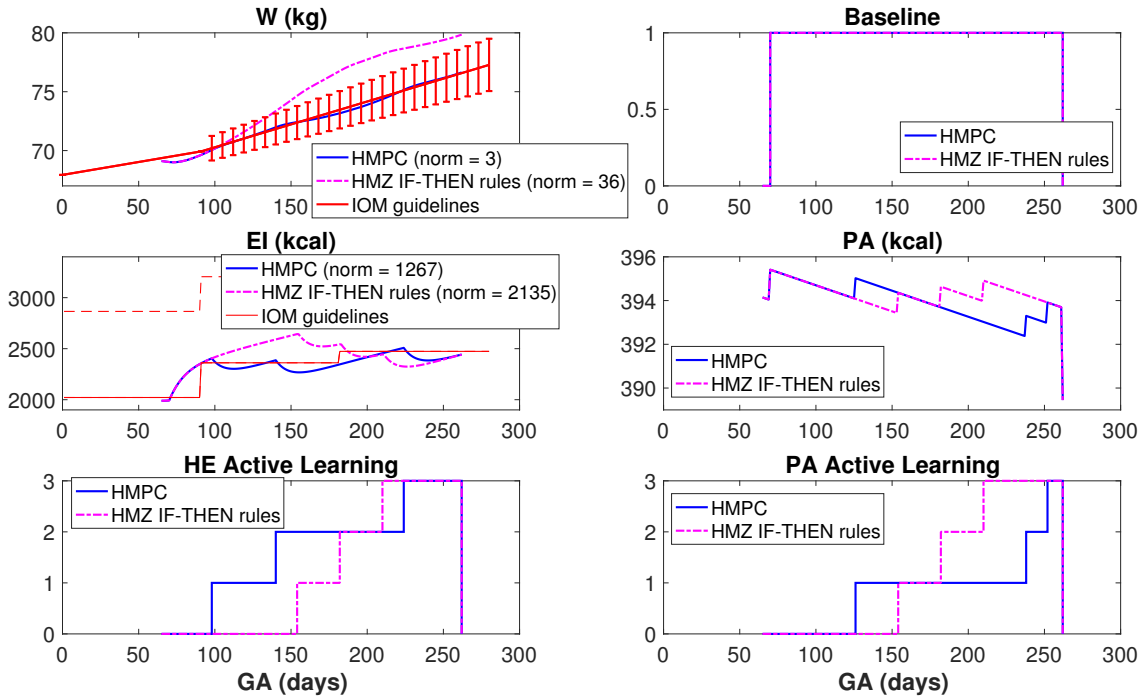

Figure 6.14: HMPC results comparison with HMZ IF–THEN rules for PID 2072 from Phase II study. (HMPC: noise-free signals only; $Q_y = [0,\ 10]$; $\alpha_r = \alpha_d = 0$; Type I filer for measured disturbance rejection; $f_a = 1$; $p = 25$, $m = 20$.

rules in general, and the adjustable parameters from the 3DoF tuning framework provide us the flexibility to accommodate variability of implementation due to real-life constraints. The interventions given by IF–THEN rules are usually delayed or too aggressive, and the decision from IF–THEN is also substantially subject to measurement noise. On the other hand, the performance of HMPC is more consistent under a variety of uncertainties.

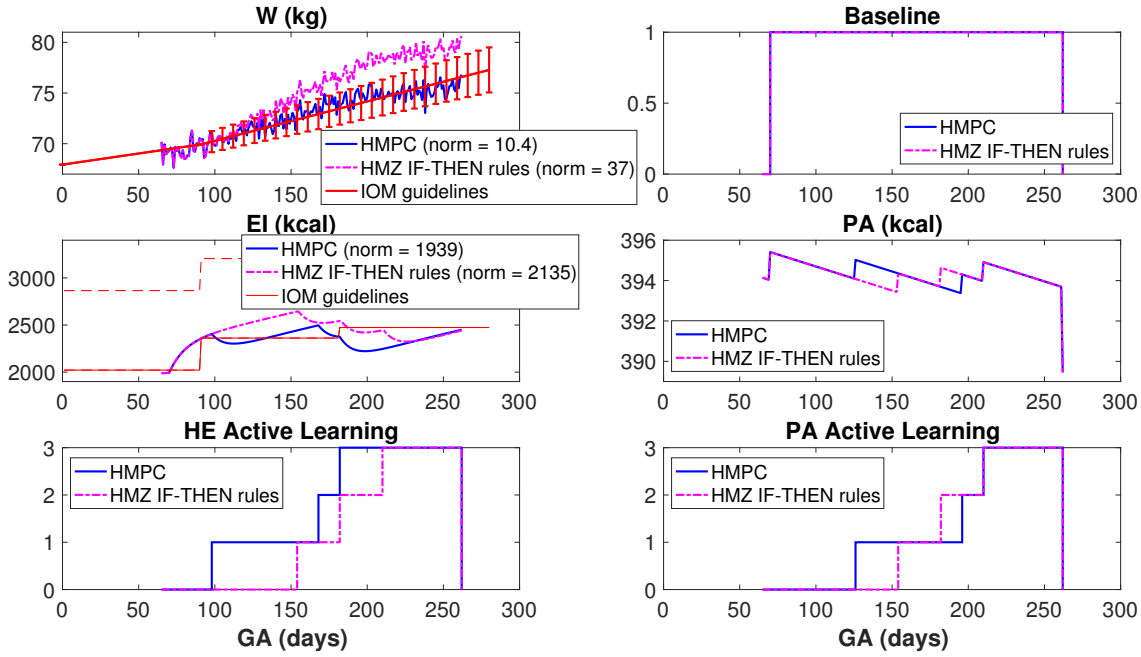

Figure 6.15: HMPC results comparison with HMZ IF–THEN rules for PID 2072 from Phase II study. (HMPC: noise signal included (covariance $R = 0.5$); $Q_y = [0,\ 10]$; $\alpha_r = \alpha_d = 0$; Type I filer for measured disturbance rejection; $f_a = 1$; $p = 25$, $m = 20$.

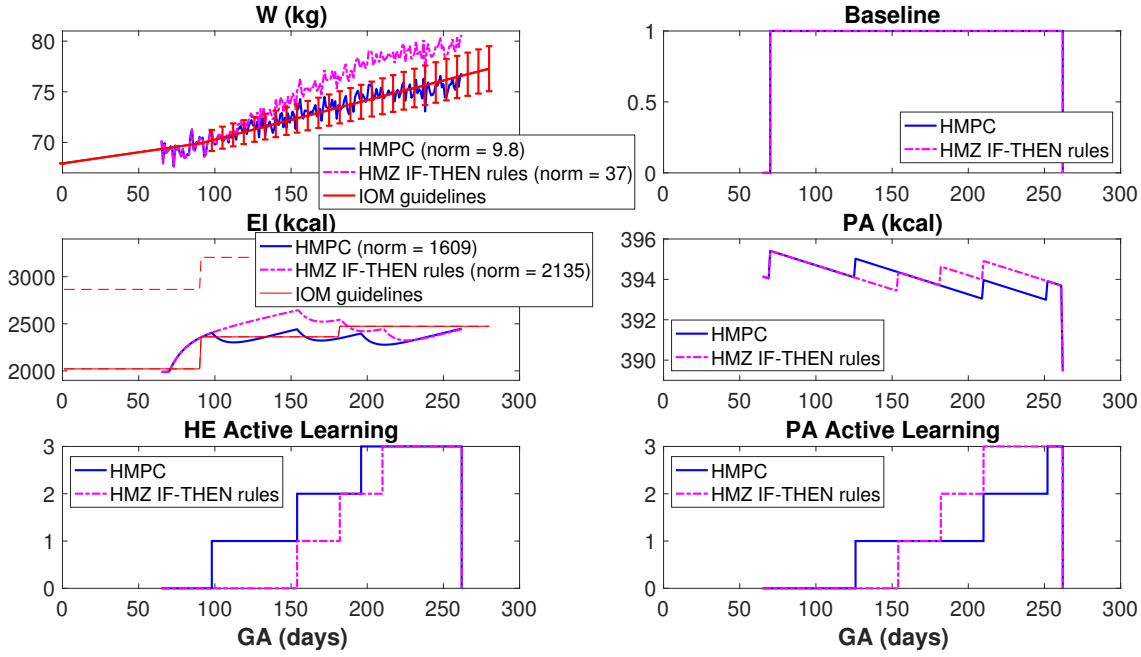

Figure 6.16: HMPC results comparison with HMZ IF–THEN rules for PID 2072 from Phase II study. (HMPC: noise signal included (covariance $R = 0.5$); $Q_y = [0,\ 10]$; $\alpha_r = \alpha_d = 0.3$; Type I filer for measured disturbance rejection; $f_a = 0.3$; $p = 25$, $m = 20$.

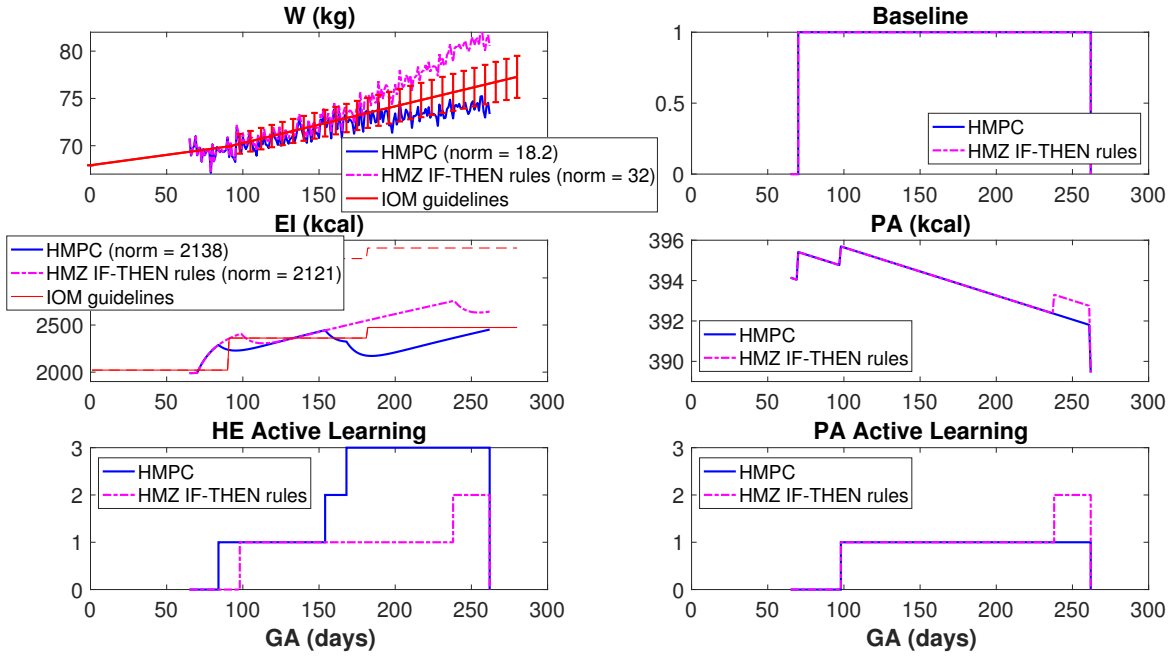

Figure 6.17: HMPC results comparison with HMZ IF–THEN rules for PID 2072 from Phase II study. (HMPC: noise signal included (covariance $R = 0.5$); $Q_y = [0,\ 10]$; $\alpha_r = \alpha_d = 0$; Type I filer for measured disturbance rejection; $f_a = 1$; $p = 25$, $m = 20$.

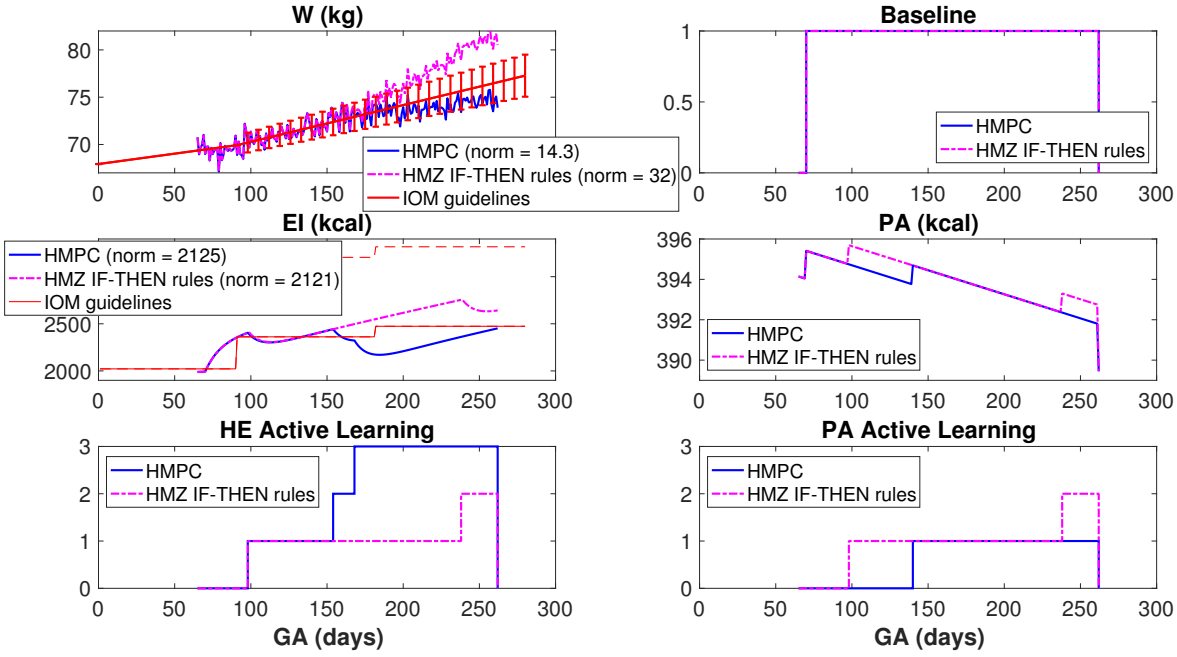

Figure 6.18: HMPC results comparison with HMZ IF–THEN rules for PID 2072 from Phase II study. (HMPC: noise signal included (covariance $R = 0.5$); $Q_y = [0,\ 10]$; $\alpha_r = \alpha_d = 0$; Type I filer for measured disturbance rejection; $f_a = 0.5$; $p = 25$, $m = 20$.

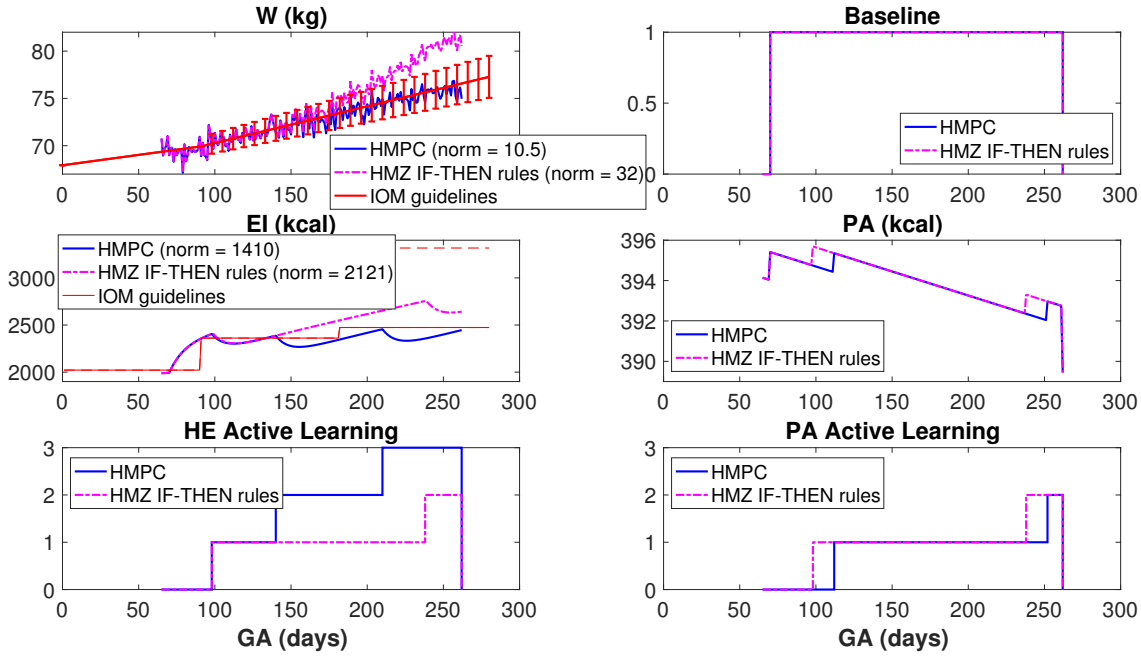

Figure 6.19: HMPC results comparison with HMZ IF–THEN rules for PID 2072 from Phase II study. (HMPC: noise signal included (covariance $R = 0.5$); $Q_y = [0,\ 10]$; $\alpha_r = \alpha_d = 0.3$; Type I filer for measured disturbance rejection; $f_a = 0.1$; $p = 25$, $m = 20$.

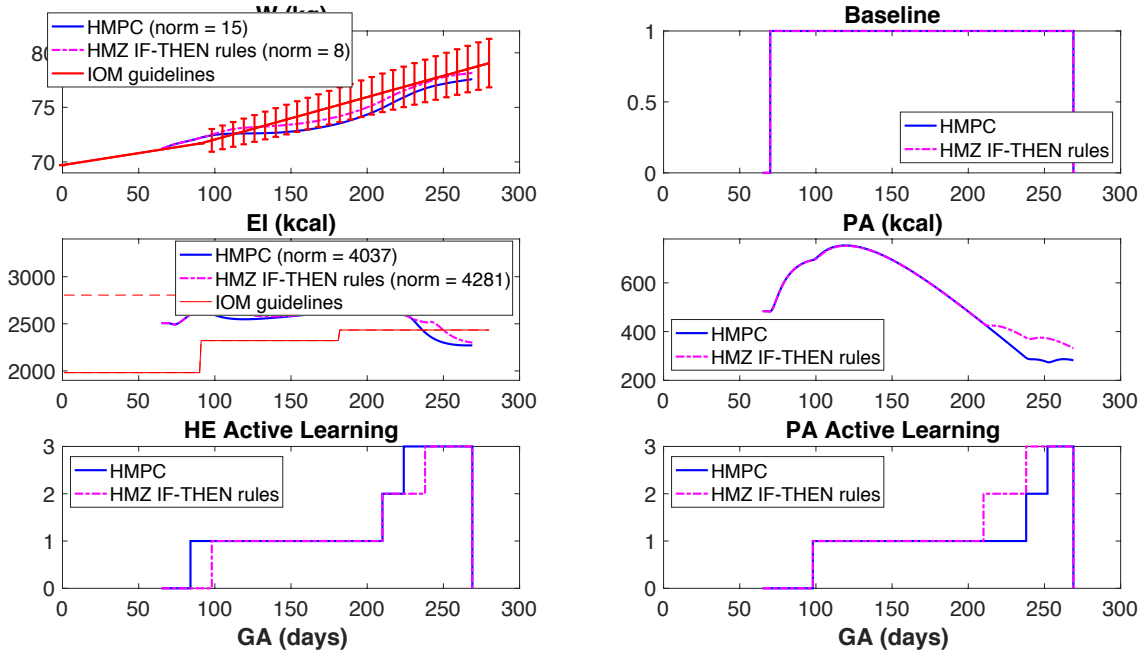

Figure 6.20: HMPC results comparison with HMZ IF–THEN rules for PID 2062 from Phase II study. (HMPC: $Q_y = [0,\ 10]$; $\alpha_r = \alpha_d = 0$; Type I filer for measured disturbance rejection; $f_a = 1$; $p = 28$, $m = 25$.

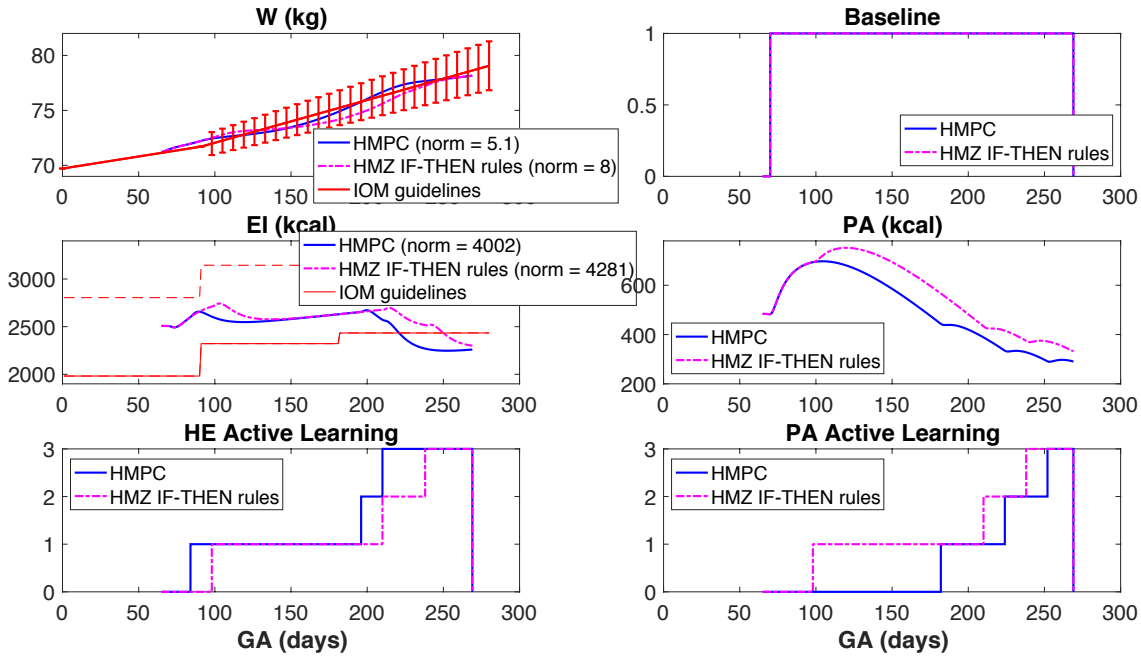

Figure 6.21: HMPC results comparison with HMZ IF–THEN rules for PID 2062 from Phase II study. (HMPC: $Q_y = [0,\ 10]$; $\alpha_r = \alpha_d = 0.9$; Type I filer for measured disturbance rejection; $f_a = 0.9$; $p = 28$, $m = 25$.

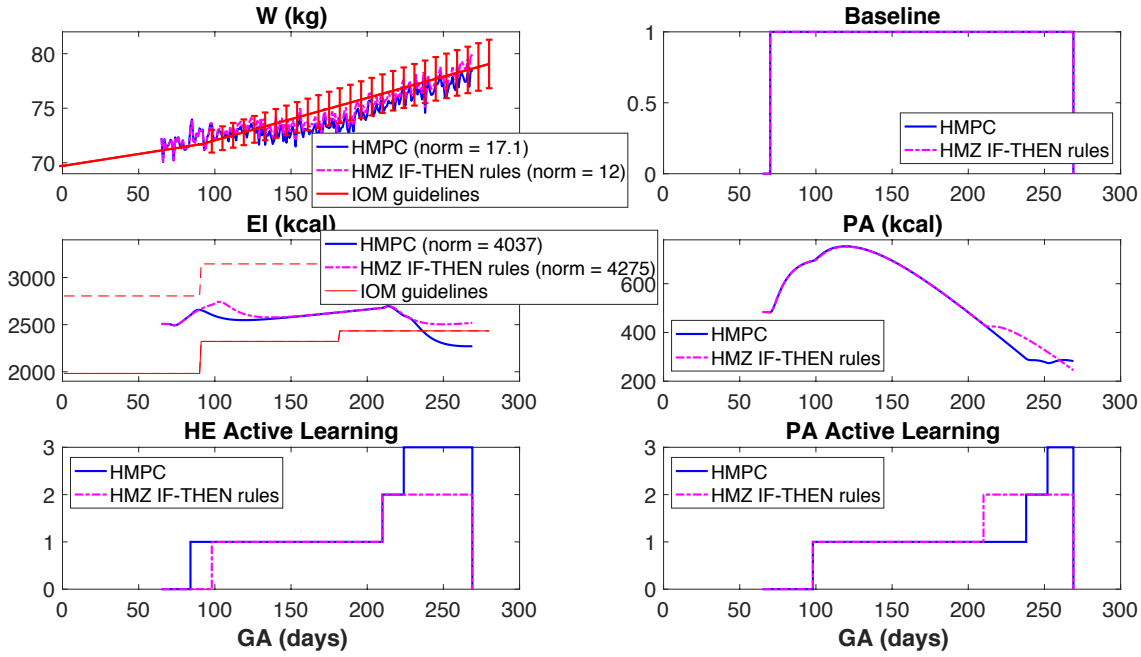

Figure 6.22: HMPC results comparison with HMZ IF–THEN rules for PID 2062 from Phase II study. (Noise signal included (covariance $R = 0.5$, realization 1); HMPC: $Q_y = [0,\ 10]$; $\alpha_r = \alpha_d = 0$; Type I filer for measured disturbance rejection; $f_a = 1$; $p = 28$, $m = 25$.

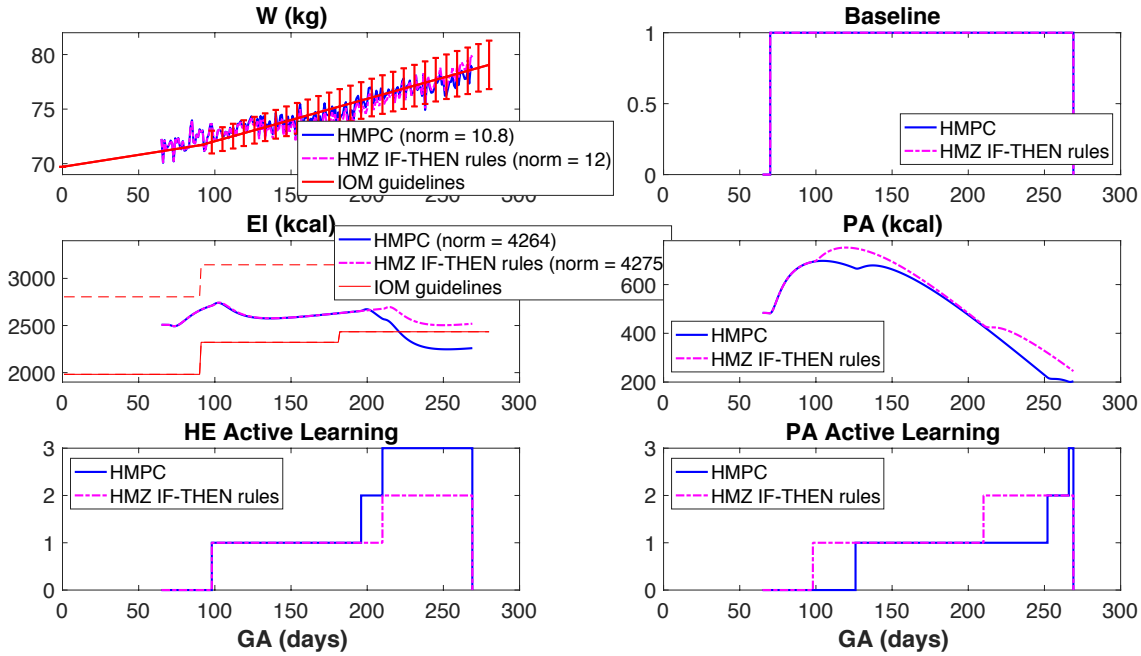

Figure 6.23: HMPC results comparison with HMZ IF–THEN rules for PID 2062 from Phase II study. (Noise signal included (covariance $R = 0.5$, realization 1); HMPC: $Q_y = [0,\ 10]$; $\alpha_r = \alpha_d = 0.9$; Type I filer for measured disturbance rejection; $f_a = 0.5$; $p = 28$, $m = 25$.

6.3 Conclusions

In this chapter, an appealing HMPC framework based on MLD structure for the design of optimized behavioral interventions is presented. It has been demonstrated that the design of such an HMPC controller can systematically assign the dosages of intervention components in a pre-determined sequenced manner. Specifically, relying on the additional constraints using binary variables in the MLD structure, the logical specifications associated with the sequential decision policies in adaptive interventions can be easily addressed, and embedded into HMPC formulation. The very common clinical requirement that the intervention decisions are made less frequently than the sampling interval is also systematically taken into account by adding extra constraints to allow for dosage changes only at fixed time frames.

In prior work, the developed HMPC algorithms have only been tested with hypothetical

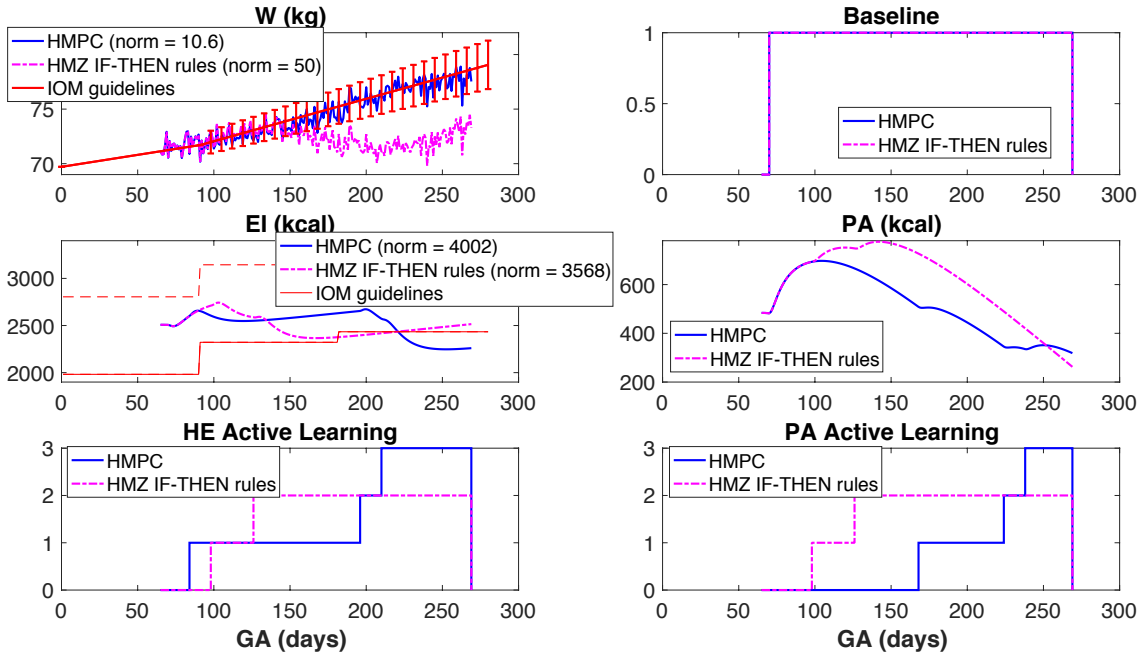

Figure 6.24: HMPC results comparison with HMZ IF–THEN rules for PID 2062 from Phase II study. (Noise signal included (covariance $R = 0.5$, realization 2); HMPC: $Q_y = [0,\ 10]$; $\alpha_r = \alpha_d = 0.5$; Type I filer for measured disturbance rejection; $f_a = 0.7$; $p = 28$, $m = 25$.

participants based on assumed parameter values. Now with the participant data available from Phase II study of the HMZ, the control problems can be reformulated based on participant-validated models as presented in Chapter 5. To represent actual circumstances in the HMZ study, the developed HMPC framework can be adjusted to accommodate real-life settings, in order for a parallel comparison with different IF–THEN rules.

Two simulation studies using the integrated participant-validate models are presented in this chapter: one study to compare HMPC with standard IF–THEN rules that follow the same sequence rules as proposed for the HMPC, and one study to compare with HMZ IF–THEN rules that is more close to actual interventions in HMZ study. Both studies demonstrate the superior performance of the HMPC to the simple IF–THEN rules. The performance of HMPC can be tuned with a set of adjustable parameters which can independently change the speed of set-point tracking and the speed of measured/unmeasured disturbance rejection. If the control action is too aggressive, the performance can be im-

Table 6.5: Tabulation of adjustable parameters and norms from HMPC and norms from HMZ IF–THEN rules for different scenarios involved in Section 6.2.2.

		HMPC									HMZ IF–THEN	
PID	Noise	α_r	α_d	ω	f_a	p	m	Q_y	norm		norm	
									GWG	EI	GWG	EI
2072	N	0	0	–	1	25	20	[0,10]	3	1267	36	2135
	Y1	0	0	–	1	25	20	[0,10]	10.4	1939	37	2135
		0.3	0.3	–	0.3	25	20	[0,10]	9.8	1609	37	2135
	Y2	0	0	–	1	25	20	[0,10]	18.2	2138	32	2121
		0	0	–	0.5	25	20	[0,10]	14.3	2125	32	2121
		0.3	0.3	–	0.1	25	20	[0,10]	10.5	1410	32	2121
2062	N	0	0	–	1	25	20	[0,10]	15	4037	8	4281
		0.9	0.9	–	0.9	28	25	[0,10]	5.1	4002	8	4281
	Y	0	0	–	1	28	25	[0,10]	17.1	4037	12	4275
		0.9	0.9	–	0.5	25	20	[0,10]	10.8	4264	12	4275

proved by detuning the controller, and vice versa. Hence, it can properly adjust participant responses under a variety of uncertainties.

In addition, it has been found that HMPC with setpoints on GWG and EI is less preferable to a setpoint-only on GWG (assigning zero weight on EI tracking), especially considering the ballpark values used for EI guidelines. This work further proves the potential that HMPC-based intervention can better improve the participant's response, increase the effectiveness of the intervention and enable less waste of resource relying on the dynamical model, measured outcomes, and predicted measured disturbance (if applicable).

Chapter 7

SUMMARY, CONCLUSIONS AND FUTURE DIRECTIONS

7.1 Conclusions

This dissertation has demonstrated how system identification, state estimation approaches can be used to assist in dynamical systems modeling, and further enhance the performance of the closed-loop control system for interventions. Excessive maternal weight gain during pregnancy represents a major public health concern that calls for novel and effective gestational weight management interventions. *Healthy Mom Zone study* (HMZ) aims to develop and validate an individually tailored intensively adaptive intervention, and has demonstrated significant potential in effectively managing gestational weight gain (GWG) for overweight or obese pregnant women (OW/OBPW).

Prior work by Dong (2014) proposed a comprehensive dynamical systems model for GWG behavioral interventions, and a closed-loop framework based on Hybrid Model Predictive Control (HMPC) algorithm designed for adaptive interventions. This model and control system were only tested with hypothetical data. In this work, the model and control algorithm have been re-evaluated with participant data from the HMZ study, and efforts have been made to address issues of erroneous self-report, missing data and measurement noise that are commonly observed in real-life interventions.

From the evaluation of the energy balance (EB) model against participant data in the HMZ study, it has been found that underreporting of energy intake is a significant issue of concern for the use of EB model as well as for the implementation of closed-loop control systems. This issue is common in weight interventions relying on self-reports, and introduces significant error in the input measurements. To understand the extent of underreporting, algebraic estimation of energy intake for participants are obtained by back-calculation from a discretized version of the reformulated EB model. Furthermore, the formulation of a

semi-physical identification problem using batch data to estimate the extent of systematic underreporting is proposed; a global estimation approach is applied to solve the identification problem and contrasted with a local modeling technique based on "Model-on-Demand" concept. To better address the issue of noise in the measurements, a recursive method based on Kalman filtering is also developed to enable sequential estimation of energy intake in real time. All the three methods for estimating energy intake have been compared across participants and the pros and cons for each method have been analyzed comprehensively.

From the estimation results, it has been realized that understanding energy intake underreporting is an important consideration in a gestational weight control intervention for overweight or obese pregnant women, which must be recognized in order to obtain meaningful weight predictions from energy balance models. The identification and characterization of energy intake underreporting is helpful in providing informative guidance to participants in the course of the intervention, and also improves the usefulness of energy balance modeling as part of an intensively adaptive intervention. From the examination of the three developed methods, it is shown that all are amenable for use in real-time clinical settings, which remains a topic for further study.

In the addition to the estimation work using the energy balance model, substantial efforts have also been dedicated to semi-physical identification of a behavioral model. The behavioral model, as described in Chapter 2, incorporates some well-accepted concepts in psychology and behavioral science, such as the Theory of Planned Behavior (TPB), self-regulation theory and intervention delivery dynamics. However, the parameters involved in the theoretical model need to be identified for individual participants in order to be used for the design of adaptive interventions, or more specifically, for control purpose.

System identification analyses based on HMZ Phase I participants were useful to learn how to modify the intervention and measurement protocols and how to make other improvements for Phase II Study. Specifically, after examining the variation, correlation and dynamics of the TPB constructs, it was decided to only keep the subjective norm (SN),

perceived behavioral control (PBC), and intention (INT) in the model structure and to increase the measurement frequency of these constructs from monthly to weekly for Phase II study while measuring the other constructs less frequently on a monthly basis. The modified identification techniques and model structures are tested on Phase II participants, from which participant-validated models are obtained and used for closed-loop implementation and demonstration.

The HMPC algorithm to assign optimized dosages in response to participant real time intervention outcomes is designed based on a Mixed Logical Dynamical framework which can address the categorical dosage components, and convert sequential decision rules and other clinical considerations into mixed-integer linear constraints. The time-varying adaptive framework developed based on HMPC algorithm has been tested with participant-validated models in this work and compared to different "IF–THEN" rules, one of these patterned after the decision rules used in HMZ Phase II study. The three degree of freedom parametrization displays ease of tuning that is amenable to robust performance in closed-loop systems. The HMPC shows consistent superior performance than "IF–THEN" rules under different uncertainties.

In this work, substantial research has been conducted based on the participant data from HMZ study, from which we have developed multiple estimation algorithms that are able to address the issues of observation loss and measurement noise in the collected data. The estimation approaches and the control algorithms designed in this study have demonstrated the potential of increasing intervention effectiveness and improving participant response. Focus of our work can be extended to the generalization of the developed algorithms for broader applications in the future.

7.2 Future Research Directions

As this dissertation presents an initial demonstration of the potential for real-world applications of adaptive sequential behavioral interventions and provides a plausible "proof of concept" of the approach, there are several interesting directions for future work.

7.2.1 Gain-Scheduling Parameter Varying Control for GWG Intervention

In the work so far, it has been assumed that the comprehensive model for individual participants is a linear time-invariant model. However, the variations of participant's attitude and behavior during pregnancy indicate the potential parameter changes in the model in real life, especially for pregnant women from different stages of gestation, leading to a linear time-varying model. Therefore, instead of using a single participant-validated model by averaging the dynamics of individual woman over the span of entire gestation, two or more models can be obtained by partitioning the collected data set into different stages in gestation for semi-physical identification analyses. The intervention problems with time-varying models can be addressed using gain scheduling parameter varying control, which will help better improve the prediction of controlled variables over the receding horizon using an HMPC strategy.

This model scheduling strategy for HMPC control algorithm has been proposed in previous work (Dong (2014)) and tested with hypothetical participants. Re-evaluating the algorithm with HMZ participant data will provide valuable insights into the design. It has to be noted that such exploration is subject to the limitations in the size of the available data set.

7.2.2 HMPC applied in real-life intervention settings

System identification of the participant-validated models and the ensuing implementation of the closed-loop control schemes in this work are performed after the actual interventions and data collection are completed for Phase II study. Hence HMPC-based control was not performed online, i.e., the HMPC was not used to determine dosage changes during the Phase II HMZ intervention. As a direction for future research, it would be useful to examine how models could be obtained for the intervention in practice.

For the purpose of closed-loop implementation, a model that describes behavioral dynamics for individual participants during gestation is necessary but will not be available for

women going through first pregnancy. Hence, model estimation might need to be performed before or at the same time with control implementation for real-life settings. Regardless of what strategy to be used for addressing such problems, intensive data collection may be necessary. However, it is difficult to obtain intensive measurements that favors online identification during pregnancy. Considering intervention participants as a special group of populations (OW/OBPW), the risks of pregnancy and participant burden are important issues to be accounted for the design of measurement protocol. These issues bring further challenges to the success of real-life implementations.

With these considerations in mind, two options that might be feasible for this problem are listed below:

1. Develop a model to describe the averaged behavioral dynamics for women from different sub-populations, for example, by BMI, or age. Such a model can be obtained by performing semi-physical identification over grouped participant data, leading to an averaged model suited for corresponding populations. Hence, parts of the model can be specified before an intervention starts based on the category a participant belongs to.

2. Develop an initial model and recursively adapt the model parameters based on new measurements as the intervention moves along. The initial model can be either an averaged model proposed above, or an individualized model based on measurements from baseline of the intervention. For the latter option of obtaining an individualized model from start, a more intensive measurement schedule needs to be planned at the early stage of interventions in order to make the initial model estimation possible, but it can be less intensive during the model update phase. As mentioned earlier, participant burden and the risks of pregnancy have to be taken into account carefully if data needs to intensively collected. In addition, if such a time varying model is used, the HMPC needs to be revised to incorporate adaptive control performance.

7.2.3 *Incorporate developed estimation approaches for energy intake into HMPC framework*

As described in earlier chapters, the HMPC algorithm relies on energy intake (one of the inputs the controller uses) to determine the optimal control action. The self-reported energy intake during interventions are subject to underreporting issue, hence cannot be used for control purpose. Chapter 3 and 4 present a variety of estimation methods with the ultimate goal to provide a reliable energy intake estimate to enhance the performance of closed-loop control.

The estimation methods developed in this work have not yet been tested in real intervention applications or used in collaboration of HMPC framework. Among these three methods, the first method of using algebraic back-calculation is the easiest and quickest to implement and might be better of practical use for behavioral scientists. However, this method cannot provide estimates instantaneously but has to wait for a few days. In addition to the delay, its use is substantially subject to noise and missing data. The semi-physical identification methods estimate systematic underreporting using self-reported energy intake and can provide point-wise estimates as long as the self-reports are available. But this method is sensitive to noise as well, and significant input noise can generate biased estimates. From this standpoint, the Kalman filtering approach is a more rigorous approach to the other two methods, and gives real-time estimation of energy intake in the presence of measurement loss.

Based on these pros and cons for each method, the Kalman filtering approach that can address intermittent measurements is the most suitable option to combine with the HMPC for online optimization. It will be useful to evaluate the algorithm in practice and further assist the interventions for real.

REFERENCES

Dietary Reference Intakes for Energy, Carbohydrate, Fiber, Fat, Fatty Acids, Cholesterol, Protein and Amino Acids (National Acadamies Press, 2005).

Ahmad, H. and T. Namerikawa, "Extended Kalman filter-based mobile robot localization with intermittent measurements", Systems Science & Control Engineering: An Open Access Journal **1**, 1, 113–126 (2013).

Ajzen, I., *Action Control*, chap. From intentions to actions: A theory of planned behavior, pp. 11–39 (Springer Berlin Heidelberg, 1985).

Ajzen, I., "The theory of planned behavior", Organizational behavior and human decision processes **50**, 2, 179–211 (1991).

Akhlaghi, S., N. Zhou and Z. Huang, "Adaptive adjustment of noise covariance in Kalman filter for dynamic state estimation", Submitted to arXiv (2017).

Armitage, C. J. and M. Conner, "Distinguishing perceptions of control from selfefficacy: Predicting consumption of a lowfat diet using the theory of planned behavior", Journal of applied social psychology **29**, 1, 72–90 (1999).

Arulampalam, M. S., S. Maskell, N. Gordon and T. Clapp, "A tutorial on particle filters for online nonlinear/non-gaussian bayesian tracking", Signal Processing, IEEE Transactions on **50**, 2, 174–188 (2002).

Baeten, J. M., E. A. Bukusi and M. Lambe, "Pregnancy complications and outcomes among overweight and obese nulliparous women", American Journal of Public Health **91**, 3, 436 (2001).

Bandura, A., *Social foundations of thought and action: a social cognitive theory* (Prentice-Hall series in social learning theory, 1986).

Bastien, M., P. Poirier, I. Lemieux *et al.*, "Overview of epidemiology and contribution of obesity to cardiovascular disease", Progress in Cardiovascular Diseases **56**, 4, 369–381 (2014).

Bemporad, A. and M. Morari, "Control of systems integrating logic, dynamics, and constraints", Automatica **35**, 3, 407–427 (1999).

Borrelli, F., A. Bemporad and M. Morari, *Predictive Control For Linear And Hybrid Systems* (Cambridge University Press, 2017).

Braun, M. W., D. E. Rivera and A. Stenman, "A 'Model-on-Demand' identification methodology for non-linear process systems", International Journal of Control **74**, 18, 1708–1717 (2001).

Butte, N. F., W. W. Wong, M. S. Treuth *et al.*, "Energy requirements during pregnancy based on total energy expenditure and energy deposition", The American Journal of Clinical Nutrition **79**, 6, 1078–1087 (2004).

Camacho, E. F. and C. Bordons Alba, *Model Predictive Control* (Springer Science & Business Media, 2013).

Carreno, C. A. *et al.*, "Excessive early gestational weight gain and risk of gestational diabetes mellitus in nulliparous women", Obstetrics and Gynecology **119**, 6, 1227–1233 (2012).

Chen, C. T., *Linear System Theory and Design* (Oxford University Press, Inc., 1995).

Chu, S. Y., W. M. Callaghan, S. Y. Kim, C. H. Schmid, J. Lau, L. J. England and P. M. Dietz, "Maternal obesity and risk of gestational diabetes mellitus.", Diabetes Care **30**, 8, 2070–2076 (2007).

Collins, L. M., S. A. Murphy and K. L. Bierman, "A conceptual framework for adaptive preventive interventions", Prevention Science **5**, 3, 185–196 (2004).

Deshmukh, S., B. Natarajan and A. Pahwa, "State estimation over a lossy network in spatially distributed cyber-physical systems", IEEE Transactions on Signal Processing **62**, 15, 3911–3923 (2014).

Diabetes Prevention Program (DPP) Research Group, "The diabetes prevention program (dpp) description of lifestyle intervention", Diabetes Care **25**, 12, 2165–2171 (2002).

Dong, Y., *A novel control engineering approach to designing and optimizing adaptive sequential behavioral interventions*, Ph.D. thesis, Arizona State University (2014).

Dong, Y., D. E. Rivera, D. Symons Downs, J. S. Savage, D. M. Thomas and L. M. Collins, "Hybrid model predictive control for optimizing gestational weight gain behavioral interventions", in "Proceedings of 2013 American Control Conference (ACC)", pp. 1970–1975 (2013).

Dong, Y., D. E. Rivera, D. M. Thomas, J. E. Navarro-Barrientos, D. Symons Downs, J. S. Savage and L. M. Collins, "A dynamical systems model for improving gestational weight gain behavioral interventions", in "Proceedings of 2012 American Control Conference (ACC)", pp. 4059–4064 (2012).

Galtier-Dereure, F., C. Boegner and J. Bringer, "Obesity and pregnancy: complications and cost", The American Journal of Clinical Nutrition **71**, 5, 1242s–1248s (2000).

Gilmore, L. A., M. Klempel-Donchenko and L. M. Redman, "Pregnancy as a window to future health: Excessive gestational weight gain and obesity", in "Seminars in Perinatology", vol. 39, pp. 296–303 (2015).

Gordon, N., "On-line filtering for nonlinear/non-gaussian state space models", in "European Conference on Simulation Methods in Econometrics", (1996).

Guo, P., D. E. Rivera, D. Symons Downs and J. S. Savage, "State estimation under correlated partial measurement losses: Implications for weight control interventions", in "Proceedings of 20th World Congress, The International Federation of Automatic Control (IFAC)", pp. 14074–14079 (2017).

Guo, P., D. Symons Downs and J. S. Savage, "Semi-physical identification and state estimation of energy intake for interventions to manage gestational weight gain", in "Proceedings of 2016 American Control Conference (ACC)", pp. 1271–1276 (2016).

Hall, K. D. and C. C. Chow, "Estimating changes in free-living energy intake and its confidence interval", The American Journal of Clinical Nutrition **94**, 1, 66–74 (2011).

Haugen, M. *et al.*, "Associations of pre-pregnancy body mass index and gestational weight gain with pregnancy outcome and postpartum weight retention: a prospective observational cohort study", BMC Pregnancy and Childbirth **14**, 1, 201 (2014).

Hu, J., Z. Wang, H. Gao and L. K. Stergioulas, "Extended Kalman filtering with stochastic nonlinearities and multiple missing measurements", Automatica **48**, 9, 2007–2015 (2012).

Jazwinski, A. H., *Stochastic Processes and Filtering Theory* (Academic Press, 1970).

Jemmott III, J. B., L. S. Jemmott and G. Fong, "Abstinence and safer sex hiv risk-reduction interventions for african american adolescents: a randomized controlled trial", Jama **279**, 19, 1529–1536 (1998).

Johansen, T. A. and T. I. Fossen, "Nonlinear filtering with exogenous Kalman filter and double Kalman filter", in "2016 European Control Conference (ECC)", pp. 1722–1727 (2016).

Johansson, L., K. Solvoll, G. E. Bjørneboe and D. C. A., "Under-and overreporting of energy intake related to weight status and lifestyle in a nationwide sample", The American Journal of Clinical Nutrition **68**, 2, 266–74 (1998).

Kumar, S., W. Nilsen, M. Pavel and M. Srivastava, "Mobile health: Revolutionizing healthcare through transdisciplinary research", Computer **46**, 28–35 (2013).

Lichtman, S. W. *et al.*, "Discrepancy between self-reported and actual caloric intake and exercise in obese subjects", New England Journal of Medicine **327**, 27, 1893–1898 (1992).

Liu, X. and A. Goldsmith, "Kalman filtering with partial observation losses", in "43rd IEEE Conference on Decision and Control (CDC)", vol. 4, pp. 4180–4186 (2004).

Locke, E. and G. Latham, *Motivation: Theory and Research*, chap. Goal-setting theory, pp. 13–29 (Hillsdale, NJ: Lawrence Erlbaum, 1994).

Lutomski, J. E., J. van den Broeck, J. Harrington, F. Shiely and I. J. Perry, "Sociodemographic, lifestyle, mental health and dietary factors associated with direction of misreporting of energy intake", Public Health Nutrition **14**, 3, 532–541 (2011).

McGowan, C. A. and F. M. McAuliffe, "Maternal nutrient intakes and levels of energy underreporting during early pregnancy", European Journal of Clinical Nutrition **66**, 8, 906–913 (2012).

Moran, L. J., S. A. McNaughton, Z. Sui, C. Cramp, A. R. Deussen, R. M. Grivell and J. M. Dodd, "The characterisation of overweight and obese women who are under reporting energy intake during pregnancy", BMC Pregnancy and Childbirth **18**, 204 (2018).

Mullaney, L., A. C. O'higgins, S. Cawley, A. Doolan, D. McCartney and M. J. Turner, "An estimation of periconceptional under-reporting of dietary energy intake", Journal of Public Health **37**, 4, 728–736 (2014).

Nandola, N. N. and D. E. Rivera, "An improved formulation of hybrid model predictive control with application to production-inventory systems", IEEE Transactions on Control Systems Technology **21**, 1, 121–35 (2013).

Navarro-Barrientos, J. E., D. E. Rivera and L. M. Collins, "A dynamical model for describing behavioural interventions for weight loss and body composition change", Mathematical and Computer Modelling of Dynamical Systems **17**, 2, 183–203 (2011).

Nehring, I., S. Schmoll, A. Beyerlein, H. Hauner and R. Von Kries, "Gestational weight gain and long-term postpartum weight retention: a meta-analysis", The American Journal of Clinical Nutrition **94**, 5, 1225–1231 (2011).

Norman, P., M. Conner and R. Bell, "The theory of planned behavior and smoking cessation", Health psychology **18**, 1, 89 (1999).

Nowicki, E., A. M. Siega-Riz, A. Herring, K. He, A. Stuebe and A. Olshan, "Predictors of measurement error in energy intake during pregnancy", American Journal of Epidemiology **173**, 5, 560–568 (2011).

Ogden, C. L., M. D. Carroll, B. K. Kit *et al.*, "Prevalence of childhood and adult obesity in the United States, 2011-2012", JAMA **311**, 8, 806–814 (2014).

Olson, C. M., M. S. Strawderman and R. G. Reed, "Efficacy of an intervention to prevent excessive gestational weight gain", American Journal of Obstetrics and Gynecology **191**, 2, 530–536 (2004).

Phelan, S., "Pregnancy: a "teachable moment" for weight control and obesity prevention", American Journal of Obstetrics and Gynecology **202**, 2, 135.e1–135.e8 (2010).

Phelan, S., M. G. Phipps, B. Abrams, F. Darroch, A. Schaffner and R. R. Wing, "Randomized trial of a behavioral intervention to prevent excessive gestational weight gain: the fit for delivery study", The American Journal of Clinical Nutritionion **93**, 4, 772–779 (2011).

Piers, L. S., S. N. Diggavi, S. Thangam, J. M. V. Raaij, P. S. Shetty and J. G. Hautvast, "Changes in energy expenditure, anthropometry, and energy intake during the course of pregnancy and lactation in well-nourished indian women", The American Journal of Clinical Nutrition **61**, 3, 501–513 (1995).

Polley, B. A., R. R. Wing and C. J. Sims, "Randomized controlled trial to prevent excessive weight gain in pregnant women", International Journal of Obesity & Related Metabolic Disorders **26**, 11 (2002).

Poslusna, K., J. Ruprich, J. H. de Vries, M. Jakubikova and P. van't Veer, "Misreporting of energy and micronutrient intake estimated by food records and 24 hour recalls, control and adjustment methods in practice", British Journal of Nutrition **101**, S2, S73–85 (2009).

Rasmussen, K. M. and A. L. Yaktine, eds., *Weight Gain During Pregnancy: Reexamining The Guidelines* (National Academies Press, 2009).

Ravussin, E. and C. Bogardus, "A brief overview of human energy metabolism and its relationship to essential obesity", The American Journal of Clinical Nutrition **55**, 1, 242S–245S (1992).

Risuleo (KTH Royal Institute of Technology, Sweden), R. S., *Personal Communication* (2017).

Sabounchi, N. S., P. S. Hovmand, N. D. Osgood, R. F. Dyck and E. S. Jungheim, "A novel system dynamics model of female obesity and fertility", Amer. Journal of Public Health **104**, 7, 1240–1246 (2014).

Schack-Nielsen, L., K. F. Michaelsen, M. Gamborg, E. L. Mortensen and T. I. Sørensen, "Gestational weight gain in relation to offspring body mass index and obesity from infancy through adulthood", International Journal of Obesity **34**, 1, 67–74 (2010).

Schifter, D. E. and I. Ajzen, "Intention, perceived control, and weight loss: an application of the theory of planned behavior", Journal of personality and social psychology **49**, 3, 843 (1985).

Sinopoli, B., L. Schenato, M. Franceschetti *et al.*, "Kalman filtering with intermittent observations", IEEE Transactions on Automatic Control **49**, 9, 1453–1464 (2004).

Söderström, T., "System identification for the errors-in-variables problem", Transactions of the Institute of Measurement and Control **34(7)**, 7, 780–792 (2012).

Söderström, T., *Error-in-Variables Methods in System Identification* (Springer International Publishing, 2018).

Subar, A. F., F. E. Thompson, N. Potischman *et al.*, "Formative research of a quick list for an automated self-administered 24-hour dietary recall", J Am Diet Assoc **107**, 1002-1007 (2007).

Symons Downs, D., "Obesity in special populations: Pregnancy", Primary Care: Clinics in Office Practice **43**, 1, 109–120 (2016).

Symons Downs, D., J. M. DiNallo, E. L. Rauff, J. S. Ulbrecht, L. L. Birch and I. M. Paul, "Pregnant women's exercise motivation and behavior: Preliminary findings from a randomized physical activity intervention", Journal of Sport & Exercise Psychology **32**, S157–S158 (2010).

Symons Downs, D. and H. A. Hausenblas, "Exercising during pregnancy and postpartum: an elicitation study using the framework of the theory of planned behavior", J Midwifery Womens Health **49**, 138–144 (2004).

Symons Downs, D., J. S. Savage and E. L. Rauff, "Falling short of guidelines? nutrition and weight gain knowledge in pregnancy", Journal of Women's Health Care **3** (2014).

Symons Downs, D., J. S. Savage, D. E. Rivera, J. M. Smyth, B. J. Rolls, E. E. Hohman, K. M. McNitt, A. R. Kunselman, C. Stetter, A. M. Pauley, K. S. Leonard and P. Guo, "Individually tailored, adaptive intervention to manage gestational weight gain: protocol for a randomized controlled trial in women with overweight and obesity", JMIR Res Protoc **7**, 6, e150, DOI: 10.2196/resprot.9220 (2018).

The Look AHEAD Research Group, "Baseline characteristics of the randomized cohort from the look ahead (action for health in diabetes) study", Diabetes & Vascular Disease Research **3**, 3, 202–215 (2006).

Thomas, D. M., "A dynamical fetal-maternal model of gestational weight gain", Personal Communication (2009).

Thomas, D. M., A. Ciesla, J. A. Levine *et al.*, "A mathematical model of weight change with adaptation", Mathematical Biosciences and Engineering **6**, 4, 873 (2009).

Thomas, D. M., J. E. Navarro-Barrientos, D. E. Rivera *et al.*, "Dynamic energy balance model predicting gestational weight gain", The American Journal of Clinical Nutrition **95**, 1, 115–122 (2012).

Trabulsi, J. and D. A. Schoeller, "Evaluation of dietary assessment instruments against doubly labeled water, a biomarker of habitual energy intake", American Journal of Physiology-Endocrinology And Metabolism **281(5)**, 5, E891–E899 (2001).

Westerterp, K. R., "Diet induced thermogenesis", Nutrition & Metabolism **1**, 1, 5 (2004).

Willett, W., *Nutritional Epidemiology* (Oxford University Press New York, 1990).

Wu, Q. and M. Suzuki, "Parental obesity and overweight affect the bodyfat accumulation in the offspring: the possible effect of a highfat diet through epigenetic inheritance", Obesity Reviews **7**, 2, 201–208 (2006).

Xian, X., A. Quach, D. Bridgeman *et al.*, "Personalized indirect calorimeterfor energy expenditure (ee) measurement", Glob J Obes Diabetes Metab Syndr **2**, 1, 107 (2015).